6-10-2009

Biochemical and Spectroscopic Characterization of Tryptophan Oxygenation: Tryptophan 2, 3-Dioxygenase and Maug

Rong Fu
Georgia State University

BIOCHEMICAL AND SPECTROSCOPIC CHARACTERIZATION OF TRYPTOPHAN OXYGENATION: TRYPTOPHAN 2,3-DIOXYGENASE AND MAUG

by

RONG FU

Under the Direction of Aimin Liu

ABSTRACT

TDO utilizes *b*-type heme as a cofactor to activate dioxygen and insert two oxygen atoms into free L-tryptophan. We revealed two unidentified enzymatic activities of ferric TDO from *Ralstonia metallidurans*, which are peroxide driven oxygenation and catalase-like activity. The stoichiometric titration suggests that two moles of H_2O_2 were required for the production of one mole of *N*-formylkynurenine. We have also observed monooxygenated-L-tryptophan. Three enzyme-based intermediates were sequentially detected in the peroxide oxidation of ferric TDO in the absence of L-Trp including compound I-type and compound ES-type Fe-oxo species. The Fe(IV) intermediates had an unusually large quadrupole splitting parameter of 1.76(2) mm/s at pH 7.4. Density functional theory calculations suggest that it results from the hydrogen bonding

to the oxo group. We have also demonstrated that the oxidized TDO was activated via a homolytic cleavage of the O-O bond of ferric hydroperoxide intermediate via a substrate dependent process to generate a ferrous TDO. We proposed a peroxide activation mechanism of the oxidized TDO. The TDO has a relatively high redox potential, the protonated state of the proximal histidine upon substrate binding as well as a common feature of the formation of ferric hydroxide species upon substrate or substrate analogues binding. Putting these together, we have proposed a substrate-based activation mechanism of the oxidized TDO. Our work also probed the role of histidine 72 as an acid-base catalyst in the active site. In H72S and H72N mutants, one water molecule plays a similar role as that of His72 in wild type TDO.

MauG is a *c*-type di-heme enzyme which catalyze the biosynthesis of the protein-derived cofactor tryptophan tryptophylquinone. Its natural substrate is a monohydroxylated tryptophan residue present in a 119-kDa precursor protein of methylamine dehydrogenase (MADH). We have trapped a novel *bis*-Fe(IV) intermediate from MauG, which is remarkably stable. A tryptophanyl radical intermediate of MADH has been trapped after the reaction of the substrate with the *bis*-Fe(IV) intermediate. Analysis by high-resolution size-exclusion chromatography shows that MauG can tightly bind to the biosynthetic precursor and form a stable complex, but the mature protein substrate does not.

INDEX WORDS: Tryptophan 2,3-dioxygenase, MauG, Hydrogen peroxide, Ferryl species, *Bis*-Fe(IV) intermediate, Ferric hydroperoxide, Ferric hydroxide, Protein radical, Acid-base catalyst, Protein-substrate complex, Mössbauer spectroscopy, Electron paramagnetic resonance sepectroscopy, Site-directed mutagenesis

BIOCHEMICAL AND SPECTROSCOPIC CHARACTERIZATION OF TRYPTOPHAN OXYGENATION: TRYPTOPHAN 2,3-DIOXYGENASE AND MAUG

by

RONG FU

A Dissertation Submitted in Partial Fulfillment of the Requirements for the Degree of

Doctor of Philosophy

in the College of Arts and Sciences

Georgia State University

2009

BIOCHEMICAL AND SPECTROSCOPIC CHARACTERIZATION OF

TRYPTOPHAN OXYGENATION:

TRYPTOPHAN 2,3-DIOXYGENASE AND MAUG

by

RONG FU

Committee Chair: Aimin Liu

Committee: Binghe Wang
Giovanni Gadda

Electronic Version Approved:

Office of Graduate Studies
College of Arts and Sciences
Georgia State University
August 2009

DEDICATION

This thesis is dedicated to my wonderful parents, Jinhui Fu and Yuanyan Wu. Thank you for all the unconditional love, guidance, and support.

谨以此文献给我敬爱的父亲和母亲：傅金辉先生和吴元燕女士！

ACKNOWLEDGEMENTS

I would like to thank my supervisor, Dr. Aimin Liu, an excellent scientist, who has guided me with his enthusiasm, inspiration, persistent and integral view on research to think and behave like a scientist. I have benefited greatly from his vast knowledge and skills in many areas.

I would like to thank the other members of my committee. I wish to thank Dr. Binghe Wang for his support and guidance. I sincerely thank Dr. Giovanni Gadda for his insight and guidance during the thesis preparation. I wish to thank Dr. Dabney White Dixon for helping me revise resume and giving me career advices.

I am deeply indebted to the professors sitting in my former committee at the University of Mississippi Medical Center: Dr. Victor L. Davidson, Dr. Johathan P.Hosler, Dr. Drazen Raucher and Dr. Parminder J.S.Vig. I would like to express my appreciation to Dr. Davidson for the access to the stopped-flow and redox titration equipment as well as assistance with the kinetic analysis, insightful discussions about the experiment. I thank Dr. Hosler for his kindly providing help on the ICP experiments, and for allowing me to use oxygen electrode and valuable advice. I am very grateful to Dr. Raucher for allowing me to use the sonicator in his lab and early training on the molecular cloning technique. I want to articulate my sincere thanks to my class instructors Dr. Mark Olson, Dr. Donald B. Sittman, Dr. Michael Hebert, Dr. David T. Brown, Dr. Charles L. Woodley, and Dr. John J. Correia.

I would like to express my appreciation to Dr. Siming Wang for helping conducting mass spectrometry and invaluable discussions. I would like to express my gratitude to Professor

Michael P. Hendrich of Carnegie Mellon University for the Mössbauer spectroscopy experiments and providing insightful discussions on TDO project. My thanks also go out to Professor Castern Krebs of Pennsylvania State University for the Mössbauer spectroscopy analyses on the MauG samples. I wish to thank Professor Tadhg P. Begley of Texas A&M University for generously providing the TDO plasmid for me to start the TDO project. I thank Professor Drs. Rodney C. Baker and Dr. Naila M. Mamoon for their assistance in the initial stage of the mass spectrometry analysis on TDO. My appreciation also goes out to Professor David Brown of the Genomics facility in theUniversity of Mississippi Medical Center for helping constructing the TDO mutants.

I want to articulate my sincere thanks to Dr. Xianghui Li for assisting me conducting stopped-flow and redox potential experiments. I wish to thank to Mr. Lakshman Varanasi for helping me with the oxygen electrode experiment. I am grateful to Dr. Hongzhi Xu who has provided me help in pirin project. I want to express my sincerely thanks to my co-workers, Dr. Tingfeng Li, Mr. Thomas W. Flanagan, Mr. Channing Twyner, Ms. Antoinetter L. Waler, Mr. Nafez Abu Tarboush, Mr. Ian Davis, Ms. Yan Chen, Ms. Fange Liu, Mr. Kednerlin Dornevil, Ms. Heyne Lee for their cooperation in experiments, for correcting the grammar of my manuscripts and this thesis, for exchanging knowledge, skills, and venting of frustration during my graduate program. The four years have been quite an experience and they all have made it a memorable time of my life.

I must acknowledge the faculty and students of the Department of Biochemistry at University of Mississippi Medical Center for their assistance during my Ph.D study. I wish to thank the

faculty, staff and students of the Department of Chemistry at Georgia State University for their assistance after I was transferred to here.

Last but not the least, my greatest appreciation goes out to all my beloved family members for their sustaining love, support and encouragement. No matter how far, how long I am away from them, I can always feel the warmest and strongest support from them.

I acknowledge a fellowship support from the Molecular Basis of Disease (MBD) program of GSU. I wouldn't be able to complete my research work and this thesis without the generous MBD support.

TABLE OF CONTENTS

LIST OF TABLES

LIST OF FIGURES

LIST OF SCHEMES

CHAPTER 1

INTRODUCTION

1.1 The Properties of Heme

A heme is a large tetrapyrrole macrocycle that contains an iron atom in the center of protoporphyrin ring. Hemes differ in terms of both the types and the substitution of the porphyrin. To date, there are a total of six known types of hemes, the most common and abundant heme of which is heme *b* (Figure 1.1), also called protoporphyrin IX. Other common types include heme *c* and heme *a*.

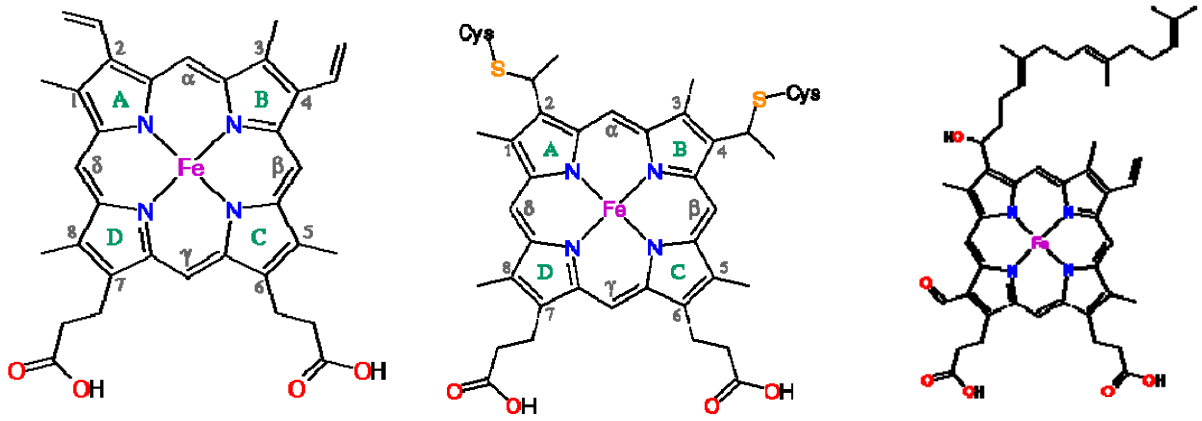

Heme *b* Heme *c* Heme *a*

Figure 1.1. The chemical structures of heme moieties.

Heme *b* (protoporphyrin IX) is the active site prosthetic group for a number of proteins, including myoglobins and hemoglobins, cytochrome P450s (CYP450), peroxidases, catalase and tryptophan 2,3-dioxygenase (TDO) (*1*). It is held in the protein matrix by a non-covalent bond by

an axial ligand and hydrophobic interactions that are provided by the protein environment. Since there is only one non-covalently bonded ligand, heme *b* is easily lost from the heme pocket during protein manipulation.

Heme *c* is synthesized from heme *b*. There are some differences between the two types of hemes. For instance, compared to the *b*-type heme, the *c*-type heme is covalently bound to a protein by two thioether bonds between two heme peripheral vinyl groups and two cysteine amino acid side chains at the 2 and 4 positions (*2, 3*). Most cytochromes utilize *c*-type heme as cofactors to function as electron carriers in a large number of redox processes found in nature. Another example of heme utilization is the *a*-type heme in cytochrome *c* oxidase (C*c*O). In this case, heme *a* differs from heme *b* in the substitution at the 2- and 8- positions of 17-hydroxyethyfarnesyl moiety and formyl group in place of 2-vinyl and 8-methyl respectively (Figure 1.1). Less commonly, there are also heme *d*, heme *d1*, and heme *o* in nature (*1-3*).

1.2 The Functions of Heme Proteins

The common oxidation states for heme iron are ferrous (Fe^{2+}), ferric (Fe^{3+}), and ferryl (Fe^{4+}). The ferryl species found in biology all have an inherent exogenous oxygen in the oxo form which usually refers to Fe(IV)=O. The electronic energy level diagrams depicted in Figure 1.2 show the common spin states of iron in heme proteins. In most cases, the resting formal oxidation state of heme proteins is in ferric form. The porphyrin ring possesses an extensive conjugation structure that allows the electron to delocalize. Often, the porphyrin ring participates in a one-electron transfer process. It is also possible for the electron to transfer from the

porphyrin ring to the nearby amino acids such as tryptophan, tyrosine, or cysteine to form protein-based radicals.

The heme prosthetic group carries out a wide range of biological functions including oxygen transport and storage, electron transfer, chemical catalysis such as monooxygenation, peroxidation, dioxygenation and oxygen reduction as well as gas sensing (*4*). Heme *b* is an extremely versatile prosthetic group in biological systems. The various functionalities of heme proteins are attributed to the various protein environments they operate in. For example, in the heme type, the metal ligands to iron, the distribution of amino acid residues around the active site, and the iron coordination number and formal oxidation state of iron all affect its ultimate function. The proximal ligand in heme *b* includes histidine, cysteine, tyrosine and methionine, whereas in heme *c*, the ligand is generally histidine (*4*).

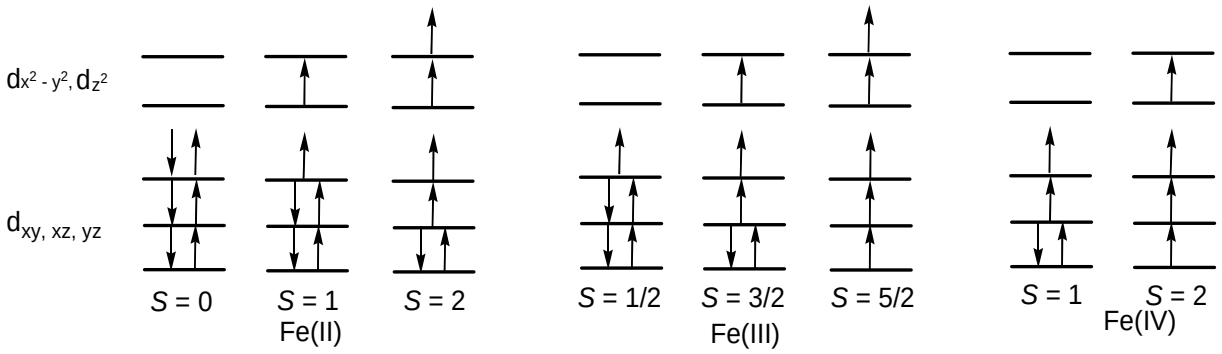

Figure 1.2. The electronic structure of iron at various formal oxidation states.

1.2.1 Monooxygenation

Cytochrome P450 (CYP450) is a superfamily of enzymes that activates dioxygen and catalyzes monooxygenation reactions, incorporating one oxygen atom to an organic substrate. The other oxygen is reduced to a water molecule during catalysis (*4*). A variety of reactions are catalized

by CYP450 such as aliphatic and aromatic hydroxylations, epoxidations, *N-, S-,* and *O*-dealkylation, the oxidation of heteroatoms, among others (*4*).

The active site of CYP450 contains a heme *b* iron center. The *b*-type heme group is embedded in a hydrophobic environment without significant exposure to the solvent. The fifth ligand is cysteine. The substrate binding pocket is relatively flexible when compared to other heme proteins, an aspect that allows large substrates to access the active site.

A normal catalytic cycle of CYP450 mediated reaction requires two electrons and two protons from an exogenous donor, such as NADH + H^+. The resting state of CYP450 contains a six-coordinate low-spin ferric form (S = ½) in which water coordinates on the distal ligand site. Substrate addition induces a change in the conformation of the active site, which results in displacing the water molecule and forming a five-coordinate high-spin ferric state (S = 5/2). This spin state facilitates an electron transfer from the exogenerous reductant, usually in the form of a closely associated CYP450 reductase. Dioxygen then binds to the ferrous enzyme and generates a low-spin ferrous-dioxygen complex or a ferric superoxide complex (Scheme 1.1).

The catalytic cycle continues as a second electron is transferred to form a ferric peroxide species. This is the rate limiting step of the CYP450 reaction during which the ferric peroxide intermediate is transient. This is rapidly followed by the acceptance of a proton to generate a ferric hydroperoxide intermediate. This intermediate accepts a second proton and undergoes heterolytic O-O bond cleavage to generate an oxoferryl porphyrin π cation radical intermediate, which is widely known as compound I. compound I is the central catalytic competent intermediate in CYP450 reaction cycle with a strong oxidizing capacity. It is capable of inserting

an oxygen atom into organic substrates to complete the monooxygenation reaction. Upon completion of the cycle, the enzyme returns to the ferric state with water rebound to the sixth ligand position of the active site. (Scheme 1.1)

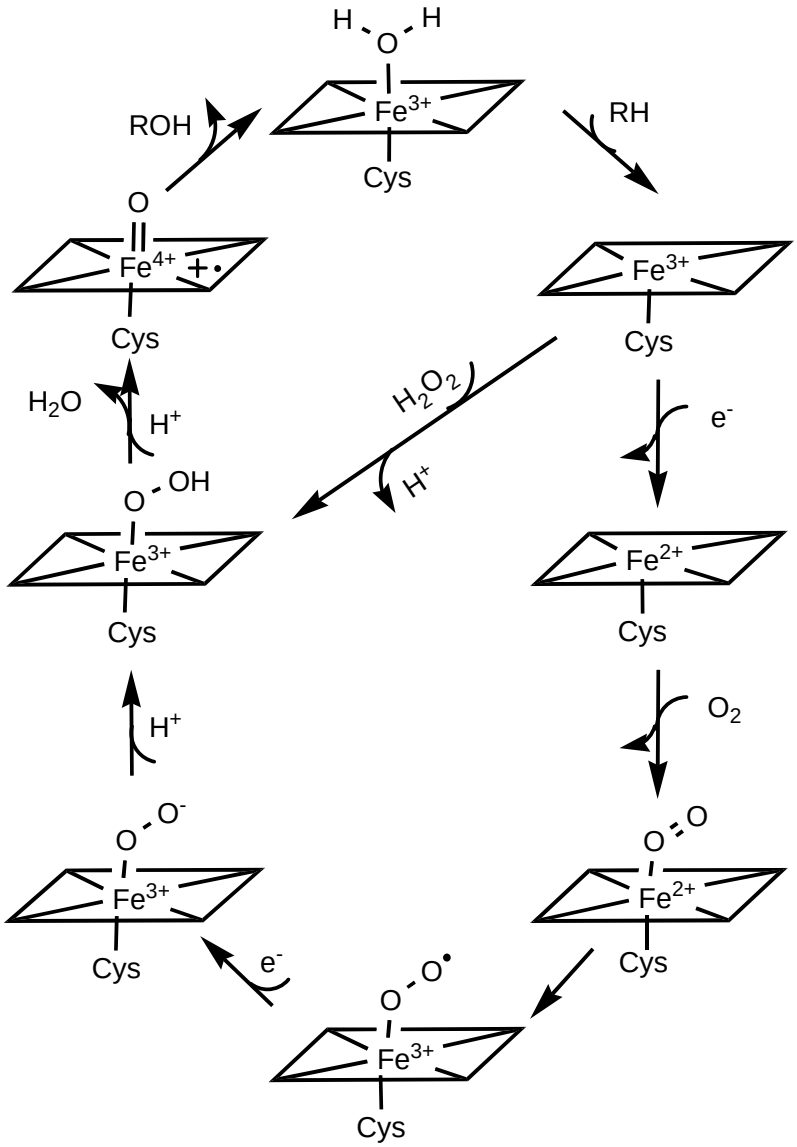

Scheme 1.1. Catalytic cycle of CYP450.

The ferric peroxide and ferric hydroperoxide intermediates of CYP450 have been observed using cryoradiolysis in conjugation with Electron Paramagnetic Resonance (EPR) spectroscopy (*5*). The oxoferryl species in CYP450 is short-lived. It has been demonstrated that hydrogen peroxide, peracids, and alkyl hydroperoxide can provide both the oxygen and electrons required to generate the same ferric hydroperoxide and compound I species from the ferric enzyme as would occur in normal catalytic cycle (*6*). This provides an alternative shunt pathway to generate and characterize the high-valent intermediate during the CYP450 reaction. In employing this advantage, both compound I and compound ES have been observed in stopped-flow studies when mixing *meta*-chloroperoxybenzoic acid (*m*-CPBA) with ferric CYP119, which is a CYP450 enzyme from the thermophile *Sulfolobus solfactaricus* (*7*). Compound ES results from intramolecular electron transfer from a nearby amino acid to the porphyrin ring cation radical of compound I. Recent EPR and Mössbauer studies using peracetic acid as oxidants have indicated that the compound ES species of CYP450 are associated with tyrosyl or tryptophanyl radicals (*8-11*).

It has been demonstrated that the active site environment plays an important role on the cleavage of the O-O bond of ferric hydroperoxide to generate compound I. Scheme 1.2 shows that the hydrogen bond network of CYP450 at the distal pocket and the proposed mechanism of the "pull-push" effect are responsible for compound I formation (*12*). The cysteine axial ligand functions as a strong electron donor, which lowers the redox potential for electron transfer and increases the basicity of the heme group. The process results the provision of a push effect on the electron transfer to the heme group. On the other hand, the two conserved distal site amino acids, Thr and Asp provide a pull effect that facilitates the protonation of the terminal oxygen of the

ferric hydroperoxide intermediate and the subsequent O-O bond heterolytic cleavage (*13*). Site-directed mutagenesis has been employed to investigate the stated role of the above active site amino acids. When Thr is replaced with Ala, or Asp is mutated to Asn, the rate of the protonation step is dramatically reduced (*14, 15*). The alternative of the hemolytic O-O bond cleavage generates compound II species, which has been thought to not be involved in the normal process (*4*).

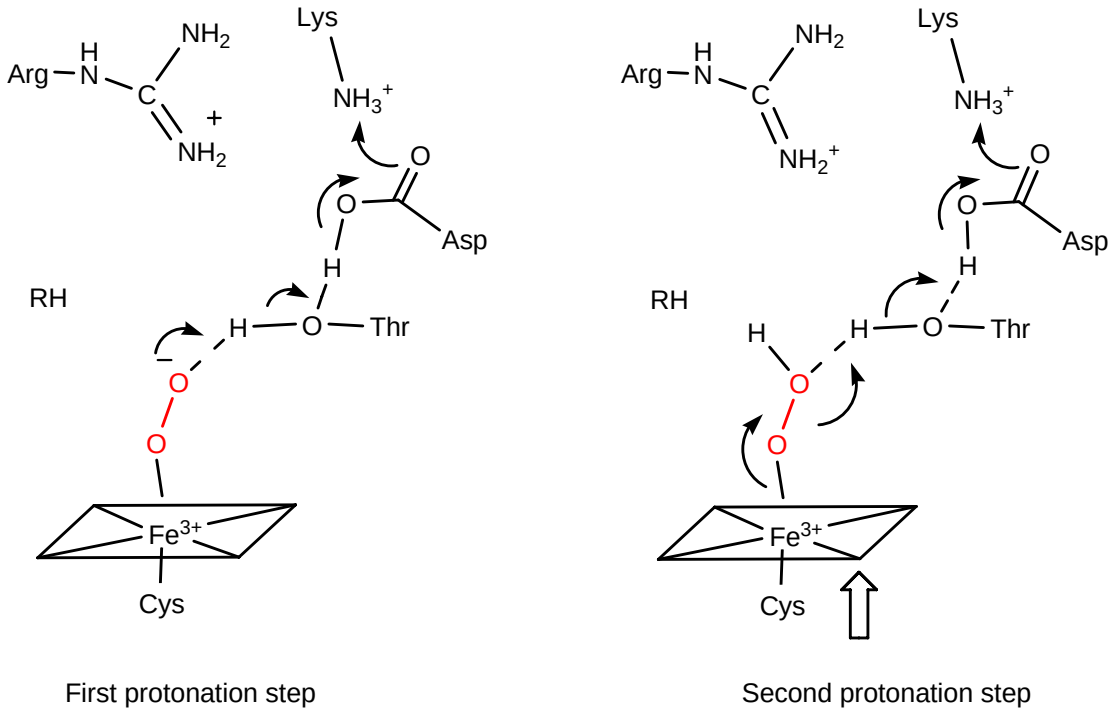

Scheme 1.2. The pull-push effect in cytochrome P450.

1.2.2 Heme Degradation

Heme oxygenase (HO) catalyzes the degradation of heme to biliverdin and carbon monoxide. It plays a vital role in maintaining iron homeostasis and other important biological functions, such as antioxidant defenses, a messenger in signaling pathways by generating CO (*16*). HO is not a

heme protein but it is known to utilize heme as both a prosthetic group and substrate, in which heme is bound to HO in a 1:1 ratio and held in distal site for a site-specific, oxidative degradation of heme itself (*4, 17*).

The ligands of the iron center are comprised of histidine residue and a water molecule in HO (*18-20*). The resting state enzyme is in a ferric from. Upon one electron reduction, dioxygen binds to the ferrous ion center. A second electron reduction and protonation of the ferrous-dioxygen complex generate a ferric hydroperoxide complex, Fe-OOH, which is proposed as the active oxygen species of the enzyme (*21, 22*). This catalytic reactive species initiates an electrophilic attack at the *α-meso* position of the porphyrin to generate an *α-meso*-hydroxyheme species. This species undergoes oxidative ring opening and releases iron and carbon monoxide. This hydroxylation reaction is highly stereospecific at the *α* position due to the blocking of all other *meso*- directions by the nearby amino acids (*18, 23*) (Scheme 1.3).

Most heme enzymes utilize high-valent iron species as the oxidizing species, whereas HO utilizes ferric hydroperoxide as the *meso*-hydroxylating active intermediate (*16, 21, 22*). This intermediate is thought to be generated in the normal catalytic cycle by dioxygen, cytochrome P450 reducatase, and NADPH. It has been proposed that the ferric hydroperoxide can undergo either heterolytic or homolytic cleavage to generate three different species as OH^+, OH^- and $OH^\cdot$ for the hydroxylation reaction. Either electrophilic hydroxylation generating ferric-OOH^+ intermediate or nucleophilic attack generating ferric-OOH^- species form via a concerted pathway that is assisted by a general acid-base catalyst and a chain of water molecules (*16, 24, 25*). A tetrahedral hydroxylated-heme intermediate is formed, which then undergoes a rearrangement and loss of H_2O to generate *α-meso*-hydroxyheme (*16, 26*).

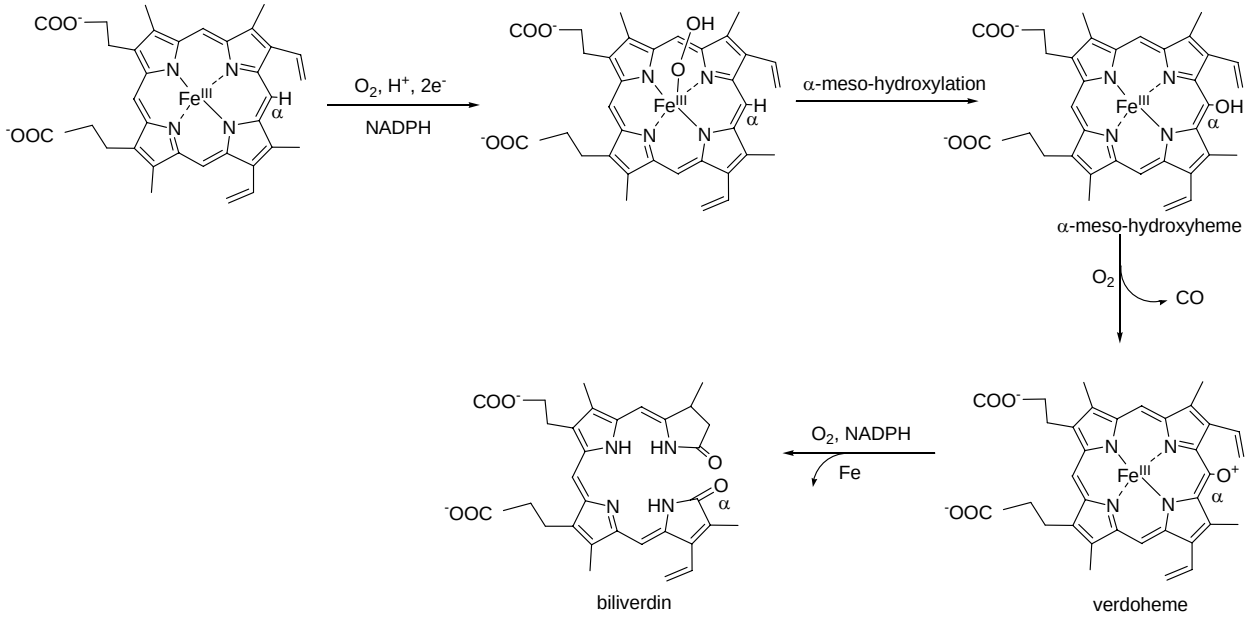

Scheme 1.3. The proposed mechanism of HO.

H_2O_2 can substitute for both of the oxygen and electron donors to produce *α-meso*-hydroxyheme. There is no ferryl intermediate generated during the reaction of ferric HO with H_2O_2 (*25, 27*). High-valent species with one oxidizing species in a protein radical and the other in porphyrin can be observed when using other peroxide analogues, such as alkyl and acyl hydroperoxide as an oxidant. However, there was no *α-meso*-hydroxyheme product observed, which indicates that the ferryl species is not involved in biliverdin formation, thus it is insignificant (*27*). Using the cryoreduction technique, the ferric hydroperoxide intermediate has been detected by EPR and ENDOR (*26, 28*).

The crystallographic studies show that the *α-meso*-edge of the heme is partially exposed at the surface of the protein to allow the electron transfer and oxidation reaction. There are several water molecules in the active site that form an extensive network of hydrogen bonds. Of these,

one of the water molecules is bound to the heme iron ion (*18, 29, 30*). EPR analysis suggests that the metal-bound dioxygen ligand is hydrogen bonded (*31*), however there is no polar amino acid, and particularly no histidine to form a hydrogen bond with the iron bond oxygen atoms. It has been proposed that the water molecules also provide hydrogen bonds (*18, 29, 30*). An interesting feature of the structure of heme oxygenase is its similarity to that of myoglobin rather than to other heme-containing enzymes. When the axial ligand of histidine has been mutated to either cysteine or tyrosine, neither of the mutant proteins has catalytic activity (*32*).

1.2.3 Peroxidation

Peroxidase catalyzes one electron peroxide oxidation of different exogenous electron donors. It is termed based on the various substrates, such as horseradish peroxidase, choloperoxidase, and cytochrome *c* peroxidase. Peroxidases utilize heme *b* as a cofactor and are only partially exposed to solvent. Histidine is the proximal ligand bound to the iron center (*33, 34*).

The general catalytic oxidation-reduction cycle of peroxidases is shown in Scheme 1.4. The resting state of peroxidase contains a high-spin ferric form ($S = 5/2$). Hydrogen peroxide displaces the water molecule and binds to the iron center. A conserved histidine is proposed to abstract a proton from hydrogen peroxide, which leads to a ferric hydroperoxide intermediate. An arginine facilitates the heterolytic O-O bond cleavage to release a water molecule, which generates an oxoferryl species that is two oxidizing equivalents above the ferric iron. In most eukaryotic peroxidases, the oxidizing equivalents manifest as an Fe(IV)-oxo and a porphyrin π cation radical (*35*). Alternately, in some cases, the two oxidizing equivalents are stored in an Fe(IV)-oxo center and nearby amino acid residue, such as a tryptophan radical in cytochrome *c*

peroxidase (*36*). An electron provided either by cytochrome *c* or an organic substrate like aromatic phenol reduces compound I to compound II. In such a case, a second electron transfer to regenerate the resting state of the ferric form followed (Scheme 1.4).

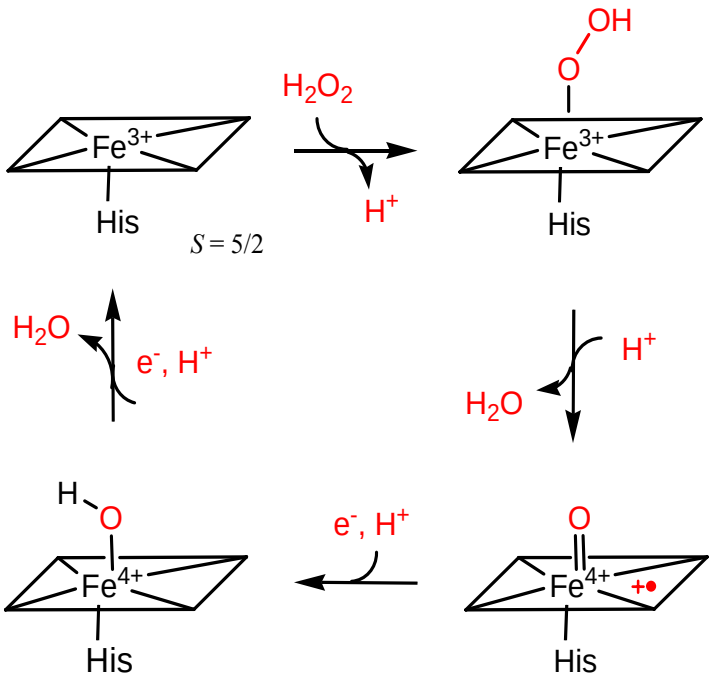

Scheme 1.4. The catalytic cycle of peroxidase.

It should be noted that both compound I and compound II species are active in peroxidases and are relatively long-lived in comparison to those found in other heme proteins. Horseradish peroxidase (HRP) has well-studied active site machinery for the formation of oxoferryl species (Scheme 1.5). The conserved histidine shown in Scheme 1.5 is proposed to function as an active site acid-base catalyst which accepts a proton from the hydrogen peroxide to form ferric hydroperoxide intermediate and then donate the proton to form a leaving water (*4, 37-39*). The conserved distal Arg stabilizes the negative charge on the exiting hydroxide during bond cleavage. Also, the neutral proximal His ligand differs from the cysteine ligand in CYP450 due

to its ability to donate electrons. The His ligand can, however, stabilize higher oxidation states on the heme iron by the strong hydrogen bond network, thus effectively stabilizing the positive charge of the Fe ion (*40, 41*).

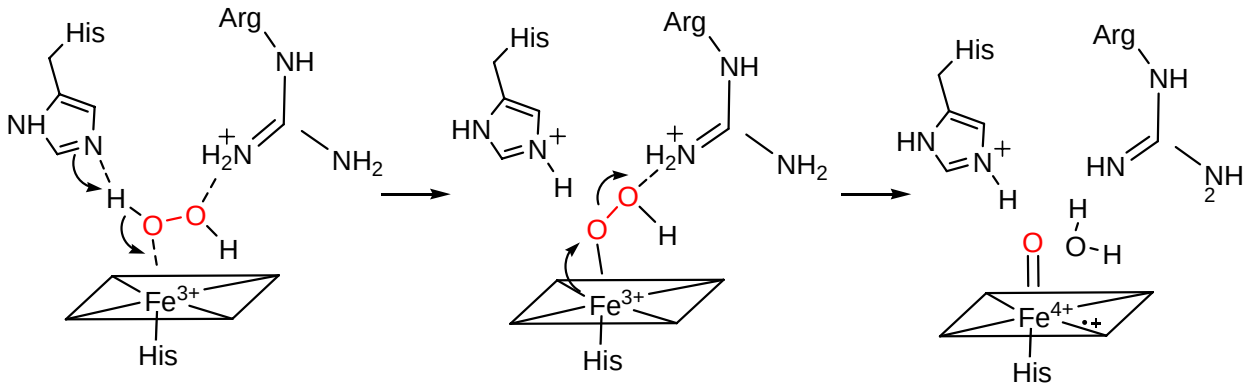

Scheme 1.5. The mechanism for O-O bond cleavage in HRP.

Chloroperoxidase (CPO) from *Caldariomyces fumango* catalyzes the oxidative chlorination of substrates using hydrogen peroxide and Cl^- as substrate. The marked difference between CPO and HRP is the axial ligand; in CPO it is cysteine, while in HRP, it is histidine (*41*).

In CPO, the ferric enzyme reacts with hydrogen peroxide to generate a known compound I species. Compound I may be reduced by two electrons to the ferric enzyme, which generates a water molecule. On the other hand, CPO is capable of inserting one oxygen atom into a substrate when performing epoxidation (*42*) and sulfoxidation (*43*). The source of the oxygen atom incorporated into the epoxide comes from hydrogen peroxide, which is identified by ^{18}O-labeled H_2O_2 (*44*). These elements make CPO a better model for the studies of heme monooxygenation. The active site of CPO is hydrophilic, which is similar to peroxidases. On the other hand, the distal site polar residue of CPO is a glutamic acid. A histidine residue is located near Glu but is away from the Fe center. The arginine in peroxidases active site pockets is not present in CPO

(Scheme 1.6) *(41).*The glutamic acid functions first as proton acceptor and then proton donor, which facilities by the active site histidine.

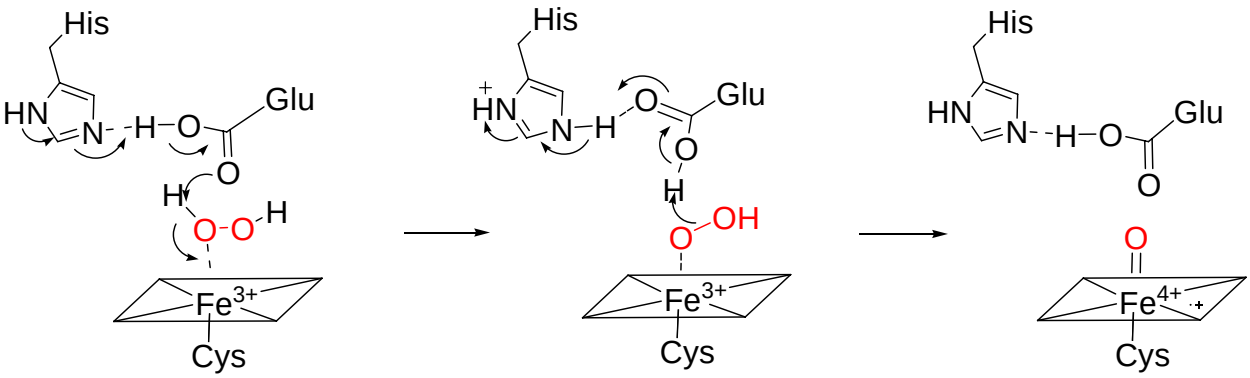

Scheme 1.6. The active site structure and acid-base function in chloroperoxidase.

Cytochrome *c* peroxidase (C*c*P) catalyzes the reduction of peroxide to water. In C*c*P, a compound I species is generataed and reduced by two successive one-electron transfer reactions back to ferric form.Yeast C*c*P is the first heme enzyme for which a high-resolution crystal structure of the oxoferryl species was determined (*45*). EPR spectrum suggests that the Fe(IV)-oxo radical species is located on a nearby tryptophan residue of the protein, while in other peroxidase the radical is located on the porphyrin (*46*). The hydrogen bond network in the distal site of C*c*P is a Trp-His-Arg triad while it is a Phe-His-Arg triad in HRP (*47*). Trp contributes to the stabilization of oxyferryl intermediate via a hydrogen bond interaction. Since Phe is not a hydrogen bond donor, the effect of the triad is different between HPR and C*c*P in oxoferryl species generation. This also explains the formation of tryptophan radical in C*c*P but not in HRP. Site-directed mutagenesis analysis has been conducted to elucidate the functions of the active site amino acids residues. For example (*48-50*), the mutants of Arg to Leu or Lys suggest that the arginine residue makes the distal side more polar and help to the cleavage of the O-O bond of the bound peroxide by stabilizing the separating charge (*51*). Kinetic studies of the distal histidine

mutant shows distal site histidine is an essential acid-base catalyst for proton transfer (*52, 53*). On the other hand, the enzyme activities can partially rescured if imidazole is supplemented to the histidine mutant in the active site. Notably, when the axial His was mutated to Cys in HRP, a low-spin ferric EPR signal resembling that of ferric substrate-bound CYP450cam was observed. However, little peroxidase activity was detected of the mutant (*54*).

Bacterial C*c*P contains two *c*-type hemes. Recently, two crystal structures were obtained for two diheme peroxidase enzymes from both *Pseudomonas aeruginosa* and *Paracoccu spantatrophus* (*55, 56*). The oxidized form of the enzyme exhibits low-spin six-coordinate conformation for both hemes, but different distal ligand coordination in which one is His/His while the other is a His/Met coordination. The two hemes have distinct redox potential due to their different protein environments. In general, the heme with His/His coordination has low redox potential whereas that with His/Met coordination has high redox potential. The resting state of the enzyme is inactive in the fully oxidized form. During activation, the high redox potential of heme obtains one electron from a redox protein such as ferrocyt. c551 or the Cu^{1+} in azurin (*57*) and forms ferrous His/Met form. At the same time, a conformational change of the low redox potential of heme results in the displacment of histidine residue from the heme center, which leads to the formation of high-spin ferric form (*58-61*). This mixed-valent species is catalytically active for hydrogen peroxide binding, followed by producing ferric hydroperoxide intermediate (*58-61*). Upon reduction of hydrogen peroxide, one electron is transferred from the reduced high-potential heme, which is then oxidized to ferric form. The low-potential heme porphyrin group provides the second electron with the formation of an oxyferryl center. Differing from the monoheme peroxidase, the second heme with the His/Met coordination functions as an electron reservoir

where an electron is stored. This stands in contrast to other peroxidase where the second electron is stored on nearby active site residue or porphyrin. The oxoferryl species accepts two electrons from the exogenous donor and is reduced to ferric state. This process requires intramolecular electron transfer from the high-redox potential to low-redox potential heme (Scheme 1.7).

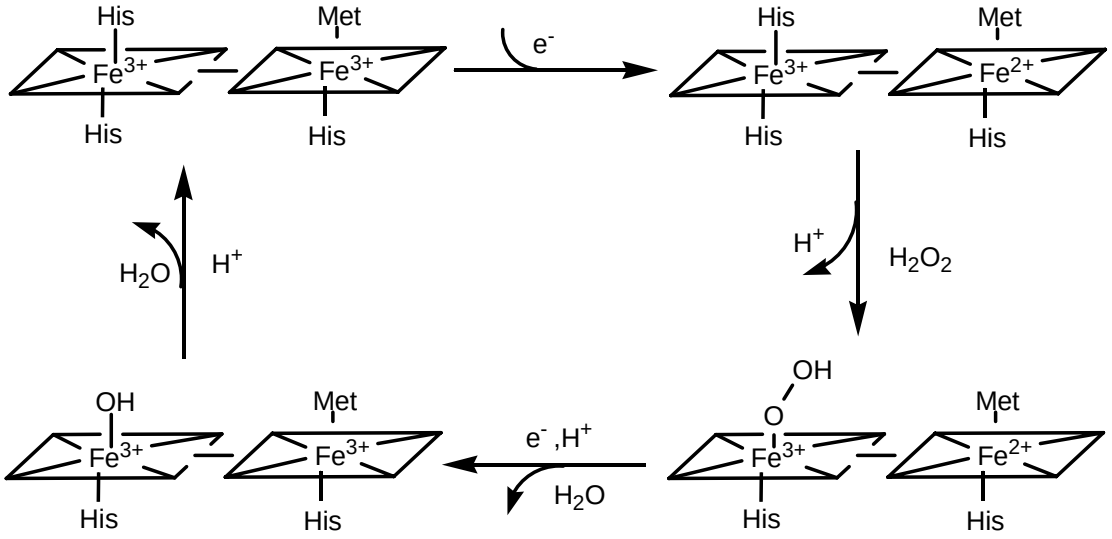

Scheme 1.7. The mechanism of cytochrome *c* peroxidase.

1.2.4 Dismutation of H_2O_2

Catalase is the enzyme that catalyzes the decomposition of hydrogen peroxide and generates water and dioxygen molecule. Catalase can also oxidize different toxins, such as formaldehyde, formic acid, phenols, and alcohols. Catalase is one of the most efficient enzymes in nature (*62*).

Catalase is a tetramer with four identical subunits that has been identified in many sources including bacterial and mammalian cells. Each subunit contains one heme *b* prosthetic group with tyrosine as axial ligand. The heme is deeply buried in the enzyme and is accessible by the

20 Å hydrophobic channel, which allows hydrogen peroxide (but not dioxygen) to get into the distal pocket (*63-65*).

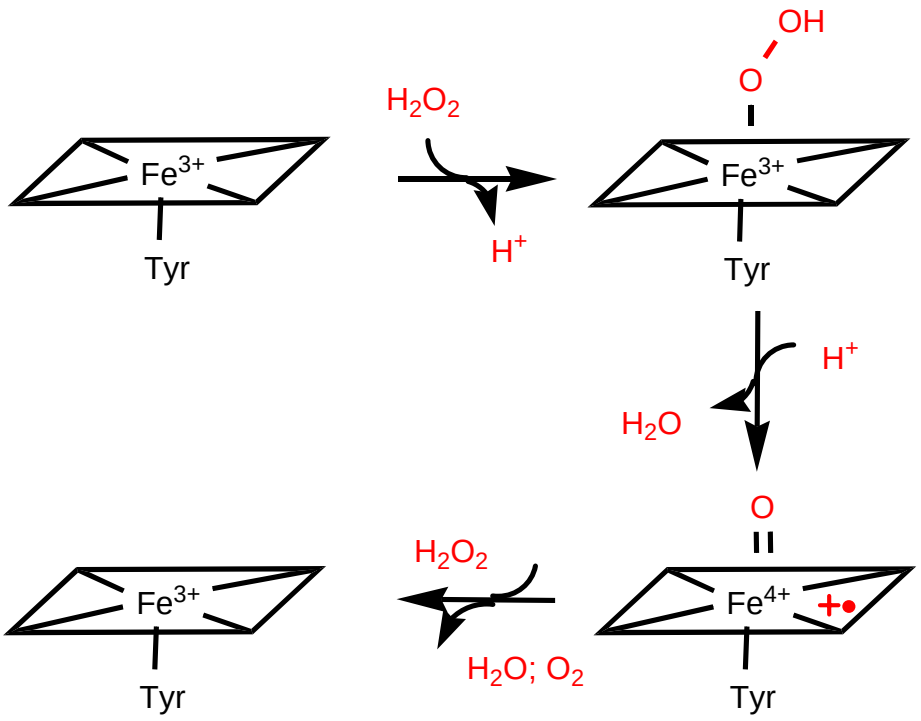

Scheme 1.8. The catalytic mechanism of catalase.

The resting state of catalase contains a high-spin ferric ion. The current working hypothesis (Scheme 1.8) contends that the first hydrogen peroxide enters the iron center, and then one proton of the hydrogen peroxide is abstracted by an active site base to form a ferric hydroperoxide intermediate. The O-O bond heterolytic cleavage of the intermediate generates a compound I species and a water molecule by accepting the proton from the active site base (*66*). This process is facilitated by two active site residues, asparagine and histidine (*67*). The relatively short Fe-phenolic oxygen distance with 1.9 Å and the proximal Arg residue contribute to the ionization of proximal tyrosine residue (*68*). The tyrosine residue, being negatively

charged, also contributes to the generation of compound I. Compound I species reacts with a second hydrogen peroxide molecule and is reduced to one dioxygen and one water molecule. After the catalytic cycle, the enzyme returns to ferric form.

1.2.5 O_2 Transportation and Storage

Myoglobin and hemoglobin are well known for their oxygen storage and transportation capabilities. Both of these proteins contain *b*-type heme and bind dioxygen reversibly. The heme group is located in a crevice in myoglobin and is surrounded by non-polar residues, except for two polar histidine residues which are important for the functionality of myoglobin. One axial histidine is bound to the iron center as a metal ligand and one histidine is located at the distal side (*69, 70*). The native deoxy form of myoglobin is a ferrous ion with a five-coordinate high-spin state (S =2), dioxygen is reversibly bound to the sixth vacant coordination site (*71*). The distal site histidine controls the correct shape of the active site cavity, which allows only small molecules (such as O_2) to access and react with the iron atom. It also helps to make the O_2 biding reaction reversible (*72, 73*). The ferrous heme binds oxygen as a ferric superoxide complex. Due to the antiferromagnetic coupling, there is no EPR signal detected for the ferric superoxide species, although Mössbauer quadruple splitting of the heme iron has demonstrated a ferric state (*74*). Myoglobin is a monomer whereas hemoglobin is a tetrameric protein with four subunits that bind oxygen cooperatively and allow the binding and dissociating of oxygen in a narrow range of oxygen partial pressure (*75-77*). Accordingly, it is ideal for O_2 transportation. On the other hand, the well-designed heme binding pocket of myoglobin allows it to be a good storage area for O_2 in the body.

Myoglobin is a well-studied heme protein with a small molecular weight of 17 kDa. Myoglobin has been used as a model for structure and functionality studies to provide additional insights about other heme-containing proteins. Myoglobin can react with peroxide in a manner similar to peroxidases to form compound I species (*78*), which is unstable in wild type myoglobin. It is, however, detected to be stable in F43H/H64L mutant wherein the His43 can stabilize the porphyrin π cation radical species (*79-81*). Myoglobin has also been engineered to perform peroxidase, catalase (*82, 83*) and monooxygenase activities (*81, 84*). L29H/H64L and F43H/H64L mutants are constructed to possess peroxidase and catalase activity to oxidize peroxidase substrate such as ABTS and guaiacol and dismutate H_2O_2 (*81, 84*). One tryptophan residue has been engineered into the active site to mimic the substrate binding site for aromatic compounds as seen in the CYP450 monooxygenation reaction (*85*).

Although myoglobin can mimic multiple functionalities, the reaction rates are much slower when compared to the naturally-occuring enzyme. It has been proposed that at least three strategies can be employed in the stabilization and cleavage of the active site intermediate in heme proteins. One such strategy involoves stabilizing the negative charge on the oxygen atoms of the leaving group by a polar amino acid is one strategy, such as Arg in peroxidase and Asn in catalase. The proper position and distance of the active site acid-base catalyst to the heme center can facilitate the heterolytic O-O bond cleavage. For example, the distances between the heme iron centers to Nε of the distal histidine are 5.6 and 4.8 Å in C*c*P and beef liver catalase, respectively (*39, 64, 86*). It has been suggested that about 5.0-5.5 Å could be the optimal distance for the hydrogen bonding interactions between the protonated distal histidine and the terminal oxygen of the iron bound hydroperoxide (*87*). Finally, hydrogen bond networks play a role in compound I

formation in both distal and proximal site. In peroxidase, Asp forms a hydrogen bond to the proximal His to compensate for the neutral feature of histidine for electron transfer. Replacement of Asp in HRP with Val could decreases the compound I formation (*39, 86*).

1.2.6 Electron Carrier and Gas Sensors

The *c*-type hemes covalently attach to the protein via thioether bonds, which are derived from the two cysteine residues of the conserved CXXCH motif and the vinyl groups of the heme. Most of the *c*-type cytochromes have a histidine as the fifth axial ligand that is provided in the CXXCH motif (*1-3*). The most common function of *c*-type heme is to work as an electron carrier that is involved in a wide range of redox processes, including photosynthesis, various processes of respiration, and the cycling of nitrogen and sulfur. Redox potential is an important measure of cytochrome *c* because it determines the direction of the electron flow and controls the driving force of the electron transfer kinetics (*1-3*). Cytochrome *c* has an amazingly wide range of redox potentials covering over 1V, from +640 mV in cytochrome *c*552 of *Thiobacillus ferrooxidans* to -400 mV in cytochrome *c*3 of *Desulfovibrio* (*88*). The redox potential of cytochrome *c* can be tuned by the heme environment, heme structure itself and the character of the axial His ligand. Cytochrome *c* generally has either His/Met or *bis*-His heme axial ligation (*1-3*). The redox potential of His-Met coordination tends to be higher than that of *bis*-His coordination due to the weak methionine-heme interaction (*3*).

Cytochrome *c* peroxidase contains two *c*-type hemes with well-separated midpoint redox potentials, as discussed in the peroxidase section above. The bifunctional catalase-peroxidases also contain two *c*-type hemes and have some similarities with the bacterial cytochrome *c*

peroxidase (*89-91*). Other enzymes utilize *c* type heme as the redox center, such as the tetraheme cytochrome *c*554 in *Nitrosomanas europaea* (*92*) and monoheme in hydroxylamine oxidoreductase (*93*), both of which have biological nitrification activity. Also, the SoxAX complex, which is a heterodimeric *c*-type heme-containing protein is involved in thiosulfate oxidation (*94*) and the rubber oxygenase RoxA which cleaves the carbon backbone of ploy (*cis*-1,4-isoprene) (*95*)

Some *c*-type heme proteins have been identified as gas or redox sensors (*2*). For example, tetraheme cytochrome c3 binds CO at the heme center and acts as a CO sensor; cytochrome *c* binds NO to suppress the toxic levels of NO. The *c*-type heme sensor proteins are generally 5-coordinate when oxidized, thus leaving an open coordination site for the physiological effectors molecules to access. Oxygen binding is uncommon for *c* type heme proteins, which are normal in heme *b*-containing proteins. Although the function is still unknown, oxygen binding characteristics have been identified in *Sphaeroides* heme *c* protein (*96*).

1.2.7 Heme Dependent Dioxygenase

1.2.7.1 Tryptophan 2, 3-dioxygenase (TDO)

TDO is a heme-containing enzyme that catalyzes the oxidative cleavage of the indole ring of L-tryptophan (L-Trp), converting it to *N*-formylkynurenine (NFK) (Scheme 1.9) (*4, 97, 98*). TDO was first discovered in mammalian liver by Kotake and Masayama in 1936 (*99*) and was first characterized in rat liver at its purified protein level in 1955. A decade later, its isoform enzyme indoleamine 2,3-dioxygenase (IDO) was discovered and isolated from rabbit intestine (*100, 101*).

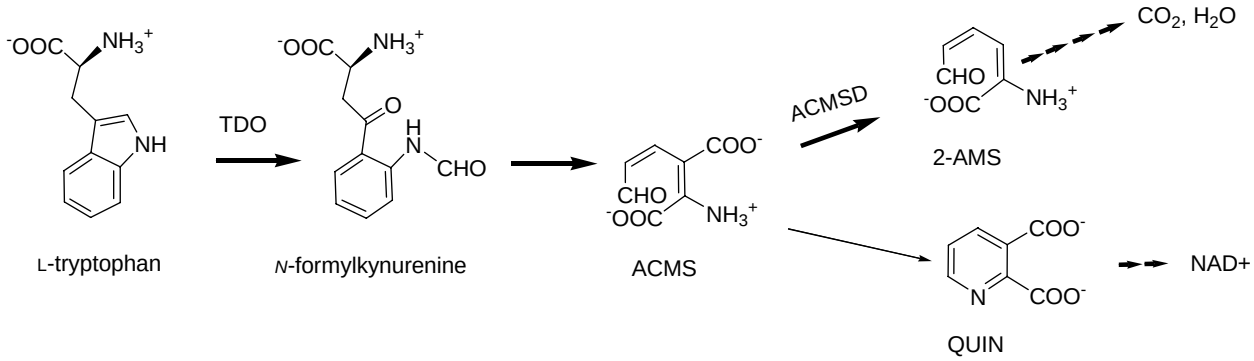

Scheme 1.9. The tryptophan kynurenine pathway.

TDO is mostly present in the liver, but has also been found in mammalian mucous membranes, and in a few cases in epididymic and brain of mouse (*102, 103*). It has also been found outside of mammals in mosquitoes and bacteria such as *Pseudomonas acidovorans* (*4, 97*). IDO is primarily present in mammals, however and is ubiquitously distributed in various tissues of mammals except liver (*4*). TDO has a high specificity to L-tryptophan. It can also use a few tryptophan derivatives as substrate, for example, 6-fluoro-tryptophan. IDO has a much broader substrate specificity; it can utilize D-tryptophan, tryptamine and 5-hydroxytryptamine (serotonin) other than L-Trp as its substrate (*4*). The expression of IDO is induced by interferon-γ and linked to various immune-related pathophysiological conditions wherein TDO is induced by glucocorticoid hormones and regulated by its physiological substrate, L-Trp (*4, 104-109*).

TDO is a biologically significant enzyme. It catalyzes the first and committing step of L-Trp degradation in the kynurenine pathway (Scheme 1.9). The kynurenine pathway constitutes the major route of *de novo* biosynthesis of NAD, which is one of the essential redox cofactors in all living systems (*110*). Excessive accumulation of many of the intermediate metabolites of this pathway can lead to numerous physiological and pathological conditions, including cataract formation, cerebral malaria, Alzheimer's disease, HIV infection, Huntington's disease and

ischemic brain injury (*111-120*). TDO is responsible for oxidizing over 99% of the free L-Trp in intracellular and extracellular pools. Less than 1% Trp is metabolized via the serotonergic pathway, which synthesizes very important neurotransmitters such as serotonin and melatonin (*104*). Therefore, TDO plays a critical role in controlling the relative Trp metabolic flux between the serotonergic and kynureninic pathways.

TDO/IDO is also one of the earliest enzymes explored in dioxygen chemistry. In the 1950s, Mason and Hayaishi, upon using an ^{18}O labeling experiment demonstrated that one or both of the oxygen atoms of dioxygen could be incorporated into substrate during an enzymatic reaction (*121, 122*). The revelation changed traditional views about how nature uses dioxygen. Hayaishi designated this kind of enzyme as oxygenase. Shortly after the discovery of oxygenase, Hayaishi further identified that both of the atoms from dioxygen were incorporated into TDO/IDO and he named it as tryptophan 2,3-dioxygenase which was exclusively used until now (*123*). The discovery of the oxygenase enzyme has provided a great opportunity for chemistry research.

1.2.7.2 The cofactor of TDO/IDO

Hemoproteins perform a wide range of biological functions including oxygen transport and storage, electron transfer, monooxygenation, and reduction of dioxygen (*4*). However, they rarely express a dioxygenase activity as their native biological function. Dioxygenation reactions are typically catalyzed by non-heme metalloenzymes (*124*) but TDO is the first described exception. As an oxygenation enzyme, TDO/IDO are distinctive members of the dioxygenase family as they utilize a histidine-ligated ferrous heme rather than a non-heme iron to carry out the oxygen activation and insertion reactions.

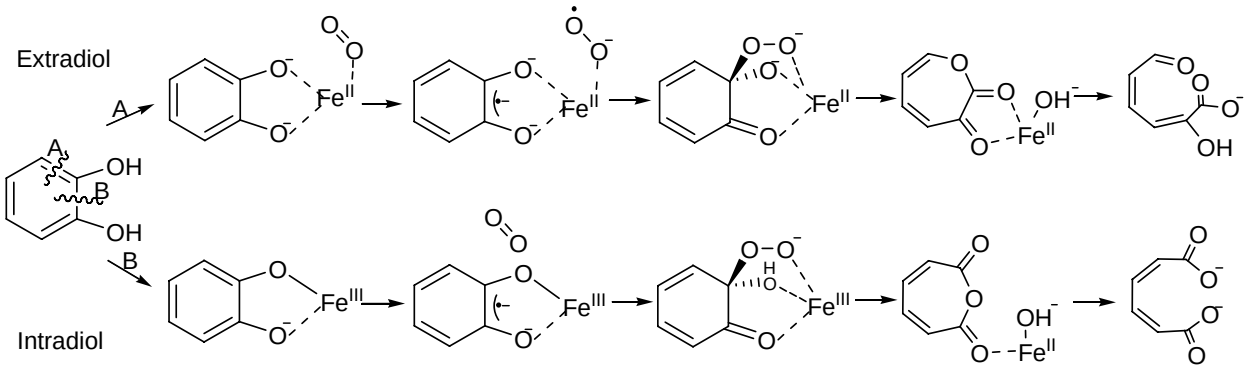

Scheme 1.10. The catalytic mechanisms of oxygen activation of extradiol and intradiol non-heme Fe dioxygenases.

The role of the metal in non-heme Fe-dependent dioxygenases is to facilitate a shift in electron density from the aromatic substrate to the bound oxygen (*125*). As for most of the non-heme iron dioxygenase, the non-heme iron active sites generally have two histidines, one carboxylate and two or three water ligands, which allow simultaneous binding of both substrate and dioxygen (*124*). The substrate and oxygen are activated and each presents some type of radical character so that the subsequent attack of oxygen on the aromatic substrate is spin allowed (*124*).

Most of the non-heme iron dioxygenases can be classified into extradiol and intradiol dioxygenase, which differ in their mode of ring cleavage and the oxidation state of the active-site metal (Scheme 1.10). The ferrous extradiol enzymes activate O_2 directly for reaction, whereas the ferric intradiol enzymes activate the substrate for O_2 attack. Although they have different mechanisms, they share same common features, one of which is substrate directly binds to iron ion and forms the common enzyme-substrate complex. However, this mechanism cannot be applied to the enzymes with a heme cofactor because heme enzymes would not allow a simultaneous binding of the two substrates onto the Fe ion. In the ligand-bound crystal structure of TDO, the primary substrate (L-Trp) binds to a relatively hydrophobic pocket near (but not

directly at) the Fe ion (Figure 1.3) (*126*). The role of the Fe cofactor in the heme-dependent dioxygenase cannot be the same as the well-studied non-heme Fe counterpart. The dioxygenase activity of TDO must therefore proceed using a distinct new mechanism relative to that of the non-heme Fe-dependent dioxygenases. A recent discovery has exposed a third hemoprotein (PrnB) with dioxygenase activity (*127*). Therefore, a potential heme-dependent dioxygenase enzyme superfamily of which TDO is a prototype member has been suggested (*127*).

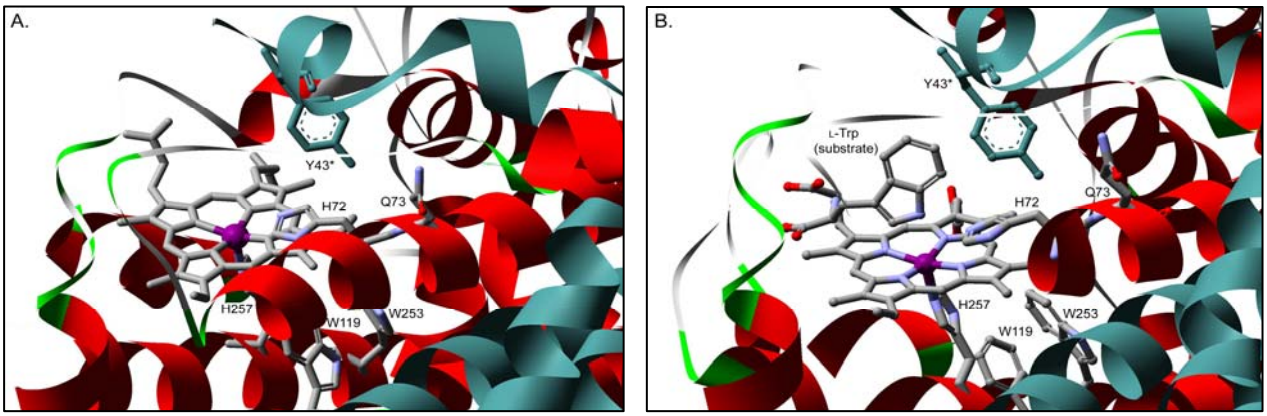

Figure 1.3. The active site of *X. campestris* TDO in absence of substrate (A) and presence of substrate (B). The protein residues are numbered according to the corresponding rmTDO sequence.

1.2.7.3 Crystal structure of TDO/IDO

The crystal structures of TDO, from *Xanthomonas campestris* and *Ralstonia metallidurans*, and IDO from humans have provided critical insights into the molecular details of the active site architecture (*128-130*). More studies on TDO either from human or bacteria sources have been performed to elucidate substrate recognition and the role of active site environment (*131-136*).

TDO is a tetrameric protein that contains four subunits. The overall structure of TDO exhibits as a dimer of dimers in which the *N*-terminal amino acid from the adjacent subunits swapps into another subunit and provids part of the area of the binding cavity for substrate binding (*128-130*). In contrast, IDO is a monomeric protein. It contains two distinct, large *C*-terminal and small *N*-terminal domains. The large domain of IDO is almost superimposed with a monomer of TDO and the active site structures are essentially identical. These enzymes have similar structures but share less than 14% amino acid sequence identity (*137*).

The crystal structure of TDO in a binary complex with L-Trp has been determined from xcTDO in the reduced form. In the ligand-bound crystal structure of xcTDO, the primary substrate (L-Trp) binds to a relatively hydrophobic pocket near but not directly to the Fe ion (Figure 1.4) (*126*). The structure in Figure 1.4 reveals the detailed interactions between substrate and the surrounding amino acids residues in the active site of xcTDO. In the structure of xcTDO, the NH of the indole ring forms a hydrogen bond with His55 (corresponding to His72 in rmTDO and Ser167 in hIDO); the carboxyl group of L-Trp form hydrogen bonding and ionic bonding with Tyr113, Arg117 and Thr254 (corresponding to Tyr130, Arg134 and Thr271 in rmTDO; Phe226, Arg231in hIDO); whereas, the ammonium group of L-Trp forms hydrogen bonds with the side chain hydroxyl group of Thr254 and the 7-propionate group of heme. The active site cavity is surrounded by several hydrophobic residues, including Phe51 and Tyr24 (corresponding to Phe68 and Tyr43 in rmTDO and Phe163 and Tyr126 in hIDO). The indole ring of L-Trp forms a stacking interaction with the aromatic ring of the amino acid residues around the active site. Though the extensive interactions, L-Trp is bound to the active site.

The large domain of the monomeric IDO contains a complete active site that is almost conversed to that of TDO. Based on the similar functions and structure in the active site, the substrate bound IDO is assumed to be similar to that observed in TDO. However, IDO has less extensive hydrogen bonding interaction with the carbonyl group of the bound L-Trp. In this case there is no residue corresponding to Thr254 in xcTDO in the active site and Arg117 residue is away from the active site to form a hydrogen bond with the carbonyl group of L-Trp. These structural arrangements appear to allow the flexibility of the substrate binding.

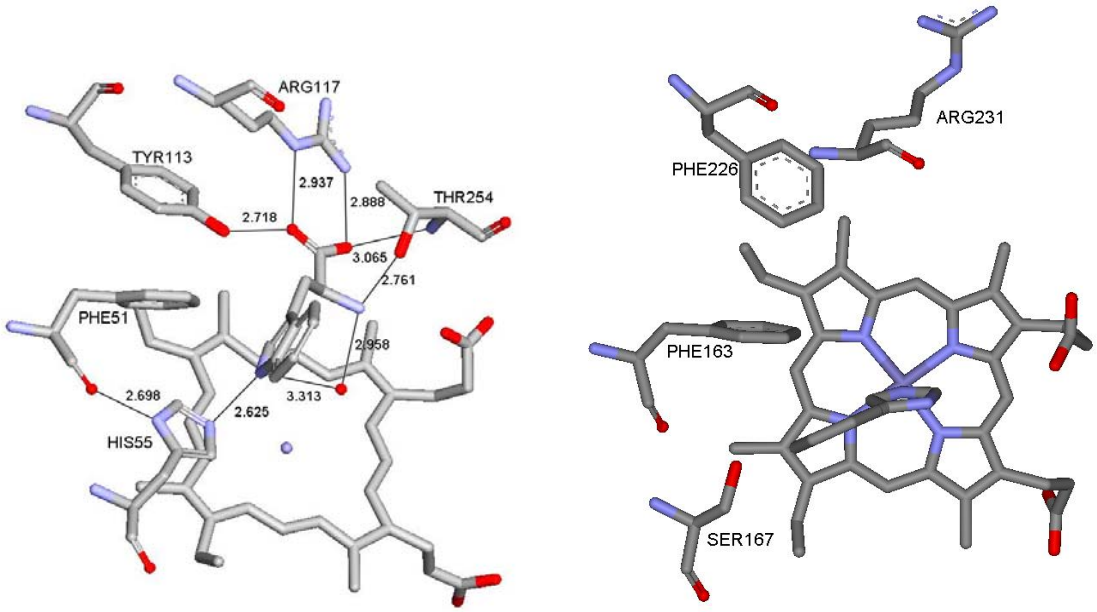

Figure 1.4. (A) The active site hydrogen bond network in the presence of L-Trp in *X. campestris* TDO (PDB 2NW8) and (B) The active site residues in the presence of 4-phenylimidazole in human IDO (PDB 2D07).

1.2.7.4 Spectroscopic methodology of binding of substrate or substrate analogue

Spectroscopic methodology has been applied to help distinguish the differences in substrate binding as well as the substrate and cofactor interactions in oxygen activation. The effect of L-Trp on the active site environment has been detected by EPR spectroscopy (*134, 135, 138-140*).

Taking the advantage that NO can be used as a probe for a ferrous ion center, the EPR spectra suggests that the symmetry of the heme is changed upon binding of L-Trp (*138*). Ferric TDO exhibits high-spin Fe EPR signal. The spin transition of ferric TDO has been observed in the presence of L-Trp (*135, 139*).This is indicated by the conversion of EPR high-spin signal at $g = 6$, 2 to low-spin signal at $g = 2.66, 2.20, 1.81$ (*139*). A recent EPR study of rhTDO and hIDO shows a mixture of a high-spin and a low-spin signals (*135*). The *g* values of the low-spin species are similar to that observed in rhIDO (*140*). Resonance Raman spectroscopy demonstrates the formation of ferric hydroxide species (*132, 141*). Thus, the low spin signal has been interpreted as a ferric hydroxide species in the substrate bound form.

Resonance Raman spectroscopy is sensitive to hydrogen bonds, hydrophobic interactions, and steric interactions. This method is employed to detect the substrate-protein interactions and provides structural information regarding the active site structures of heme proteins. The resonance Raman spectra of TDO indicated that the L-Trp binds in the vicinity of the heme, triggering the spin transition from the high-spin to low-spin state of the ferric ion (*131-133*). CO is used as a structural probe for distal ligand binding site of heme proteins since it has a high affinity toward the ferrous ion. In hTDO, the NH group of L-Trp forms a hydrogen bond with histidine residue but not CO, while in hIDO it forms a hydrogen bond with CO (*132, 133*). This suggests that the active site substrate binding geometry of CO and ferrous ion is different in TDO and IDO. Batabyal and colleagues utilized tryptophan analogues such as L-Trp, D-Trp, tryptamine and indole propionic acid as structural probes to distinguish the substrate-protein interaction among different mutants in the presence of CO. Four possible conformers of L-Trp or L-Trp analogue-bound enzymes were proposed (*132*).

1.2.7.5 O_2 binding and redox properties

In TDO, the Michaelis–Menten complex is formed by L-Trp binding to the active site, followed by dioxygen binding to the ferrous iron center. Moreover, the substrate binding order is much more flexible in IDO, in which it can bind to dioxygen regardless of L-Trp (*142, 143*). Both TDO and IDO can be activated by the binding of superoxide to the ferric enzyme as well as dioxygen to the ferrous form (*4, 144*). The spectroscopic evidence of the oxy-intermediate has been reported for a bacterial TDO from *Pseudomonas fluorescens*, which shows a Soret band at 417 nm and visible region at 543 nm and 576 nm (*145*) (*146*). H72S which mimic the active site residue of serine in IDO and H72A which replaces the only polar active site residue in TDO are constructed. The oxy-intermediate of H72S and H72A mutants are more stable compared to wild type TDO (*132*). hTDO and hIDO have similar redox potential. Upon substrate binding, the electrochemical midpoint redox potential for both of them increased (*129, 135, 140, 147*). This type of an increase leads to the thermodynamic stabilization of the active ferrous form.

1.2.7.6 Catalytic mechanism of TDO

TDO was identified over seventy years ago (*148*) and was studied at several well-established laboratories (*149-156*). Hamilton has proposed an ionic mechanism for the formation of a hydroperoxide intermediate at C_3 position of the indole ring. It is generally believed that the further reaction proceeds through either a Criegee rearrangement or a concerted dioxetane mechanism (Scheme 1.11) (*4, 128, 157-160*). In the dioxetane mechanism, dioxygen inserts into the substrate in a concerted manner, while in the Criegee rearrangement, dioxygen molecule inserted into the substrate one by one. An alternative radical- based mechanism has also been

proposed by Leeds, in which electron transfer from the deprotonated L-Trp to ferric TDO is followed by radical recombination to generate the common hydroperoxide intermediate (*161*). However, previous studies have not been able to find solid evidence establishing either mechanism.

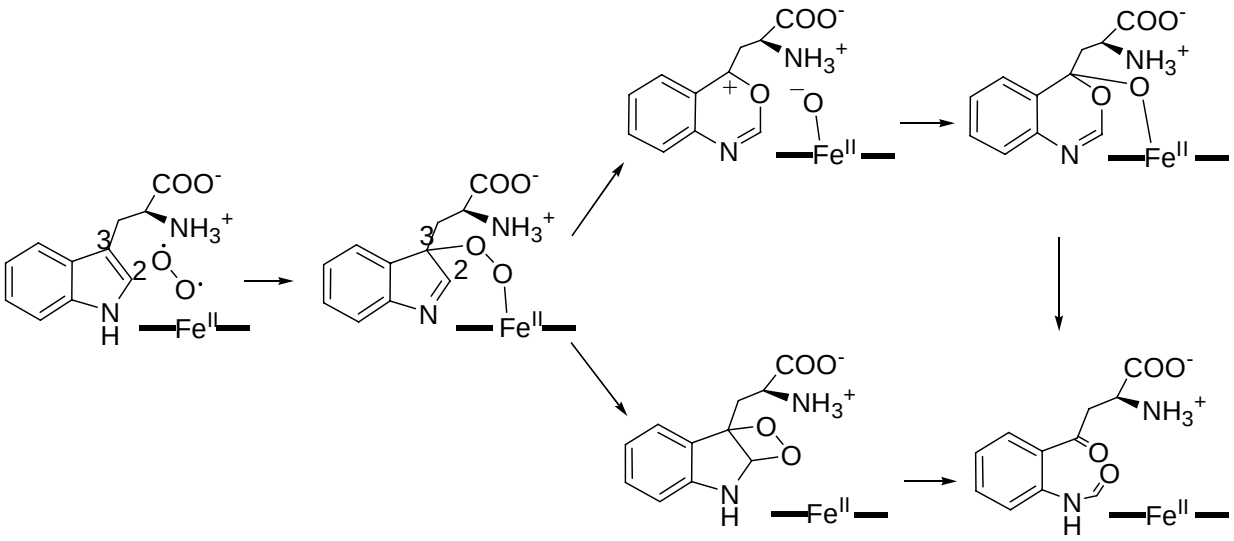

Scheme 1.11. The mechanistic models of Criegee rearrangement and dioxetane mechanisms.

It has been suggested that both the dioxetane and Criegee rearrangement mechanisms are possible in enzymatic reactions (*4*). The dioxetane pathway is controversial because of the thermodynamic consideration of ring strain. It is less favorable to go through this pathway due to the formation of the highly strained dioxetane intermediate. The Criegee rearrangement pathway has been described in catechol dioxygenases (*162, 163*). Criegee rearrangement types of reactions require an acid-base catalyst for the proton transfer in order to facilitate the O-O bond cleavage. It has been proposed that the active site histidine residue in TDO functions as an acid-base catalyst to facilitate the O-O bond cleavage (*132, 133, 141*). However, the IDO active site does not have the conserved amino acid required. It is proposed that dioxygen itself can function

as an acid-base catalyst for dioxygen activation in IDO (Scheme 1.12B) (*134, 140, 147*). Most recently, an electrophilic addition mechanism (Scheme 1.12C) was proposed based on knowledge on indole chemistry when reexamining the activity of TDO/IDO with 1-methyl-L-Trp (*164*). It was proposed that C_2 or C_3 position of the indole ring of substrate was attacked by electrophilic addition and a cation at N_1 was formed. Density functional theory (DFT) calculations by Chung and colleagues provides computational support for this mechanism (*165*).

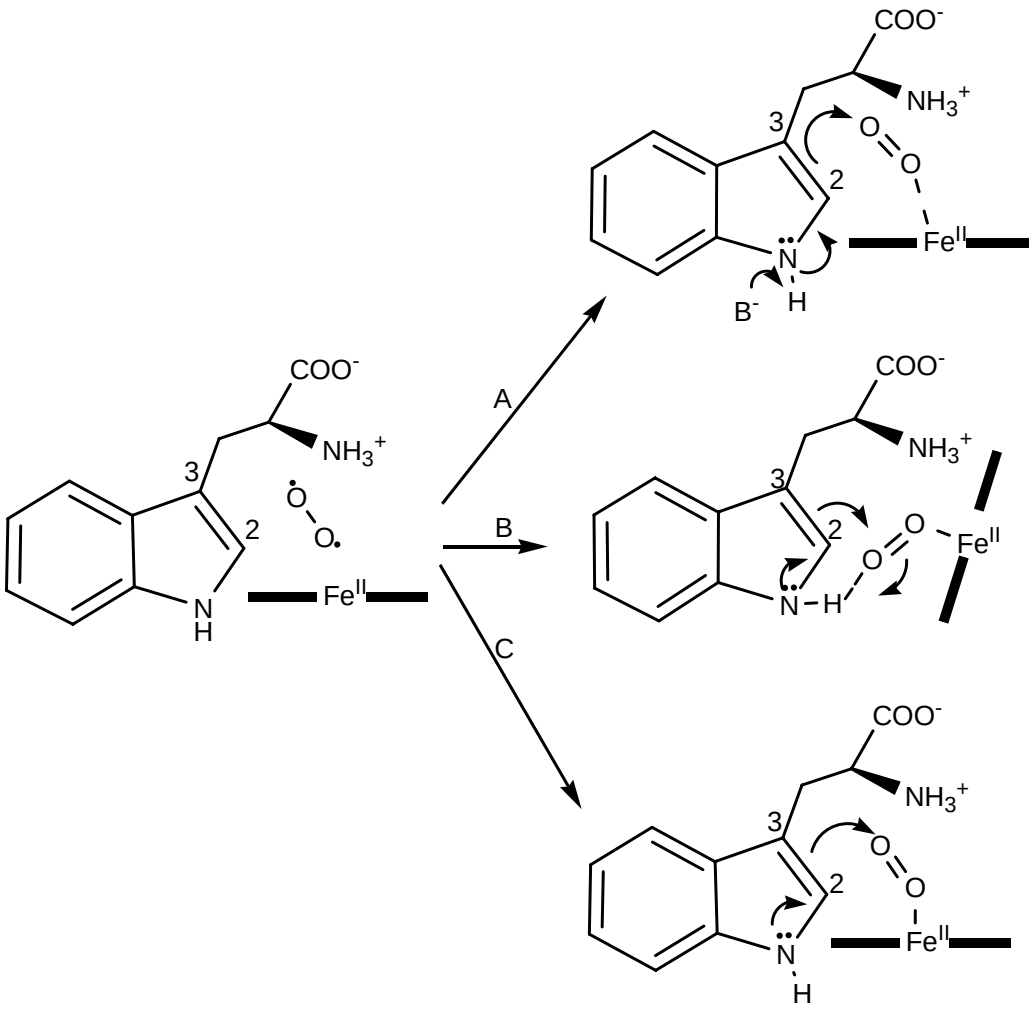

Scheme 1.12. Proposed mechanism of ferric hydroperoxide intermediate formation at C3 position of L-Trp.

1.2.8 Protein Cofactor Synthesis

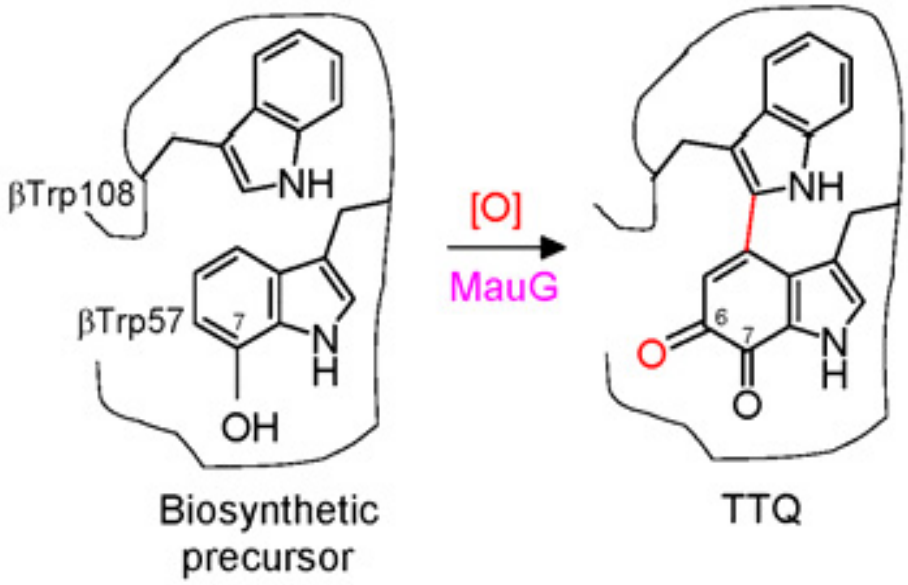

Scheme 1.13. TTQ biogenesis mediated by MauG.

TTQ is the protein-derived catalytic cofactor for amine oxidations in several enzymes (*166-169*). In methylamine dehydrogenase (MADH) from *Paracoccus denitrificans*, TTQ is present on each β subunit of the 119 kDa hetero-tetrameric $\alpha_2\beta_2$ protein (Figure 1.5) (*170, 171*). The biogenesis of TTQ requires incorporation of two oxygen atoms into Trp57 and a cross-linking of the indole rings of Trp57 and Trp108 of the β subunits (Scheme 1.13). Such a biosynthesis is not a self-processing event but an enzyme-mediated posttranslational process that requires the action of at least one processing enzyme encoded in the methylamine utilization (*mau*) gene cluster (*172, 173*). It has been shown that MauG, the *mauG* gene product, is the crucial enzyme for tryptophan tryptophylquinone (TTQ) biogenesis (*174, 175*). Deletion of *mauG* in the *mau* gene cluster causes accumulation of a 119 kDa biosynthetic precursor of MADH in which Trp57 is mono-hydroxylated at C7 and the cross-link is absent (*174*). This 119 kDa protein precursor of MADH

is the natural substrate of MauG. MauG-dependent TTQ-biosynthesis from the precursor is achievable *in vitro* using either O_2 plus electrons from an external donor or H_2O_2 (*175-178*).

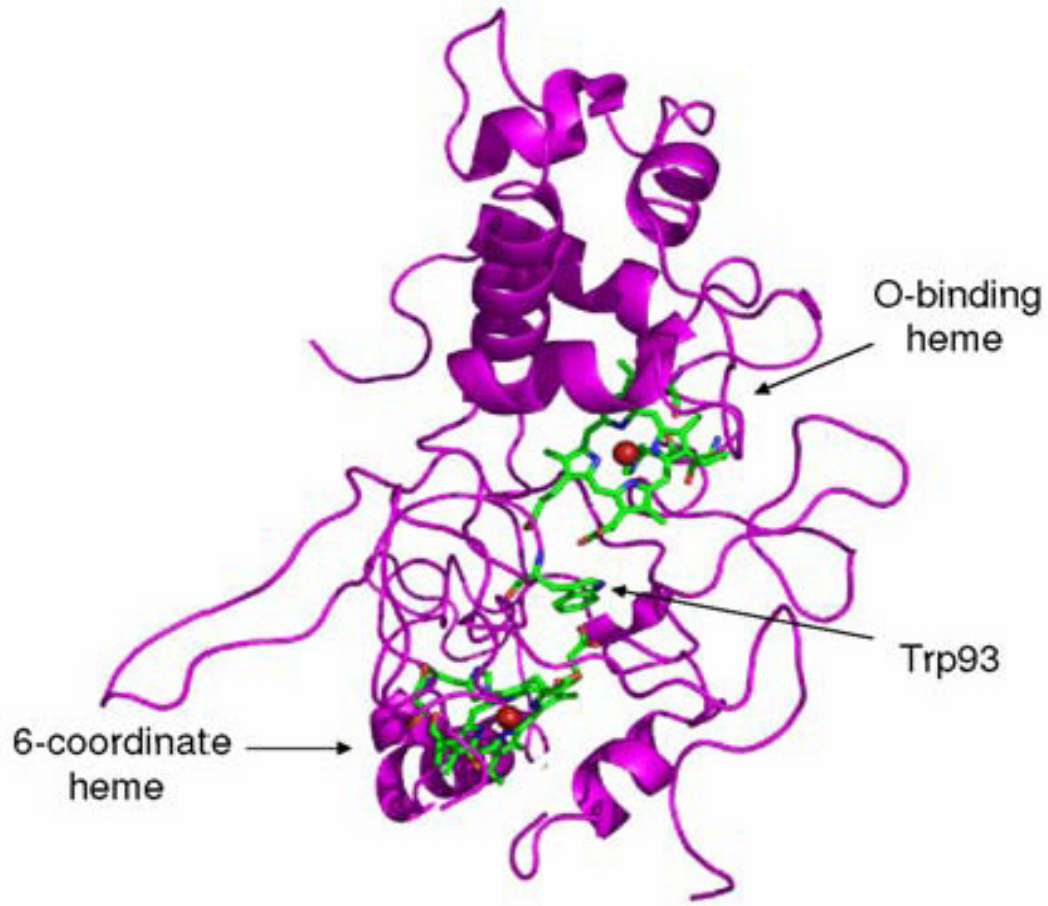

Figure 1.5. Crystal structure of MauG at 2.1 Å resolution (courtesy C. M. Wilmot).

MauG is a 42.3 kDa protein containing two covalently bound *c*-type hemes, one low-spin and one high-spin (*176*). MauG catalyzes the second oxygenation at C6 of the Trp57 phenyl ring, the cross-linking of the two tryptophan residues Trp53 and Trp108, and the oxidation of the semiquinone intermediate during the TTQ biogenesis (Scheme 1.13) (*177*). Overall the MauG-mediated reaction is a six-electron oxidative process.

MauG is the first enzyme described that utilizes *c*-type hemes to catalyze an oxygenation reaction. Its sequence is homologous to that of bacterial di-heme cytochrome *c* peroxidase, but it possesses negligible peroxidase activity (*176*). The initial EPR study performed provides important clues into MauG's biological activity debunking the hypothesis that MauG is a peroxidase on the basis of a sequence similarity to di-heme cytochrome *c* peroxidase (*176*). The EPR spectra of the ferric hemes of oxidized MauG are atypical of *c*-type cytochromes and different from di-heme cytochrome *c* peroxidases (*176*). The high-spin heme EPR signal has been found to be similar to those of myoglobin and the heme oxygenase-heme complex. The low-spin heme EPR signal is similar to those of complexes of CYP450cam with an exogenous axial sixth ligand (*176*). The intrinsic oxidation-reduction midpoint potential study of MauG has suggested a redox cooperativity, i.e. facile equilibration of electrons, between the two hemes (*179*). However, our EPR study shows that the two hemes are not spin-coupled (*176, 180*). Therefore, the two hemes must be distantly located even though they efficiently share electrons. A recent resonance Raman study confirms that one heme is 5-coordinate and the other is 6-coordinate (*179*). The crystal structure of MauG, which is currently under refinement, confirms our EPR results in that the two Fe ions are physically separated, at ~ 21 Å distance. The heme edges are within 10 Å of each other and are connected by Trp93 (Figure 1.5). Two His residues, His35 and His205, were also confirmed to provide the proximal axial heme ligands (C. M. Wilmot of University of Minnesota, unpublished results). Surprisingly, it is a Tyr residue, rather than a His residue suggested by the Raman study (*179*), that provides the distal axial ligand in the low-spin heme.

One special aspect of MauG is its cofactor utilization. MauG employs two *c*-type hemes to perform oxygenation and subsequent oxidation reactions. This is in contrast to other hemoproteins that generally utilize *b*-type hemes, such as CYP450 [3-5], for the oxygenase activities. Most recently, a few other enzymes have also been found to utilize *c*-type hemes to perform similar reactions. For instance, RoxA is a rubber oxygenase that utilizes two *c*-type hemes for an oxidative cleavage of poly(*cis*-1,4-isoprene) (*181*). MauG remains the best characterized protein in this emerging new class of hemoproteins. Therefore, MauG is an ideal model system for studying the catalytic mechanisms of those covalently bound *c*-type heme cofactors. Another special aspect of MauG is that its substrate is a 119 kDa protein, which is about 3-fold larger than the enzyme. Therefore, characterization of the MauG-mediated process introduces a new dimension to our current views about protein evolution and protein structure-function relationships, and provides insight for protein engineering strategies to introduce new functional groups into proteins.

1.3 High-valent Iron-oxo Intermediates in Heme-Containing Proteins

High-valent iron (IV)-oxo species have been identified as the oxidizing species in many heme and non heme Fe enzymes (*4, 182-184*). The oxidation state of compound I and II species are identical. Compound ES species is one electron more oxidized than compound II. The six-coordinate ferryl porphyrins are low-spin (S =1) d^4 complexes. In compound I, the radical can couple with the ferryl moiety (S = 1) in a ferromagnetic (S = 3/2) or antiferromagnetic (S = 1/2) fashion (*185, 186*). The high-valent iron intermediates have been trapped and are characterized and distinguished by the heme-containing proteins mentioned above, with an exception for TDO/IDO. They are also observed in nitric oxide synthase (NOS) with cysteine ligand (*187*),

prostaglandin H synthase (PGHS) (*188*), and cytochrome *c* oxidase (C*c*O) (*189*). These intermediates have been characterized by various spectroscopic techniques, including EPR, Mössbauer, resonance Raman, extended X-ray absorption fine structure (EXAFS), and electron-nuclear double resonance (ENDOR) spectroscopy (*182, 183, 190, 191*).

The formation and stabilization of high-valent iron-oxo species is dependent on the nature of the heme active-site environment, the axial ligand, and the oxidants. The axial ligand in C*c*P, myoglobin and HRP is a histidine while in CYP450 it is a cysteine, and in catalase, it is tyrosine. The optical features of the high-valent Fe species of some heme-containing proteins are listed in Table 1.1. In most *b* type heme, compound I or II can be characterized by the shift of Soret band in UV-Vis spectroscopy.

Compound I species of HPR exhibits a green color with a broad Soret band at 400 nm and 651 nm, which is similar to that of metalloporphyrin π cation radical; compound II has absorption at 418, 527 and 554 nm. A Mössbauer spectroscopy analysis indicates that the Fe ion in compound I and II have the same oxidation state. The EPR spectrum of compound I shows a broad signal around the $g = 2$ region, which suggests the radical is located in the porphyrin ring and it is spin ferromagnetic coupled with the ferryl species.

The first high-resolution crystal structure of the oxoferryl species in heme enzymes was determined in C*c*P. The brown compound I species of C*c*P exhibits a different UV-Vis spectrum compared to that of HRP and other heme enzymes. The compound I species had been previously characterized by EPR and Mössbauer spectroscopy. It has been concluded that the second oxidizing equivalent is located on a nearby tryptophan residue (*192*) (*46*), which has been termed

as compound ES. Using site-directed mutagenesis analysis, the protein radical was identified and pointed to Trp119 (*193*).

The compound I of chloroperoxidase (CPO) has a thiolate axial ligand and represents the best characterized enzymatic model for the oxyferryl intermediate of CYP450. Compared to those histidine- and tyrosine-ligated oxoferryl species, the Soret band of the thiolate ligated oxoferryl species in CPO shifts away from the resting state with absorption at 367 nm and 689 nm. The intermediate has a transient lifetime--around 30 ms at room temperature. The rapid-freeze quench EPR spectrum of the CPO compound I exhibits signals at g = 2.00, 1.73, 1.64 with a much larger ferromagnetic exchange interaction when compared with that of HRP (*185, 194*). This variation might be due to the thiolate axial ligand acquiring some radical characters during oxoferryl formation.

Compound I in catalase has a much shorter lifespan than peroxidase and is thus hard to detect using hydrogen peroxide as oxdiant. Using a peroxide analogue, such as peroxyacetic acid, compound I species was observed. The EPR spectrum of compound I from *Micrococcus luteus* catalase (MLC) shows an EPR signal at g = 3.3, 2.0, which suggests a porphyrin π cation radical quite different from those reported previously for the compounds I from horseradish peroxidase and chloroperoxidase (*195*). A similar EPR signal has also been detected in bovine liver catalase (BLC), in which the porphyrin π cation radical intratransfer to a Tyr residue within 0.04 - 15 s (*196*).

The compound I intermediate has never been detected in the native dioxygen-driven catalytic reaction of CYP450 because of the very short-lived transient state. Many attempts, including the

use of the cryoradiolysis method and various computational chemistry approaches, have been made to characterize the compound I intermediate in CYP450 (*5, 197, 198*). Taken the advantage of peroxide shunt pathway which has much slower reation rate relative to the normal catalytic cycle, the proton transfer and compound I formation can be investigated. The reaction of CYP101 and *meta*-chloroperbenzoic acid (*m*CPBA) generated an intermediate with UV-Vis spectrum at 367 nm and 690 nm which is similar to the π cation radical of compound I (*199*). The assignments are supported by subsequent DFT studies. (*200, 201*) Similar results have been observed in CYP119 in the peroxide reaction. Further EPR analysis suggests the presence of a ferryl ion and a protein radical species (*7*). Multifrequency EPR studies indicate that the radical is harbored by a tyrosine residue (*9*). Due to the difficulties in isolating high-valent intermediate during catalytic cycle, Davydov and his colleagues have developed a cryoradiolysis method coupled with EPR or ENDOR spectroscopy to characterize the high-valent intermediate (*5, 197*).

Since the first successful determination of crystal structure of C*c*P compound I in 1987 (*45*), several crystal structures of the high-valent intermediates of C*c*P, catalase, CYP450, myoglobin and HRP have been reported. Table 1.2 summarizes of the Fe-O distance in heme proteins determined by crystallography (*202*). It should be noticed that C*c*P intermediate has a radical located on a nearby amino acid, thus its Fe-O bond length is close to compound II species.

Computational studies have been employed to generate structural information about high-valent intermediates. These methods use some approximations to then choose the specific surrounding environment of the protein to obtain the bond length information after energy minimizations. The studies on the geometric and electronic structure of heme-containing protein have been reviewed

Table 1.1. Comparison of UV-Visible characteristics of heme proteins.

	Resting state	Compound I	Compound II	Heme Type	Radical	Fifth ligand
Horseradish peroxidase	402,490,640 (*203-206*)	400,577,620,651 (*205, 206*)	418,527,554 (*205-207*)	Heme *b*		His
Chloroperoxidase	399,514,650 (*208*)	367,610,689 (*209*)	438,542,571 (*209*)	Heme *b*		Cys
Mitochondrial cytochrome *c* peroxidase	406,630 (*210*)	414,528,556 (*211*)		Heme *c*	Trp	His
Lignin peroxidase	409,502 (*212*)	409 (*213*)		Heme *b*		His
Yeast cytochrome *c* peroxidase	408,507,647 (*214*)	419-420;529-530;560-561 (*214*)	418,530,560 (*215*)	Heme *c*	Trp	His
Catalase	405	405,660 (*195*)	424,534,567 (*195*)	Heme *b*		Tyr
CYP450 101	417,535,571	367,694 (*216*)	429,536,568	Heme *b*		Cys
CYP450 119	415,533,566 (*217*)	370,608,690 (*7*)	n.d	Heme *b*	Tyr	Cys

Table 1.2. The Fe-O distances in heme proteins determined by crystallography.

	Compound I	Compound II	Axial ligand	pH
HPR (*47, 218*)	1.70	1.84	His	6.5
C*c*P (*219*)	1.87		Cys	6.0
Mb (*220, 221*)	1.76	1.92	His	5.2
CYP450 (*222, 223*)	1.67		Cys	7.4
Catalase (*224*)	1.76*	1.86	Tyr	5.2

*The compound II from *Micrococcus lysodeikticus* (MLC) and compound I from *Proteus mirabilis* (PMC).

[223, 224]. Green and his colleagues use the empirical Badger's rule, which is based on the Fe(IV)-O stretching frequencies obtained from resonance Raman spectroscopy to predict the bond length information (*225*). Mössbauer spectroscopy is the classical standard in determining the formal oxidation state of iron. Experimental data suggest the isomer shift parameter of Fe(IV) is in the range of 0-0.2 mm/s (*226*).

1.4 The Protonation of Ferryl Species

Compound I and II are traditionally described as Fe(IV)-oxo species. Recent studies suggest that the ferryl oxygen can be protonated in enzymes. Upon protonation, the spin population is transferred from the oxo ligand to the iron, thus the protonated ferryl species will have a longer bond length with a single bond characteristic when compared to the unprotonated one (*227*).

Although protons cannot be observed in X-ray structure determination, its protonation state can be interpreted based on the bond length. It has also been suggested by experimental data and DFT calculation that the quadrupole splitting parameter for Fe(IV) corresponding to the protonation state of ferryl ion (*227*). Recent crystallographic studies, Mössbauer spectroscopy, resonance Raman studies of ferryl ion are consistent with the predication. In crystallographic studies, a relatively long bond length ranging from 1.82 to 1.92 Å are observed in CPO-II, C*C*P-I, CAT-II, Mb-II and HRP-II (*47, 219, 221, 228, 229*) which suggest a protonated form in CPO-II species. Mössbauer spectra of Catalase II, CPO II, $CYP450_{BM3}$ and $CYP450_{cam}$ identifies two Fe(IV) species, one with quadruple splitting of 1.0-1.6 mm/s and the other one with 2.0-2.3 mm/s, which are assigned respectively to unprotonated ferryl and protonated ferryl species (Table 1.3). The bond length of Fe(IV)-OH is also interpreated to be in the range of 1.76-1.81 Å or 1.81-1.85 Å using density functional calculations on heme model systems (*225, 230*), which is in line with the bond length of X-ray crystal structure. Resonance Raman is applied for the bond distance calculation based on the stretching frequency with 750-840 cm^{-1} for Fe(IV)=O whereas 540-630 cm^{-1} for Fe(IV)-OH (*225*). Comparative EPR, ENDOR and annealing studies have been conducted on a cryoreduced group of heme protein to identify the protonated features (*197, 227, 231*).

The discovery of basic ferryl species provides further insights into the heme-driven hydroxylation reaction, especially in CYP450. In CYP450 (Scheme 1.14), compound I withdraws one electron and proton from the C-H bond to form an Fe(IV)-OH intermediate, which rapidly recombines with cation carbon radical of substrate to generate hydroxylation

Table 1.3. Summary of Mössbauer parameters for ferryl species.

Intermediate	Iron species	Spin	δ (mm/s)	ΔE_Q (mm/s)
CcP-I (*232*)	$[Fe^{4+}=O_2^-]^{+\bullet}$	$S = 1$	0.05	1.55
HRP-I (*233*)	$[Fe^{4+}=O_2^-]^{+\bullet}$	$S = 1$	0.08	1.25
HRP-II (*47, 192*)	$Fe^{4+}=O_2^-$	$S = 1$	0.03	1.61
JRP-I (*234*)	$[Fe^{4+}=O_2^-]^{+\bullet}$	$S = 1$	0.10	1.33
JRP-II (*235*)	$Fe^{4+}=O_2^-$	$S = 1$	0.03	1.59
Mb-II (*221*)	$Fe^{4+}=O_2^-$	$S = 1$	0.09	1.43
Mb (annealed) (*236*)	$Fe^{4+}=O_2^-$	$S = 1$	0.10	1.49
Catalase-II (*237*)	$Fe^{4+}=O_2^-$	$S = 1$	0.07(2)	1.47(2)
Basic Catalase-II (*237*)	$[Fe^{4+}=O_2^-]H^+$	$S = 1$	0.03(2)	2.29(2)
CPO-I (*238*)	$Fe^{4+}=O_2^-$	$S = 1$	0.14	1.02
CPO-II (*238*)	$Fe^{4+}=O_2^-$	$S = 1$	0.11(3)	1.59
Basic CPO-II(*238*)	$[Fe^{4+}=O_2^-]H^+$	$S = 1$	0.10(3)	2.06(3)
$CYP450_{BM3}$-II (*190*)	$Fe^{4+}=O_2^-$	$S = 1$	0.11	1.05
Basic $CYP450_{BM3}$ (*190*)	$[Fe^{4+}=O_2^-]H^+$	$S = 1$	0.09	2.17
$CYP450_{cam}$-II (*190*)	$Fe^{4+}=O_2^-$	$S = 1$	0.14	0.66
Basic $CYP450_{cam}$-II (*190*)	$[Fe^{4+}=O_2^-]H^+$	$S = 1$	0.11	1.84

product. It has been shown that the capability of metal-oxo to abstract hydrogen increased in conjunction with an increase in the strength of the formation of O-H bond (*239*).

The protonation status of the ferryl species and the distal site hydrogen bond to the oxygen atom of oxoferryl ligand may play important roles in proton transfer during the reaction. High-valent ferryl species are generally to be electrophilic in nature; the basic ferryl species has been proposed as a general feature in which hydrogen abstraction of the substrate can be facilitated.

The formation of compound II in peroxidases is accompanied by the uptake of a proton. The ferryl species is modulated by a carboxylate side chain that is hydrogen-bonded to a proximal histidine. This might increase the basicity of ferryl species and the enzyme activity. In myoglobin, the proximal histidine ligand is hydrogen-bonded to a neutral backbone carbonyl group, implying a smaller proton affinity. It has been observed that the lower pH associates with increased reactivity in myoglobin, which is consistent with the increased proton affinity of the protonated ferryl species. (*240*)

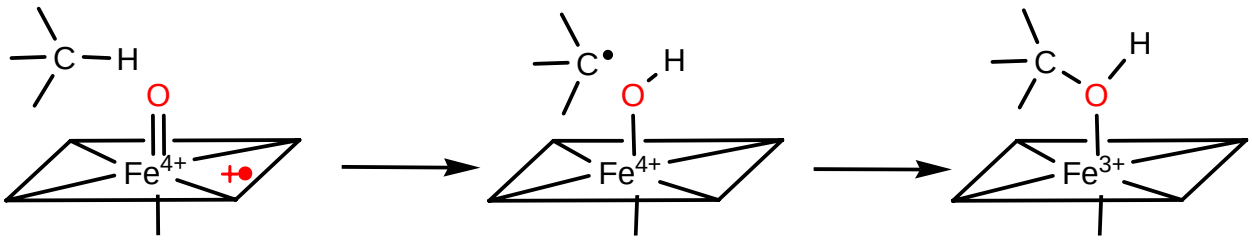

Scheme 1.14. Rebound mechanism for CYP450 hydroxylation reaction.

1.5 The Protein Radical Formation and Identification by EPR Spectroscopy

In the past three decades, evidence has strengthened for the hypothesis that enzyme-based protein radicals are the catalytic driven force or the key transient intermediate in enzymatic

reactions. Spectroscopic data from EPR implicate these highly reactive species can be stored with remarkable stability inside an enzyme either as a transient intermediate or a paramagnetic center, and they catalyze a wide range of biological reactions in electron transfer and oxidation/reduction.

It was not known that a protein can harbor a stable free radical derived from an amino acid residue until the discovery and later identification of the first tyrosyl radical from the smaller R2 subunit of the *Escherichia coli* ribonucleotide reductase (RNR) in the 1970's (*241*). Later it was discovered that a transient cysteine-based thiyl radical is formed at the expense of the tyrosyl radical during catalysis and that the transient thiyl radical is responsible for the catalytic reduction of the ribonucleotide substrates (*242, 243*).

Tyrosine and tryptophan are the common sites of free radical location in proteins. Tyrosyl radicals have been found in bovine catalase, human hemoglobin, soybean leghemyoglobin, horse and sperm whale myoglobin treated with H_2O_2 (*244*) (*196*) (*245-248*), in *Mycobacterium tuberculosis* catalase-peroxidase treated with peroxyacetic acid (*249*), turnip isoperoxidases (*250*), and in PGHS (*251*) (*252*). Tryptophan-based radicals have been observed in C*c*P (*46*), peroxidase from *Bjerkandera adusta* (*253*), in recombinant pea cytosolic ascorbate peroxidase (rAPX) reacting with H_2O_2 (*254*). Site-directed mutagenesis provides the information on the radical location of specific amino acid residues within the protein. However, these studies would not be conclusive. For example, wild type sperm whale Mb can generate a Tyr103 radical, while in Y103F mutant, a radical signal still be observed which is located in Tyr151 instead of the original location on Y103 (*247*).

Most of the known protein-based tyrosyl radicals, either stable or transient, exhibit a lineshape resembling one of the above unless they are strongly spin-coupled with another paramagnetic center, such as that found in galactose oxidase (*255, 256*). An intriguing finding is although the EPR spectra are distinct; the spin density distributions of the unpaired electron in these tyrosyl radicals are almost invariant. Although the observed EPR spectra are distinct, the differences in EPR spectral characteristics are mainly due to the dihedral angles θ_H, defined by the locations of the β-methylene protons, β-methylene carbon, ring carbon C_1, and its $2p_z$ axis relative to the phenyl ring of the side chain (*257*).

It should be noted that no structure analysis is available for the radical-containing form in the above enzymes with the exception of one radical-containing form obtained by oxidizing the crystals of *E. coli* R2 by H_2O_2 (*258*). The electronic structure and orientation of the active tyrosyl radical are determined by EPR-based techniques in conjunction with isotope-labeling of the radicals in ribonucleotide reductase (*259, 260*) and in PGHS (*261*). The tyrosyl radicals in R2 proteins are stable because the free electron is delocalized to the phenyl ring and the radical center is shielded from reaction by a hydrophobic pocket.

It is rare to obtain the crystal structure of a biological radical within its catalytic site In most other cases, free radical intermediates are not sufficiently stable to survive crystallization and the X-ray diffraction, thus EPR spectroscopy is the most pertinent tool to for defining structures of the radicals.

1.6 The Objectives

Our objective in this thesis is to study the molecular biochemistry exhibited by two structurally diverse heme-containing enzymes that oxidize either free tryptophan or protein-bound tryptophan residues. Tryptophan 2,3-dioxygenase (TDO) inserts two oxygen atoms into free tryptophan in a four electron oxidizing process by a *b*-type heme cofactor. This enzyme is a representative of a potentially new hemoprotein dioxygenase superfamily, whose oxygenase activity remains poorly understood. MauG is a novel enzyme that utilizes two *c*-type hemes to catalyze a posttranslational modification of a 119 KDa protein. Such a modification endows endogenous tryptophan residues with a new catalytic activity. The reaction is a six-electron oxidation and the utilization of two *c*-type hemes by MauG to perform a hydroxylation reaction and the subsequent oxidation reactions is unprecedented.

A biochemical and spectroscopic research study with two intellectually distinct aims is conducted to characterize the unique catalytic and structural properties of the two tryptophan oxidizing enzymes:

1) Elucidation of the capability of oxidized TDO using hydrogen peroxide as a competent oxygen and electron donor in an oxidized TDO mediated tryptophan oxygenation process; spectroscopic characterization and a computational study of the intermediates generated during the peroxide-driven reaction catalyzed by the oxidized TDO; providing insights into a peroxide activation mechanism of oxidized TDO; illustration of the substrate activation mechanism of oxidized TDO; probing the contribution of the conserved active site histidine residue to the catalytic reaction via site-directed mutagenesis, and constructing mutants with regard to the

conserved Trp and Tyr residues in the active site to identify the radical generated during the peroxide-driven oxygenation.

2) Probing of protein structure-function relationship of MauG, MADH biosynthetic precursor and mature MADH via chromatographically studies; spectroscopically trapping the intermediates during the H_2O_2-dependent oxygenation and further characterization of the chemical properties and reactivity of the intermediates; identification of the protein-based radical intermediate generated on the substrate protein during the H_2O_2-dependent oxygenation.

CHAPTER 2

MATERIALS AND METHODS

2.1 Chemicals

$H_2{}^{16}O_2$ (30%, v/v), L-tryptophan, D-tryptophan, 5-hydroxy-L-tryptophan, 5-fluoro-DL-tryptophan were obtained from Fisher Scientific. The concentration of H_2O_2 was calculated based on the extinction coefficient of $\varepsilon_{240} = 43.6\ M^{-1}cm^{-1}$. $H_2{}^{18}O_2$ (2% v/v solution) and $H_2{}^{18}O$ were obtained from Icon Isotopes, New Jersey, at 90 and 97.6 atom %, respectively. All experiments were performed in 50 mM Tris-HCl pH 7.4 buffer unless otherwise specified.

2.2 Overexpression and Preparation of TDO

The construction of the plasmid encoding full-length *Ralstonia metallidurans* TDO has been described elsewhere (*262, 263*). Cultures were started by streaking the frozen glycerol stock cells into an ampicillin agar plate. The plate was incubated at 37 °C overnight. A single ampicillin-resistant colony of *E. coli* cells was picked up and inoculated in 20 ml of Luria-Bertani (LB) media containing 100 μg/ml ampicillin at 37 °C until the $OD_{600\ nm}$ reached 0.6. This starter culture was then inoculated into 500 ml of LB media containing 100 μg/ml ampicillin with an initial $OD_{600\ nm}$ of 0.002. The cells were grown under a constant shaking rate of 200 rpm at 37 °C until an $OD_{600\ nm}$ value of 0.3 was reached. Aminolevulinic acid was added to a final concentration of 10 mg/500 ml of culture; ferrous ammonium sulfate was added to reach 35 μM final concentrations. The cells were allowed to grow until $OD_{600\ nm}$ reached 0.6. Next, Isopropyl-

β-D-thiogalactopyranoside (IPTG) was added to a final concentration of 0.6 mM after which the culture was allowed to proceed for additional 12 h at 28 °C with agitation at 200 rpm. The cells were then harvested by centrifugation at 8000 × g for 15 min at 4°C and stored at -80 °C.

The frozen cells were resuspended in a 50 mM potassium phosphate buffer pH 7.6 containing 5% glycerol and 20 mM *β*-mercaptoethanol. Protease inhibitors including 1 mM PMSF, 2 μM leupeptin, and 0.02 mg/ml aprotinin were added, and the cells were sonicated in ice. The debris of the cells was removed by centrifugation at 20,000 *g* for 20 min at 4°C. The protein purification was conducted using ÅKTA FPLC protein purification system. The clear supernatant was then applied to 80 mL Ni-NTA-affinity chromatography (Qiagen) equilibrated with a 50 mM potassium phosphate buffer pH 7.6 containing 150 mM NaCl; 20 mM imidazole and 5% glycerol. Before application to the Ni-NTA column, the imidazole concentration of the supernatant solution was adjusted to 20 mM. TDO was eluted from the column with 50 mM potassium phosphate buffer pH 7.6 containing 150 mM NaCl, and 5% glycerol with an imidazole gradient from 20 mM - 350 mM over 7 column volume (CV). The fractions containing TDO were combined and exchanged into 50 mM Tris pH 7.4 containing 10% glycerol using a Sephadex G50 column (GE healthcare, NJ). The desalted fractions were pooled and concentrated using an Amicon Ultra (Millipore) centrifugal device with a 10,000 Da molecular weight cut-off. Concentrated protein was frozen by liquid nitrogen and stored at -80 °C.

2.3 Overexpression and Preparation of ^{57}Fe-enriched TDO

The ^{57}Fe-enriched TDO was obtained by growing cell culture with metal-depleted medium supplemented with ^{57}Fe. The ^{57}Fe stock solution was prepared by dissolving the ^{57}Fe-enriched

metal foil (95.38% ^{57}Fe-enrichment) in 2.5 M sulfuric acid under O_2-free condition. The mixture was incubated at 60°C while stirred using septum-sealed vials under anaerobic condition until the metal totally dissolved. This stock solution was ready to be added directly to the medium.

For expression of the ^{57}Fe-enriched TDO for Mössbauer spectroscopy, the LB culture medium was forced through a Chelex-100 column which eliminated naturally abundant ^{56}Fe from the medium. The following reagent grade compounds were also added at the final concentrations: 5 μM ^{57}Fe solution, 90 μM $MgSO_4$ and 140 μM $CaCl_2$. When cultures enriched in ^{57}Fe reached an $OD_{600\ nm}$ of 0.3, aminolevulinic acid was added to a final concentration of 10 mg/500 ml of culture and ^{57}Fe stock solution was added to reach 35 μM final concentration. The cells were allowed to grow until $OD_{600\ nm}$ reach 0.6. Then IPTG was added to a final concentration of 0.6 mM and the culture was allowed to proceed for an additional 14 h at 28 °C with shaking at 200 rpm. The cells were then harvested by centrifugation at 8000 × *g* for 15 min at 4°C and stored at -80°C.

^{57}Fe enriched TDO was purified using the same procedure as that used for ^{56}Fe TDO purification.

2.4 Construction of TDO Derivatives by Site-directed Mutagenesis

The plasmid containing His-tagged TDO was used as a template for construction of all of the mutants, including H72S, H72N, Q73F, Y43W, Y43F, W119F, W253F, W119F/W253F, and H257C. The constructions were conducted by Dr. David T. Brown (the Genomics facility at University of Mississippi Medical Center, Jackson, MS). Y130F was kindly provided by Dr. Tadhg P. Begley (Department of Chemistry, Texas A&M University, TX).

2.5 Electrophoretic Analysis and Concentration Determination of Protein

The expression levels and enzyme purities of TDO and its mutants were determined by SDS-PAGE on 12% polyacrylamide gels. SDS polyacrylamide gels were prepared as described by Laemmli (*264*). SDS-PAGE was performed in a Mini Protein II electrophoresis apparatus (Bio-Rad) with a constant voltage of 200 volts. The gel was then stained using Coomassie blue solution for 5 min and then destained with Coomassie blue destaining solution for at least 1 hr with rotational shaker.

Protein concentration was determined by using Coomassie Plus protein assay reagent (Pierce, IL). Albumin was used as standard and added to the reagent at the final concentrations of 0 μg/ml, 25 μg/ml, 125 μg/ml, 250 μg/ml, 500 μg/ml, 750 μg/ml, 1000 μg/ml, 1500 μg/ml and 2000 μg/ml. Absorbance at 595 nm was measured on an Agilent 8453 spectrophotometer (Agilent Technologies, CA) after mixing the varied concentration of albumin with the assay reagent. The absorbance values were then plotted over the albumin concentrations to obtain the protein concentration standard curve. An appropriate amount of desired protein was mixed with the assay reagent and the absorbance at 595 nm was recorded. The amount of protein was adjusted until the recorded absorbance value fell into the range of the standard curve. The reading value was fitted into the standard curve to calculate the concentration of the desired protein. Unless otherwise stated, all protein concentrations are listed as monomer concentrations.

2.6 Steady State Kinetic Analysis of TDO and Its Derivatives

All TDO samples were prepared in 50 mM Tris-HCl pH 7.4. The absorption spectra were obtained with an Agilent 8453 UV-Vis spectrophotometer with ChemStation A09.01.76 software or a Cary 50 UV-Vis spectrophotometer (Varian Inc, CA) with a 1 cm light path.

The enzyme activity of WT TDO and its mutants was measured by monitoring the rate of the production of NFK at 321 nm by a spectrophotometric assay. Reactions were performed at room temperature in 50 mM Tris-HCl pH 7.4 containing 1 mM ascorbic acid and varied concentrations of L-Trp. The reactions were initiated by addition of TDO; the initial rates were calculated from the absorbance increase at 321 nm with an extinction coefficient of 3,150 M^{-1} cm^{-1}. Apparent K_m and k_{cat} values were determined by varying the concentration of each substrate and fitting the data to the Michaelis-Menten equation using Origin software (eq. 2.1),

$$\upsilon/[E] = k_{cat}[S]/(K_m + [S]) \qquad \text{(eq 2.1)}$$

where υ is the steady state velocity; [E] is the concentration of enzyme; [S] is the concentration of L-Trp; k_{cat} is the catalytic rate, K_m is the Michaelis-Menten constant.

2.7 Mass Spectrometry

The preparations of samples and data analysis were conducted by Rong Fu. Mass spectrometry was preformed by Dr. Siming Wang at Georgia State University.

Samples for ESI-MS were prepared for infusion with 50:50 acetonitrile/water in 0.1% formic acid. Water Q-TOF micro (Milford, Massachusetts) equipped with an electrospray ionization

source was operated in positive ionization mode. In the MS-MS experiment, the collision energy was set at 30 V. The Waters 2695 Alliance HPLC system (Milford, Massachusetts) was used for the LC-MS analyses. Chromatographic separation was achieved on the analytical column Restek Allure C18 column (100 mm × 2 mm i.d., 3 μM). Mobile phase A was composed of water containing 0.1% formic acid and mobile phase B was composed of acetonitrile containing 0.1% formic acid. The gradient was developed from 100% A over 5 min; to 0% A over 10 min; to 0% A over 15 min; to 100% A over 20 min at the flow rate of 200 μL/min. MassLynx 4.1 software was used for instrument control and data acquisition.

2.8 Oxygen Production

Oxygen production was measured using an YSI oxygen electrode coupled to a Hansatech Oxygraph (Kings Lynn, Norfolk, U.K.) at 25 °C. The stirred cell was capped, and reagents were added with a Hamilton syringe. Oxygen levels were continuously monitored in real-time during reaction.

2.9 Rapid Freeze Quench EPR Samples

Rapid freeze quench EPR samples were prepared using Update Instruments Model 715 freeze-quench apparatus (Madison, WI). Ferric TDO (400 μM) or MauG (400 μM) were mixed with 6 equivalents of H_2O_2 or 1 equivalents of H_2O_2 in a 1 : 1 ratio. Reactants were mixed through the shortest aging line (5.3 μl) and sprayed into an EPR tube, followed by freezing in 1 s in cold isopentene, -140 °C.

2.10 Stopped-flow Spectroscopy

Pre-steady-state kinetic analysis of the ferric TDO oxidation reaction with H_2O_2 was performed using a RSM16 stopped-flow rapid scanning spectrophotometer (OLIS, Bogart, GA). Dead time of the instrument is ca. 2 milliseconds. One syringe contained 13 μM ferric TDO, and the other contained 6 equivalents of H2O2. The reaction temperature was controlled at 25 ºC by a water bath.

2.11 Electron Paramagnetic Resonance Spectroscopy

All the EPR samples were prepared in 50 mM Tris pH 7.4 containing 10% glycerol unless otherwise stated. The enzyme concentrations used were heme concentration. EPR samples were made in reaction vials, transferred to EPR tubes and quickly frozen in cold isopentane (-140 °C) or liquid nitrogen after the desired reaction time. X-band EPR spectra were recorded in perpendicular mode on a Bruker EMX spectrometer at 100-kHz modulation frequency using a 4119HS high-sensitivity resonator. The EPR measurement temperature was maintained with an ESR910 liquid helium cryostat, LLT650/13 coolant transfer tube, Oxford ITC503S and Bruker ER4131VT temperature controllers. Spin concentration was determined by double integration of the sample spectrum obtained under low microwave power conditions and comparing the resulting intensity to that of a copper standard (0.5 mM $CuSO_4$, 5 mM EDTA) obtained under identical conditions. Spectral baseline corrections were performed using the WinEPR software package (Bruker). EPR simulation was accomplished by using the WEPR program developed by Dr. Frank Neese (*265*) and by the theoretical predictions according to the spin Hamiltonian

described in SimFonia version 1.25 (GmbH, 1995). No assumptions were made regarding the orientations of the principal axis of *g* and A in the calculations.

For the experiments of ferric TDO and its derivatives with peroxide and its analogues in the absence of L-Trp, typically EPR samples with 0.15 – 0.20 mM TDO or its derivatives were made in each set of experiments with 6 equivalents of H_2O_2 in different experiments in 50 mM Tris pH 7.4 buffer containing 10% glycerol. The samples were transferred into EPR tubes and frozen in liquid nitrogen as soon as they were adequately mixed.

In the reaction of ferric TDO with peroxide in the presence of L-Trp, EPR samples with 0.15 – 0.20 mM TDO were mixed with 10 equivalents of L-Trp and 6 equivalents of H_2O_2 at the same time and mixed well, followed by transferring to EPR tubes and frozen in liquid nitrogen. The total time was 30 s.

For experiments with ferric TDO derivative binding to substrate or substrate analogues, TDO was mixed well with varied concentrations of substrate or substrate analogues, followed by transferring to an EPR tube and frozen in liquid nitrogen. The total time was 30 s. Experimental EPR spectra were recorded at 10 K with 3 mW microwave power at 9.4 GHz.

The EPR relaxation property of the free radical at different temperatures was analyzed from the EPR spectra obtained with microwave power added in triplets of dB. At each given temperature, sixteen EPR spectra were recorded within 0.002 – 200 mW of microwave power. The values of half-saturation parameter ($P_{1/2}$) were obtained by fitting the data according to eq 2.2:

$$I \propto 1/(1 + P/P_{1/2})^{b/2}$$

[eq 2.2]

where I is the EPR signal amplitude, b is an inhomogeneous broadening parameter, and P is microwave power.

2.12 Mössbauer Spectroscopy

The preparation of samples was performed by Rong Fu. The measurements were conducted by Professor Michael P. Hendrich and his student, Rupal Gupta (Department of Chemistry Carnegie Mellon University, Pittsburgh) and Professor Castern Krebs at Pennsylvania State University.

The Mössbauer samples were prepared from 1.7 mM TDO (70% ^{57}Fe/^{56}Fe ratio) reacting with either six or eight equivalents of peroxide and frozen in liquid nitrogen. The experiments were conducted for three times. The total reaction time for the intermediate samples was between 28 s and 50 s. As for substrate-bound ferric ^{57}Fe-TDO, 1.5 mM sample was mixed well with 10 equivalents of L-Trp in a sealed vial for 3 min under anaerobic condition before being frozen. Around 460 µl of mixture was transfered into a Mössbauer cap using a gas-tight syringe and slowly frozen in liquid nitrogen.

Ferrous ^{57}Fe-TDO sample was prepared by treating with 10 equivalents of sodium dithionite under anaerobic conditions. The sample was allowed to incubate under anaerobic condition for an additional 15 min, followed by transfer into a Mössbauer cap using a gas-tight syringe, and then slowly frozen in liquid nitrogen. Substrate-bound ^{57}Fe ferrous with 1.5 mM concentration was prepared by mixing enzyme prepared as above with 10 equivalents of L-Trp under anaerobic

condition. CO bubbled into a substrate-bound ^{57}Fe ferrous sample to generate a substrate-bound ^{57}Fe ferrous-CO complex.

To detect the formation of ferrous ion in the reaction of ^{57}Fe ferric TDO treated with H_2O_2 in the presence of L-Trp, 1.5 mM ^{57}Fe ferric TDO was treated with 10 equivalents of L-Trp followed by bubbling with CO, then 2 equivalents of H_2O_2 were added into the reaction mixture and mixed well before being transferred into a Mössbauer cap and frozen in liquid nitrogen.

Mössbauer spectra were recorded on a constant acceleration instrument with an available temperature range of 1.5 to 200 K. Isomer shifts are reported relative to Fe metal at 298 K. Least-square fitting of the spectra was performed with the WMOSS software package (WEB Research, Edina, MN). The low-temperature Mössbauer spectra of resting TDO were fit with the standard spin Hamiltonian of eq 2.3:

$$H = g\beta B\cdot S + D[S_z^2 - S(S+1)/3] + E(S_x^2 - S_y^2) + A_{iso}(S\cdot I) - g_n b_n B\cdot I + (eQV_{zz}/12)\,[3I_z^2 - I(I+1) + \eta(I_x^2 - I_y^2)]$$

[eq 2.3]

2.13 Metal Content Analysis

The preparation of samples and data analysis was conducted by Rong Fu. The measurements were conducted by Dr. Johnathan P. Hosler at the University of Mississippi Medical Center.

Metal contents were determined by inductively coupled plasma optical emission spectroscopy (ICP-OES) using a Spctro Genesis spectrometer (Spectro Analytical Instrument GmbH & Co.

KG, Germany). The spectro genesis ICAL calibration standard (GENESIS-ICAL) and transition elements ICP-MS standard (CCS-6) (Inorganic Ventures Inc, Lakewood, NJ) were used as standards for instrument setup and calibration. Calibration curves were obtained by measuring the standards at the concentrations of each element at 0, 0.1, 0.3, 0.5, 1.0 and 10 ppm (mg/L).

All the samples for ICP-OES experiments were prepared in 25 mM Tris pH 7.4. Before metal analysis, the proteins were desalted on a 5 ml HiTrap column (GE Healthcare, NJ) using an ÅKTA FPLC protein purification system to change the protein buffer into metal free 25 mM Tris pH 7.4 buffer. Protein concentrations were determined before and after the metal analysis as described before. The blank ICP buffer was also measured and the result was used as a control for subtraction. The measurement was repeated three times. Metal concentrations were converted from ppm to molar concentrations.

2.14 UV-Vis Spectra of the Ferric TDO upon Reacting with Hydrogen Peroxide in the Presence of L-Trp under Anaerobic Condition

L-Trp and H_2O_2 were freshly prepared in 50 mM Tris-HCl pH 7.4 buffer which had been previously degassed and purged with argon. A vial containing concentrated ferric TDO was gently vacuumed and refilled with argon, and the enzyme was diluted into the O_2-free buffer in a sealed cuvette containing 5 mM L-Trp. A gas-tight microsyringe was used for the addition of 6 equivalents of H_2O_2 of argon-saturated oxygen-free H_2O_2 to ferric TDO. Ferrous TDO-L-Trp complex was prepared by adding 10 equivalents of sodium dithionite under the same anaerobic condition in the presence of 5 mM L-Trp. In another parallel experiment, ferric TDO was mixed

with 5 mM L-Trp and bubbled with carbon monoxide for 5 min to allow equilibrium, followed by adding 6 equivalents of H_2O_2.

2.15 Effect of the Concentration of L-Trp on Reduction of Ferric TDO

The reduction of ferric TDO upon peroxide activation was performed under anaerobic condition. Stock solution of H_2O_2, L-Trp were freshly prepared using 50 mM Tris pH 7.4 buffers which had been previously degassed and purged with nitrogen gas. The stock ferric TDO was gently vacuumed and refilled with argon repeatedly. Ferric TDO and L-Trp were transferred with a gas-tight syringe into a sealed cuvette in which ferric TDO has a final concentration of 5 μM, whereas L-Trp concentration ranged from 200 μM to 6,200 μM. The reaction mixture was vacuumed and refilled with argon by repeated cycles. The mixture was filled with 100% CO and allowed to reach equilibrium for 5 min. Six equivalents of H_2O_2 were added into the mixture and the optical absorption spectra were recorded with an Agilent 8453 UV-Vis spectrophotometer. The formation of ferrous-CO-L-Trp complex was monitored at 421 nm. The value of 421 nm was obtained from the difference spectrum between the recorded spectrum after and before peroxide activation. The extinction coefficient of ε_{405} = 130 $mM^{-1}cm^{-1}$ and ε_{421} = 123 $mM^{-1}cm^{-1}$ was used to determine the concentration of ferric TDO and ferrous TDO-CO-L-Trp complex, respectively.

2.16 Effect of the Concentration of H_2O_2 on the Activity of Ferric TDO for Dioxygenation Reaction

The reaction mixture contained 0.77 μM ferric TDO, 5 mM L-Trp in 50 mM Tris pH 7.4 buffer. H_2O_2 was added into the mixture to initiate the reaction. The concentration of H_2O_2 ranged from

2 to 20 equivalents over the concentration of ferric TDO. The enzyme activity of ferric TDO was measured by monitoring the rate of production of NFK at 321 nm by a spectrophotometric assay with an Agilent 8453 UV-Vis spectrophotometer.

2.17 Stoichiometry of Hydrogen Peroxide Consumption to Product Formation under Anaerobic Conditions in the Presence or Absence of Hydroxyurea

L-Trp and H_2O_2 were freshly prepared in 50 mM Tris-HCl pH 7.4 buffer which had been previously degassed and purged with argon. Concentrated ferric TDO was gently vacuumed and refilled with argon and diluted into the O_2-free buffer in a sealed cuvette containing 5 mM L-Trp. A gas-tight microsyringe was used for stepwise additions of 5 equivalents of argon-saturated oxygen-free H_2O_2 to ferric TDO in the presence or absence of 10 mM hydroxyurea. The total amount was 35 equivalents of H_2O_2 over the enzyme concentration.

2.18 The Effect of Hydroxyurea on the Catalytic Reaction of Ferric TDO upon Reacting with H_2O_2

The reactions were conducted in 50 mM Tris pH 7.4. Three sets of experiments were designed to investigate the effect of a potential radical, generated via O-O bond cleavage of ferric hydroperoxide intermediate, on the enzymatic activity. Ferric TDO was mixed with 6 equivalents of H_2O_2. The reaction mixtures were incubated for varied times ranging from 5 s to 100 s, followed by adding 2 mM L-Trp to initiate the catalytic reaction. In another set of experiments, the reaction mixtures were initiated by adding 5 mM hydroxyurea and 2 mM L-Trp at the same time. Experiments were also set up for the reaction in which ferric TDO was mixed with 6 equivalents of H_2O_2 and 5 mM hydroxyurea. The reaction mixture was incubated for a

various time ranging from 5 s to 100 s, followed by adding 2 mM L-Trp to initiate the catalytic reaction. The rate of the reactions was measured by monitoring the rate of the production of NFK at 321 nm by a spectrophotometric assay with an Agilent 8453 UV-Vis spectrophotometer.

2.19 Substrate Activation of Ferric TDO under Anaerobic Conditions

All TDO samples were prepared in 50 mM Tris-HCl pH 7.4. The reactions were conducted under anaerobic condition using a homemade long-arm sealed cuvette. The absorption spectra were recorded with an Agilent 8453 UV-Vis spectrophotometer with ChemStation A09.01.76 software at room temperature. All reagents were degassed and purged with argon prior to the actual experiments. The cuvette was evacuated by vacuum, and refilled with argon repeatedly. Around 900 μl buffer containing 20 mM substrate analogue including D-Trp, 5-OH-Trp and 6-F-Trp was transfered into the cuvette using a gas-tight syringe. The solution was evacuated by vacuum and again refilled with argon repeatedly. 5-6 μM ferric TDO was transferred into the mixture under anaerobic conditions to start the incubation. The incubations were conducted under anaerobic conditions for 3 h.

2.20 Preparation of His72 and Its Mutants at Different pH Conditions

The buffer with 50 mM Tris pH 7.4, containing 10% glycerol, of the stock proteins of WT TDO, H72S, H72N and Q73F were exchanged to various pH conditions on 5 ml HiTrap Desalting column (GE healthcare, NJ) using ÅKTA FPLC protein purification system. The buffers corresponding to different pH values of 6.0, 7.4 and 10.0 were 50 mM MES pH 6.0, 50 mM Tris pH 7.4 or 50 mM CHES pH 10.0 containing 10% glycerol. The desalted fractions were pooled and concentrated using an Amicon Ultra (Millipore) centrifugal device with a 10,000 Da

molecular weight cut-off to around 200 μM concentration. Concentrated protein was frozen by liquid nitrogen and stored at -80 °C.

2.21 PH Dependence Studies

Studies on pH dependence were performed on ferric TDO, H72S, H72N and Q73F over the pH range of 6.0-10.5 using a multicomponents buffer which contained 50 mM Tris, 50 mM MES and 50 mM glycine. This buffer was used to minimize the effects of using different buffers over a wide range of pH. NaCl was added to normalize the ionic strength effects in the buffer. The pH of the buffers was adjusted with 1 M NaOH or 1 M HCl with a pH meter. Steady-state kinetic assays were conducted at room temperature in 50 mM Tris-HCl pH 7.4 containing 1 mM ascorbic acid and 20 mM L-Trp. The reactions were initiated by addition of enzymes and the initial rates were calculated from the absorbance increase at 321 nm with extinction coefficient of 3,150 M^{-1} cm^{-1}.

2.22 Redox Titrations of TDO

The redox potentials of TDO were determined with a Corning combination redox electrode in 100 mM potassium phosphate pH 7.0 buffer under anaerobic condition. The electrode was calibrated using quinhydrone (1:1 mixture of hydroquinone and benzoquinone) as a standard with an E_m value of 280 mV at pH 7.0 (*266*). The electrode was tested by measuring the known potentials of 2,6-dichlorophenolindophenol (DCPIP), and amicyanin. The mediators used were 10 μM 1,2-naphthoquinone,10 μM phenazine methosulfate and 10 μM 1,2-naphthoquinone mixture. The TDO sample was subjected to repeated cycles of evacuation by vacume and replacement with argon to remove O_2 and then transferred into a sealed cuvette to a final

concentration of 5 μM. Sodium dithionite and potassium ferricyanide were used as titrants and the stock solutions were freshly prepared in 100 mM potassium phosphate pH 7.0, which had been previously degassed and purged with nitrogen gas. A gas-tight syringe was used for titration. The concentrations of the oxidized and reduced TDO were determined by comparison with the spectra of the completely oxidized and reduced forms of TDO. E_m values were obtained by fitting the experimental data to the Nernst equation (eq 2.4) for a single electron process. Potentials are quoted against the standard hydrogen electrode (SHE).

$$\text{Fraction (reduced)} = 1/(1+10^{(E-E\text{m}) / 0.059}) \qquad \text{(eq 2.4)}$$

CHAPTER 3

HYDROGEN PEROXIDE AS A SUBSTRATE OF OXIDIZED TRYPTOPHAN 2,3-DIOXYGENASE

The section of chapter 3 is a direct copy of our prepared manuscript on TDO: Hydrogen peroxide as a substrate of oxidized tryptophan 2,3-dioxygenase. Rong Fu, Siming Wang, Michael P. Hendrich, Tadhg P. Begley, and Aimin Liu. (2009). The expression and purification of TDO protein, anaerobic and aerobic UV-Vis spectroscopy, kinetic assay, stopped-flow spectroscopy, as well as the preparation of samples for mass spectrometry, and the oxygen electrode experiments were all conducted by Rong Fu (Department of Chemistry, Georgia State University, Atlanta). Mass spectrometry was conducted by Dr. Siming Wang (Department of Chemistry, Georgia State University, Atlanta). Catalase-like activity of ferric TDO was suggested by Dr. Michael P. Hendrich (Department of Chemistry Carnegie Mellon University, Pittsburgh). The rmTDO plasmid was provided by Tadhg P. Begley (Department of Chemistry, Texas A&M University, Austin). The manuscript was prepared by Rong Fu and Dr. Aimin Liu. Other authors provided input for the manuscript. We thank Drs. Rodney C. Baker and Naila M. Mamoon for the initial attempts in the mass spectrometry analysis, Dr. Jonathan P. Hosler and Mr. Lakshman Varanasi for assistance with the oxygen electrode experiments, and Dr. Victor L. Davidson for access to the stopped-flow spectrophotometer as well as assistance with the kinetic analysis. This work is supported by the National Institutes of Health grants GM069618 (to TPB) and GM077387 (to MPH), and National Science Foundation (NSF) grant MCB 843537 (to AL). RF acknowledges a

fellowship support from the Molecular Basis of Disease (MBD) program of Georgia State University (GSU).

3.1 Abstract

Tryptophan 2,3-dioxygenase (TDO) utilizes a ferrous heme to catalyze the dioxygenation reaction of L-tryptophan (L-Trp) to produce *N*-formylkynurenine (NFK). Here we report that the ferric form of TDO possesses two previously unknown catalytic activities with hydrogen peroxide as a substrate. Under either aerobic or anaerobic conditions, ferric TDO utilizes two moles of H_2O_2 to produce one mole of NFK from L-Trp. In the presence of ^{18}O-enriched H_2O_2 or H_2O, ESI-MS, LC-MS, and ESI-MS-MS spectrometric analyses show that both oxygen atoms inserted in NFK are derived from H_2O_2 and one of the oxygen atoms is solvent exchangeable, as suggested by the ^{18}O-incorporation results. This observation is further validated by the experiment dissolving ^{16}O-NFK into $H_2{}^{18}O$ followed by mass spectrometry analysis and re-dissolving in $H_2{}^{16}O$ and analyzed by mass spectrometry again. One ^{18}O-incorporation and expulsion are observed from these experiments. Importantly, a monooxygenated product of L-Trp with m/z of 221 in the ^{16}O experiments, or 223 with ^{18}O, is also observed. These results point to a sequential addition of two oxygen atoms to L-Trp during catalysis, as opposed to a one-step concerted dioxygenation reaction. In the absence of L-Trp, peroxide is also able to react with TDO and O_2 is produced as a result of the reaction, which indicates that the ferric enzyme possesses catalase activity. However, the production of O_2 from H_2O_2 is significantly suppressed when L-Trp is present. These findings propose the potential function of TDO as a peroxide scavenger, suggesting important implications for understanding the biological role of this enzyme under oxidizing environments.

3.2 Introduction

Tryptophan 2, 3-dioxygenase (TDO) catalyzes oxidative cleavage of the indole ring of L-tryptophan (L-Trp), converting it to *N*-formylkynurenine (NFK). TDO is a biologically significant enzyme. It utilizes a *b*-type heme to catalyze the first committed step for L-Trp degradation through the kynurenine pathway (*155, 267-272*). The kynurenine pathway constitutes the major route of *de novo* biosynthesis of NAD which is one of the essential redox cofactors in all living systems (*267*). The intermediate metabolites of this pathway can lead to numerous physiological and pathological conditions, including: cataract formation, cerebral malaria, Alzheimer's disease, HIV infection, Huntington's disease and ischemic brain injury (*268-271*). TDO is responsible for oxidizing over 99% of the free L-Trp in intracellular and extracellular pools (*268*). In addition, the levels of tryptophan regulated by TDO can affect the synthesis of serotonin (*268, 273-275*), a known neurotransmitter.

Hemoproteins perform a wide range of biological functions including oxygen transport, storage, electron transfer, monooxygenation, and reduction of dioxygen; however, they rarely express a dioxygenase activity as their native biological function. TDO is the first described exception (*148, 155, 276*). As an oxygenation enzyme, TDO and its orthologue, indoleamine 2,3-dioxygenase (IDO) are distinctive members of the dioxygenase family in that they utilize a histidine-ligated ferrous heme rather than a non-heme iron to carry out the oxygen activation and insertion (*126, 137, 262*). A number of recent biochemical and spectroscopic studies on substrate recognition have clarified the role of active site environment (*277-283*); however, the catalytic mechanism of TDO and IDO still remains to be elucidated. The heme binding site of TDO has only one axial position for O_2 binding and activation (*126, 262, 282*), and the primary

substrate, L-Trp, must bind to a pocket adjacent to the Fe ion (*126*). In contrast, the non-heme iron or manganese dioxygenases typically have active sites with two histidines, one carboxylate and two or three solvent-derived ligands, which allow simultaneous binding of both substrate and dioxygen to the metal ion (*124*). The oxygen activation and insertion of O-atoms catalyzed by TDO must therefore proceed via a distinct mechanism relative to the non-heme iron dependent enzymes. The crystal structures of TDO, from *Xanthomonas campestris* and *Ralstonia metallidurans* (*126, 262, 282*), and IDO from human (*137, 139*) have provided critical insights into the molecular details of the active site architecture. These two enzymes have similar structures but share less than 14% sequence identity. A recent discovery has exposed a third hemoprotein, PrnB, with dioxygenase activity (*284*). Therefore, the existence of a potential heme-dependent dioxygenase enzyme superfamily of which TDO is a prototype member has been suggested (*284*). This intriguing property of TDO has generated much attention (*126, 137, 262, 277-283, 285-287*).

Hydrogen peroxide is known to activate oxidized TDO (*285, 288, 289*), but its activation mechanism has not been thoroughly studied. In cytochrome P450, the oxidized enzymes can utilize peroxide as a substrate for catalysis, which is known as peroxide shunt mechanism (*290-295*). For those enzymes, hydrogen peroxide is used as the source for an oxygen atom and two electrons for substrate oxygenation, thereby bypassing the requirements of the normal catalytic cycle for dioxygen and exogenous electron donors. Through biochemical and mass spectrometric analyses, two previously unidentified catalytic activities of oxidized TDO are revealed in this work. Hydrogen peroxide is found to be an oxygen donor in the enzyme-

mediated NFK production. A sequential oxygen insertion into the L-Trp at the enzyme active site is also demonstrated by the mass spectrometry analyses.

3.3 Materials and Methods

Chemicals — $H_2{}^{16}O_2$ (30%, v/v) was obtained from Fisher. The concentration of H_2O_2 was calculated based on the extinction coefficient of $\varepsilon_{240\ nm} = 43.6\ M^{-1}cm^{-1}$. $H_2{}^{18}O_2$ (2% v/v solution) and $H_2{}^{18}O$ were obtained from Icon Isotopes, New Jersey, at 90 and 97.6 atom %, respectively. All experiments were performed in 50 mM Tris-HCl pH 7.4 buffer unless otherwise specified.

Expression and purification of ferric TDO — The construction of the plasmid encoding full-length *Ralstonia metallidurans* TDO has been described elsewhere (*262, 267*). Cultures were started by streaking the frozen glycerol stock cells into an ampicillin agar plate. The plate was incubated at 37 °C overnight. A single ampicillin-resistant colony of *E. coli* cells was picked up and inoculated in 20 ml of Luria-Bertani (LB) media containing 100 μg/ml ampicillin at 37 °C until the $OD_{600\ nm}$ reached to 0.6. This starter culture was then inoculated into 500 ml of LB media containing 100 μg/ml ampicillin with an initial $OD_{600\ nm}$ of 0.002. The cells were grown with constant agitation at 200 rpm at 37 °C until an $OD_{600\ nm}$ value of 0.3 was reached. Then *δ*-aminolevulinic acid was added to a final concentration of 10 mg/500 ml of the culture and ferrous ammonium sulfate was added to reach a final concentration of 35 μM. The cells were allowed to grow until $OD_{600\ nm}$ reached 0.6. Isopropyl-*β*-D-thiogalactopyranoside (IPTG) was added to a final concentration of 0.6 mM and the culture was allowed to proceed for an additional 12 h at 28 °C with agitation at 200 rpm. The cells were then harvested by centrifugation at 8000 × g for 15 min at 4°C and stored at -80 °C.

The frozen cells were resuspended in 50 mM potassium phosphate buffer pH 7.6 containing 5% glycerol 20 mM *ß*-mercaptoethanol. Protease inhibitors including 1 mM PMSF, 2 µM leupeptin, and 0.02 mg/ml aprotinin were added, and the cells were sonicated in ice. The debris of the cells was removed by centrifugation at 20,000 *g* for 20 min at 4°C.The clear supernatant was applied to 80 mL Ni-NTA-affinity chromatography (Qiagen) equilibrated with 50 mM potassium phosphate buffer, pH 7.6 containing 150 mM NaCl; 20 mM imidazole and 5% glycerol. Before applying to the Ni-NTA column, the imidazole concentration of the supernatant solution was adjusted to 20 mM. TDO was eluted from the column with 50 mM potassium phosphate buffer pH 7.6 containing 150 mM NaCl; 5% glycerol with a imidazole gradient from 20 mM - 350 mM over 7 column volume (CV). The fractions containing TDO were combined and exchanged into 50 mM Tris pH 7.4 containing 10% glycerol using a Sephadex G50 column (GE healthcare, NJ) using ÅKTA FPLC protein purification system. The desalted fractions were pooled and concentrated using an Amicon Ultra (Millipore) centrifugal device with a 10,000 Da molecular weight cut-off. Concentrated protein was frozen by liquid nitrogen and stored at -80 °C. The optical absorption spectrum of the as-isolated TDO enzyme used in this work typically displays a 405/280 nm ratio greater than 1.4:1.

Enzyme assay — All TDO samples were prepared in 50 mM Tris-HCl pH 7.4. The absorption spectra were obtained with an Agilent 8453 UV-Vis spectrophotometer with ChemStation A09.01.76 software at room temperature. The kinetics of the peroxide-driven oxygenation reaction were determined under anaerobic condition using a homemade long-arm sealed cuvette. All the reagents had been degassed and purged with argon prior to the actual experiments. A vial containing concentrated ferric TDO was gently evacuated by vacuum, refilled with argon and

diluted into the O_2-free buffer in a sealed cuvette containing 3 mM L-Trp either in the absence or in the presence of 50 mM glucose and 50 μg/ml glucose oxidase. The final concentration of TDO in the reaction system was 5 μM. A gas-tight microsyringe was used for additions of various amounts of argon-saturated oxygen-free H_2O_2 to initiate the reaction. The concentration of H_2O_2 was ranged from 25 μM to 250 μM. NFK concentration was determined with $\varepsilon_{310\ nm}$ = 3,150 $M^{-1}cm^{-1}$. The apparent rates of the dioxygnation reactions were determined from the initial velocity of the NFK formation. Oxygen production was measured using an YSI oxygen electrode coupled to a Hansatech Oxygraph Plus (Kings Lynn, Norfolk, U.K.) at 25 °C. In the absence of L-Trp, the reaction was initiated by adding H_2O_2 to a final concentration of 10 μM to 50 mM. In the presence of L-Trp, the contration of H_2O_2 was ranged from 50 μM to 1.5 mM with the ratio of L-Trp to H_2O_2 fixed at 50:1. The oxygen in the reaction mixture was consumed by adding 0.2 equivalents of H_2O_2 to 5 μM ferric TDO containing L-Trp. The catalase-like reaction was initiated by adding H_2O_2. Kinetic data were fitted to the following equation using Microcal Origin package:

$$\upsilon/\ [E] = k_{cat}[S]^n/(K_m{}^n + [S]^n) \qquad (4.1)$$

where υ is the steady state velocity; [E] is the concentration of ferric TDO; [S] is the concentration of H_2O_2; k_{cat} is the reaction rate; K_m is the Michaelis-Menten constant and n is the Hill number or cooperativity index.

Stoichiometry of hydrogen peroxide consumption to product formation under anaerobic conditions — L-Trp and H_2O_2 were freshly prepared in 50 mM Tris-HCl pH 7.4 buffer which had been previously degassed and purged with argon. A vial containing concentrated ferric TDO

was gently vacuumed and refilled with argon, and the enzyme was diluted into the O_2-free buffer in a sealed cuvette containing 5 mM L-Trp. A gas-tight microsyringe was used for stepwise additions of equimolar amounts of argon-saturated oxygen-free H_2O_2 to TDO.

$H_2{}^{16}O_2/H_2{}^{18}O_2$-driven reaction mediated by ferric TDO in the presence of L-Trp — 50 mM Tris pH 7.4 buffer was bubbled and purged with argon for hours. All the reagents were prepared using the anaerobic 50 mM Tris pH 7.4 buffer in a sealed vial and vacuumed and refilled with argon repeatedly prior to the experiments. The reactions were performed on ice with stirring using septum-sealed vials. Ferric TDO (100 μM) was allowed to react with H_2O_2 in the presence of 5 mM L-Trp, in which either $H_2{}^{16}O_2$ or $H_2{}^{18}O_2$ was added to a total of 4 mM concentration with a stepwise addition. After 20 minutes of reaction, TDO was removed from the reaction system using a Centriprep-10 at 3000×*g* for 10 min, and the filtrate was collected for electrospray ionization-mass spectrometry (ESI-MS) analysis.

Solvent exchange of the dioxygenation product (NFK) — Unlabeled NFK was prepared according to the procedures described above for the $H_2{}^{16}O_2$-driven reaction mediated by ferric TDO**.** A sample of ^{16}O-NFK was dissolved in $H_2{}^{18}O$ (75% ^{18}O) on ice for 20 min and used for ESI-MS analysis. Also, a parallel sample of ^{16}O-NFK in $H_2{}^{18}O$ (75% ^{18}O) was further diluted with $H_2{}^{16}O$ to a final 60:1 ratio of $H_2{}^{16}O$:$H_2{}^{18}O$. The ^{18}O-incorporation was analyzed by mass spectrometry for the above samples. In another set of experiments involving $H_2{}^{16}O_2$, L-Trp and ferric TDO were prepared and dissolved in $H_2{}^{18}O$ buffer. The reaction was performed with the procedure described in $H_2{}^{16}O_2$-driven reaction mediated by ferric TDO experiment above. The ^{18}O-incorporation was analyzed by ESI-MS.

Mass spectrometric identification — Mass spectrometry (MS) analyses were conducted on a Waters ESI-Q-TOF micro mass spectrometer equipped with a Wates alliance 2695 HPLC system (Milford, Massachusetts) in a positive mode. Samples were analyzed through either a direct infusion or through HPLC separation before MS analysis. The samples were mixed with 50% acetonitrile in water containing 0.1% formic acid before analysis. In MS-MS analysis, collision energy was set to 30 V. HPLC separation was achieved on Restek Allure C18 column (100 mm × 2 mm i.d., 3 μM). Mobile phase A was composed of water which contains 0.1% formic acid and mobile phase B was composed of acetonitrile which contains 0.1% formic acid. The gradient was developed from 100% A over 5 min; to 0% A over 10 min; to 0% A over 15 min; to 100% A over 20 min at the flow rate of 200 μL/min. MassLynx 4.1 software was used for instrument control and data acquisition.

Oxygen production — Oxygen production was measured using an YSI oxygen electrode coupled to a Hansatech Oxygraph Plus (Kings Lynn, Norfolk, U.K.) at 25 °C. The stirred cell was capped, and reagents were added with a Hamilton syringe. Oxygen levels were continuously monitored in real-time during reaction. In glucose/Glucose oxidase (GO) system, 50 mM D-glucose and 50 μg/ml glucose oxidase were added to the cell and allowed to equilibrate.

Stopped-flow spectroscopy — Pre-steady-state kinetic analysis of the ferric TDO oxidation reaction with H_2O_2 was performed using a RSM16 stopped-flow rapid scanning spectrophotometer (OLIS, Bogart, GA). Dead time of the instrument is ca. 2 milliseconds. One syringe contained 13 μM ferric TDO, and the other contained 6 equivalents of H_2O_2. The reaction temperature was controlled at 25 ºC by a water bath.

Stoichiometry of hydrogen peroxide consumption to the formation of product in the presence of oxygen scavenger — L-Trp, H_2O_2, glucose and glucose oxidase were freshly prepared in 50 mM Tris-HCl pH 7.4 buffer which had been previously degassed and purged with argon. A vial containing concentrated ferric TDO was gently vacuumed and refilled with argon, and the enzyme was diluted into the O_2-free buffer in a sealed cuvette containing 5 mM L-Trp, 50 mM glucose and 50 μg/ml glucose oxidase. A gas-tight microsyringe was used for stepwise additions of argon-saturated oxygen-free H_2O_2 to TDO. The total addition is 40 equivalents of H_2O_2.

3.4 Results and Discussion

Stoichiometry of hydrogen peroxide consumption with ferric TDO and L-Trp in the absence of dioxygen — To determine if H_2O_2 can function as a substrate of ferric TDO and be used as the sole oxidant of the dioxygenation reaction, we performed a set of experiments in the absence of O_2 and reducing agents. Under strictly anaerobic condition, equimolar amounts of H_2O_2 were repeatedly added to ferric TDO and L-Trp, and the reaction was followed spectrometrically.

These multiple small additions of H_2O_2 were designed to minimize potential oxidative damage to TDO by H_2O_2 during the measurements of product formation. Figure 3.1 shows the development of a broad absorbance at 310 nm. A similar absorbance development at 321 nm was observed when the reaction was mediated by reduced TDO and using O_2 as the oxidant. The absorbance in this region has previously been used to measure the formation of NFK (*262, 267, 280, 285, 296*), because the synthesized NFK exhibits a similar absorbance band at 315 nm in water (*296*). The broad 310 nm chromophore observed in the peroxide-driven reaction is consistent with the formation of the dioxygenation product. Using the extinction coefficient of

NFK, the inset shows that the formation of the product was linear with respect to the amount of H_2O_2 added. When H_2O_2 was incubated with L-Trp in the absence of TDO, the development of the 310 nm chromophore did not occur, confirming that the peroxide-driven oxygenation reaction is an enzymatic process.

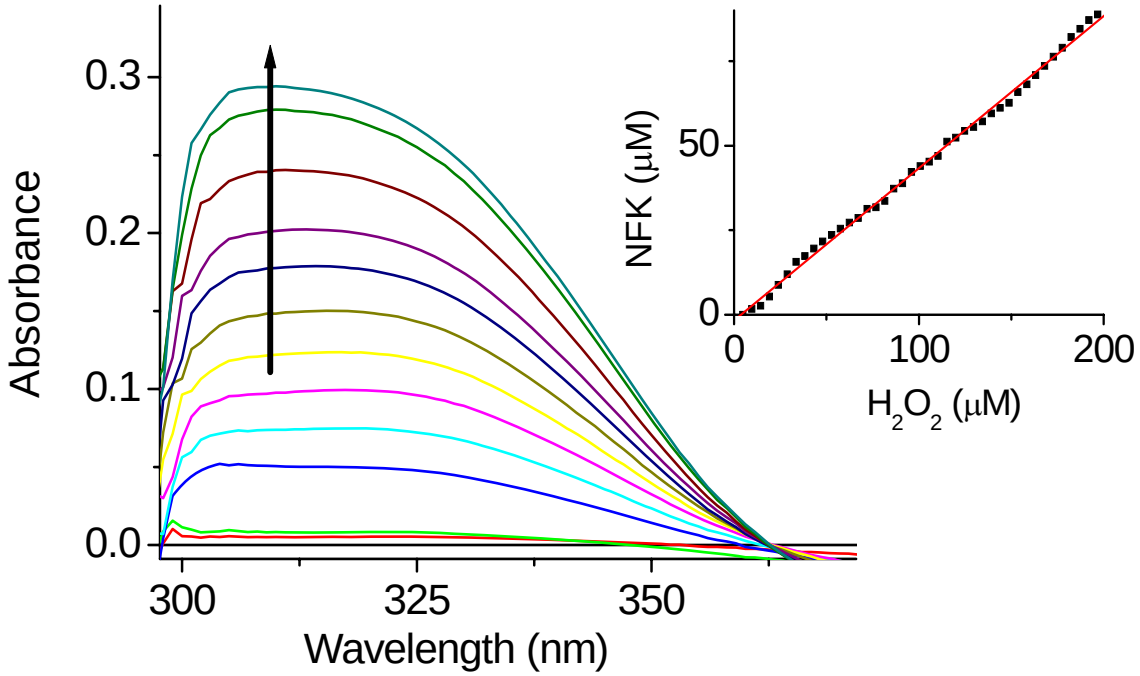

Figure 3.1. Difference spectra for each 5 equivalents of the titration of H_2O_2 with 5 μM ferric TDO in the presence of 5 mM L-Trp under anaerobic conditions. The initial L-Trp and the enzyme absorption are subtracted from each trace. The arrow indicates development of absorbance at the 310 nm region. The inset is the calculated product concentration as a function of the added peroxide.

After a 40-step anaerobic addition of a total of 200 μM H_2O_2 in the presence of 5 μM of ferric TDO, approximately 90 μM of the product formed (Figure 3.1, inset). These results indicate that 2 moles of H_2O_2 are required for the formation of 1 mol of product under ideal conditions in

which two oxygen atoms are incorporated into L-Trp, and presumably, two other oxygen atoms have been reduced to water molecules (Scheme 3.1).

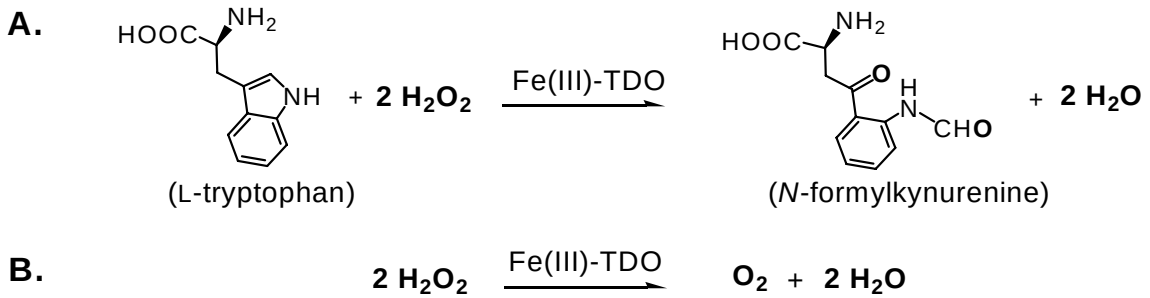

Scheme 3.1. The chemical reactions catalyzed by ferric TDO using H_2O_2 as a substrate in the presence (A) or absence of (B) L-Trp.

Mass spectrometry identification of the N-formylkynurenine product formation — To firmly establish that the broad 310-nm species from the peroxide-driven reaction is indeed NFK, a mass spectrometric analysis was conducted using $H_2{}^{16}O_2$ (Figure 3.2B) and $H_2{}^{18}O_2$ (Figure 3.2C) as oxidant. L-Trp alone exhibits an ion of mass-to-charge ratio (*m/z*) 205 (Figure 3.2A), corresponding to the anticipated $[M+H]^+$ form. A new ion at *m/z* 237 is present in the reaction mixture with $H_2{}^{16}O_2$ as the oxidant in addition to the unreacted L-Trp (Figure 3.2B). The 32-Dalton mass shift compared to the substrate is consistent with the anticipated production of NFK in which 2 oxygen atoms have been inserted into L-Trp. Thus, the development of the broad 310-nm chromophore, with H_2O_2 as the oxidant, corresponds to the NFK formation in the ferric TDO mediated system.

When $H_2{}^{18}O_2$ was used instead of $H_2{}^{16}O_2$, the mass spectrum in Figure 3.2C shows an ion of *m/z* 241, which is consistent with the incorporation of two ^{18}O atoms derived from $H_2{}^{18}O_2$ to the substrate. It has been previsously known that oxidized TDO could be activiated by H_2O_2 for the

normal catalytic reaction. A small peak at 237 is also shown in this figure, which is likely produced during the process of removing enzyme from the system by filtration/centrifugation under non-anaerobic conditions in which O_2 is available. The mass spectrum in Figure 3.2C also shows an ion of *m/z* 239 which corresponds to the incorporation of one ^{16}O and one ^{18}O atom into L-Trp. The source of the ^{18}O scrambling is presumably due to solvent exchange. To prove this, a sample of ^{16}O-NFK was prepared, which presents the ion of *m/z* 237 as shown in Figure 3.2B. This ^{16}O-NFK sample was re-dissolved in solvent with 1:4 ratio of $H_2{}^{16}O$:$H_2{}^{18}O$ after a speed vacuum treatment. While the ion of *m/z* 237, which corresponds to the ^{16}O-NFK in Figure 3.3A, is still present, a new ion of *m/z* 239 is generated by the $H_2{}^{18}O$ dilution, indicating that one ^{18}O from solvent, rather than two, has been exchanged to the ^{16}O-NFK.

To provide further evidence for solvent exchange on one of the oxygen site in NFK, we diluted the above sample with $H_2{}^{16}O$ to reach a $H_2{}^{16}O$:$H_2{}^{18}O$ ratio of 60:1. Figure 3.3B shows that the *m/z* 239 peak is substantially reduced while the original *m/z* 237 ion becomes the major peak in the mass spectrum. This is consistent with the notion that the solvent exchange of NFK is readily reversible with solvent. Since there is no *m/z* 241 peak in either case in this set of the experiments, we conclude that one and only one oxygen site in the product NFK is solvent exchangeable. Furthermore, these observations rule out the possibility that the *m/z* 241 ion in Figure 3.2C is due to the solvent exchange. Taken together, these observations suggest that the two new oxygen atoms in the NFK are derived from hydrogen peroxide, and one of them is exchangeable with solvent. Unlike the *m/z* 237 ion in Figure 3.2C, which is due to the small amount of O_2 contamination during the centrifugation step for removing TDO from the reaction

mixtures, the occurrence of *m/z* 243 in some of the samples is an experimental artifact. This ion is derived from Tris-HCl. It is not always present, due to sample dilution by water or acetonitrile.

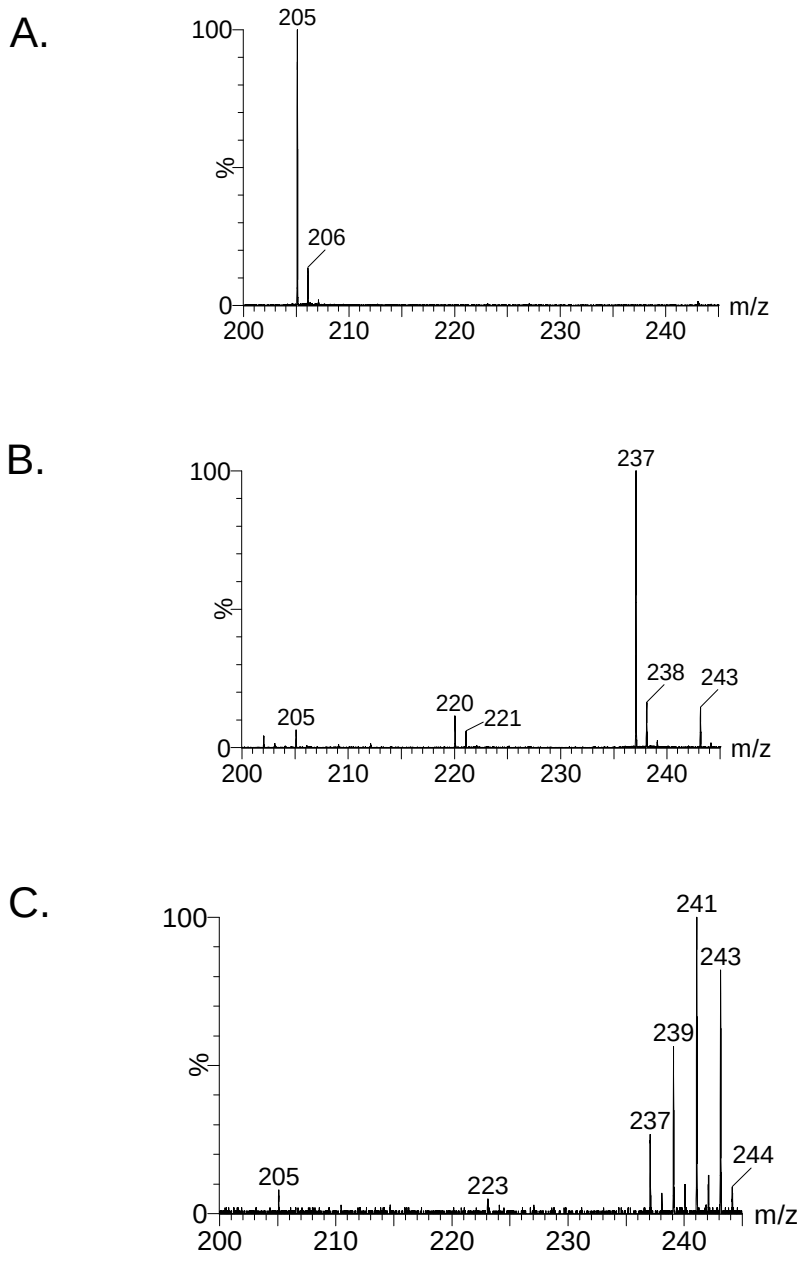

Figure 3.2. ESI-Mass spectrometric characterization of (A) L-Trp, (B) the product of $H_2{}^{16}O_2$ driven oxygenation mediated by ferric TDO and (C) the product of $H_2{}^{18}O_2$ driven oxygenation mediated by ferric TDO.

To test whether a water molecule contributes oxygen to NFK during reaction and prior to the solvent exchange, we performed experiments using unlabeled $H_2{}^{16}O_2$ as oxidant in $H_2{}^{18}O$ solvent (Figure 3.3C) and labeled $H_2{}^{18}O_2$ as oxidant in $H_2{}^{16}O$ solvent (same as Figure 3.2C), respectively. If water contributes oxygen to the substrate during catalytic reaction or through solvent-exchange with an iron-bound oxygen intermediate, it should generate an oxygen scrambled NFK product with *m/z* 237 ion and *m/z* 239 in both of the mass spectra. The *m/z* 237 and 239 ions are indeed present in the $H_2{}^{16}O_2/H_2{}^{18}O$ sample (Figure 3.3C), whereas *m/z* ions of 239 and 241 are present in the $H_2{}^{18}O_2/H_2{}^{16}O$ sample (Figure 3.2C). The former is consistent with the post-catalytic reaction solvent exchange. However, the *m/z* 241 ion is not present in the $H_2{}^{18}O$ solvent sample while it is observed with the sample containing $H_2{}^{16}O$ solvent. These results indicate that H_2O is not directly involved in the catalytic reaction. These observations are also consistent with the conclusion that one, and only one, carbonyl group is exchangeable with solvent in NFK.

Based on the fact that ketonic oxygen exchanges with water (*297-299*) and the amide group of NH-COH exchanges with solvent slower than aldehyde and ketone, we propose that the ketone group is the only exchangeable carbonyl group which exchanges oxygen atom with solvent via a diol- intermediate mechanism and two possible mechanisms are proposed for the solvent exchange (Scheme 3.2). In Scheme 1A, a transient state of a six-member ring structure facilitates the electrophilical attack at the ketone carbon by water to generate a diol-intermediate. While in Scheme 1B, the lone pair electron of the amide nitrogen atom nucleophilical attacks the carbonyl group of the ketone for the solvent exchange. However, considering the stability of the benzene ring structure, the solvent exchange reaction favors the mechanism in Scheme 1A.

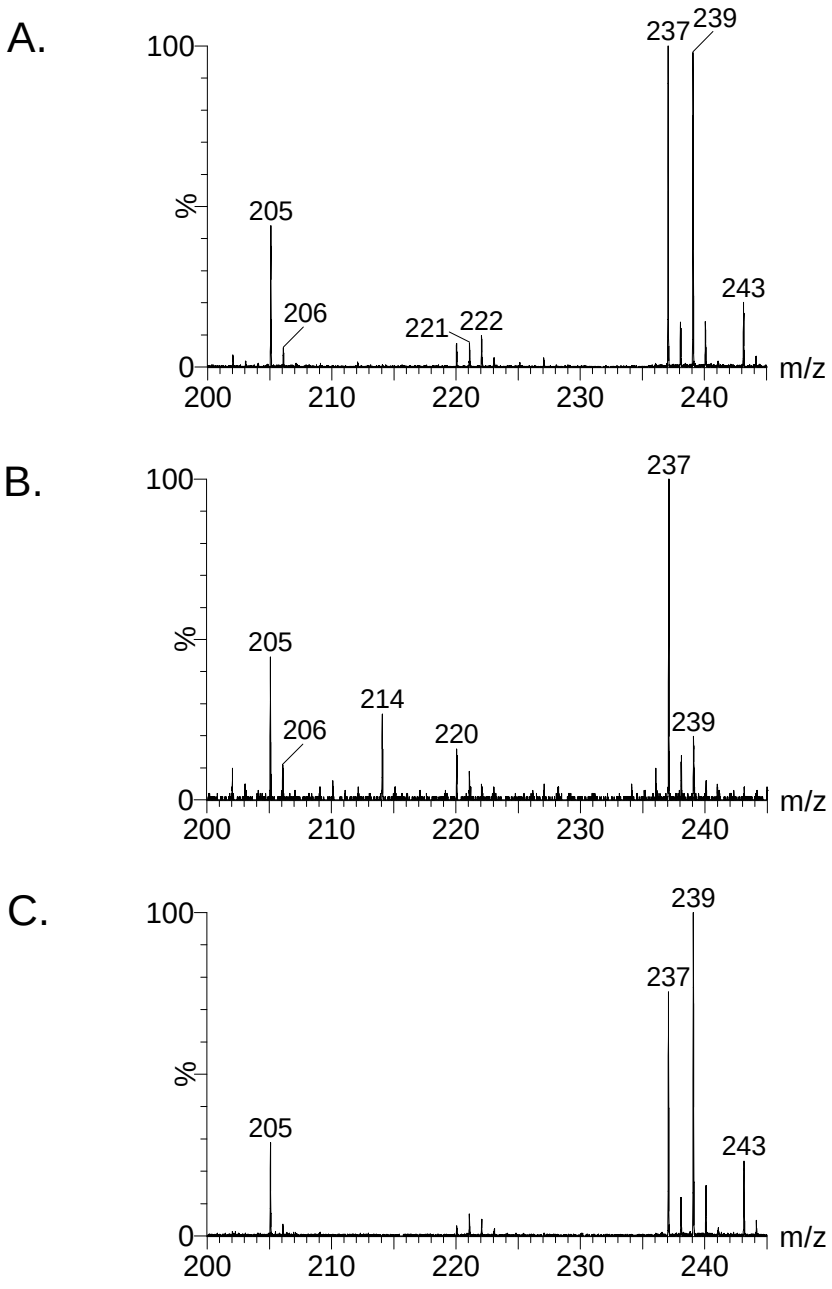

Figure 3.3. Solvent exchange of NFK characterized by ESI-Mass spectrometry. (A) unlabeled NFK dissolved in $H_2{}^{16}O$: $H_2{}^{18}O$ (1:4) solvent, (B) Sample from Figure 3.3A dissolved in $H_2{}^{16}O$: $H_2{}^{18}O$ (60:1), (C) Sample of the reaction of $H_2{}^{16}O_2$-driven oxygenation mediated by ferric TDO performed in $H_2{}^{18}O$.

A.

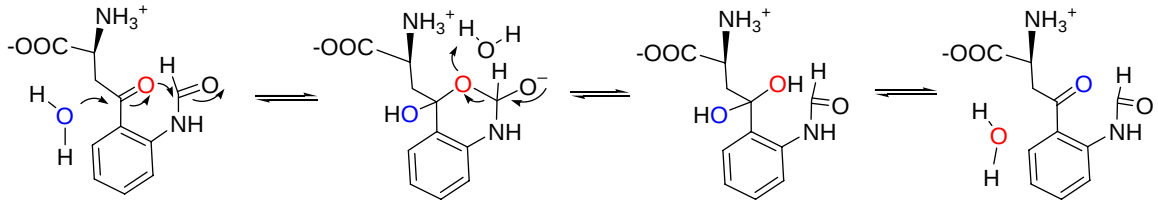

B.

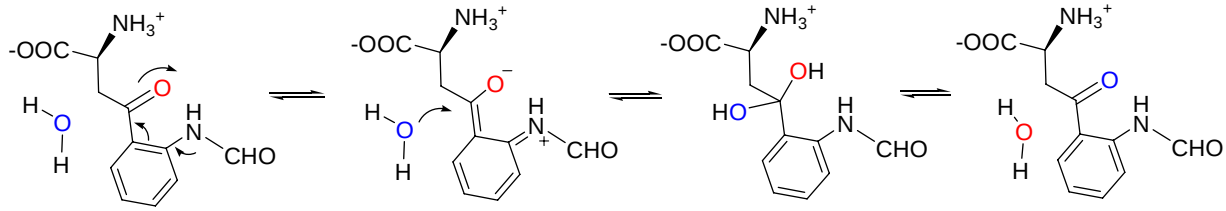

Scheme 3.2. The proposed two possible mechanisms of solvent exchange with carbonyl group of NFK.

It should be noted that a small, but reproducible, peak for an ion at *m/z* 221 (Figure 3.2) appears when $H_2{}^{16}O_2$ was used. This ion is a 16-Dalton shift over L-Trp. A corresponding *m/z* 223 ion, 18-Dalton shift over L-Trp, is observed when $H_2{}^{18}O_2$ was used as oxidant. This corresponds to the mass in positive mode of a monooxygenated L-Trp in which only one oxygen atom is inserted into the substrate. Figure 3.4 shows the result from LC-MS analysis to identify the oxygenation products generated in the ferric TDO-mediated reaction using $H_2{}^{16}O_2$ as oxidant in the presence of $H_2{}^{18}O$. The species with *m/z* 221/223 indication of the formation of a monooxygenated L-Trp was eluted at the retentioin time of 5.25 min. The 6.08 min species is the dioxygenation product of NFK. The *m/z* 243 ion with a 2.88 min retention time was an ion peak giving rise from Tris buffer used during sample preparation.

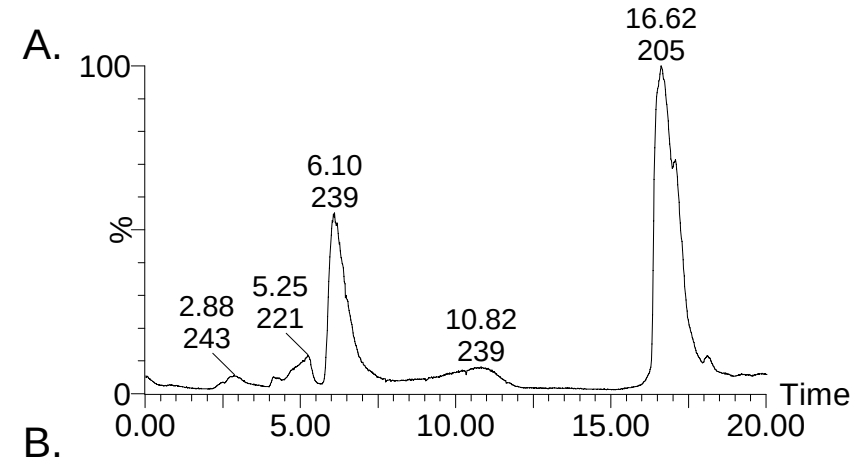
A.
100
%
0
16.62
205
6.10
239
5.25
221
2.88
243
10.82
239
Time
0.00
5.00
10.00
15.00
20.00

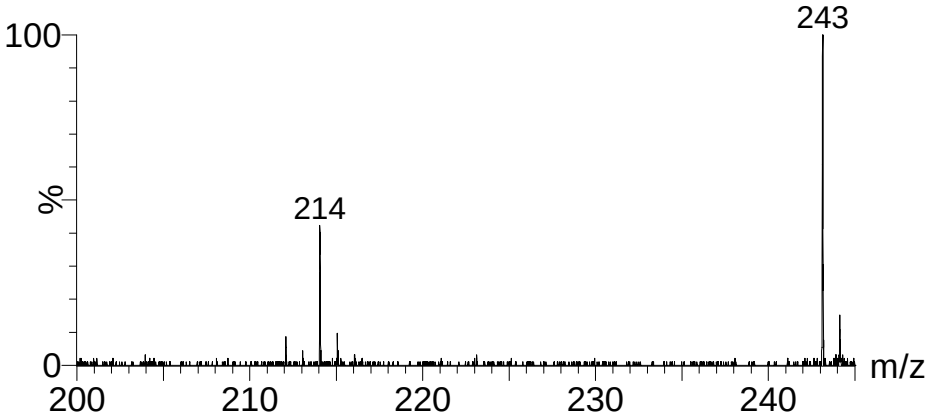
B.
100
%
0
243
214
m/z
200
210
220
230
240

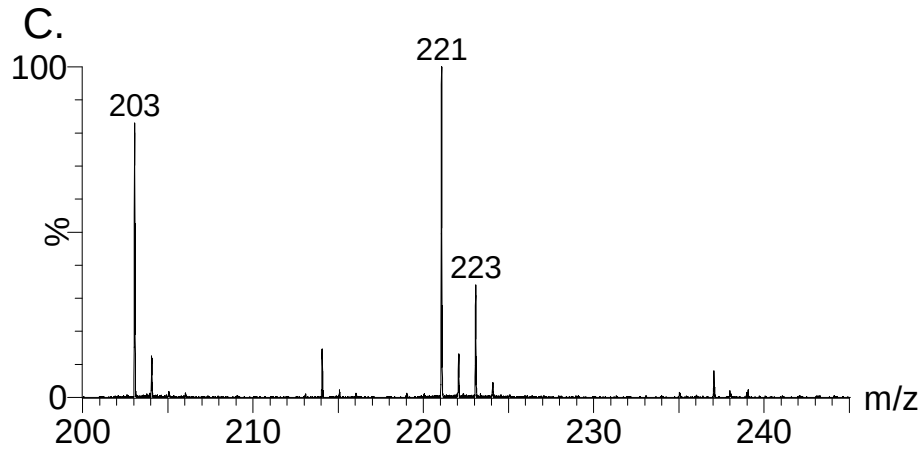
C.
100
%
0
221
203
223
m/z
200
210
220
230
240

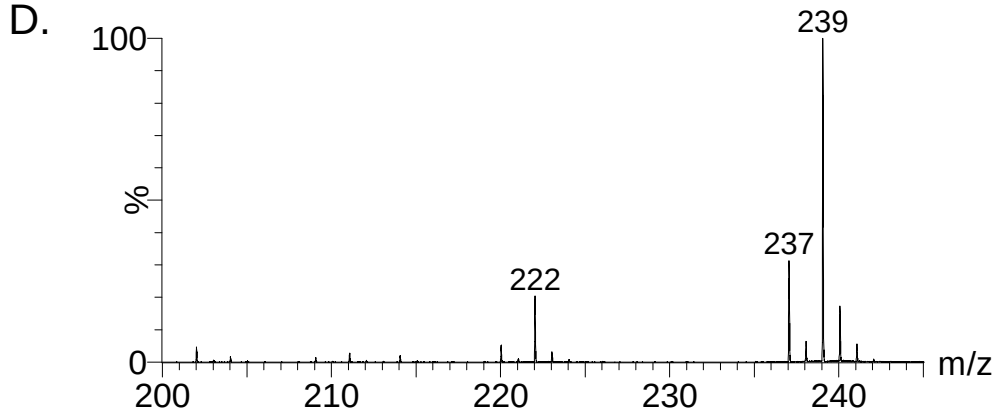

Figure 3.4. LC-MS characterization of the product formation of monooxygenated L-Trp and NFK. (A) Chromatography of the reaction mixture of $H_2{}^{16}O_2$ driven oxygenation mediated by ferric TDO performed in $H_2{}^{18}O$. MS spectrum at retention time at (B) 2.88 min (C) 5.25 min (D) 6.08 min.

To better understand the origin of the *m/z* 221 ion and other small ions in the same region, ESI-MS-MS experiments were also conducted to characterize the major products of *m/z* 237 and 239 ions. Figure 3.5 shows that *m/z* 220/202 and 222/204 are associated with *m/z* 237 and 239, respectively, as a consequence of one lost –OH or $-{}^{18}OH$ group during ionization. Therefore, the *m/z* 220 and 222 ions are not associated with formation of the monooxygenated L-Trp. These results also demonstrate that *m/z* 221 and, *m/z* 223 ion in the ^{18}O case, are not the fragments of the NFK with *m/z* 237 and 239 ions. Combined with the consistent presence of *m/z* 221 and *m/z* 223 species when using $H_2{}^{16}O_2$ and $H_2{}^{18}O_2$ as oxidant, these results give an indication of the formation of monooxygenated L-Trp. This is also consistent with the fact that the heme cofactor in TDO does not allow a simultaneous coordination of two molecules of peroxide molecules. The heme group can only bind one peroxide molecule at a time. The monooxygenated L-Trp therefore must be generated by the reaction of TDO with the first peroxide molecule, which

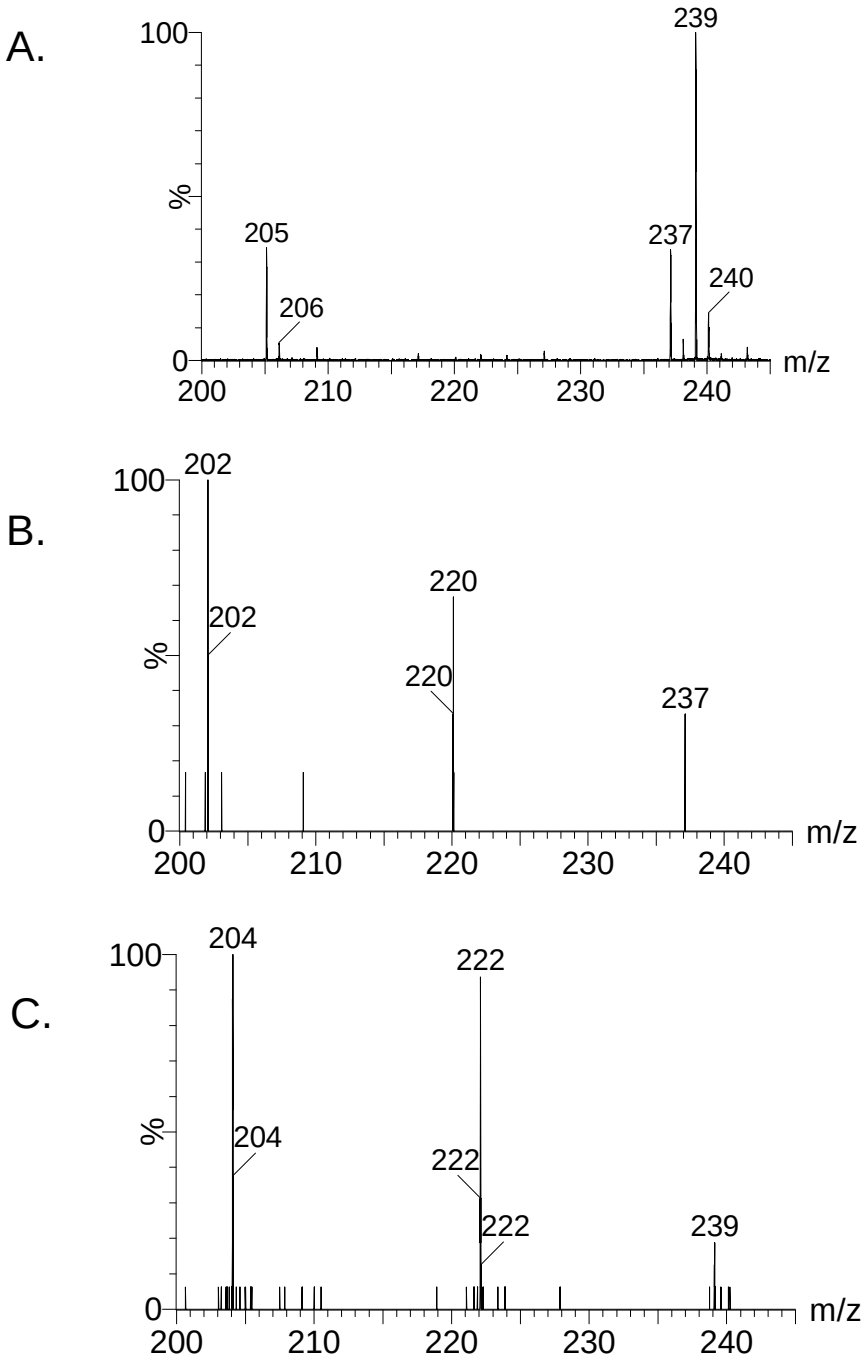

Figure 3.5. Mass spectrometric characterization of m/z 220 and m/z 222 ion peaks. (A) ESI-MS spectrum of the product of $H_2{}^{16}O_2$ driven oxygenation mediated by ferric TDO in $H_2{}^{18}O$ solvent. MS/MS characterization of ion peak in (A) at (B) *m/z* 237 (C) *m/z* 239.

binds to the ferric heme and generates an enzyme-based intermediate. This Fe-intermediate is capable of inserting an oxygen atom into L-Trp, as described in the monooxygenase reactions.

These results suggest that the peroxide-driven oxygenation reaction must undergo sequential addition of two oxygen atoms to L-Trp during catalysis (Scheme 3.3A), as opposed to a one-step concerted dioxygenation reaction mechanism. The *m/z* 221 ion peak was present after the reaction of mixed TDO-free monooxygenated L-Trp with excess H_2O_2 to proceed for 20 min. This suggests that the monooxygenated L-Trp does not further convert to NFK via a non-enzymatic reaction. However, since the *m/z* 221 might also arise from by-product during the peroxide driven oxygenation, it remains unclear whether the oxidation of the monooxygenated L-Trp to NFK by peroxide is necessarily enzyme-dependent. An alternative mechanism is that it reacts with H_2O_2 in a non-enzymatic process as shown in Scheme 3.3B.

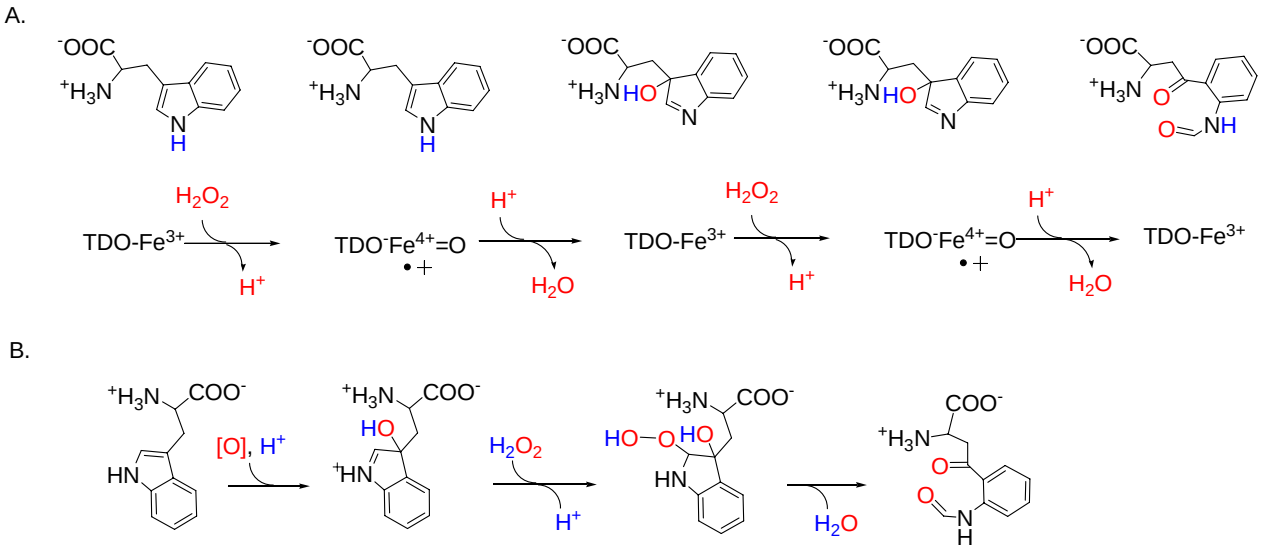

Scheme 3.3. The proposed ferric TDO dioxygenation mechanisms using H_2O_2 as oxidant.

Catalase-like activity of ferric TDO in the absence of L-Trp — In the absence of L-Trp, ferric TDO is also able to consume large excess of H_2O_2, but at a much slower rate. Figure 3.6 shows

an UV-visible spectral change of the Soret band of the enzyme induced by the addition of H_2O_2. The Soret band at 405 nm in the initial spectrum decreased in intensity and slightly red-shifted to 406 nm (Figure 3.6 inset), which gives an indication of a compound I-like or compound ES-like species (for review, see refs. (*292, 300, 301*)). Such an absorption change at Soret band is not due to enzyme activation by peroxide, because the activation process leads to a significant shift of the Soret band from 405 nm to 432 nm and requires a different reaction condition (*289*) .

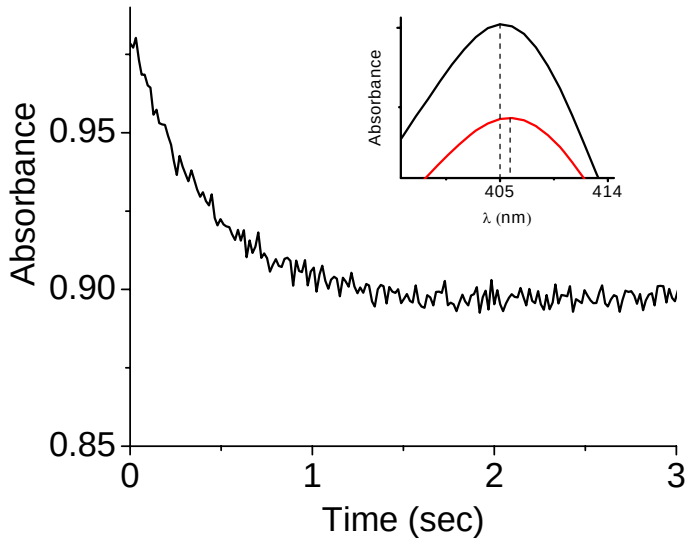

Figure 3.6. Stopped flow UV-visible spectral changes of ferric TDO reacting with 6 equivalents of H_2O_2 at 405 nm versus time. The inset is UV-visible spectral change at 405 nm.

In the mechanism of catalase, the ferric heme reacts with the first peroxide molecule to produce H_2O and a reactive oxoferryl (compound I), which subsequently reacts with a second peroxide to produce an O_2 molecule and a second water. Indeed, a ferryl intermediate species from TDO has been trapped (Fu, Gupta, Begley, Hendrich, and Liu, manuscript in preparation). Similar high-valent Fe intermediate has also recently been characterized in the reaction of oxidized MauG,

another heme-dependent enzyme oxidizing protein-bound tryptophan residues, with H_2O_2 (*302*). To understand the consumption of H_2O_2 by ferric TDO in the absence of the primary substrate L-Trp, and to determine if ferric TDO possesses catalase-like activity, we examined the reaction using an oxygen electrode in a stirred cell at 25 °C to detect the generation of O_2 via potential catalase-like activity. The addition of 5 μM ferric TDO to the reaction buffer did not alter the O_2 concentration (Figure 3.7). However, the addition of 15 equivalents of H_2O_2, in the absence of L-Trp resulted in an immediate increase in the oxygen concentration. Oxygen generation at the same rate could be reinitiated by a second excessive addition of H_2O_2. These results show that O_2 is produced from H_2O_2, and hence demonstrates that ferric TDO possesses a catalase-like activity with H_2O_2 in the absence of L-Trp (Scheme 3.1).

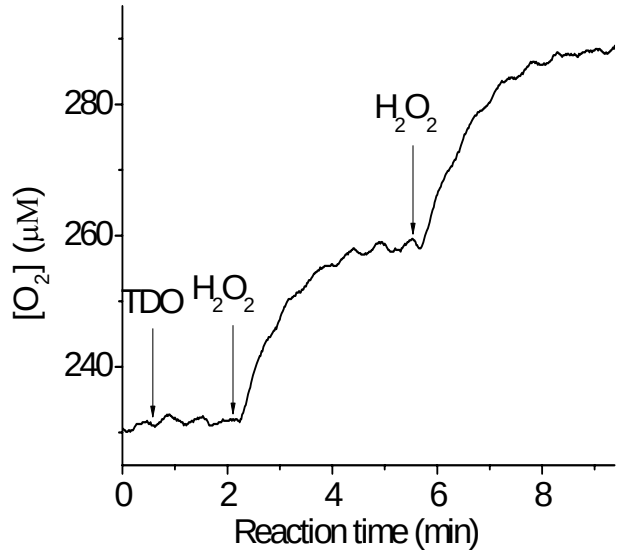

Figure 3.7. The increase of O_2 concentration after addition of 75 μM hydrogen peroxide to 5 μM ferric TDO. Arrows indicate the time points in which the ferric TDO or H_2O_2 was added to the O_2-electrode cell.

In steady state analysis, the apparent k_{cat} and K_m values of the TDO catalase-like activity are ca. 13.5 s^{-1} and 16 mM, respectively (Table 3.1). With the ratio of L-Trp to H_2O_2 as 50:1, the oxygen-electrode experiments suggest that the catalase-like activity is a minor but concomitant reaction with the apparent k_{cat} and K_m values of 0.9 s^{-1} and 1.2 mM, respectively. The fact that both values of apparent k_{cat} and K_m undergo a more than 90% decrease but k_{cat}/K_m does not change significantly indicates that the peroxide-driven oxygenation reaction is in competition with the catalase-type of dioxygen production. It appears that upon L-Trp binding, the active site of TDO shifts to an appropriate conformation in which the second substrate, H_2O_2, would be ligated to the Fe ion, and positioned at the correct distance and orientation for the peroxide-driven dioxygenation reaction. In subsequent experiments, we have found that the apparent k_{cat}/K_m value of the peroxide-driven dioxygenation reaction is ca. 4-fold higher than that of the catalase-like reaction either in the presence or in the absence of an oxygen scavenger system. These results suggest that the oxygenation reaction does not couple with the catalase-like reaction. The K_m of H_2O_2 in the oxygenation reaction is 77 μM, while it is 16 mM in the catalase-like reaction. The large difference in H_2O_2 binding indicates that the incorporation of L-Trp to the active site will facilitate the H_2O_2 binding. In comparison with L-Trp, H_2O_2 is a small hydrophilic molecule to access the active site.

As shown in Table 3.1, the kinetic of TDO is cooperative for the substrate of H_2O_2 in the peroxide driven oxygenation reaction. This gives an indication that there are at least two active site conformations for H_2O_2 binding which is consistent with two hydrogen bonding networks in the active site in the crystal structure of substrate-bound xcTDO. TDO is a tetrameric protein; the cooperative index is probably mediated by the subunit-subunit interaction. The central region of

the interaction between the subunits is in a hydrophobic active site binding pocket, in which Tyr43 is intruded from one subunit inserted from the adjacent subunit.

Table 3.1. Kinetic properties of the ferric TDO catalized reactions.

Peroxide-driven oxygenation[a]	K_m (μM) (H_2O_2)	k_{cat} (s^{-1})	n	k_{cat}/K_m ($M^{-1}s^{-1}$)
no glucose / GO	77.0 ± 22.0	0.24 ± 0.10	1.8 ± 0.5	3,140.0 ± 584.0
with glucose / GO	247.0 ± 37.0	0.70 ± 0.08	1.3 ± 0.1	2,728.0 ± 95.0

Catalase-like reaction[b]	K_m (μM) (H_2O_2)	k_{cat} (s^{-1})	n	k_{cat}/K_m ($M^{-1}s^{-1}$)
no L-Trp	16,110 ± 3320	13.50 ± 1.60	1.0 ± 0.1	1,152.0 ± 65.0
with L-Trp	1,200 ± 99	0.90 ± 0.10	4.0 ± 0.8	784.0 ± 13.0

a. The peroxide-driven reaction mixtures contain 5 μM TDO and 3 mM L-Trp in 50 mM Tris-HCl pH 7.4 in a sealed cuvette at 25°C. The reactions were performed either in the presence or in the absence of 50 μg/ml glucose oxidase and 50 mM glucose under anaerobic conditions.

b. The catalase-like reactions were performed in an oxygen electrode cell. In the presence of L-Trp, the concentration of H_2O_2 was ranged from 25 μM to 1500 μM with a ratio of L-Trp to H_2O_2 fixed at 50:1. In the absence of L-Trp, the H_2O_2 concentration was ranged from 25 μM to 50 mM.

In the contrast, there is no cooperative effect on the catalase-like activity in the absence of L-Trp. This is consistent with the relative small molecule of H_2O_2 which may not be able to induce the cooperative effect at the active site. On the other hand, a significant positive cooperative index was observed on the catalase-like activity of TDO in the presence of L-Trp. This suggests that L-Trp facilitates the binding of H_2O_2 to the ferric heme. In addition, high concentration of H_2O_2, even in the presence of L-Trp, favors to the catalase-like activity of TDO and contributes to the relative big cooperative index.

Peroxide-driven oxygenation in the presence of an oxygen scavenger — The discovery of a second catalytic activity of ferric TDO with peroxide as substrate raises the question whether the oxygenation of L-Trp is due to the production of O_2 from catalase-like activity. This is unlikely a process because the O_2 production process is more than one order of magnitude slower than the oxygenation reaction. So, the catalase-like activity is not capable of for providing enough O_2 for the oxygenation reaction. To further eliminate this concern, we introduced in a separate set of experiments an enzyme-based oxygen scavenger reaction system. Glucose and glucose oxidase (glucose/GO) were employed as the oxygen scavenger which rapidly converts O_2 generated by TDO's catalase-like activity back to H_2O_2. Figure 3.8A clearly indicates that the O_2 consumption via 50 mM glucose and 50 μg/ml glucose oxidase exceeded O_2 production via the catalase-like activity of ferric TDO reacting with 50 equivalents of H_2O_2. In the presence of this enzyme-based oxygen scavenger system, ferric TDO was added either in the absence (Figure 3.8B) or presence of L-Trp (Figure 3.8C). The O_2 concentration did not change in either case. The source of peroxide in Figure 3.8B & 8C was from the reaction of glucose and O_2 catalyzed by glucose oxidase. In a parallel experiment shown in Figure 3.8C, either with or without

externally supplied H_2O_2, the electronic absorption spectra monitored in the 310 nm region indicate the formation of NFK (Figure 3.8C inset).

The ability of H_2O_2 to function as an oxygen donor in the enzymatic oxidization of L-Trp by ferric TDO has not been previously established, although ferric TDO has been shown to be partially activated by superoxide or hydrogen peroxide under certain conditions. The activation mechanism by H_2O_2 is not yet fully understood and thus a subject area for further investigation. To a great extent, the dioxygenase catalytic activity of ferric heme resembles the peroxide shunt activity described for various heme Fe-dependent oxygenase enzymes (*4, 290, 291*). The detection of an intermediary monohydroxylated product of L-Trp in the present work suggests a stepwise oxygen insertion. However, whether the ferrous enzyme and dioxygen share the same mechanism is a provoking question yet to be answered.

It is remarkable that TDO is such an extraordinarily versatile enzyme, functionally active at both the oxidizing and reducing states and able to utilize either dioxygen or peroxide and superoxide as an oxidant. It is also intriguing that ferric TDO expresses two distinct catalytic functions with H_2O_2 under the circumstances in which the primary substrate is present. In the present mass spectrometry analyses, the L-Trp and peroxide ratio used was nearly 1:1 in most of the experiments. Under this condition, the dioxygenase reaction is the dominating activity. In the absence of L-Trp, TDO functions as a catalase. It has been known that catalases display no or little peroxidase activity, and peroxidases exhibit very little catalase activity. There are indeed some heme-dependent bifunctional enzymes that use a single heme active site to catalyze two distinct functions, such as catalase-peroxidases (*89-91, 303, 304*). A rather unique feature of TDO is that the ferric form of the enzyme possesses both the dioxygenase and catalase activities,

depending on the availability of the primary substrate, from a single heme active site. It has been reported that the catalase from *Bacillus stearothermophilus* possessed indole dioxygenase activity (*305*); however, in this case, catalase activity dominates over dioxygenase activity. In our studies, this is a unique example of a dioxygenase that expresses a catalase-like activity, i.e., a two-in-one enzyme with two competing catalytic activities, only one of which is pronounced at a time in most of the cases.

The elucidation of activities for ferric TDO may be related to the normal regulation of the kynurenine pathway for tryptophan degradation. It is known that H_2O_2 production is stimulated during apoptosis or when regulatory T-cells are suppressed as a result of infection, oxidative stress, or chemotherapy (*306-309*). The results described here suggest that tryptophan degradation could be enhanced by increased levels of H_2O_2, causing depletion of the precursor for serotonin biosynthesis and accumulation of a downstream neurotoxin quinolinic acid (*269, 310*). On the other hand, the catalase activity of ferric TDO suggests that the enzyme could function as a peroxide scavenger when levels of L-Trp are low.

3.5 Acknowledgements

We thank Drs. Rodney C. Baker and Naila M. Mamoon for helping us with the initial attempts in the mass spectrometry analysis, Dr. Jonathan P. Hosler and Mr. Lakshman Varanasi for assistance with the oxygen electrode experiments, and Dr. Victor L. Davidson for access to the stopped-flow spectrophotometer as well as assistance with the kinetic analysis.

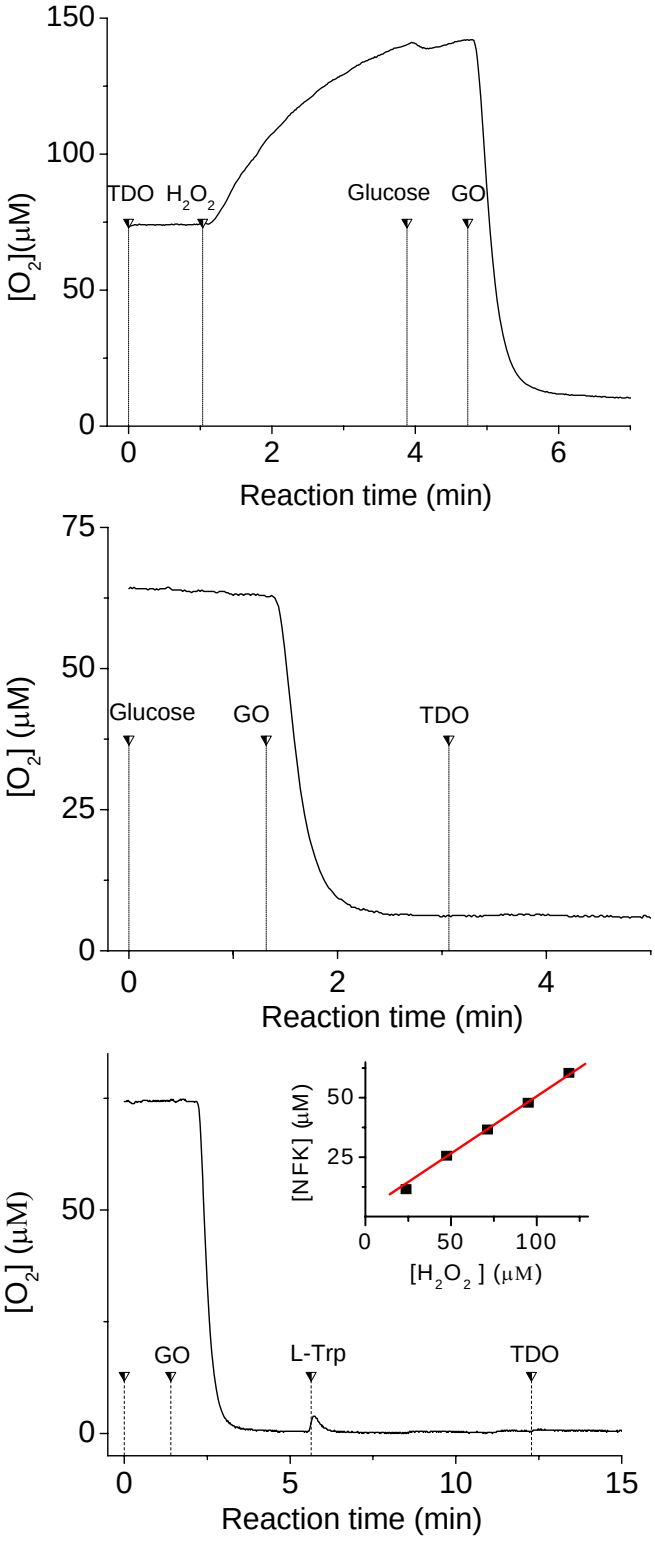
150
100
50
0
[O2](μM)
TDO
H2O2
Glucose
GO
0
2
4
6
Reaction time (min)
75
50
25
0
[O2] (μM)
Glucose
GO
TDO
0
2
4
Reaction time (min)
50
0
[O2] (μM)
GO
L-Trp
TDO
0
5
10
15
Reaction time (min)
50
25
[NFK] (μM)
0
50
100
[H2O2] (μM)

Figure 3.8. The ferric TDO mediated reaction carried out in an oxygen electrode cell at 25°C, 50 mM Tris-HCl pH 7.4 in the presence of glucose and glucose oxidase. Arrows indicate the additions of (A) 5 μM TDO; 50 equivalents H_2O_2; 50 mM glucose; 50 μg/ml glucose oxidase and (B) 50 mM glucose; 50 μg/ml glucose oxidase; and 5 μM TDO (C) 50 mM glucose; 50 μg/ml glucose oxidase; 2.5 mM L-Trp; 5 μM TDO, respectively. Inset is the plot of NFK formation with the H_2O_2 concentration in the presence of 50 mM glucose and 50 μg/ml glucose oxidase.

CHAPTER 4

EXPERIMENTAL AND COMPUTATIONAL INVESTIGATIONS OF AN AUTHENTIC FERRYL INTERMEDIATE IN TRYPTOPHAN 2,3-DIOXYGENASE

The following section of chapter 4 is a direct copy of our prepared manuscript on TDO: Experimental and computational investigations of an authentic ferryl intermediate in tryptophan 2,3-dioxygenase. Rong Fu, Yong Zhang, Rupal Gupta, Tadhg P. Begley, Michael P. Hendrich, and Aimin Liu (2009). EPR experiments were performed by Rong Fu (Department of Chemistry, Georgia State University, Atlanta). Mössbauer samples were prepared by Rong Fu and the spectroscopic analysis was conducted by Professor Michael P. Hendrich and his graduate student, Rupal Gupta (Department of Chemistry Carnegie Mellon University, Pittsburgh). Density functional theory (DFT) calculations were performed by Professor Yong Zhang (Department of Chemistry and Biochemistry, University of Southern Mississippi). The rmTDO plasmid was provided by Tadhg P. Begley (Department of Chemistry, Texas A&M University, TX). The manuscript was prepared by Dr. Aimin Liu, Dr. Yong Zhang, Dr. Michael P. Hendrich and Rong Fu. This work is supported by the National Institutes of Health grants GM069618 (to TPB), GM077387 (to MPH), and GM085774 (to YZ), and National Science Foundation (NSF) grants MCB 843537 (to AL) and EPSCoR award OIA-0556308 (to YZ). RF acknowledges a fellowship support from the Molecular Basis of Disease (MBD) program of GSU. YZ is also grateful to the Mississippi Center for Supercomputing Research and the USM Vislab for the generous use of the computing facilities.

4.1 Abstract

The dioxygenation of L-tryptophan to *N*-formylkynurenine is catalyzed by tryptophan 2,3-dioxygenase (TDO). The ferric form is catalytically active when treated with H_2O_2. Three enzyme-based intermediates were sequentially detected in the peroxide oxidation of ferric TDO. These spectroscopically distinguishable intermediates are: An Fe(IV)-oxo species coupled with a porphyrin cation radical (compound I-type), an Fe(IV)-oxo species and a distant protein radical (compound ES-type), and a ferric intermediate that is more axial than the initial ferric ion. The last two species have also been characterized by Mössbauer spectroscopy. The authentic oxyferryl species is demonstrated by an isomer shift of 0.05(2) mm/s. However, the oxyferryl species exhibits an unusually large quadrupole splitting parameter of 1.76(2) mm/s at pH 7.4. Based on DFT calculations that evaluates all the possible structural influences to the iron axial ligands: 1) protonation of the oxo group, 2) hydrogen bonding to the oxo group, 3) hydrogen bonding to the proximal His, and 4) conformation of the proximal His, this unusual quadrupole splitting was proposed as a result of the hydrogen bonding to the oxo group due to a unique active site environment in TDO.

4.2 Introduction

Tryptophan 2,3-dioxygenase (TDO) inserts two oxygen atoms into tryptophan by a four electron oxidizing process utilizing a *b*-type heme as cofactor. This enzyme is a representative of a potentially new hemoprotein dioxygenase superfamily, whose oxygenase activity remains poorly understood. TDO is catalytically active with O_2 as the oxidant at the ferrous oxidation state. It is known that peroxide is able to activate the resting state of TDO (*4, 311-313*), but the mechanism

of which is not well understood. The resting state of TDO contains a ferric heme. We have recently found that TDO can utilize peroxide as the sole oxygen donor for tryptophan dioxygenation (Scheme 4.1). An Fe(IV)-oxo species is proposed for the peroxide driven reaction (Scheme 4.2). In this study, such an intermediate is trapped in the peroxide oxidation of ferric TDO and characterized by using electron paramagnetic resonance (EPR) and Mössbauer spectroscopy.

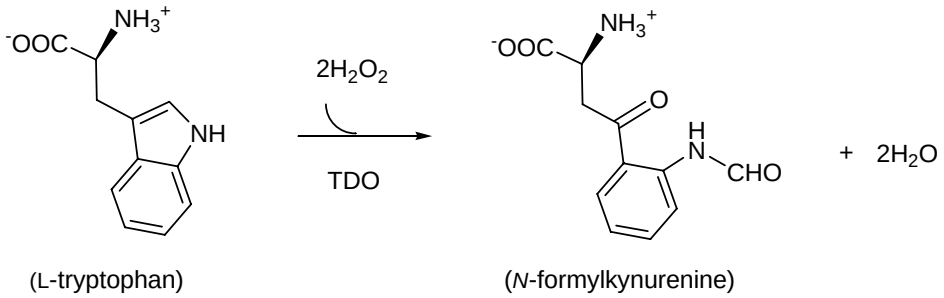

Scheme 4.1. The dioxygenation reaction catalized by oxidized TDO.

4.3 Results and Discussion

TDO at the resting state displays a nearly axial EPR signal with resonances at the g = 1.999, 5.690, and 6.091, typical a high-spin ferric ion in the heme environment (Figure 4.1A). Upon addition of 6-8 equivalents of H_2O_2 or *m*-CPBA , the high-spin ferric heme EPR signal at the g = 6 region is shown to rapidly decrease concomitantly with the formation of a broad EPR signal extending from g values of 1.74 – 2.7 and a sharp signal at g = 2.002 (Figure 4.1B). The EPR signal shown in Figure 4.1B likely originated from a transient compound I (Cpd I)-type of species [Fe(IV)=O/porphyrin π-cation radical]. The broad feature is presumably due to the spin-coupling between the Fe(IV)=O and porphyrin π-cation radical, which is similar to those known

ferryl species in other hemoproteins. For example, Cpd I in catalase exhibits well-resolved $g = 2$ and 3.45 spectral components (*314*), and $g = 2$ and 3.27 resonances in ascorbate peroxidase (*315*). In P450cam, only the $g = 2.0$ free radical signal is observed for the Cpd I species by EPR spectroscopy (*316, 317*). The spin-coupling feature has not been observed from this monooxygenase.

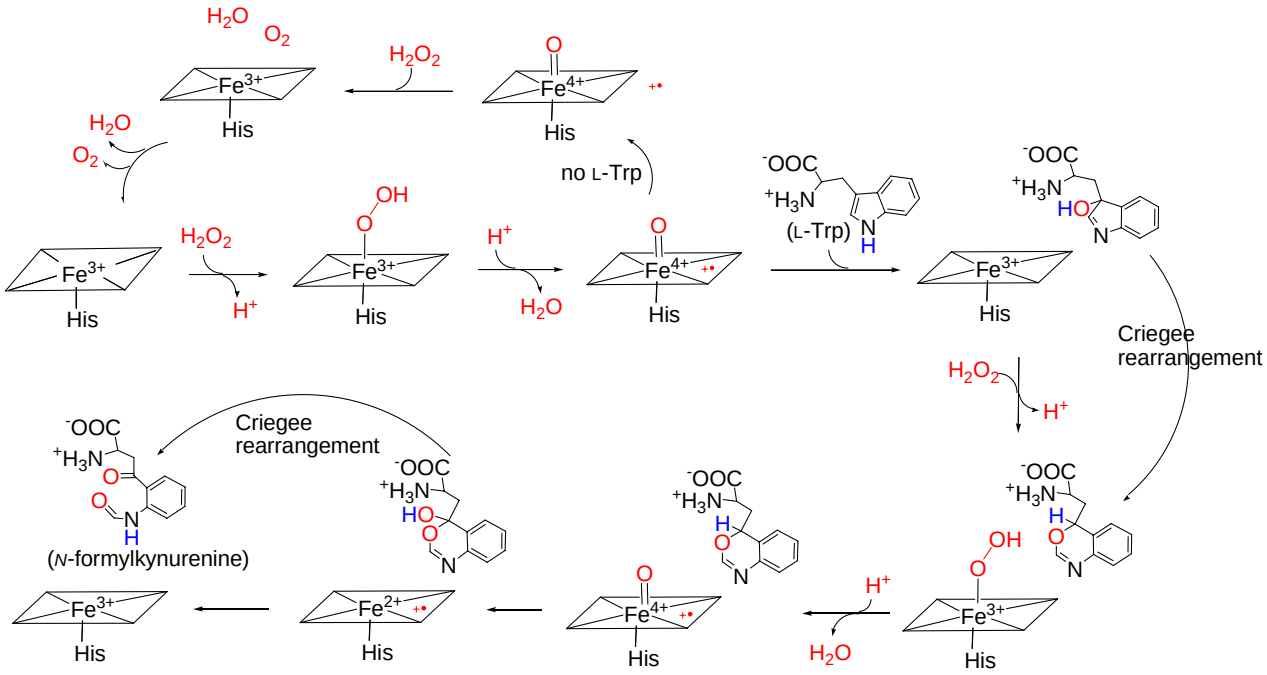

Scheme 4.2. The proposed L-Trp dioxygenation mechanism using H_2O_2 as the oxidant.

When the reaction proceeded further in the absence of substrate, the presumed Cpd I-type of species decayed to a second intermediate with a transient $g = 2.002$ signal that does not contain the broad feature assigned to the spin-coupling between Fe(IV)=O and porphyrin π-cation radical. This observation is interpreted as a result of transfer of the radical to an adjacent amino acid residue, i.e., formation of a compound ES [Cpd ES, Fe(IV)=O/amino acid radical]-type of species (*318, 319*). These intermediates are two oxidizing equivalents above the ferric state of the native enzyme. The formation of these ferryls was at the expense of the ferric heme.

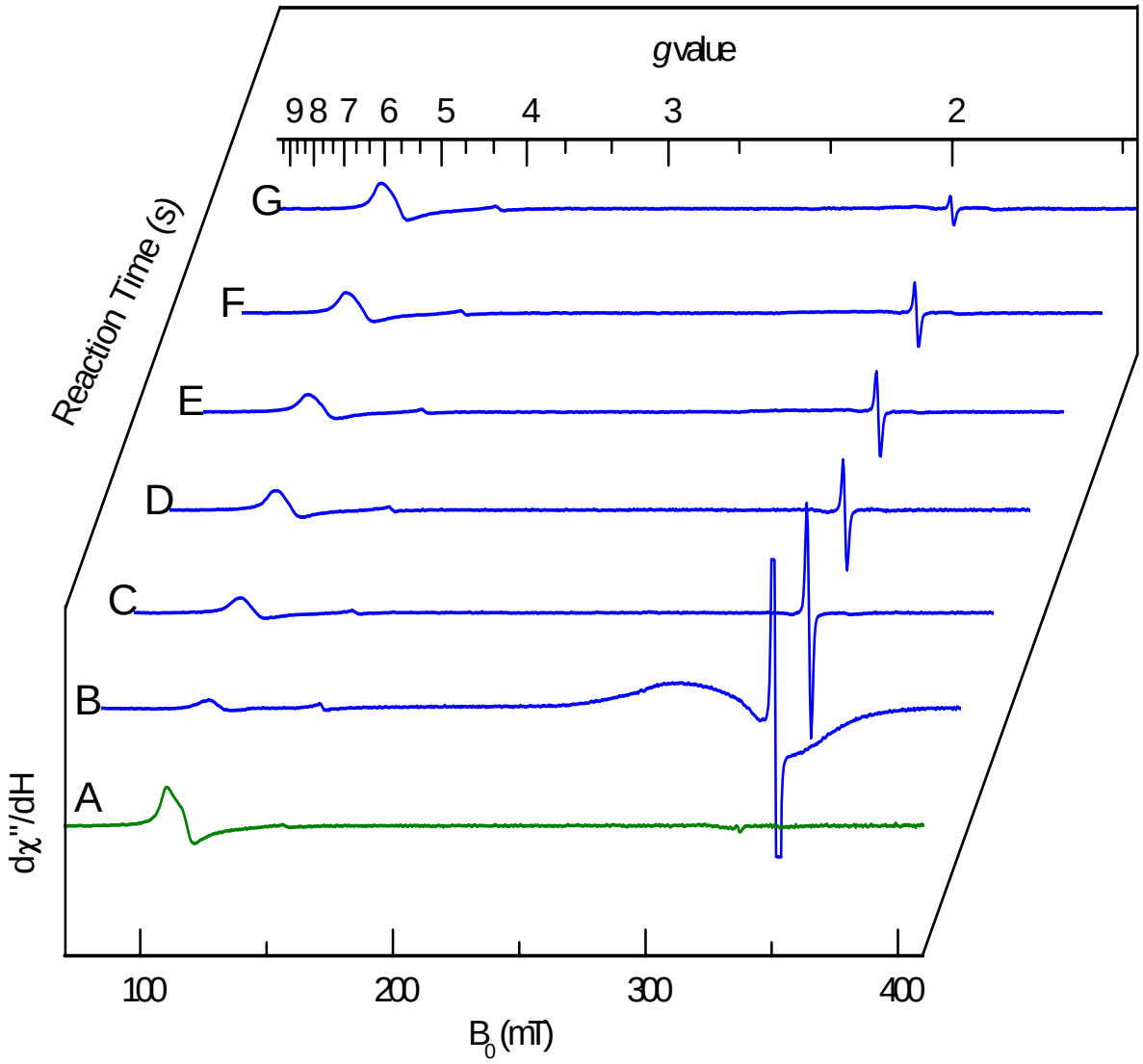

Figure 4.1. The formation and decay of the compound I-type ferryl intermediate in the reactions of ferric TDO with H_2O_2 monitored by EPR spectroscopy at 10 K. Seven representative EPR spectra (traces A to G) are shown in a 2D plot for the reaction of 0, 12, 30, 60, 90, 240, and 600 s in the parallel samples of 150 μM oxidized TDO mixed with 900 μM H_2O_2.

The high-spin ferric EPR signal gradually returned while the g = 2.002 radical decayed. The ferric ion changed to a more axial species with E/D = 0.005 comparing to the starting ferric ion

with *E/D* of 0.01 (Figure 4.2). Thus, this axial ferric species presumably originated from the decayed ferryl intermediates. The smaller *E/D* value indicates that the heme environment is not identical to the initial ferric ion, or the histidine ligand is in a different conformation. This intermediate eventually transformed to the initial ferric ion of the starting material after a prolonged time. However, the EPR signal intensity of the ferric heme did not come back to its original quantity.

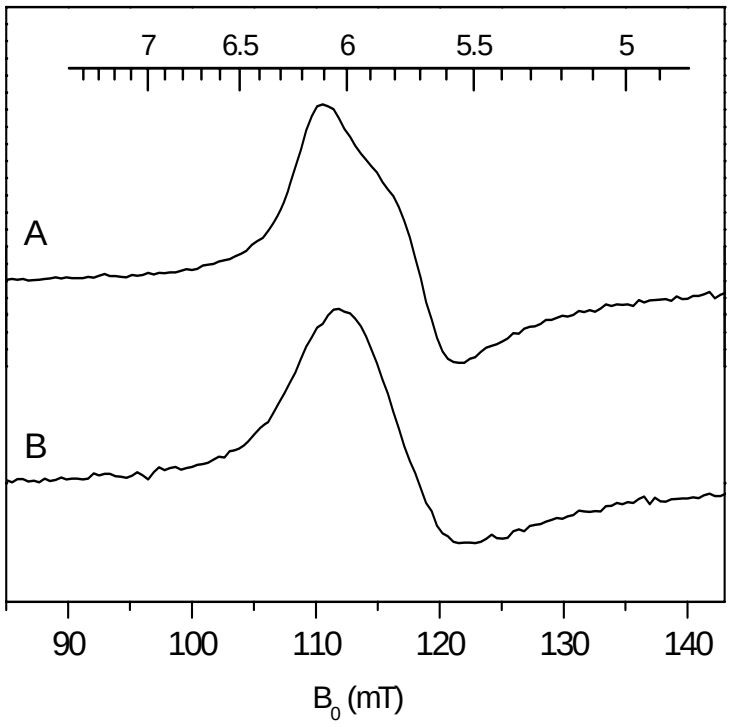

Figure 4.2. The high-spin EPR signal of TDO (A), TDO treated with H_2O_2 at 30 s (B). The samples were monitored by EPR spectroscopy at 10 K.

About 66% of the ferric signal returned after 10 minutes of reaction and 70% after 2 hours of reaction. About 30% of the heme Fe was lost after the peroxide oxidation under this condition

(Figure 4.3). This is consistent with the easy loss of the *b*-type heme cofactor in this protein. The fact that the 280 and 405 nm absorption did not change suggest that the protein was not degraded under these conditions.

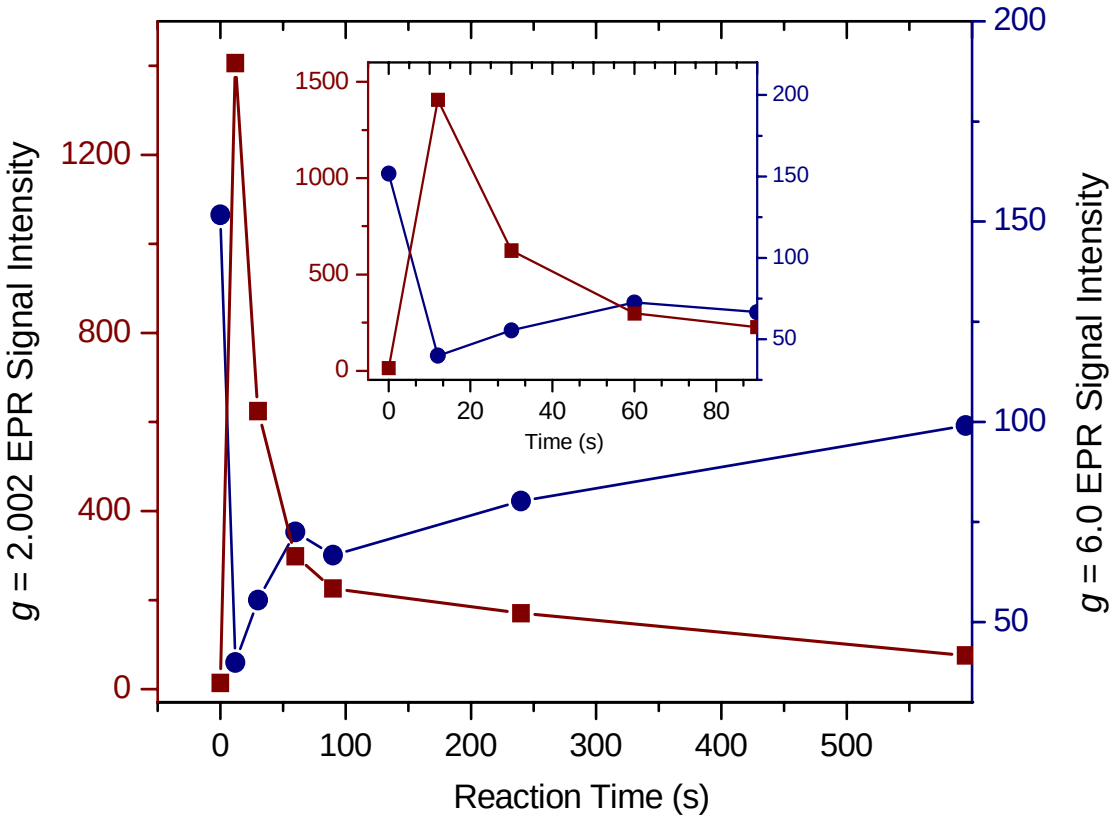

Figure 4.3. EPR signal amplitude as a function of reaction time for the $g = 2$ (wine colored trace, ■) and $g = 6$ (navy, ●), respectively. The inset is a blow up for the first 90 s of the reaction that shows the intermediate is formed concomitant with the oxidation of the ferric heme of the enzyme.

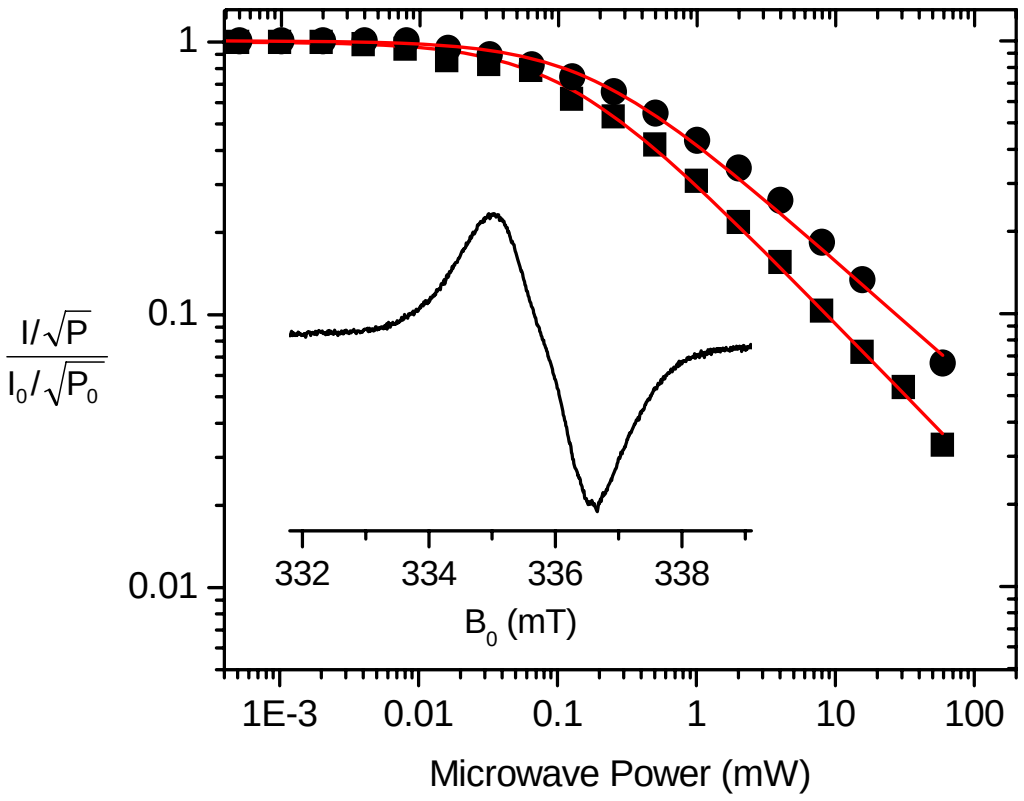

Figure 4.4. The relaxation properties of the $g = 2$ free radical. The power saturation behavior of the 10 K (■) and 100 K (●) and the fit to equation 4.1 are shown in the logarithmic scale, where I represents EPR signal intensity (amplitude in this case) and P represents microwave power. The inset is a spectrum of the radical measured at 10 K.

The microwave power saturation parameter of $g = 2.002$ EPR signal is 0.11 mW at 10 K, and 0.16 mW at 100 K, respectively (Figure 4.4). Using the $P_{1/2}$ values and the Fe–tyrosyl radical distances of mouse, *E. coli*, and *M. tuberculosis* ribonucleotide reductase enzymes (3.5 – 7.5 Å) as the comparing system (*315, 320, 321*), the greater value of the $P_{1/2}$ value at 10 K suggests that the radical is located near the active site. The relatively small $P_{1/2}$ value at 100 K suggests that the radical harboring residue has a great degree of conformational flexibility. Based on the temperature-dependence and the relaxation properties, this free radical species is not spin-

coupled with the iron ion. The radical does not reside in the porphyrin ring. It is an amino acid residue-based radical near the heme cofactor, presumably derived from the transfer of the porphyrin radical of Cpd I.

To explicitly detect the formal oxidation state of the iron ion, Mössbauer spectroscopy was employed to characterize the peroxide oxidation reaction of TDO. At 4.2 K, the resting state of the protein shows a single six-line magnetic pattern (Figure 4.5A). The simulation overlaid on the data (solid line) is calculated for an $S = 5/2$ iron site with $\delta = 0.42(1)$ mm/s, $\Delta E_Q = 1.46(1)$ mm/s, $E/D = 0.01$, and $A_{iso} = 195$ G. The standard errors indicated in the parenthesis were obtained from multiple repeating experiments. These values are indicative of high-spin ferric heme (*322*). In another set of samples, protein solution was treated with 10 mM hydrogen peroxide (six equivalents of TDO) and frozen after 20 s. The Mössbauer spectrum of this sample at 4.2 K (Figure 4.5B) is composed of four species. Figure 4.5C shows the difference spectrum of B - 0.25A. This spectrum is composed of a six-line ferric heme species and three overlapping doublets. The six-line magnetic pattern accounts for 25% of the iron in the treated sample. Combined with the EPR data, the species is decayed ferryl intermediates, however, simulations of the Mössbauer spectrum are insensitive to this small change in E/D. The fit to the three doublets (solid lines) gives Fe species of: (1) $\delta = 0.05(2)$, $\Delta E_Q = 1.76(2)$, 33%, (2) $\delta = 0.350$, $\Delta E_Q = 0.703$, 17% (3) $\delta = 0.585$, $\Delta E_Q = 1.5$, 25%. Species 1 is an authentic Fe(IV)=O heme species ($S = 1$). Since an uncoupled protein radical was also detected by EPR spectroscopy, this species is assigned to a Cpd ES intermediate of the enzyme. Other than the protein-based radical, the physical and chemical properties of the Fe center in Cpd ES and Cpd II are identical (*323*). The parameter range of isomer shift for Cpd II or Cpd ES heme species is 0 - 0.11 mm/s. The

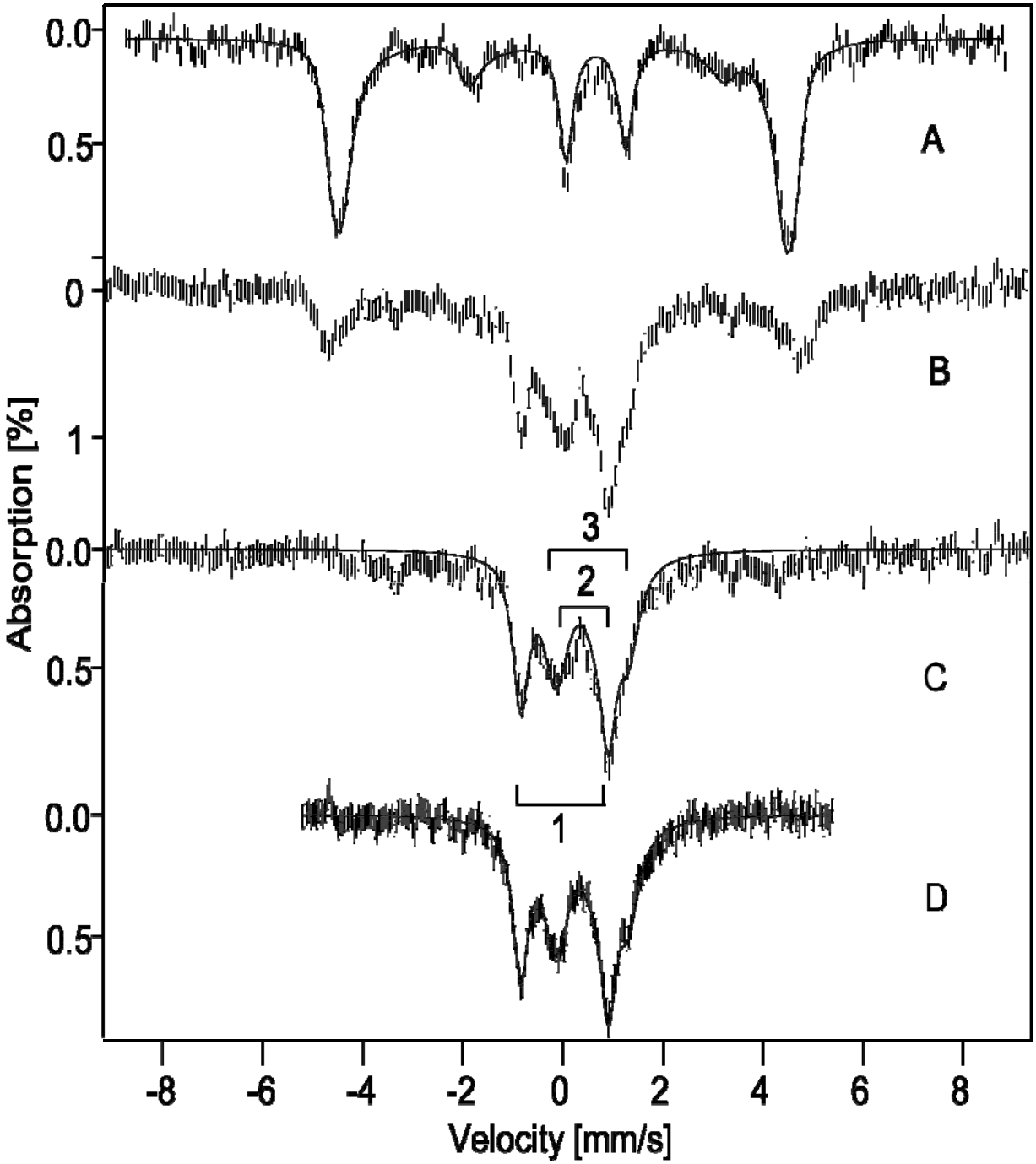

Figure 4.5. Mössbauer spectra of TDO at 4.2 K. (A) the protein in the resting state (B) the protein treated with hydrogen peroxide and. Trace C a difference spectrum (B) - 0.25(A). (D) is same as (C) except for sample temperatures of 100 K.

TDO intermediate's value is well within this range. The remaining two species appear to be degradation products of the reaction. Species 2 has parameters typical of high-spin ferric hemes, and the diamagnetic doublet indicates that the hemes are forming μ-oxo bridges (*324*). Species 3 is indicative of non-heme Fe(III) oxide formation, presumably due to loss of Fe from heme. The positions of the lines in the spectrum do not significantly change at higher temperature (Figure 4.5D). Thus, the addition of H_2O_2 resulted in a total of 42% loss of the heme and Fe from TDO and generated 58% of Fe intermediates in the Mössbauer sample holder. This ratio is higher than that of the EPR experiments (42 vs 30%), presumable due to the 11.5-fold greater concentration of protein. Similar results were observed in two other repeating Mössbauer samples.

The unusual quadrupole splitting of 1.76(2) mm/s of this ferryl intermediate is unique. Recent experimental and density functional theory calculation evidence have indicated that ΔE_Q is a sensitive indicator of the protonation state of the oxyferryl species and the length of the Fe(IV)-oxygen bond. The theoretical and experimental parameter range for a protonated Fe(IV)OH species is 2.0 – 2.5 mm/s and for unprotonated Fe(IV)=O is 1.0 – 1.62 mm/s (*323, 325-327*). The quadrupole splitting parameter of the ferryl intermediate in TDO is slightly greater than that of any other known Fe(IV)=O species (< 1.62 mm/s). On the other hand, it is significantly smaller than those of the protonated Fe(IV)-OH species (> 2.0 mm/s) (*326*). Thus, the parameters of the TDO Cpd ES species are not consistent with the values of a protonated Fe(IV)-OH heme species recently observed in several hemoproteins (*323, 325-327*).

To probe the origin of this unique Mössbauer quadrupole splitting, density functional theory (DFT) calculations were performed on eleven structural models (Table 4.1). Since the iron equatorial ligand heme in TDO is the same as found with other heme proteins that display

Table 4.1. Results of various models for TDO ferryl species 1[a]

	Model	R_{FeO} (Å)	ΔE_Q (mm/s)	δ_{Fe} (mm/s)
Expt			1.76	0.05
1A	$Fe^{IV}(Por)^{2-}(His)^0(O)^{2-}$	1.654	1.54	0.14
1B	twisted His	1.648	1.97	0.13
2A	$Fe^{IV}(Por)^{2-}$ $(His)^0(OH)^{1-}$	1.799	3.02	0.08
2B	twisted His	1.795	3.19	0.11
3A	$Fe^{IV}(Por)^{2-}$ $(His)^0(O\cdots HB)^{2-}$	1.663	**1.78**	0.12
3B	twisted His	1.657	2.20	0.11
4A	$Fe^{IV}(Por)^{2-}$ $(His\cdots H_2O)^0(O)^{2-}$	1.656	1.44	0.14
4B	twisted His	1.646	2.14	0.12
5A	$Fe^{IV}(Por)^{2-}$ $(His\cdots H_2O)^0(O\cdots HB)^{2-}$	1.665	1.66	0.11
5B	twisted His	1.660	2.11	0.11
6A	$Fe^{IV}(Por)^{2-}$ $(His)^0(OH\cdots HB)^{1-}$	1.792	3.07	0.10

[a] HB represents the Ser124-Gly125 residues hydrogen bonded to the oxo.

"normal" Mössbauer ΔE_Q values for Fe^{IV}=O species, these structural models were used to evaluate the structural contributions that can directly affect the iron axial ligands: 1) protonation of the oxo group, 2) hydrogen bonding to the oxo group, 3) hydrogen bonding to the proximal His, and 4) conformation of the proximal His. All the models were generated on the basis of the x-ray crystal structure of the substrate-free TDO (PDB ID: 2NW7), the same condition as in this

work. Geometries of these structural models were optimized (see Table 4.1 for the optimized coordinates) with the terminal atoms fixed at the x-ray crystal structure positions to mimic the protein environment effect, using the previous method for other oxoferryl species (*328*). Both the Mössbauer quadrupole splittings and isomer shifts for these models were calculated using the DFT method that enabled accurate predictions of these two properties in various iron proteins and models covering all iron spin states and coordination states (*328-332*).

As shown in Table 4.1, the predicted Mössbauer isomer shifts of these models are all close to the experimental value with no significant difference, indicating its insensitivity to the secondary structural changes along the axial positions. In contrast, the predicted Mössbauer quadrupole splittings display a large range from 1.44 mm/s to 3.19 mm/s, suggesting its role as a sensitive structural probe. Model **1A** was first evaluated as a prototype oxoferryl species for heme proteins with an axial His ligand and indeed, the predicted ΔE_Q value of 1.54 mm/s is very similar to 1.55 mm/s for cytochrome *c* peroxidase compound ES, 1.59 mm/s for Japanese radish peroxidase Cpd II, or 1.61 mm/s for horse radish peroxidase Cpd II (*333*). But clearly, the deviation from the TDO experiment indicates that this model is insufficient. We then evaluated other structural models, including the effect of the protonation of the oxo group as well as three other effects along the axial ligands based on the examination of the x-ray structures of TDO: 1) the His ligand in the substrate-free TDO structure (PDB ID: 2NW7) is twisted from a normal perpendicular position with respect to the heme ring; 2) the Ser124-Gly125 residues are so close that the amide proton is within hydrogen bonding distance (H…oxo is ca. 2.2 Å), see Figure 4.6) the proximal His group has a water molecule hydrogen bonded to the Nδ position in the substrate-bound TDO structure (PDB ID: 2NW8). Compared to 1A, the proximal His in 1B was

fixed in the twisted conformation as found in the TDO x-ray structure, and this conformation effect was also evaluated for other structural models discussed below. This kind of twisted conformation of course decreases the symmetry of the iron environment, resulting in the increase of the ΔE_Q value. But compared to 1A, this conformation effect in 1B overestimates ΔE_Q, suggesting that this is not a good model. In fact, none of the twisted His models (Table 4.1) gave good ΔE_Q predictions, so this twisted conformation is likely an artifact of the low resolution of this crystal structure (2.7 Å). To compare with the unprotonated FeIV=O models 1A and 1B, the protonated 2A and 2B models were used, which cause the largest errors in the predicted ΔE_Q values. This clearly indicates that such models are highly unlikely. Interestingly, by incorporation of the nearby hydrogen bonding residues Ser-Gly (these two residues are fixed at their X-ray positions except for the peptide bond atoms CONH, which are allowed to be optimized), the predicted ΔE_Q value of 1.78 mm/s for 3A is almost identical to the experimental measurement of 1.76 mm/s. This indicates that the unique Mössbauer quadrupole splitting of the TDO ferryl species is most probably a consequence of the unique active site environment of this hydrogen bonding that is not present in other heme proteins displaying normal Mössbauer quadrupole splittings. Models 4 and 5 were used to investigate another effect along the iron axial ligands, the effect of the hydrogen bonding to the proximal His, compared to Models 1 and 3. It can be seen from Table 4.1 that such effect generally decreases ΔE_Q by ~0.1 mm/s, which is very mild.

The best calculation of these hydrogen bonded His models is again the one (**5A**) that has the unique Ser-Gly hydrogen bond, with 1.66 mm/s, which is only second to the agreement between that for **3A** and experiment. Since the effect of a hydrogen bond to the oxo atom in ferryl species

was not reported before, we also investigated **6A**, which has this unique hydrogen bond with a protonated Fe^{IV}=O species, in addition to above investigated unprotonated ones: **3A** and **5A**, with and without a proximal His hydrogen bond, respectively. However, it again has the largest error of the predicted ΔE_Q value (Table 4.1) as with other protonated models (**2A** and **2B**), precluding its possibility as the TDO ferryl species. These results also suggest that the Mössbauer quadrupole splitting of the ferryl species has the following trend: unprotonated Fe^{IV}=O < hydrogen bonded Fe^{IV}=O < protonated Fe^{IV}=O.

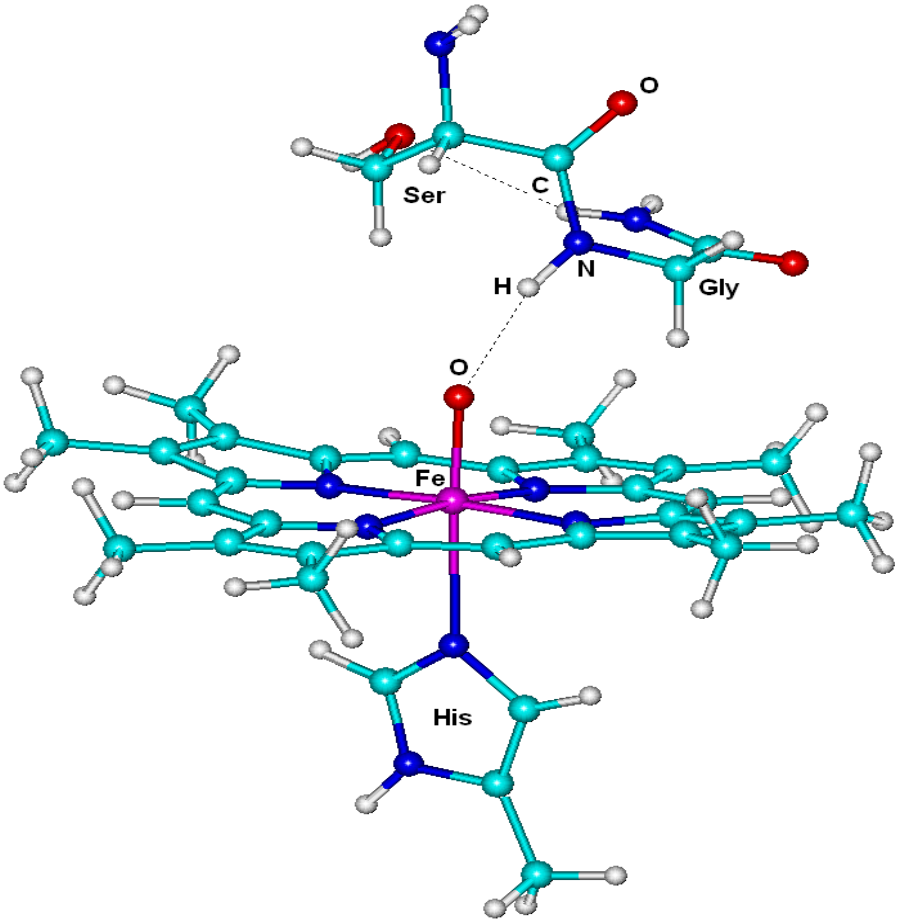

Figure 4.6. The structural model (3A) that yields the best predictions of the Mössbauer properties for the TDO ferryl species 1.

The present work suggests that the formation of ferryl intermediates upon oxidation by H_2O_2 is a general nature of TDO. The spectroscopic detection of the ferryl intermediate in TDO appears to favor the Criegee-type rearangment mechanism. However, it does not exclude the possibility that the O_2-mediated catalytic cycle proceeds through a different path, e.g. the dioxetane mechanism (Scheme 4.3). If the Cpd I intermediate is indeed formed in the catalytic cycle with dioxygen as the oxidant, its formation mechanism must differ from that of Scheme 4.2 because the ferrous ion and O_2 would give rise to an $Fe(III)O_2^{\bullet-}$ species instead of an Fe(III)OOH intermediate. Subsequent attack of L-Trp by the presumed $Fe(III)O_2^{\bullet-}$ species may require assistance of an active base catalyst. In the absence of such a base catalyst, a cationic radical would be formed on the enzyme-bound L-Trp. The formation of Cpd I is then ascribed to the O-O bond cleavage the Fe(III)-O-O$^-$ substrate moiety. The presumed Cpd I then attacks the oxazine of the L-Trp intermediate to insert the second oxygen.

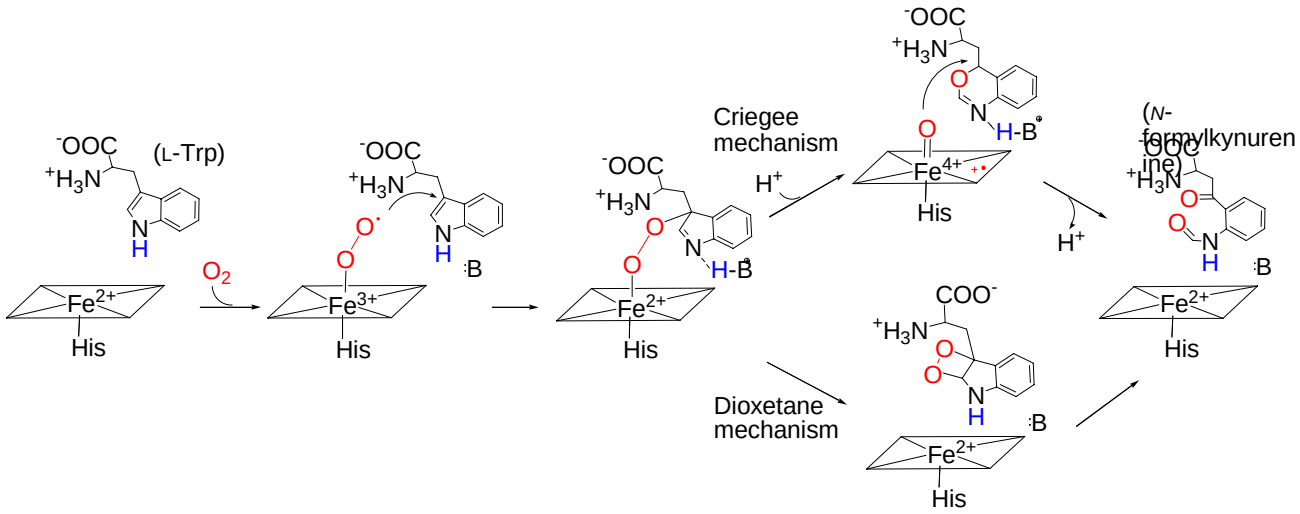

Scheme 4.3. Two parallel paths in reaction of L-Trp with O_2 catalyzed by reduced TDO which are under investigation.

4.4 Materials and Methods

Preparation of TDO — The construction of the heteroexpression plasmid encoding full-length *Ralstonia metallidurans* TDO has been described elsewhere (*262, 263*). The ^{56}Fe-containing TDO was prepared by growing the *E. coli* culture with LB medium supplemented with δ-aminolevulinic acid and ammonium ferrous sulfate prior to induction. Low-speed centrifugation was used in the protein purification to avoid loss of the heme Fe prosthetic group. TDO was obtained by using a 80 ml HiLoad nickel-affinity column and a Superdex 200 gel-filtration column on an ÅKTA FPLC system. The purified enzyme has a up to 62% of heme Fe occupancy based on the determination of protein concentration and Fe-content using inductively coupled plasma optical emission spectroscopy and electron paramagnetic resonance (EPR) spectroscopy. The optical absorption spectrum of the TDO enzyme used in this work typically displays a $405_{nm}/280_{nm}$ ratio greater than 1.4.

The ^{57}Fe-enriched TDO was obtained by growing cell culture with metal-depleted medium supplemented with ^{57}Fe. The ^{57}Fe stock solution was prepared by dissolving the ^{57}Fe-enriched metal foil (95.38% ^{57}Fe-enrichment) in concentrated sulfuric acid under O_2-free condition. The culture medium was forced through a Chelex-100 column prior to the addition of ^{57}Fe at the final concentration of 35uM.

UV-Vis spectroscopy — All TDO samples were prepared in 50 mM Tris-HCl pH 7.4, containing 10% glycerol or 100mM potassium phosphate buffer pH7.0. The absorption spectra were obtained with an Agilent 8453 UV-Vis spectrophotometer with ChemStation A09.01.76 software at room temperature.

EPR spectroscopy — EPR samples were made in reaction vials, transferred to EPR tubes and quickly frozen in cold isopentane (-140 °C) or liquid nitrogen after the desired reaction time. Typically ten EPR samples with 0.15 – 0.50 mM TDO were made in each set of experiments with 1 – 8 equivalents of peroxide or *meta*-chloroperoxybenzoic acid (*m*-CPBA) in different experiments, and multiple sets of experiments were conducted to optimize the formation of reactive intermediates. X-band EPR first derivative spectra were recorded in perpendicular mode on a Bruker EMX spectrometer at 100-kHz modulation frequency using a 4119HS high-sensitivity resonator. The EPR measurement temperature was maintained with an ESR910 liquid helium cryostat, LLT650/13 coolant transfer tube, Oxford ITC503S and Bruker ER4131VT temperature controllers. Spin concentration was determined by double integration of the sample spectrum obtained under low microwave power conditions and comparing the resulting intensity to that of a copper standard (0.5 mM $CuSO_4$, 5 mM EDTA) obtained under identical conditions.

The EPR relaxation property of the free radical at different temperatures was analyzed from the EPR spectra obtained with microwave power added in triplets of dB. At each given temperature, sixteen EPR spectra were recorded within 0.002 – 200 mW of microwave power. The values of half-saturation parameter ($P_{1/2}$) were obtained by fitting the data according to Eq 3.1:

$$I \propto 1/(1 + P/P_{1/2})^{b/2}$$

[eq 3.1]

where I is the EPR signal amplitude, b is an inhomogeneous broadening parameter, and P is microwave power.

Mössbauer spectroscopy — The Mössbauer samples were prepared from 1.72 mM TDO (70% $^{57}Fe/^{56}Fe$ ratio) reacting with either six or eight equivalents of peroxide and frozen in liquid nitrogen. The total reaction time for the intermediate samples was about 28 s to 50 s. Mössbauer spectra were recorded on a constant acceleration instrument with an available temperature range of 1.5 to 200 K. Isomer shifts are reported relative to Fe metal at 298 K. Least-square fitting of the spectra was performed with the WMOSS software package (WEB Research, Edina, MN). The low-temperature Mössbauer spectra of resting TDO were fit with the standard spin Hamiltonian:

$$H = g\beta B \cdot S + D[S_z^2 - S(S+1)/3] + E(S_x^2 - S_y^2) + A_{iso}(S \cdot I) - g_n b_n B \cdot I + (eQV_{zz}/12)\,[3I_z^2 - I(I+1) + \eta(I_x^2 - I_y^2)]$$

[eq 3.2]

4.5 Acknowledgements

This work is supported by the National Institutes of Health grants GM069618 (to TPB), GM077387 (to MPH), and GM085774 (to YZ), and NSF grants MCB 843537 (to AL) and EPSCoR award OIA-0556308 (to YZ). RF acknowledges a fellowship support from the Molecular Basis of Disease (MBD) program of GSU. YZ is also grateful to the Mississippi Center for Supercomputing Research and the USM Vislab for the generous use of the computing facilities.

CHAPTER 5

REVISITING THE MECHANISM OF HYDROGEN PEROXIDE ACTIVATION OF OXIDIZED TDO

5.1 Introduction

TDO is catalytically active at ferrous form. Reducing reagents such as ascorbic acid and sodium hydrosulfite are used to reduce the oxidized form to ferrous form. It has long been known that H_2O_2 is capable of activating the ferric form of TDO, but its activation mechanism has not been thoroughly understood (*313, 334, 335*). Until recently, this activation has been attributed to the production of Fe(II) heme from Fe(III) (eq. 5.1) (*336, 337*).

$$Fe(III) + H_2O_2 \rightarrow Fe(II)\text{-}TDO \qquad \text{(eq. 5.1)}$$

This hypothesis (eq. 5.1) is largely based on the optical evidence that the Soret band of the ferric heme is shifted upon the peroxide oxidation as observed from 405 nm towards 432 nm, which is the wavelength for the ferrous heme. The redox potential of hydrogen peroxide is around 650 mV at pH 7 (*338*), which is substantially higher than the 150 mV of heme moiety in TDO. Thus, it is difficult to understand why the Fe(III) ion becomes reduced after an oxidation reaction. One possibility is that the ferric iron is oxidized to an Fe(IV)=O species by reacting with H_2O_2. Ferryl species is a strong oxidizing species in nature and capable of withdrawing two electrons to reduce Fe(IV)=O and generate a Fe(II) ion subsequently. If so, the peroxide activation mechanism, which has been repeatedly documented and cited, deserves a careful investigation and reconsideration.

5.2 Results and Discussion

Overexpression and purification of TDO — The study of the TDO/ IDO chemical mechanism has been hampered for a long time due to a technical problem. It is difficult to obtain the pure and active enzyme with a great degree of heme Fe occupancy. The *b*-type heme Fe cofactor is located near the protein surface, and its association with the protein mainly depends on the axial histidine ligand. The heme Fe cofactor is often easily lost during protein purification and manipulation. Unfortunately, the cofactor reconstitution has not been feasible for TDO. This does not seem to be a problem for crystallization, presumably due to the fact that the holoenzyme fraction appears to fold correctly and crystallize out from the protein portion which, in a few cases, does not contain a cofactor (apoenzyme) in a few cases. The low heme occupancy is, however, a significant problem in the biochemical and especially mechanistic studies of these enzymes. The expression and purification strategy reported in (*110*) (*128*) originally obtained TDO with less than 10% heme occupancy. In an experiment, we incorporated ferrous ammonium sulfate during expression and omitted any reducing reagent and substrate during the purification. The heme occupancy in the *Ralstonia metallidurans* TDO in our preparation was up to 70% with the ratio of the absorbance of 405 nm to 280 nm more than 1.5:1.

UV-Vis spectra of TDO — The purified as-isolated TDO exhibits UV-visable absorbance characteristics of a ferric heme protein with Soret band at 405 nm. The addition of the substrate, L-Trp, to ferric TDO resulted in a shift of Soret band from 405 nm to 406 nm with a slight decrease in absorbance. This gives an indication of the formation of low-spin ferric TDO-L-Trp complex or a conformational change in the protein which modifies the surrounding environment of the heme group. Carbon monoxide (CO) is a strong field ligand for ferrous heme and forms

CO-ferrous complex with a shifted Soret band. When bubbling with CO, the spectrum of ferric TDO did not change regardless of L-Trp. When ferric TDO was reduced with sodium dithionite, the Soret band was shifted from 405 nm to 432 nm. Bubbling CO into the reduced TDO in the presence of L-Trp resulted in the formation of a ferrous TDO-CO-L-Trp complex with absorption peaks at 421 nm, 536 nm and 561 nm. In contrast, ferric TDO have small fractions of 541 nm and 576 nm in visible region (Table 5.1).

Table 5.1. UV-Vis absorption of TDO in the Soret band and visible regions.

	Soret band (nm)	$\varepsilon_{\text{Soret band}}$ (mM^{-1} cm^{-1})	Visible region (nm)
Ferric TDO	405	130	505; 541; 576; 632
Ferric TDO + L-Trp	406	127	505; 541; 576; 632
Ferrous TDO	432	104	554; 588
Ferrous TDO + L-Trp	432	89	553; 584; 657
Ferrous TDO + CO + L-Trp	421	123	536; 561

Effect of the concentration of H_2O_2 on the enzymatic activity of ferric TDO upon peroxide activation — The effect of the concentration of H_2O_2 on the enzymatic activity of ferric TDO upon peroxide activation was examined and displayed in Figure 5.1. The enzymatic activity was monitored at the development UV-visiable absorbance at 321 nm corresponding to NFK product and normalized based on the maximal rate presented here. One and two equivalents of H_2O_2 over the concentration of ferric TDO induce 50% and 65% activity compared to the maximal

activation activity, while 6 equivalents of H_2O_2 cause 80% activity. Further increasing the concentrations of H_2O_2 only resulted in only a slight increase in enzyme activity. The hyperbolic activation curve indicates that a higher concentration of H_2O_2 does not contribute to further activation of the enzyme. TDO is a tetrameric protein in which heme cofactor is buried in the protein matrix. Therefore, a little excess H_2O_2 is required to access the active site efficiently for the activation of oxidized TDO.

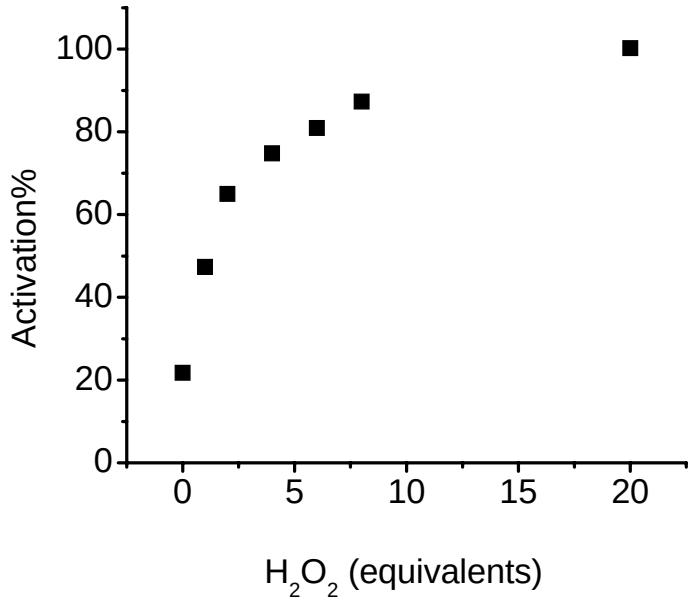

Figure 5.1. The effect of concentrations of H_2O_2 on the enzymatic activity of ferric TDO upon peroxide activation.

UV-Vis spectra of the ferric TDO upon reacting with hydrogen peroxide in the presence of L-Trp under anaerobic conditions — In order to specifically study the reaction of ferric TDO and H_2O_2, we examined the UV-Vis absorbance of the reaction under anaerobic conditions. All the buffer, stock solution and ferric TDO were vacuumed and refilled with argon in repeated cycles. As

shown in Figure 5.2, upon addition of 6 equivalents of H_2O_2 to ferric TDO in the presence of L-Trp, the Soret band of one third of the ferric TDO is shifted toward 432 nm which resembles that of the ferrous TDO. When the reaction was conducted in the presence of CO, an absorbance peak at 421 nm rather than 432 nm occurred (Figure 5.2B). The 421 nm species is similar to that observed in ferrous TDO and presumably ferrous TDO-CO-L-Trp complex corresponding to around one third ferric TDO conversion. This conversion is consistent with the observation in Figure 5.2A. In the absence of L-Trp, ferric TDO reacted with H_2O_2 does not generate the similar shift of the absorbance. These results suggest that the putative ferrous TDO was generated during the reaction of ferric TDO with H_2O_2 in the presence of L-Trp.

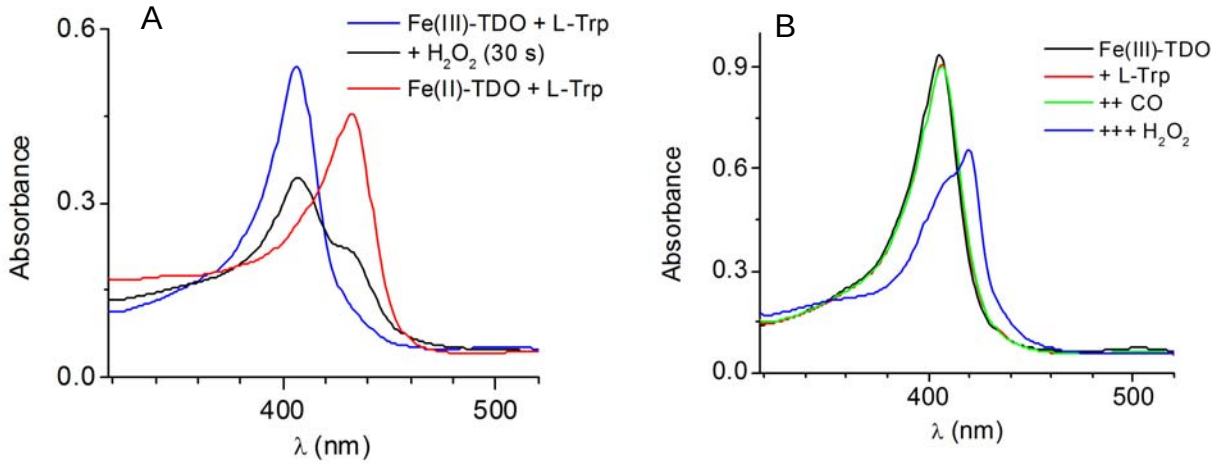

Figure 5.2. UV-Vis spectra of ferric TDO reacted with H_2O_2 in the presence of L-Trp. (A) Ferric TDO treated with 6 equivalents of H_2O_2 in the presence of 5 mM L-Trp and ferrous TDO in the presence of L-Trp. (B) Ferric TDO mixed with 5 mM L-Trp and bubbled with carbon monoxide, followed by adding 6 equivalents of H_2O_2.

Mössbauer spectroscopy characterization of the ferrous ion in the reaction of ferric TDO with H_2O_2 — Since the observation concerning optical absorption bands is not sufficient to identify a ferrous species, Mössbauer spectroscopy experiments were conducted to seek a conclusive

evidence of the formation of ferrous species in the reaction of ferric TDO with H_2O_2. Five parallel Mössbauer samples were prepared for comparison and analysis. Figure 5.3 shows the Mössbauer spectra of the ^{57}Fe-TDO obtained at 4.2 K with a magnetic field of 45 mT. The magnetic splitting pattern of spectrum A is characteristic of a ferric high-spin system with anisotropic magnetic hyperfine pattern, which coppresponds to the ferric ^{57}Fe-TDO. Figure 5.3B illustrates the Mössbauer spectrum of the ferric ^{57}Fe-TDO upon adding 10 equivalents of L-Trp followed by freezing in liquid nitrogen. Approximately 50% of the spectral area in spectrum B corresponds to a ferric low-spin ion, which suggests that around 50% of the high-spin ferric ion in the starting material is converted to the low-spin ferric ion.

In another set of experiments, ferrous ^{57}Fe-TDO was analyzed. The Mössbauer spectrum of ferrous ^{57}Fe-TDO upon adding 10 equivalents of L-Trp is shown in Figure 5.3C. The solid line is the simulation resembling the substrate-bound ferrous ^{57}Fe-TDO. The Mössbauer spectrum shows two doublets with ΔE_Q = 3.55 mm/s, δ = 1.00 mm/s and ΔE_Q = 2.55 mm/s, δ = 0.95 mm/s, respectively. The two species are present in a ratio close to 1:1, which suggests a typical high-spin ferrous heme is present with two conformations in the presence of L-Trp (more discussions in Chapter 6). Furthermore, upon bubbling CO into the substrate-bound ferrous ^{57}Fe-TDO under anaerobic conditions, a new component with ΔE_Q = 0.55 mm/s and δ = 0.27 mm/s occurs which results when 50% of both of the ferrous hemes are converted to a ferrous-CO-L-Trp adduct. This spectrum is shown in Figure 5.3D.

Figure 5.3E displays the Mössbauer spectra of the reaction of ferric TDO with H_2O_2 in the presence of L-Trp and CO. Mössbauer spectroscopy has around 5 % detectable limitation. In

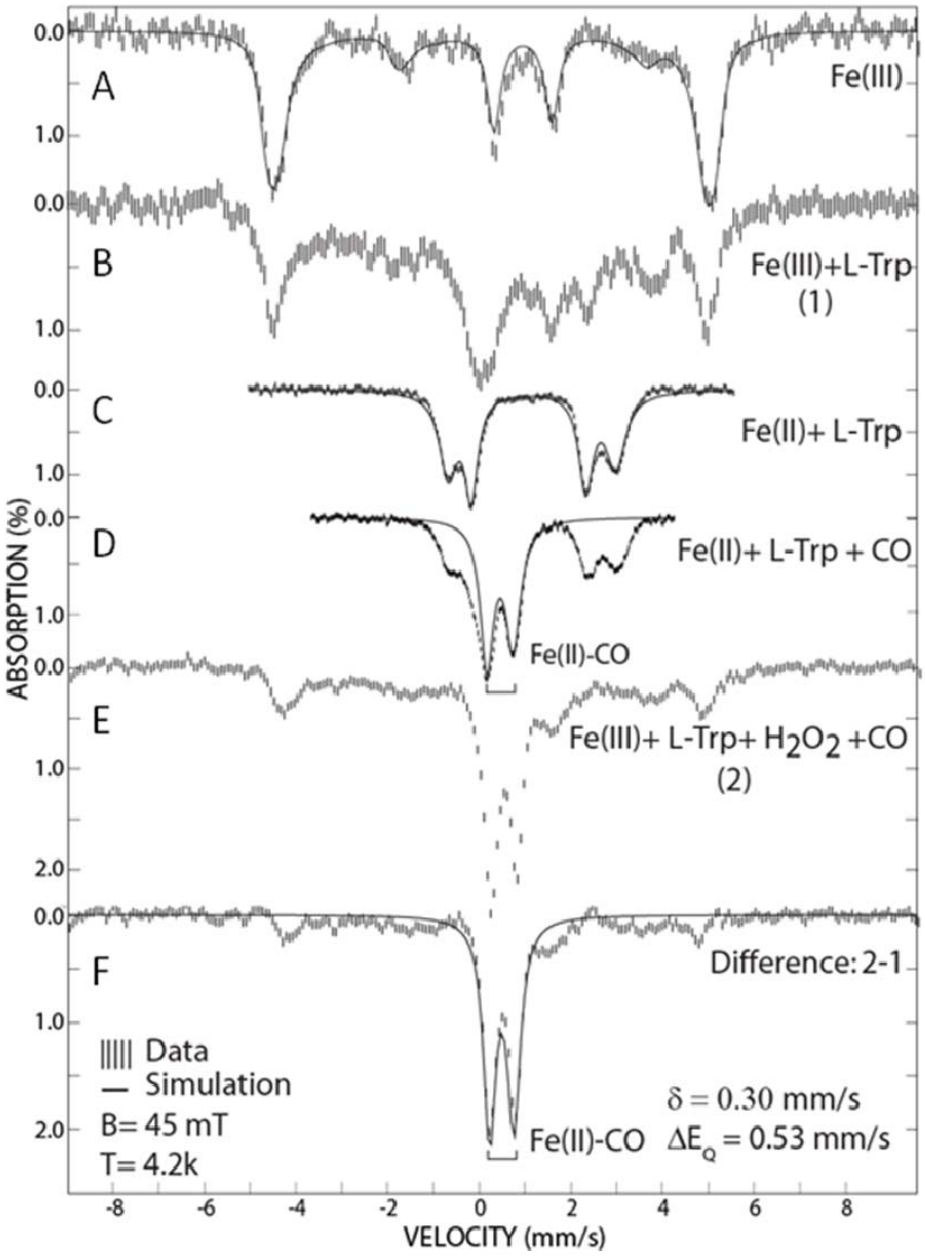

Figure 5.3. Mössbauer spectra of the ^{57}Fe-TDO mixtures. (A) Ferric ^{57}Fe-TDO; (B) Ferric ^{57}Fe-TDO mixed with 10 equivalents of L-Trp; (C) Ferrous ^{57}Fe-TDO mixed with 10 equivalents of L-Trp; (D) Ferrous ^{57}Fe-TDO mixed with 10 equivalents of L-Trp followed by bubbling with CO; (E) Ferric ^{57}Fe-TDO mixed with 10 equivalents of L-Trp and bubbled with CO, followed by adding 2 equivalents of H_2O_2; (F) Difference spectrum between spectrum E and spectrum B. The spectra were recorded at 4.2 K with a magnetic field at 45 mT.

order to stabilize and maximize the putative ferrous heme, CO was introduced into the reaction mixture. Upon adding 10 equivalents of L-Trp, the substrate-bound ferric ^{57}Fe-TDO was bubbling with CO followed by adding 2 equivalents of H_2O_2. A new doublet species occurs which arises from the starting material and is mixed with the remaining ferric high-spin signal. The solid line in Figure 5.3F shows the simulation of the difference spectrum in which spectrum B is subtracted from spectrum E. The new doublet signal has the parameters with $\Delta E_Q = 0.53$ mm/s and $\delta = 0.30$ mm/s. In comparision with the spectrum of D, the new doublet is identical to that observed for ferrous TDO-CO-L-Trp complex and assigned as a ferrous-CO-L-Trp complex. These results demonstrate that a ferrous species is generated during the reaction of ferric TDO and H_2O_2 in the presence of L-Trp, which also confirms the assignment of 432 nm species as a ferrous heme in the optical observation in Figure 5.2.

Effect of the concentration of L-Trp on reduction of ferric TDO — The effect of the concentration of L-Trp on the ferrous TDO formation in the peroxide activation reaction was examined under anaerobic conditions. Five μM ferric TDO were mixed with various concentrations of L-Trp. CO was introduced and allowed to equilibrate for 5 min before adding 6 equivalents of H_2O_2. Figure 5.4 shows the plot of the yield of ferrous TDO-CO-L-Trp complex obtained after reaction over the concentration of L-Trp. In the presence of 2 mM L-Trp, around 20% ferric TDO was converted to ferrous form, whereas 33% ferrous TDO formed when the contenctration of L-Trp was 6 mM. This is consistent with the quantitation resulting from spectral change of the optical data shown in Figure 5.2. These results suggest the peroxide reduction of ferric TDO is a L-Trp dependent process.

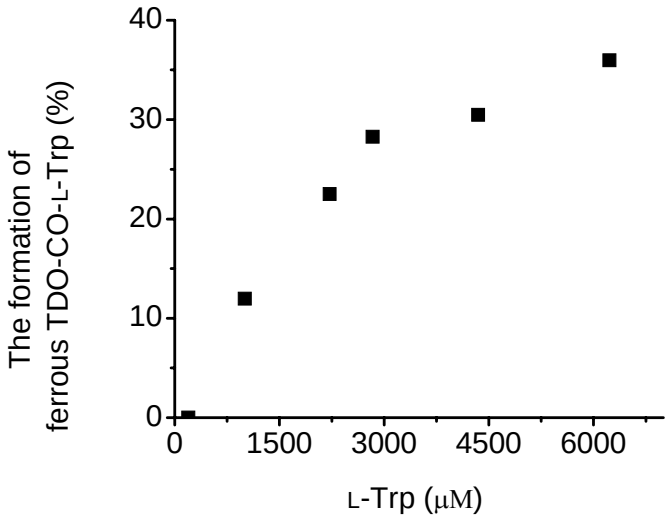

Figure 5.4. The formation of the ferrous-CO-L-Trp complex. Ferric TDO was treated with H_2O_2 in the presence of various concentrations of L-Trp in CO saturated buffer under anaerobic conditions.

Low-spin ferric hydroperoxide intermediate in the presence of H_2O_2 and L-Trp — The ferric TDO exhibits a typical high-spin ferric signal near g = 6 and g = 2 shown in Figure 5.5A. Upon addition of 10 equivalents of L-Trp and 6 equivalents of H_2O_2, the sample was frozen in liquid nitrogen in 30 s. A set of new low-spin ferric signals is observed in Figure 5.5C which contains two overlapping species with g = 2.487, 2.143, 1.891 and g = 2.467, 2.143, 1.898 with a ratio close to 1 : 2. The remaining high-spin ferric signal becomes much more axial than the original one. These g-values are similar to those previously observed in $CYP450_{Cam}$ with g = 2.55, 2.25, 1.88 using $HCOO^-$ as anionic ligand and g = 2.46, 2.25, 1.88 using CH_3COO^- or $CH_3CH_2COO^-$ as anionic ligand (*339*). Recent cryoradiolysis of oxy-ferrous complex has been utilized in heme-containing proteins to generate low-spin ferric hydroperoxide species including CYP450, HO, HRP and hemoglobin. The EPR signal of the low-spin hydrooperoxo ferric hemes exhibit a

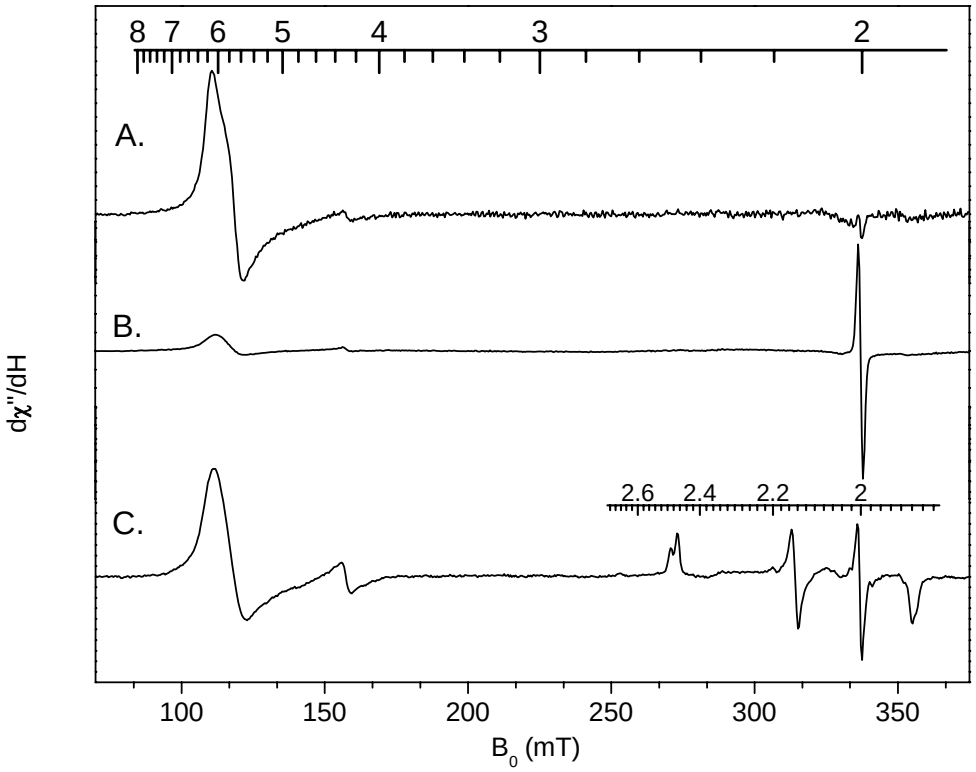

Figure 5.5. EPR spectra of ferric TDO reacted with H_2O_2 in the absence and presence of L-Trp. (A) 150 μM ferric TDO; (B) 150 μM ferric TDO mixed with 900 μM H_2O_2 at 30 s; (C) 150 μM ferric TDO mixed with 900 μM H_2O_2 and 1.5 mM L-Trp at 30 s. Experimental EPR spectra were recorded at 10 K with 1 mW microwave power at 9.4 GHz. An 8 G field modulation at 100 kHz was employed. Time constant, 40.960 ms; conversion constant, 81.920 ms and sweep time, 83.886 s.

range of the *g* values around 2.3-2.25, 2.2-2.14, and 1.94-1.97 (*300*). Thus, the low-spin ferric species here are assigned as ferric hydroperoxide intermediates of TDO during the peroxide activation reaction. The presence of two low-spin ferric species is consistent with the crystal structure of substrate-bound xcTDO, in which the active site water is involved in the formation of hydrogen bond network in two different scenarios. In one of the dimers, the water molecule forms a hydrogen bond with L-Trp while in the other dimer, it forms a hydrogen bond with the

active site histidine residue (His72) (*129*). The EPR spectra indicate that H_2O_2 displaces the active site water and generates a putative ferric hydroperoxide intermediate which maintains the similar hydrogen bond networks in the active site with either L-Trp or His72.

The putative ferric hydroperoxide species undergoes an O-O bond cleavage to generate a ferryl species. When ferric TDO reacts with H_2O_2 in the presence of L-Trp, two distinguished Soret bands are observed: one toward 432 nm is a ferrous TDO, while another one remains a ferric form. In chapter 4, ferryl species has been characterized using EPR and Mössbauer spectroscopy. These suggest that ferric TDO might utilize both of the manners to break down the O-O bond of the putative ferric hydroperoxide intermediate. The two possible manners are heterolytic cleavage and homolytic cleavage, in which heterolytic cleavage of O-O bond generates compound I or compound ES-like species and a water molecule whereas homolytic cleavage generates compound II-like species and a hydroxyl radical.

Effect of hydroxyurea on the catalytic activity of ferrous TDO — We probed the two manners of O-O bond cleavage of the putative ferric hydroperoxide intermediate by examining the effect of the potential radicals on the enzymatic activities. The protein radical in compound ES-like species is located in the nearby amino acid residues of the active site which do not migrate in the protein matrix. However, if ferric TDO also undergoes homolytic cleavage, a non-specifically located hydroxyl radical will be generated. Hydroxyl radicals are very reactive species and lead to the inactivation of the protein. A radical scavenger, hydroxyurea was introduced into the reaction to probe the potential radicals.

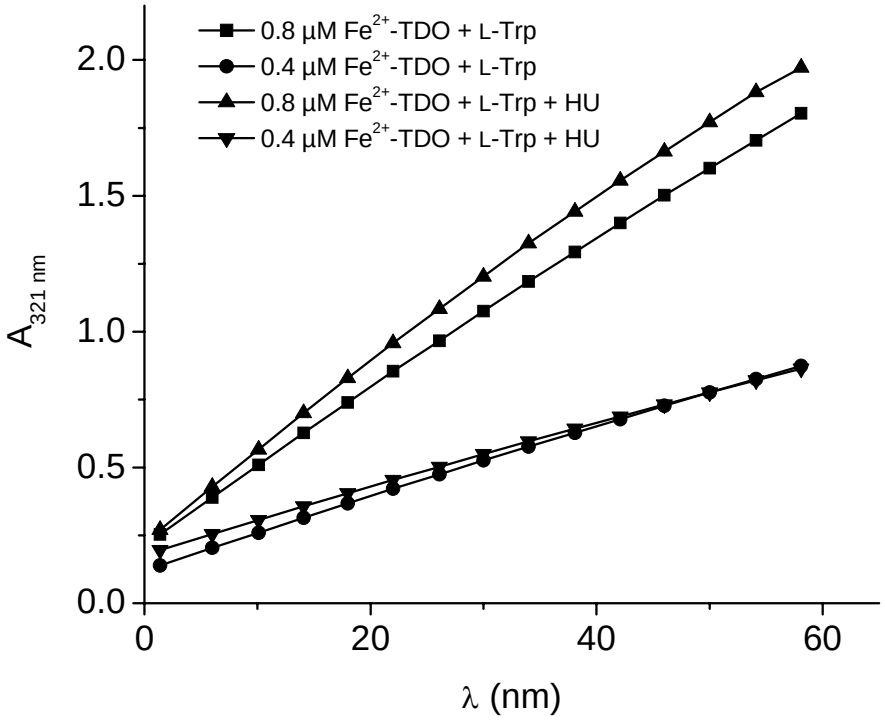

Figure 5.6. The effect of hydroxyurea on the enzymatic activity of ferrous TDO. Ferric TDO was treated with 2 equivalents of sodium dithionite and purged with argon for 15 min under anaerobic conditions. The reactions were conducted in O_2-saturated buffer containing 5 mM L-Trp in the absence or presence of hydroxyurea. 5 mM hydroxyurea is abbreviated as HU.

In order to rule out the influence of hydroxyurea on the normal catalytic cycle, the experiments were conducted using ferrous TDO as cofactor and dioxygen molecule as oxidant in the presence of hydroxyurea. Ferric TDO was reduced to ferrous form using 2 equivalents of sodium dithionite under anaerobic conditions. The reduced enzyme was 100-fold diluted into O_2-saturated buffer containing 5 mM L-Trp in the absence or presence of hydroxyurea to initiate the reaction. As shown in Figure 5.6, the reaction rates recorded as the developed absorbance at 321 nm in the presence or absence of hydroxyurea are similar with the enzyme concentration at either

0.4 μM or 0.8 μM. This indicates that hydroxyurea does not affect the normal O_2-driven dioxygenation. Thus, hydroxyurea can be used as a radical scavenger to specifically probe the peroxide activation reaction of ferric TDO.

Effect of the radical generated during the peroxide activation on the catalytic activity under aerobic conditions — The effect of the potential radical generated during the peroxide activation on the catalytic activity was investigated by designing three sets of experiments in which radical scavenger, hydroxyurea, was used. The reaction mixtures containing 0.45 μM ferric TDO and 2.7 μM H_2O_2 were initiated by adding 2 mM L-Trp. Before the initiation step, the reaction mixtures were incubated either in the presence or absence of 5 mM hydroxyurea for various times.

As shown in Figure 5.7, when ferric TDO was incubated with H_2O_2 for various times before the initiation by L-Trp, the catalytic rate decreased dramatically with increasing incubation time. After 100 s incubation with H_2O_2, ferric TDO lost more than 70% activity. A similar set of experiments were conducted with 5 mM hydroxyurea in the mixture for the incubation of ferric TDO with H_2O_2. The catalytic rate decreased much less compared with that in the absence of hydroxyurea. After 100 s incubation with H_2O_2 in the presence of 5 mM hydroxyurea, ferric TDO lost around 30% activity. In another set of experiments, hydroxyurea was included in the initiation step but not in the incubation of ferric TDO with H_2O_2. The plotted curve is similar to that in the absence of hydroxyurea.

These results suggest that the hydroxyurea might quench the potential reactive radical species generated during the reaction of ferric TDO with H_2O_2 and prevent enzyme inhibition. The

potential reactive radical is probably a hydroxyl radical arising from homolytic cleavage of O-O bond of the ferric hydroperoxide intermediate. After the activation, the addition of hydroxyurea had no effect on the enzyme activity compared with that in the absence of hydroxyurea. This is also consistent with the observation in Figure 5.1, in which the enzyme activity exhibits a hyperbolic change when the concentration of H_2O_2 increases. From the beginning, neither the presence nor absence of hydroxyurea affects reaction rate, suggesting that the activation of ferric TDO is not a radical dependent process.

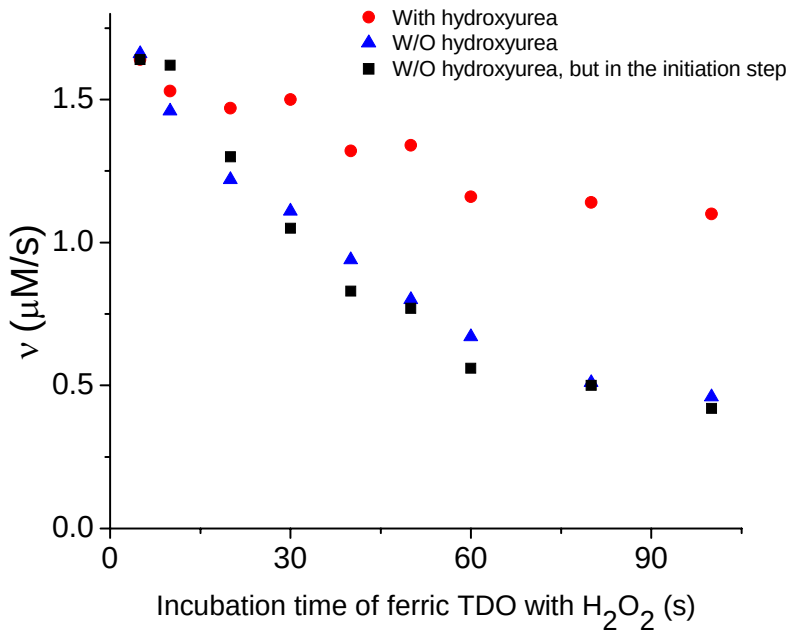

Figure 5.7. The effect of radical scavenger on the enzymatic activity of ferric TDO upon peroxide activation mixing with H_2O_2.

The catalytic relevance of the protein radical in the peroxide driven oxygenation reaction under anaerobic conditions — In Chapter 3 and 4, compound ES-like species was trapped during the

peroxide driven reaction of ferric TDO with H_2O_2 in the absence of L-Trp. This compound ES-like species must be generated via a heterolytic cleavage of O-O bond. The radical in compound ES-like species is located in the nearby amino acid residues of the active site. Protein radical generated during the reaction can be catalytic competent such as the tyrosyl radicals in PGHS and ribonucleotide reductase which are directly involved in the catalytic processes (*340*). The catalytic relevance of the protein radical species generated in the peroxide driven reaction using ferric TDO was also investigated.

A typical high-spin ferric EPR signal of ferric TDO was shown in Figure 5.5A. Figure 5.5B displays an intensive $g = 2$ signal upon adding H_2O_2 into ferric TDO in the absence of L-Trp, which was identified as a protein radical in chapter 4. Furthermore, ferric TDO was mixed with H_2O_2 in the same condition except for the presence of L-Trp. As shown in Figure 5.5C, the yield of the protein based radical upon mixing with L-Trp decreases dramatically and the high-spin ferric signal increases compared with that in spectrum B. This observation indicates that the protein radical is involved in a catalytic reaction.

In order to further clarify the catalytic competence of the protein radical in the peroxide driven oxygenation reaction, the experiment was conducted under anaerobic condition either in the presence or absence of hydroxyurea. As shown in Figure 5.8, 175 μM H_2O_2 was added stepwise to 5 μM ferric TDO in the presence of 5 mM L-Trp. After reaction, 152 μM NFK was generated using H_2O_2 as substrate and oxidant, which corresponds to around 87% conversion based on the estimated maximal product formation in which H_2O_2 is consumed. The ratio of the formation of NFK to the consumption of H_2O_2 can be normalized to 1:2. A set of parallel experiments was conducted in the presence of 10 mM hydroxyurea under the same conditions. After reaction, only

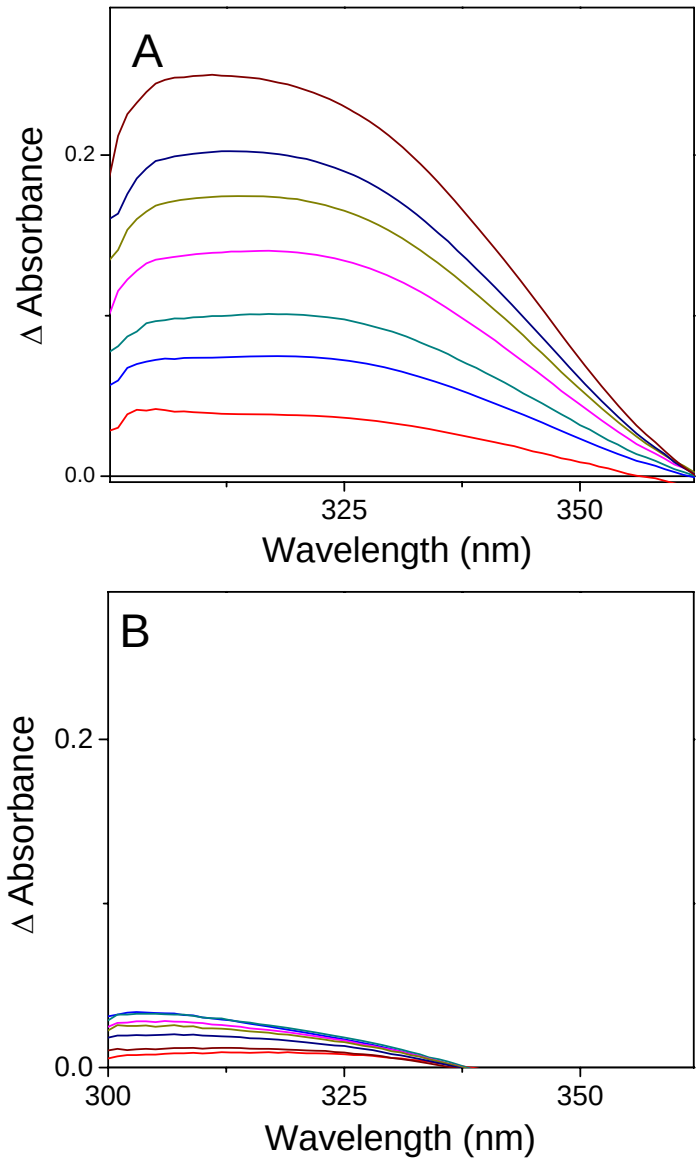

Figure 5.8. The difference spectra of 5 μM ferric TDO titrated with 35 equivalents of H_2O_2 containing 5 mM L-Trp in the absence of hydroxyurea (A); in the presence of 10 mM hydroxyurea (B).

less than 5% NFK was generated. The results clearly indicate that the protein radical is catalytically relevant in the peroxide driven reaction. In the presence of radical scavenger hydroxyurea, the catalytic active intermediate, compound ES-like species can not be generated or stabilized to fulfill the peroxide driven dioxygenation reaction.

Proposed mechanism for hydrogen peroxide activation of ferric TDO — Hydroperoxide has been frequently used in studying heme proteins such as in CYP450, in which H_2O_2 can provide both oxygen and electrons for an alternative way to bypass the requirement of a dioxygen molecule and reducing agents. In this alternative, so called peroxide shunt pathway, hydrogen peroxide binds to the ferric ion center and forms a ferric hydroperoxide intermediate.

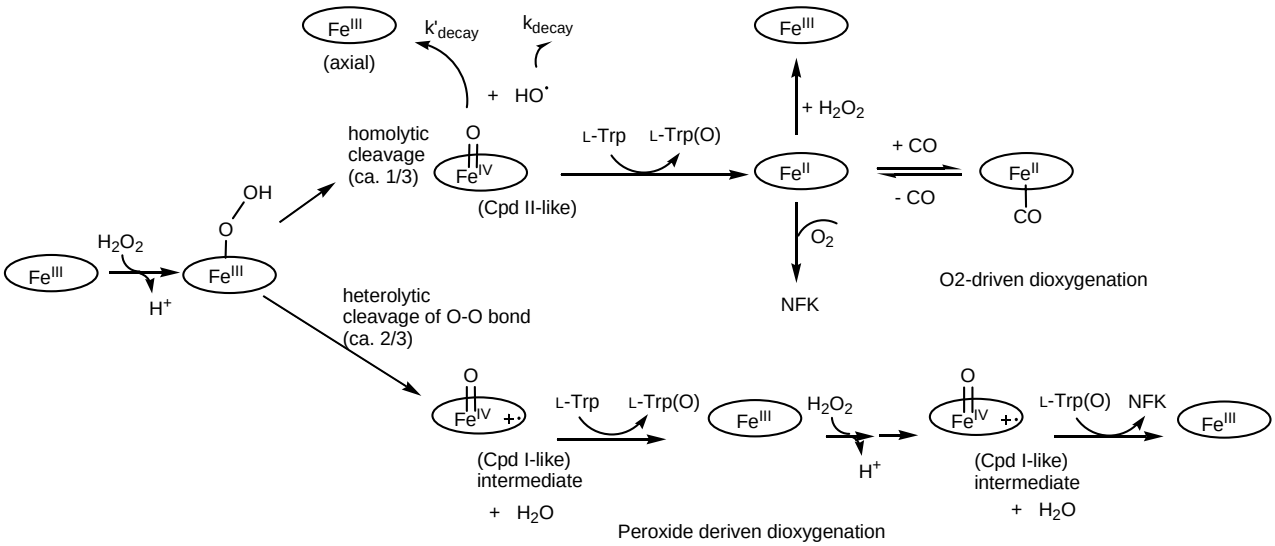

Scheme 5.1. The proposed mechanism of peroxide activation of ferric TDO.

In the presence of L-Trp, a set of low-spin ferric species is generated and proposed as a putative ferric hydroperoxide intermediate of TDO. In Chapter 4, the formation of compound ES-like species of ferric TDO reacted with H_2O_2 in the absence of L-Trp must undergo heterolytic cleavage of the ferric hydroperoxide intermediate. This compound ES-like species is catalytic

competent to generate NFK in the presence of L-Trp via peroxide driven oxygenation reaction and two-thirds of TDO remains in ferric form after reaction. On the other hand, upon peroxide activation of ferric TDO and H_2O_2, one-third of ferrous ion was observed in the presence of L-Trp and characterized by UV-Vis and Mössbauer spectroscopy. The formation of ferrous ion requires substrate; however, it is a one-electron reduction process during the peroxide activation. While compound ES-like species generated via a heterolytic cleavage is capable of inserting an oxygen atom into the substrate via a two-electron reduction process. Thus it must have a different mechanism in peroxide activation reaction, in which TDO has the possiblity to break down the O-O bond via a homolytic cleavage to generate a compound II-like species.

Mössbauer spectroscopy does not show a ferryl signal in the spectrum of ferric TDO treated with H_2O_2 in the presence of L-Trp. This demonstrates that the compound II-like species is catalytic competent, and able to provide two electrons simultaneously for a reduction. When the substrate for the oxygenation reaction is available, the peroxide activation is effective and H_2O_2 can be used as an activator to generate ferrous TDO. Thus, peroxide activation process should generate a catalytic competent intermediate, compound II-like species via homolytic cleavage of O-O bond of ferric hydroperoxide intermediate, followed by a substrate oxidation reaction to form a ferrous ion.

A possible mechanism is proposed for peroxide activation as illustrated in Scheme 5.1. In the initiate step, hydrogen peroxide binds to the high-spin ferric heme and displaces the active site water molecule to generate a ferric hydroperoxide intermediate. In the presence of substrate, L-Trp, this intermediate undergoes two manners of O-O bond cleavage, heterolytic and homolytic cleavage. Two-thirds of the enzyme goes through heterolytic cleavage in which a compound I-

like species is generated followed by one electron transfer from nearby amino acid to form a compound ES-like species. In the presence of L-Trp, the compound ES-like species is catalytically competent to perform peroxide driven dioxygenation reaction whereas in the absence of L-Trp, it is capable of performing catalase-like reaction as was discussed in Chapter 3 and 4. On the other hand, in the presence of L-Trp, another one-third of the enzyme undergoes a homolytic O-O bond cleavage, which generates a Fe(IV)=O intermediate, compound II-like species, and a hydroxyl radical. In contrast, Compound-II like species is capable of inserting one oxygen atom into L-Trp and reducing ferric TDO to ferrous form. When dioxygen is available, the active form of the ferrous enzyme enters the catalytic cycle to perform the O_2-driven dioxygenation reaction. Homolytic cleavage also generates a hydroxyl radical species which is reactive and non-specifically bound to the enzyme. This species explains the inhibition of ferric TDO during the prolonged peroxide activation.

It has been known that most heme-containing proteins undergo heterolytic cleavage to generate compound I or compound ES species as a catalytic competent species (*4, 341, 342*). However, it has also been reported that the CYP450 catalyze both heterolytic and homolytic cleavages to break down O-O bond when using H_2O_2 and peroxyacids (*343, 344*). In sperm whale myoglobin, both O-O bond cleavages have been observed (*345*).

Previous studies suggest that the heterolytic cleavage of O-O is subject to a general acid-base catalyst (*346-348*). The homolytic cleavage is relatively insensitive to general acid or base catalysis (*348*). In peroxidase, the conserved histidine and arginine residues in the active site facilitate the heterolytic O-O bond cleavage by pull-push effect. In this mechanism, the histidine residue facilitates the transfer of electron from the porphyrin ring to the oxygen atom and the

proton to the exiting oxygen atom of ferric hydroperoxide intermediate to facilitate the heterolytic O-O bond cleavage (*38, 39*).

In CYP450, although the thiolate ligand with strong electron donation features favors heterolytic cleavage of the O-O bond of the ferric hydroperoxide intermediate (*4*), it can also catalyze homolytic cleavage. It has been suggested that the hydrophobic environment of active site enhances homolytic cleavage. When the active site amino acid of Glu318 or Thr319 in CYP450 was mutated to hydrophobic amino acid residues such as Val and Ala, the portion of homolytic cleavage increased (*349*).

It appears that the nature of substrate, the active site environment, and the heme conformation are involved in the O-O bond cleavage. The active site pocket of TDO is surrounded by mostly hydrophobic amino acids. There is one active site histidine residue in the substrate binding pocket. Since TDO undergoes heterolytic cleavage and homolytic cleavage with a ratio close to 2:1, heterolytic cleavage is favored. It should be noticed that the formation of two overlapping ferric hydroperoxide intermediate at g = 2.487, 2.143, 1.891 and g = 2.467, 2.143, 1.898 has a ratio close to 1:2, which is consistent with two conformations of the active site hydrogen bonding network.The one-third portion at g = 2.487, 2.143, 1.891 species corresponds to the conformation in which the ferric hydroperoxide intermediate forms a hydrogen bond with the NH group of L-Trp, in which case the electron rich indole ring facilitates the homolytic cleavage of O-O bond. On the other hand, the two-thirds portion at g = 2.467, 2.143, 1.898 species is assigned to the conformation in which ferric hydroperoxide forms a hydrogen bond with the active site histidine which functions as an acid-base catalyst to facilitate the heterolytic cleavage.

CHAPTER 6

ENZYME ACTIVATION BY SUBSTRATE

6.1 Introduction

Most enzymes catalyzing the oxygenation reaction utilize ferrous ion as a cofactor to activate O_2. Such enzymes include extradiol dioxygenase, α-ketoglutarate dioxygenase and Rieske dioxygenase. TDO is active at ferrous state, however, it has also been reported from several research groups that ferric TDO exhibits significant activity for the oxidation of L-Trp (*141, 313*). Previous studies have shown that the reaction of TDO does not require adding an exogenous electron donor. The required electron for oxidized TDO activation should be provided by substrate.

It has been reported that intradiol dioxygenases utilize ferric ion as cofactor and the dioxygenation reaction proceeds via a substrate activation mechanism. The active site of intradiol dioxygenase is composed of two histidine, two tyrosine and one solvent-derived water ligands. Upon substrate binding, the tyrosine ligand is displaced and the substrate and dioxygen bind to Fe(III) ion center simultaneously to form a subtrate-peroxy-enzyme complex, in which the ferric ion center functions as a conduit for a shift in electron density from the aromatic substrate to the bound O_2. The heme binding site of TDO has only one axial position for O_2 binding and activation, which does not allow for the formation of substrate-peroxy-enzyme complex. The substrate-based dioxygen activation catalyzed by oxidized TDO must undergo a distinct mechanism relative to intradiol dioxygenase.

In this chapter, we investigate the substrate-based activation of oxidized TDO and propose a substrate-based activation mechanism.

6.2 Results and Discussion

UV-Vis absorbance of ferric TDO mixed with L-Trp under anaerobic conditions — In the absence of any reducing agent, incubation of ferric TDO with L-Trp resulted in the developed UV-Vis absorbance at 321 nm which corresponds to the formation of NFK product. In order to study the effect of substrate on ferric TDO, the reaction mixture containing 5.5 μM ferric TDO and 5 mM L-Trp was incubated under anaerobic conditions. Upon adding L-Trp, the Soret band of ferric TDO slightly shifted 1 nm to 406 nm which suggests that L-Trp binds to the active site and disturbs the active site environment. During the 3 h incubation, the Soret band of 405 nm decreases and the absorption at 432 nm increases (Figure 6.1B). This suggests that ferrous TDO slowly forms in the presence of L-Trp and the formation is at the expense of the ferric TDO. The absorbance at 321 nm corresponding to the NFK product does not change during the 3 h incubation, suggesting that the formation of ferrous TDO does not require an oxygenation process.

The absorption at 432 nm of the difference spectrum was used to calculate the formation of ferrous TDO. After 3 h and 6 h incubation, around 18% and 23% ferric TDO is converted to ferrous TDO, respectively (Figure 6.1A). When the 6 h-incubation reaction mixture was bubbled with CO, a shoulder peak was observed at 421 nm, corresponding to the formation of ferrous TDO-CO-L-Trp complex. The results suggest that L-Trp is an electron donor to provide one electron for the reduction of ferric TDO.

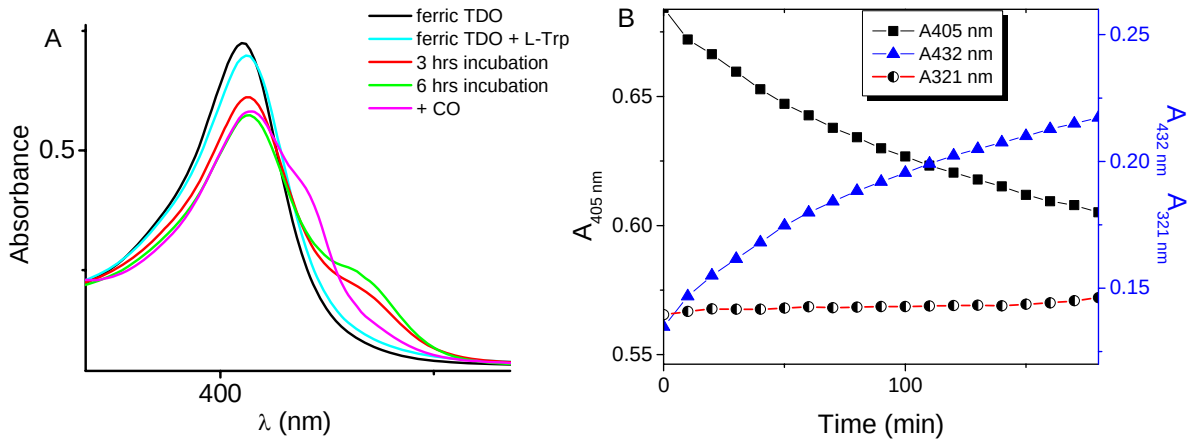

Figure 6.1. UV-Vis spectra of ferric TDO incubated with 5 mM L-Trp under anaerobic conditions. (A) The reprehensive spectra of the ferric TDO incubated with L-Trp. (B) The time trace of the absorption at 405 nm, 432 nm and 321 nm over 3 h incubation.

UV-Vis spectra of substrate analogue-bound ferric TDO — In order to obtain better understanding of the interaction between substrate and the ferric TDO, substrate analogues which includes D-tryptophan (D-Trp), 5-hydroxy-L-tryptophan (5-OH-Trp) and 5-fluoro-DL-trptophan (5-F-Trp) (Figure 6.2) were utilized to probe the interaction between the potential electron donors and the ferric TDO.

Substrate analogues were mixed with ferric TDO under anaerobic conditions to detect the effect on the formation of ferrous TDO (Figure 6.3). Similar trends to that with L-Trp were observed with substrate analogues. The different spectra show an increased Soret band at 432 nm, visible absorptions at 554 nm and 588 nm and a decreased Soret band at 405 nm, resulting from the formation of a ferrous species at the expense of ferric TDO (Figure 6.3D).

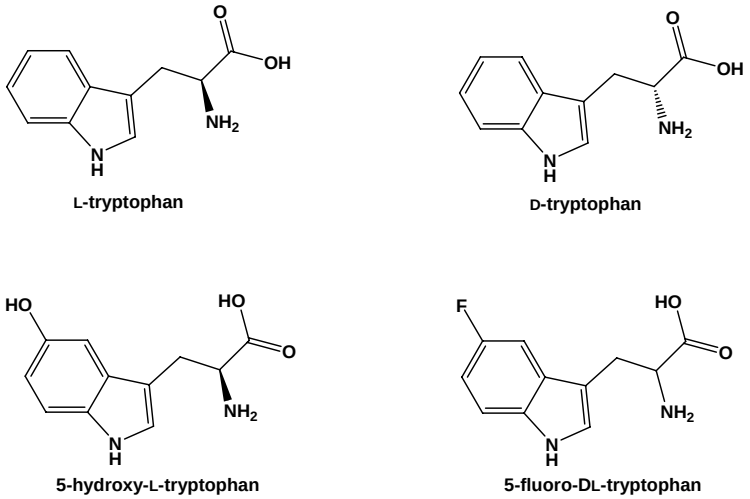

Figure 6.2. The chemical structures of substrate, L-Trp, and its analogues.

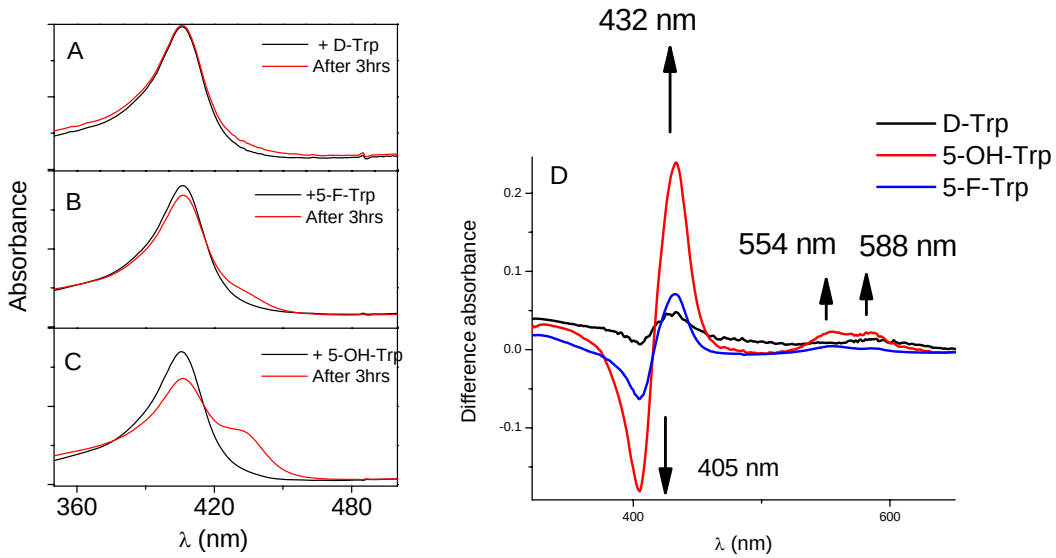

Figure 6.3. The activation of ferric TDO upon binding substrate analogues. Ferric TDO mixed with (A) 20 mM D-Trp; (B) 20 mM 5-F-Trp; (C) 20 mM 5-OH-Trp for 3 h under anaerobic conditions; (D) the difference spectra of ferric TDO reacted with D-Trp, 5-F-Trp, 5-OH-Trp for 3 h.

After 3 h incubation, the ferrous TDO formation based on the concentration of the starting ferric TDO was 11.6 % and 41.6 % for 5-F-Trp and 5-OH-Trp respectively. Compared with the 18 % ferrous TDO formation using L-Trp (Figure 6.1), 5-OH-Trp is 1.3-fold more effective whereas 5-F-Trp is 35 % less efficient. As for D-Trp, only 2.5 % ferric TDO is converted to ferrous form. The activation has the following order: 5-OH-Trp > L-Trp > 5-F-Trp > D-Trp which does not correlate to the specificity of substrate. These results clearly suggest that the formation of ferrous species is sensitive to the chemical properties as well as the geometry rather than the involvement in the catalytic reaction of the substrate or substrate analogues. Upon binding to the active site, the orientation and position of substrate analogues might be different, affecting the electron transfer from or through the indole ring of substrate or substrate analogue to the ferric heme ion.

EPR spectra of substrate- or substrate analogue-bound ferric TDO — In order to obtain more information on the binding of substrate or substrate analogues to ferric TDO, EPR spectroscopy was employed to investigate the substrate- and substrate analogues-bound ferric TDO complex.

Figure 6.4 displays the low temperature X-band EPR spectra of ferric TDO in the presence of substrate and substrate analogues. The EPR spectrum of substrate-free ferric TDO in 4A shows a rhombic high-spin ferric signal near g = 6 and 2. The samples of spectra B-E were prepared by mixing ferric TDO with 100 equivalents of L-Trp, D-Trp, 5-OH-Trp or 5-F-Trp, respectively for 25 s, followed by freezing in liquid nitrogen. The L-Trp-bound ferric TDO is shown in 4B in which a low-spin ferric signal occurs at g = 2.69, 2.19, 1.80. In another parallel experiment, the quantitation results indicate that the formation of the low-spin ferric signal is at the expense of

50% high-spin ferric signal. The *g*-values of the low-spin ferric signal is similar to those of other heme-containing proteins (*134, 135*), which have been identified as a ferric hydroxide species. Thus, the low-spin ferric signal in ferric TDO is assigned to a ferric hydroxide species. The original high-spin ferric signal becomes more axial and a small amount of high-spin ferric signal at $g = 6.66$ occurs upon the binding of substrate (more details in Chapter 7), which is indicative of a perturbation in the active site environment.

The binding of D-Trp to ferric TDO did not change the EPR signal as shown in 4C. On the other hand, the binding of 5-OH-Trp and 5-F-Trp to ferric TDO induce a similar EPR low-spin ferric signal at $g = 2.69, 2.19, 1.80$ corresponding to ferric hydroxide low-spin species as shown in 4D and 4E.

It should be noted that D-Trp has only little effect on ferric TDO activation, whereas L-Trp, 5-OH-Trp and 5-F-Trp have significant activation effect when incubated with ferric TDO under anaerobic conditions. These findings are in line with the observation in the EPR spectrum in which a low-spin ferric species was not observed when ferric TDO was mixed with D-Trp but with L-Trp, 5-OH-Trp and 5-F-Trp. This indicates the formation of ferrous TDO is correlated to the formation of hydroxide-ligated ferric intermediate. The fact that the spin transition is sensitive to the stereospecificity of the substrate reveals a conformational change upon the binding of substrate or substrate analogues.

The low-spin ferric signal upon binding L-Trp to ferric TDO — The low-spin ferric hydroxide species is most possible to provide a conduit for the electron transfer from aromatic substrate to ferric ion center. If it does, it should be long-lived for the activation as the activation can be

observed for at least 6 h. EPR spectroscopy was used to detect the stability of the low-spin ferric species over a 5 h time scale. Parallel samples were prepared under anaerobic conditions for various reaction times in which ferric TDO mixed with L-Trp for 30 min, 2 h and 5 h

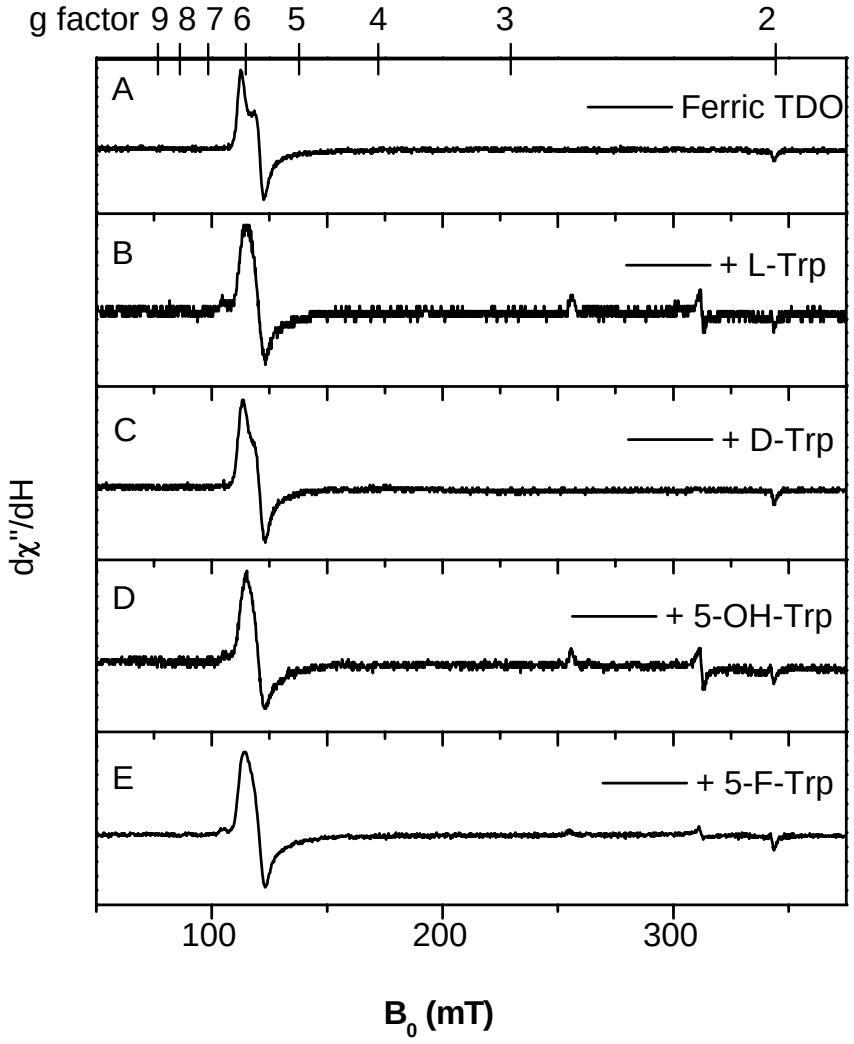

Figure 6.4. EPR spectra of ferric TDO mixed with substrate or substrate analogues. (A) 200 μM as-isolated ferric TDO; Spectra B-E shows the EPR spectra of 200 μM ferric TDO upon the reaction for 25 s with 20 mM (B) L-Trp; (C) D-Trp; (D) 5-OH-Trp; (E) 5-F-Trp. Experimental EPR spectra were recorded at 10 K with 3 mW microwave power at 9.4 GHz.

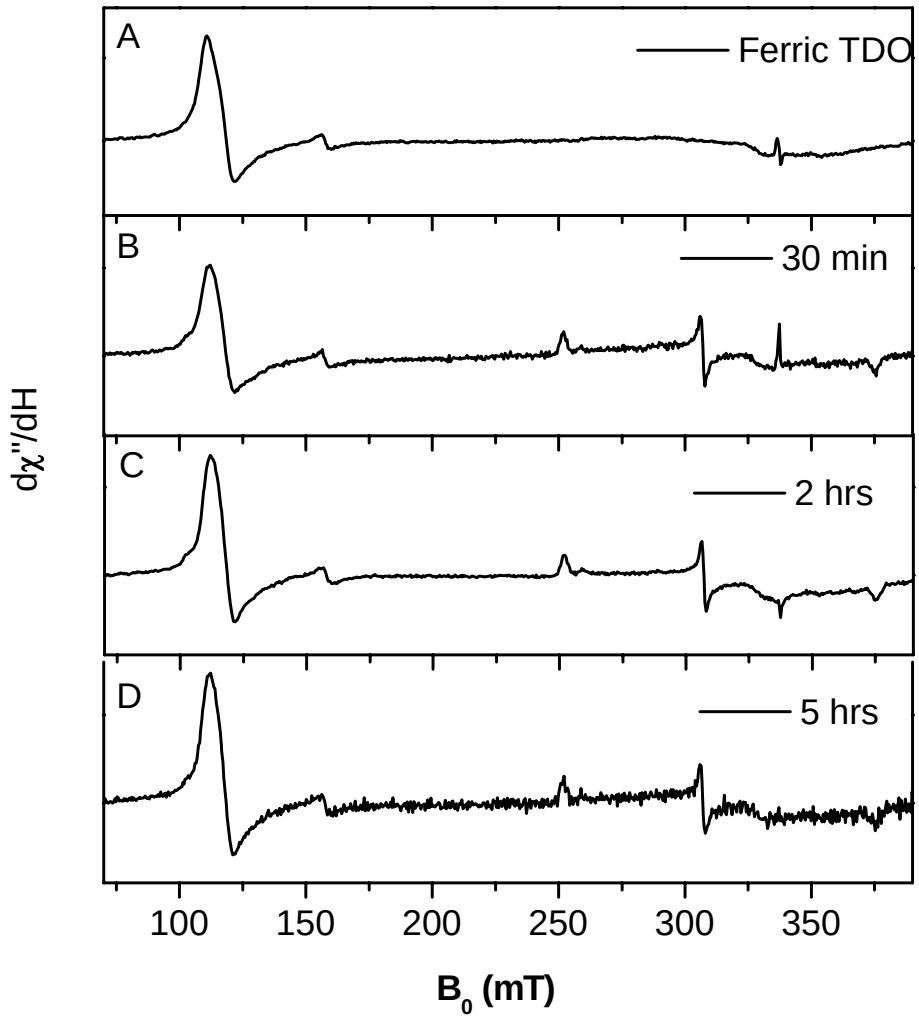

Figure 6.5. EPR spectra of the time dependence of incubation of ferric TDO with L-Trp under anaerobic conditions. EPR spectra of 200 μM as-isolated ferric TDO (A); Spectra B-D are the EPR spectra of 200 μM ferric TDO mixed with 6 mM L-Trp for (B) 30 min; (C) 2 h and (D) 5 h. Experimental EPR spectra were recorded at 10 K with 1 mW microwave power at 9.4 GHz. A 5 G field modulation at 100 kHz was employed.

respectively before freezing in liquid nitrogen for EPR spectroscopy analysis (Figure 6.5). The low-spin ferric signal is present even after 5 h incubation. The high-spin ferric signal becomes more axial compared with the original one. These results clearly suggest that the low-spin ferric signal is a property of substrate-bound ferric TDO.

Table 6.1. EPR parameters of ferric signals of TDO in the presence of L-Trp.

	Spin State	*g*	%
Site 1	High-spin	5.78	40
	Low-spin	2.61	8
Site 2	High-spin	6.6	7
	Low-spin	2.69, 2.19, 1.80	43

The simulation of the EPR spectrum of L-Trp bound ferric TDO reveals two overlapping low-spin ferric signal with a ratio of 43 : 8 at g = 2.69, 2.19, 1.80 and g = 2.61, 2.19, 1.80 (Table 6.1). This finding gives an indication of two conformers of the ferric hydroxide species in the active site.

The redox potential of TDO — In order to investigate the electron transfer driving force, redox potential of TDO was determined in the absence and presence of L-Trp. Selected spectra obtained during anaerobic redox titration of TDO are shown in Figure 6.6. Data is fitted to a single electron process (Nernst equation) at either 405 nm or 432 nm which gives results within error of one another. The reduction potential are 110 ± 2 mV for the substrate-free TDO and 191

± 10 mV for the L-Trp-bound TDO, which shows an increase of 81 mV over the value for the substrate-free TDO.

The redox potential properties of heme group can be modulated by the hydrogen bonding network, electrostatic interactions in the active site environment as well as other modifications in the heme-binding pocket upon a change in ligands (*350*). In the peroxidase family, the interaction of Asp-His-ferric heme ion at the proximal heme side mainly contributes to a low redox potential by deprotonating the NH group of the proximal histidine. In TDO, proximal His257 is surrounded by a mostly hydrophobic environment and hydrogen bonded to Arg254 through two water molecules. The His257 has no additional electrostatic interaction with the protein matrix. Putting these together contributes to the high redox potential of TDO.

It has been reported that the higher redox potential helps stabilize the catalytic oxyferrous intermediate. For example myoglobin has a redox potential around 50 mV (*351*). This suggests that the high redox potential in TDO increases the potential electron driving force of ferric heme ion of TDO. In CYP450, the resting state of the enzyme exhibits a mixture of spin state with high-spin and low-spin ferric in which the low-spin ferric state is favored in the absence of substrate. Upon substrate binding, the water molecule is displaced from the sixth ligand position. This modification increases the midpoint redox potential of iron center from -300 mV to -170 mV which facilitates the transfer of one elctron from the CYP450 reductase to activate the enzyme (*352*). It is likely that the increased redox potential in TDO upon substrate binding results in the increase in the thermodynamic driving force for electron transfer between L-Trp and the ferric ion center which facilitates the substrate-based ferric TDO activation.

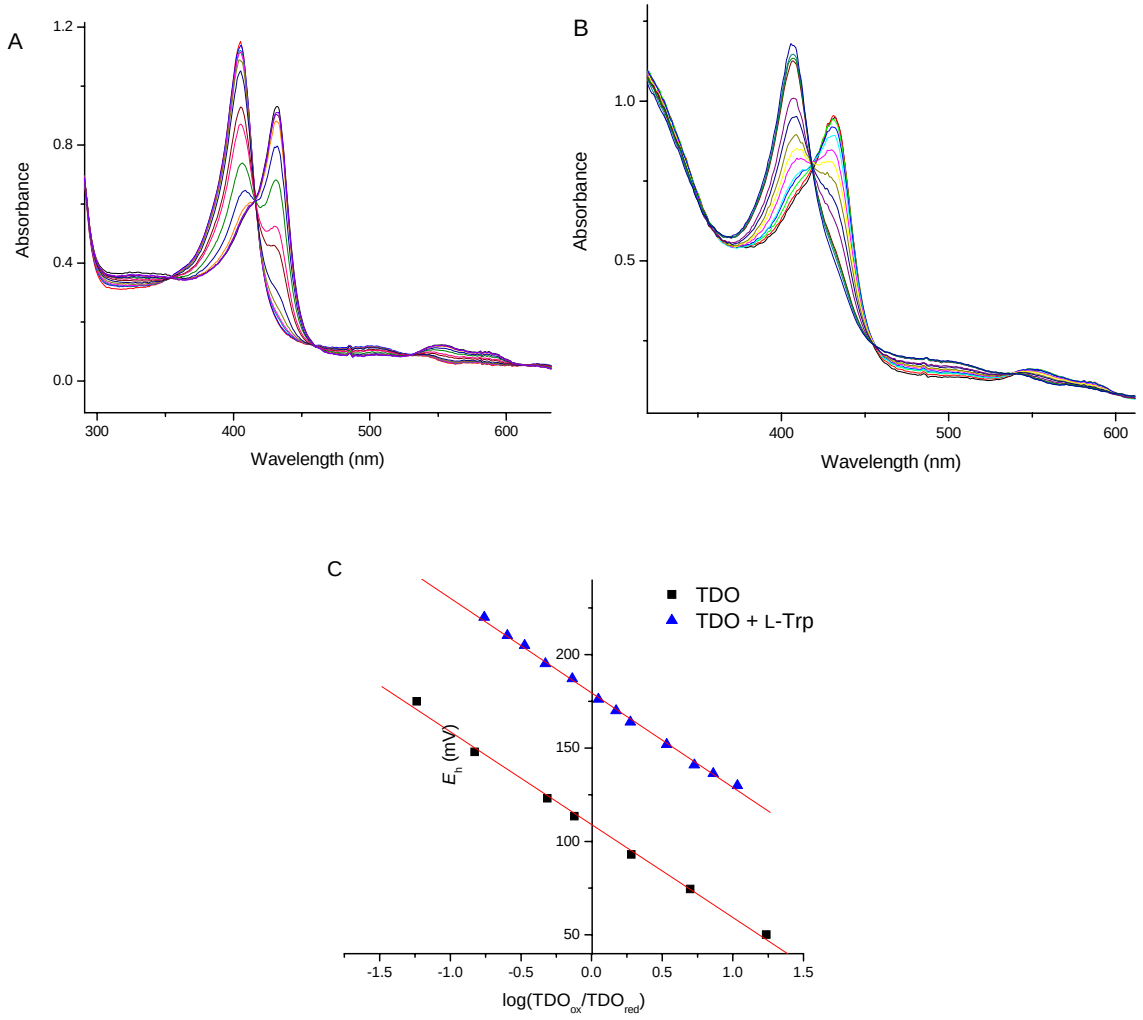

Figure 6.6. Anaerobic spectrochemical titrations of TDO at 100 mM potassium phosphate buffer pH 7.0. (A) Absorption spectra obtained during redox titration of substrate-free TDO. (B) Absorption spectra collected during redox titration of TDO in the presence of 15 mM L-Trp. (C) Nernst plot for the reductive titration of TDO. Values of log [TDO_{ox}]/[TDO_{red}] were obtained from the change of absorbance at 405 nm.

Mössbauer characterization of TDO — The iron axial ligand in heme proteins always affects the electronic property of the porphyrin ring. Mössbauer spectroscopy was conducted to provide further information on the axial ligand.

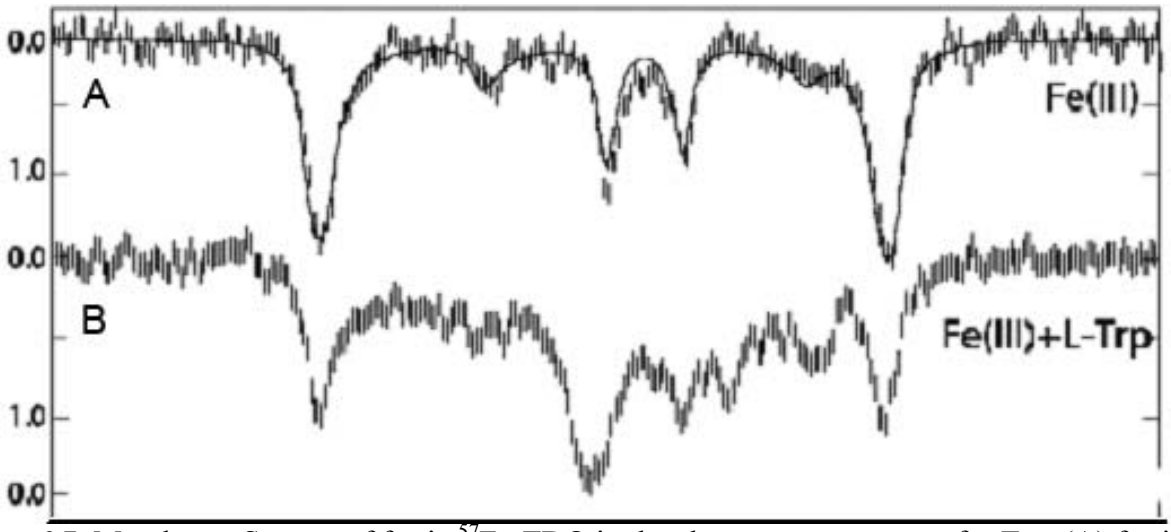

Figure 6.7. Mössbauer Spectra of ferric ^{57}Fe-TDO in the absence or presence of L-Trp. (A) ferric ^{57}Fe-TDO; (B) ferric ^{57}Fe-TDO treated with 10 equivalents of L-Trp. The spectra were recorded at 4.2 K with a magnetic field at 45 mT.

Mössbauer spectra shown in Figure 6.7 indicate that the addition of L-Trp to ferric TDO results in conversion of 60% of high-spin ferric signal to low-spin ferric signal. The ratio of the formation of low-spin ferric species in Mössbauer spectrum is consistent with the EPR experiment observation within the range of error.

The Mössbauer spectrum of ferrous TDO shows a single doublet (single species) with relatively large quadrupole splitting of 3.55 mm/s. The observed isomer shift of 1.00 mm/s and line width of $\Gamma = 0.56$ mm/s is typical of high-spin ferrous heme as shown in Figure 6.8.

Upon addition of 10 equivalents of L-Trp, 50% of the ferrous doublet is converted to a new ferrous species with a significantly smaller quadrupole splitting of 2.5 mm/s, line width of $\Gamma =$ 0.37 mm/s and the same isomer shift 0.95 mm/s (Figure 6.9). No change in isomer shift indicates that the oxidation state of iron remains high-spin ferrous.

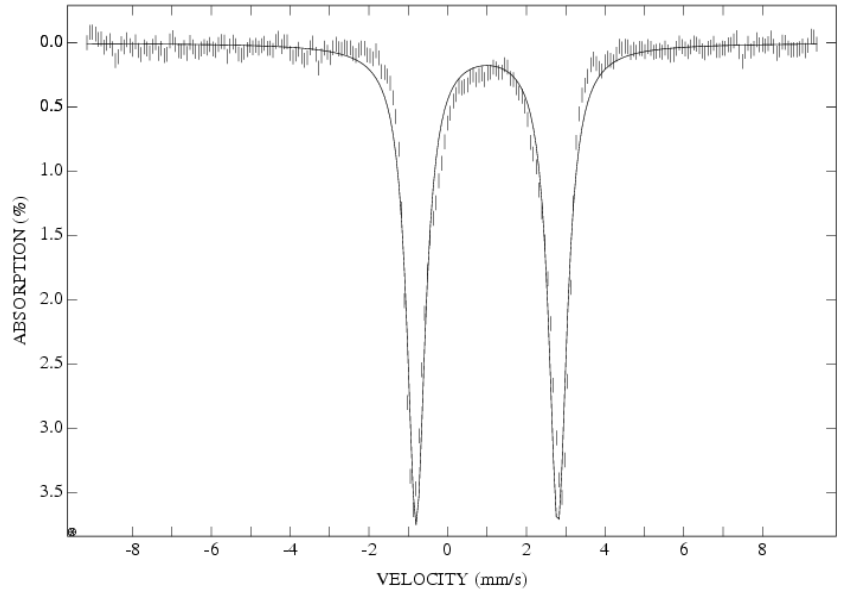

Figure 6.8. Mössbauer Spectrum of ferrous ^{57}Fe-TDO. The spectrum was recorded at 4.2 K with a magnetic field at 45 mT.

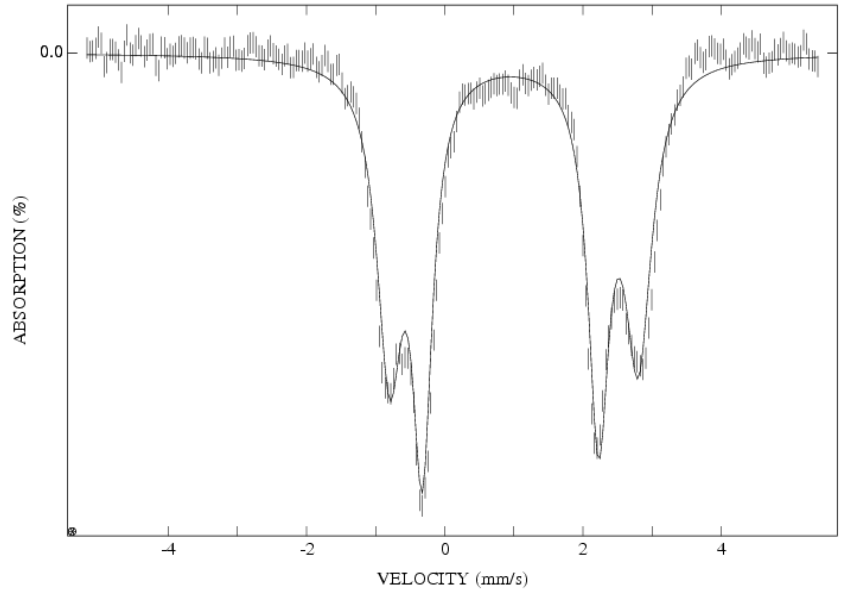

Figure 6.9. Mössbauer Spectrum of ferrous ^{57}Fe-TDO in the presence of L-Trp. The spectrum was recorded at 4.2 K with a magnetic field at 45 mT.

The lower quadrupole splitting *g*-value is typical of other heme proteins with a His proximal axial ligand, such as myoglobin (2.22 mm/s), hemoglobin (2.40 mm/s), and HRP (2.68 mm/s). The larger value of ΔE_Q is rare, but a large value has been observed in hydroxylamine oxidoredutase (4.21 mm/s). Recent studies of synthetic model complexes have correlated the shift from small to large ΔE_Q with the protonation state of N_δ of the proximal histidine (*353*). The smaller ΔE_Q is observed for neutral imidazole (N_δ protonated), and the larger value observed for imidazolate (N_δ deprotonated) complexes. Thus, the L-Trp-bound ferrous TDO with ΔE_Q = 3.55 mm/s is correlated with an imidazolate complex, whereas the one with ΔE_Q = 2.5 mm/s is correlated with a neutral imidazole complex. Site A and Site B in Scheme 6.1 refer to two different protonation states of the proximal His257 with regard to the imidazolate complex and neutral imidazole complex. In site A, the water forms hydrogen bond with N_δ of His 257 in one subunit of the substrate-bound dimer and leads to more negative δ^- in His257 compared with that of Site B, giving an imidazolate complex. On the other hand, in Site B, the proton moves from water to His257, giving a neutral imidazole complex with a small ΔE_Q.

The X-ray structure of substrate-bound xcTDO does not show difference at the water near the proximal histidine (Figure 6.10). Mössbauer data suggests that one subunit of the dimer of the histidine ligand has become more positively charged in the presence of L-Trp with a higher protonated character as shown in Scheme 6.1B. The positively charged proximal histidine influences the basicity of the four pyrrole nitrogens and thus decreases the electron density at the heme iron which facilitates electron transfer from potential nearby electron donor.

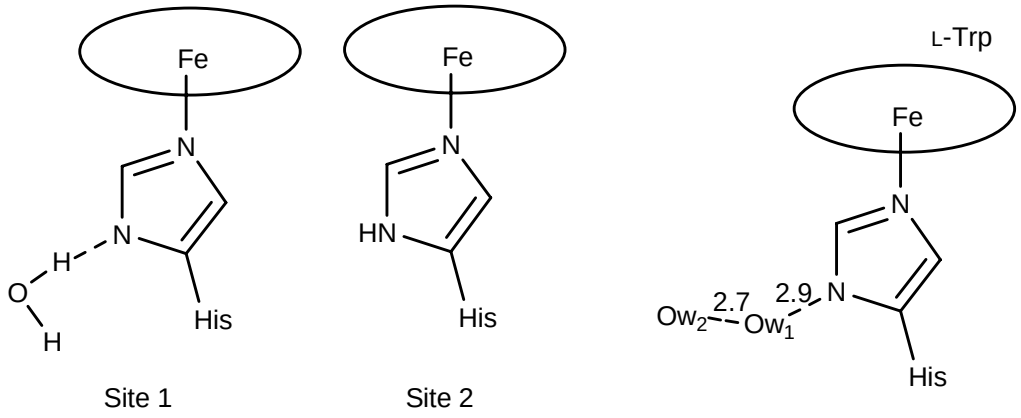

Scheme 6.1. The two protonation states of proximal His257 in TDO.

Proposed substrate activation mechanism — In TDO, the binding of substrate or substrate analogues triggers the change in spin state to form low-spin ferric hydroxide species. There are two overlapping low-spin ferric hydroxide signals at g =2.69, 2.19, 1.80 and g = 2.61, 2.19, 1.80. The X-ray structure of substrate-bound xcTDO (Figure 6.10) shows differences between Conformers A and B of the active site water molecules to the substrate and the distal site histidine. In one subunit of dimer, the active site water is close to L-Trp and forms hydrogen bond with N_δ group of L-Trp which is referred to as Conformer A. In the other subunit of dimer, the active site water is away from L-Trp and forms hydrogen bond with N_δ group of histidine, which is designated as Conformer B (Figure 6.10). Although the crystal structure of substrate-bound rmTDO is not available, a similar hydrogen bonding network in the active site is assumed in rmTDO with regard to the observation of two overlapping low-spin ferric hydroxide intermediates.

Our studies suggest the formation of ferrous TDO is sensitive to the geometry of the substrate or substrate analogues in the active site. Since electron transfer requires a conduit for the electron

shift from substrate or substrate analogue to ferric ion center, a ferric hydroxide-L-Trp complex is assumed during the substrate-based activation. Conformer A is effective for the ferric TDO activation in which the ferric hydroxide is close to C3 to form a ferric hydroxide-L-Trp complex. Conformer B has a hydrogen bond between ferric hydroxide intermediate and N_{δ} group of both of His72 and L-Trp is inefficient for the activation of ferric TDO.

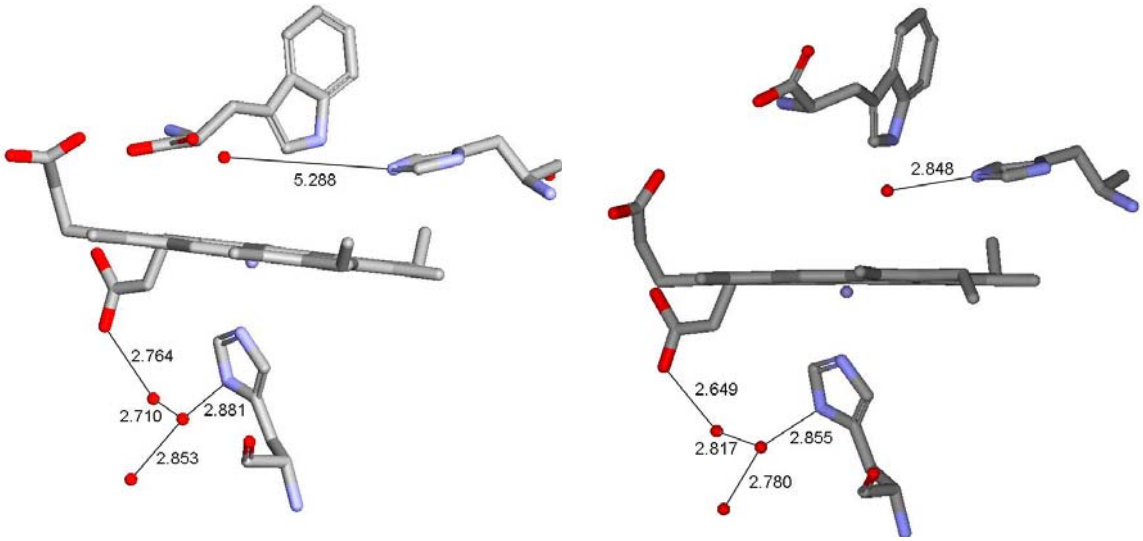

Conformer A Conformer B

Figure 6.10. Crystal structure of the water molecule near His55 in the distal site and His240 in the proximal site of xcTDO (PDB: 2NW8).

Combined with the higher redox potential, the protonation state of proximal histidine of TDO and the formation of ferric hydroxide low-spin ferric species, a substrate-based activation mechanism of ferric TDO is proposed as shown in Scheme 6.2. Upon substrate binding, the active site water shifts toward the ferric heme center which facilitates the formation of low-spin six-coordinated ferric heme complex with a hydroxide as the sixth ligand. The C2-C3 double bond of L-Trp moves close to and faces the hydroxide ferric intermediate in a hydrogen bond

distance. Based on the indole chemistry, the highest spin density is located at C3 of L-Trp. The formation of the low-spin ferric hydroxide complex triggers an electrophilic attack at C3 and generates a hydroxyl-L-Trp-ferric TDO intermediate. The increased redox potential of the ferric ion and the imidazolate character of the proximal His257 upon the binding of substrate facilitate the electron transfer from the nearby potential electron donor to the iron center. Thus, one electron reduction occurs in ferric TDO to generate a ferrous TDO. After reduction, the proton is rebound to form ferrous hydroxide TDO intermediate and generates a tryptophan cation radical intermediate. When a dioxygen molecule is available, the water molecule in the active site is displaced and O_2 driven dioxygenation reaction is initiated. However when ferric TDO was incubated with L-Trp under anaerobic condition, no protein radical is observed by EPR spectroscopy. This could be due to the very low reaction rate of the generation of the putative tryptophan cation radical. The heme binding pocket is partially exposed to the solvent, so the relatively small amount of radical is easily quenched by the solvent.

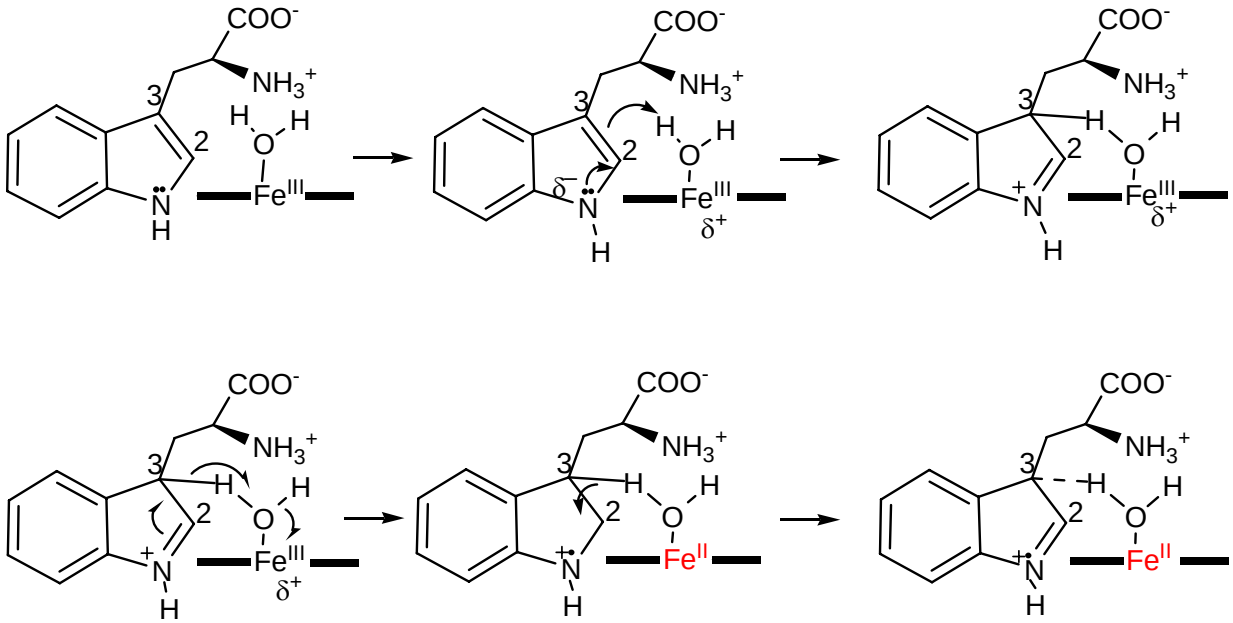

Scheme 6.2. Proposed mechanism of substrate activation of ferric TDO.

CHAPTER 7

A SITE-DIRECTED MUTAGENESIS ANALYSIS ON THE ROLE OF THE CONSERVED ACTIVE SITE RESIDUES

7.1 Introduction

In order to probe the role of the active site residues (Figure I.4), a set of TDO derivatives was constructed, which includes proximal site His72 derivatives of H72S, H72N, Q73F; distal site tyrosine residue derivatives of Y43W, Y43F, Y130F, proximal site tryptophan residue derivatives of W119F, W253F, W119F/W253F and proximal ligand derivative of H257C.

7.2 Results and Discussion

Expression, purification, and characterization of TDO derivatives — The mutant proteins were purified with the same protocol as that of the wild-type TDO (WT TDO). The UV-Vis maximal absorptions of the ferric TDO derivatives are compared in Table 7.1. All of the mutants have similar UV-Vis spectral features with a Soret band of a ferric form within 1-2 nm range of 405 nm and a ferrous form within 1-2 nm range of 432 nm, which are similar to that of WT TDO. These suggest that the corresponding mutations might not have significant effects on the active site structure of the mutants. The available crystal structures of TDO can provide reasonable information on the surrounding environments of the active sites to interprete the substrate-protein interaction of these mutants.

There are two exceptions among them. One is Y43F, in which the ferric form has maximal absorptions at 411 nm, 532 nm and 576 nm. Another one is H257C, in which the ferric form

exhibits a Soret band at 403.5 nm and visible bands at 529 nm and 603 nm. The ferrous form shows a Soret maximal at 420 nm which is much different from other TDO derivatives and better resembles the features of cysteine ligated heme proteins.

The mutants dramatically alter the heme binding capabilities as shown in Table 7.2. WT TDO and Y130F as purified isolated protein contained 63% and 62% Fe/monomer. H72S, H72N, Y43W and W253F as purified isolated protein have 51%, 45%, 46% and 47% Fe/monomer heme occupancy respectively, followed Q73F, W119F and W119F/W253F with 37%, 35% and 32% respectively, and H257C has the lowest heme occupancy with 28%, determined by ICP.

Kinetic parameters of k_{cat}, K_m and k_{cat}/K_m for all of the mutants were measured in 50 mM Tris pH 7.4 and are presented in Table 7.3. In steady state analysis, the k_{cat} and K_m values of the WT TDO are 12 s^{-1} and 215 μM, respectively. The enzyme activity decreases in the order of W119F, Q73F, W253F, W119F/W253F and Y130F with 7.60 s^{-1}, 5.0 s^{-1}, 3.4 s^{-1} and 3.3 s^{-1}, respectively. The activity of H72S and H72N with 0.68 s^{-1} and 0.020 s^{-1} are 18-fold and 630-fold slower relative to WT TDO. The two Tyr43 mutants of Y43W and Y43F have dramatically decreased activities with k_{cat} values of 0.002 s^{-1} and 0.040 s^{-1} corresponding to 6000-fold and 310-fold slower compared with WT TDO. H257C has a very low enzyme activity (k_{cat} value of 0.006 s^{-1}).

EPR spectroscopy was used to determine the heme coordination geometry of TDO derivatives. All the EPR samples were prepared in 50 mM Tris pH 7.4 containing 10% glycerol. Ferric TDO exhibits a typical rhombic high-spin ferric signal at g = 6, 2. H72N, Q73F, Y130F, W253F, W119F and W119F/W253F have similar rhombic high-spin ferric signal as that observed in WT TDO as shown in Figure 7.1 and Table 7.4. Compared with WT TDO, Y43W exhibits a much

axial high-spin ferric EPR signals. The most interesting mutant is H72S in the EPR study. A set of low-spin ferric signals is observed in the as-isolated H72S. Further discussion about the high-to-low spin transition will be is provided in later chapters. There are two sets of high-spin ferric signals observed in H257C with g = 6.64 and g = 5.15, respectively. A low-spin ferric signal is also observed at g = 2.1, 1.99, 1.90 from H257C. It is also not surprising to observe the low-spin ferric signal in H257C which is designed to mimic the cysteine ligand in CYP450. The spin mixture of low-spin and high-spin ferric signal in H257C is consistent with the observation in its UV-Vis spectrum. In most of the TDO derivatives, there is a small portion of g = 2 signals, which may be due to a free radical signal, however, the identity is not yet understood.

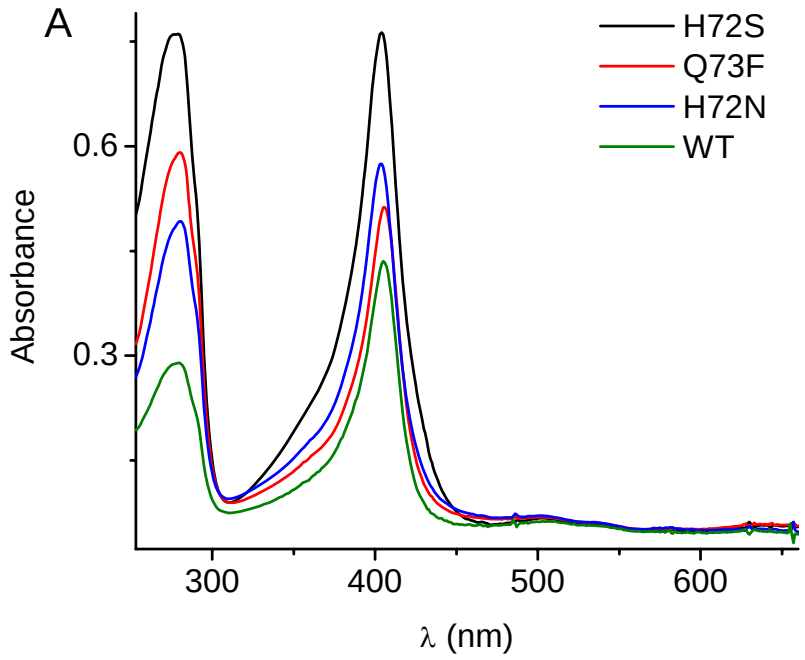

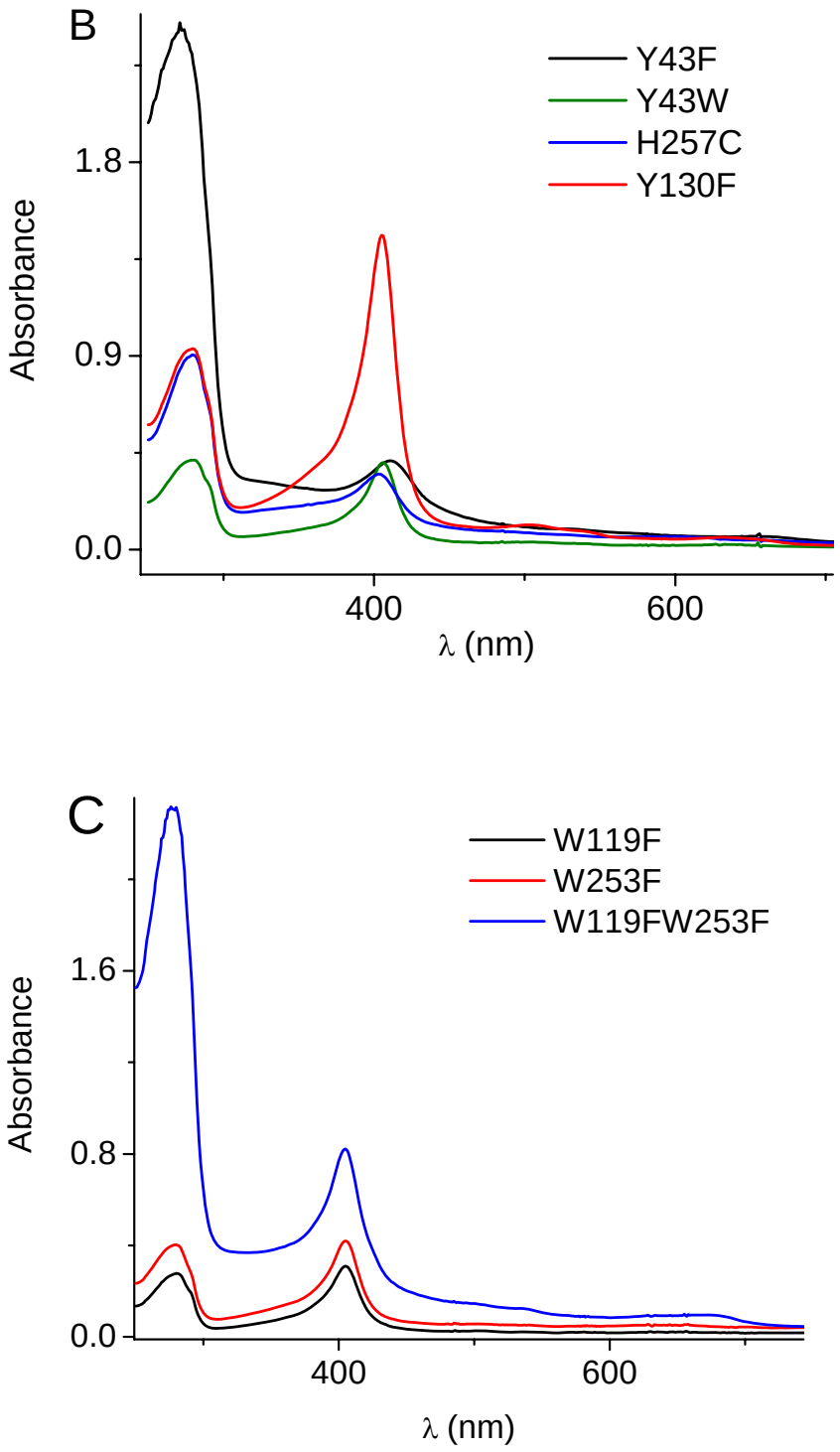

Figure 7.1. UV-Vis spectra of TDO derivatives.

Table 7.1. Absorption spectra of the TDO mutant proteins.

Sample	Ferric form (nm)	Ferrous form (nm)
WT TDO	405; 505; 541; 632	432; 554; 588; 657
H72N	403; 504; 539; 630	429; 552; 584; 656
Q73F	405; 505; 540; 637	432; 554; 587; 661
H72S	404; 504; 538; 637	430; 552; 586; 657
Y130F	405; 504; 541; 633	432; 554; 589; 660
Y43W	406; 503; 540; 636	433; 555; 589; 658
H257C	403.5; 489; 529; 603	420; 535; 570; 658
W253F	405; 502; 540; 641	430; 555; 588
W119F	405; 505; 540; 640	430; 553; 588
W119F/W253F	404; 505; 537; 631; 677	428; 555; 590; 659
Y43F	411, 532, 576, 659	426; 532; 557; 650

Table 7.2. Heme occupancy and the extinction coefficient of TDO derivatives.

TDO	Fe/Protein (%)	$\varepsilon_{\text{Soret band}}$ ($mM^{-1}\ cm^{-1}$)
WT TDO	63	130
H72S	51	120
H72N	45	120
Q73F	37	110

Y130F	62	130
Y43W	46	140
W119F	35	130
W253F	47	110
W119F/W253F	32	80
H257C	28	90
Y43F	N/A	N/A

Table 7.3. Kinetic parameters for wild-type TDO and its derivatives with L-Trp as substrate.

TDO	K_m (μM)	k_{cat} (s^{-1})	k_{cat}/K_m(M^{-1} s^{-1})
WT TDO	215.0 ± 13.0	12.0 ± 0.4	55,530.0 ± 1,680.0
H72S	586.0 ± 80.0	0.68 ± 0.08	1160.0 ± 80.0
H72N	1153.0 ± 120.0	0.020 ± 0.001	16.0 ± 1.0
Q73F	996.0 ± 130.0	5.0 ± 0.07	5,410.0 ± 620.0
Y130F	180.0 ± 10.0	3.30 ± 0.03	18,680.0 ± 1,040.0
Y43W	N/A	0.0020 ± 0.0003	N/A
Y43F	N/A	0.040 ± 0.005	N/A
W119F	450.0 ± 37.0	7.60 ± 0.20	16,900.0 ± 900.0
W253F	245.0 ± 20.0	14.50 ± 0.40	44,440.0 ± 2,380.0
W119F/W253F	270.0 ± 50.0	3.40 ± 0.30	12,760.0 ± 1,360.0
H257C	N/A	0.006 ± 0.001	N/A

N/A: 50 mM L-Trp was used for the determination of the apparent rate.

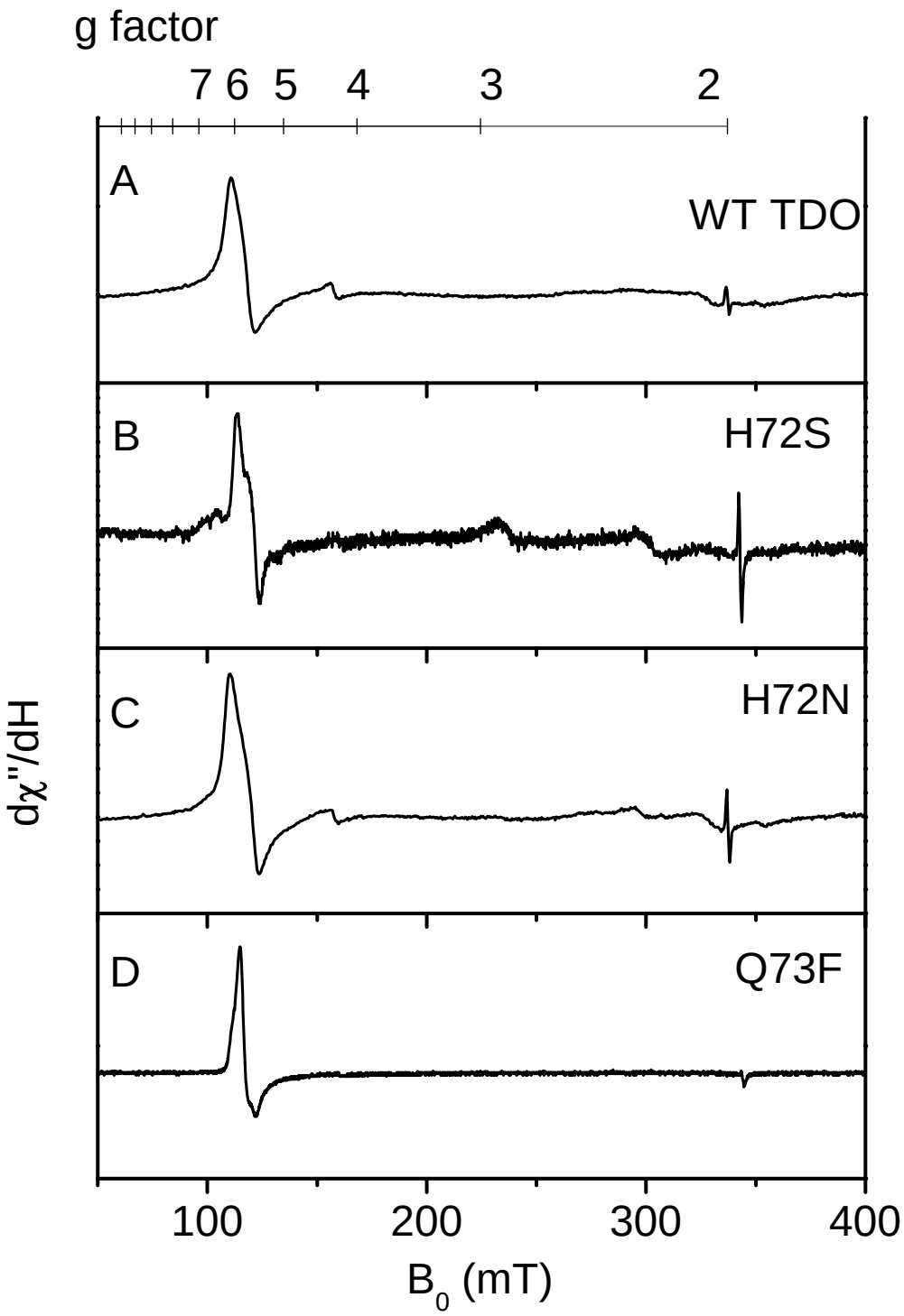
g factor
7 6 5 4 3 2
A
WT TDO
B
H72S
C
H72N
D
Q73F
dχ"/dH
100 200 300 400
B0 (mT)

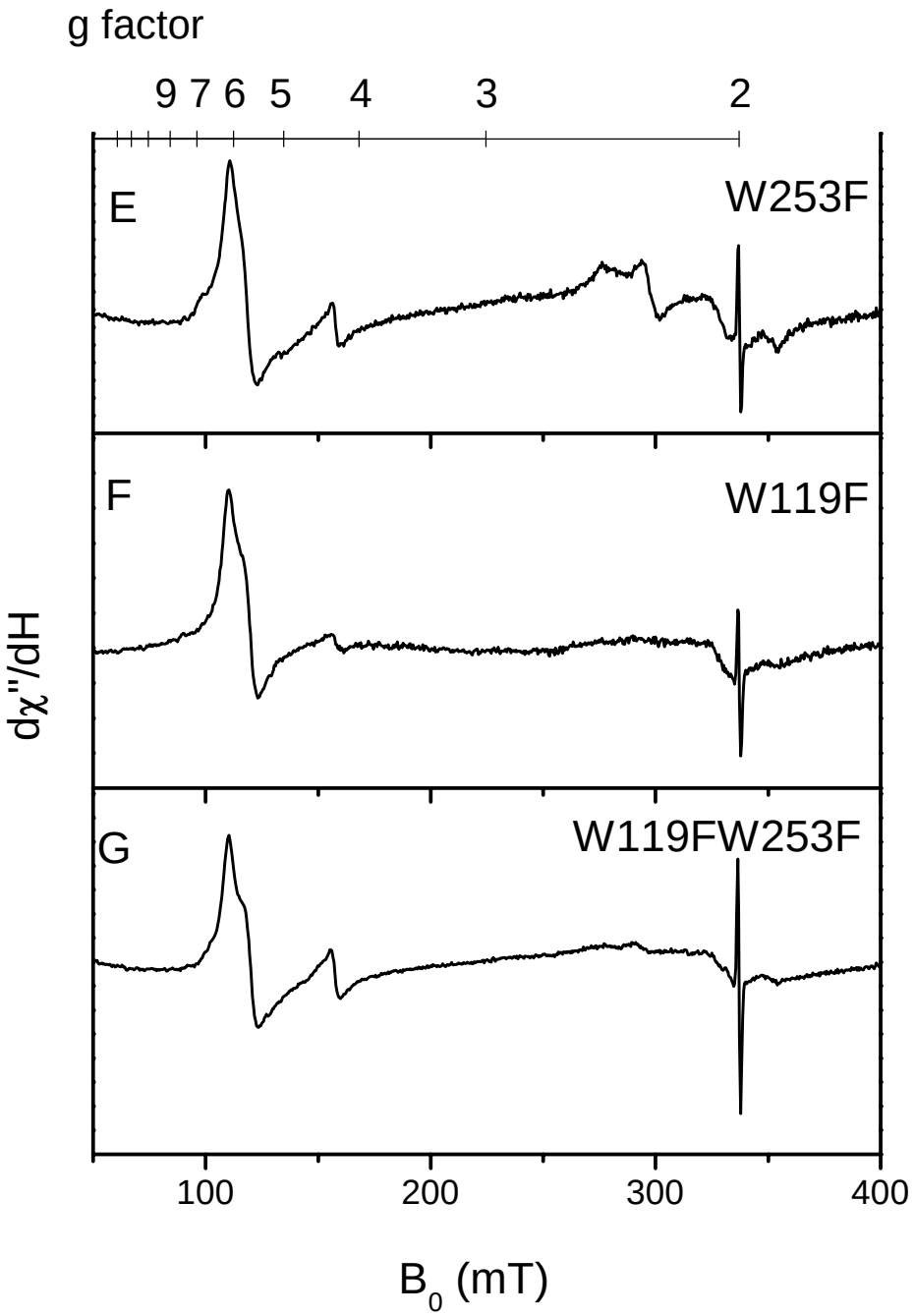
g factor
9 7 6 5 4 3 2
E
W253F
F
W119F
G
W119FW253F
dχ''/dH
100
200
300
400
B0 (mT)

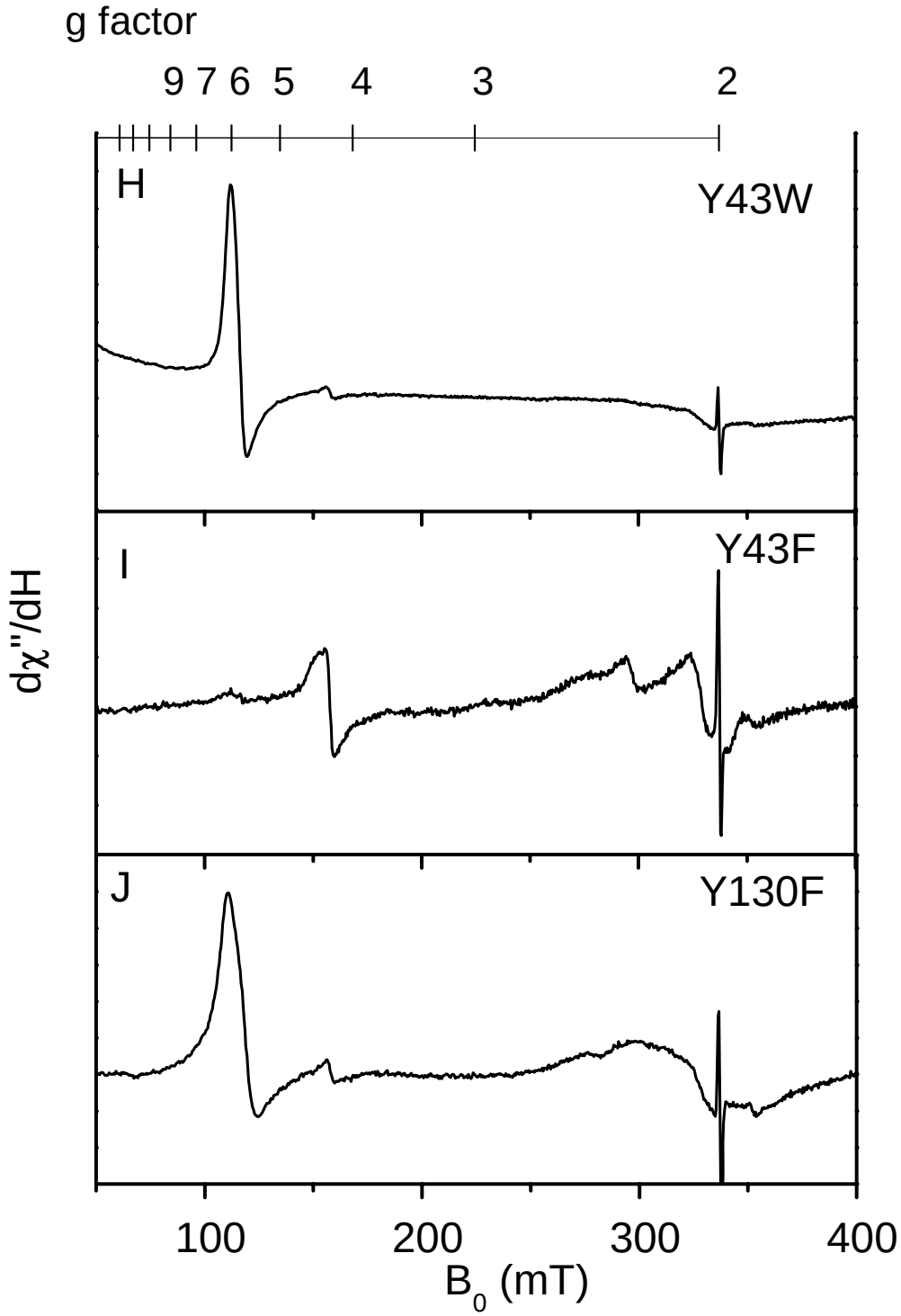
g factor
9 7 6 5 4 3 2
H
Y43W
I
Y43F
J
Y130F
dχ"/dH
100
200
300
400
B0 (mT)

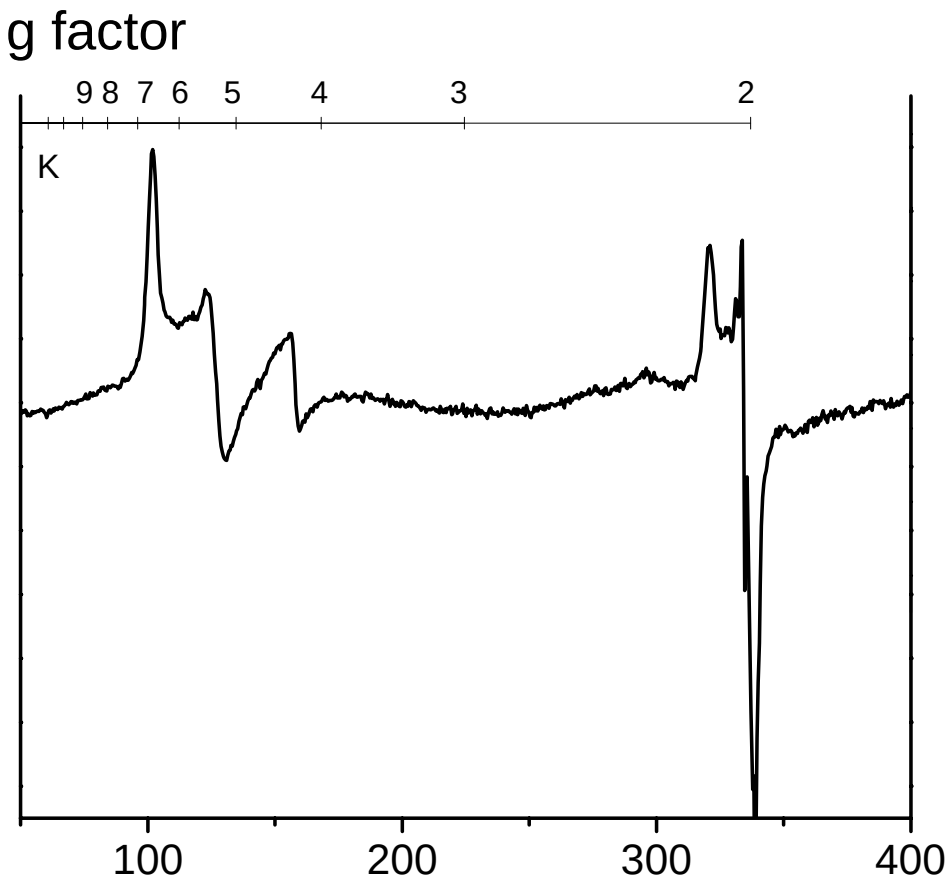

Figure 7.2. EPR spectra of TDO derivatives. The as-isolated purified TDO derivatives were prepared in ferric forms. (A) WT TDO; (B) H72S; (C) H72N; (D) Q73F; (E) W253F; (F) W119F; (G) W119F/W253F; (H)Y43W; (I) Y43F; (J) Y130F; (K) H257C. Experimental EPR spectra were recorded at 10 K with 1 mW microwave power at 9.4 GHz. A 5 G field modulation at 100 kHz was employed.

Table 7.4. The *g* parameters of as-isolated TDO derivatives.

Sample	High-spin 1		High-spin 2	Low-spin		
	g-values		*g*-values	*g*-values		
WT TDO	6.11	5.7				
H72N	6.11	5.62	6.76			
Q73F	6.00	5.87	6.87			
H72S	6.11	5.72	6.66	2.98	2.31	1.90
Y130F	6.11	5.67				
Y43W	6.0	5.8				
Y43F	6.04			2.44	2.29	1.99
W253F	6.08	5.7	6.88			
W119F	6.11	5.66				
W119F/W253F	6.11	5.62	6.6			
H257C	5.46	5.15	6.64	2.1	2.06	2.03

Distal site His72 derivatives: H72S, H72N and Q73F — His72 forms a hydrogen bond with the only distal water molecule in the active site in the ligand-free structure of the enzyme (*262, 354*). In the ligand-bound crystal structure in xcTDO, the indole nitrogen atom of the substrate is directly hydrogen-bonded to the His55 which corresponds to His72 in rmTDO (Figure 1.4) (*354*). The residue of His72 is the sole candidate, should an active site acid-base catalyst be required in the catalytic mechanism. However, it is serine in the corresponding position of IDO, which

appears less likely to play this role (*130*). The role of the histidine in the active site is still controversial.

Site-directed mutagenesis of the distal histidine to serine or alanine decreases the reaction but can not eliminate the reaction (*129, 132, 133*). Recent resonance Raman studies suggest that His72 plays a role in regulating substrate binding (*132*). The intriguing observation in the crystal structures of H55S and H55A is that one additional water molecule is introduced to the active site when histidine is replaced (*133*).

In order to determine the role of His72, three mutants, H72N, H72S, and Q73F, were constructed. The mutation of His72 to an asparagine (Asn) is capable of maintaining the hydrogen bonding interactions (though less effectively) or is incapable of functioning as an acid-base catalyst. Likewise, H72S is capable of forming hydrogen-bonds with its hydroxyl group but would be an ineffective acid-base catalyst. Gln73 is a conserved residue next to His72. The apparent role of this residue is to maintain the proper position of His72 in the active site. The substitution of Q73 by a bulky and hydrophobic residue such as phenylalanine will not directly change His72, but will most likely affect its physical position. This would consequently interrupt the interactions between His72 and its hydrogen-bond partners.

UV-Vis features of His72 derivatives — The UV-Vis spectra of H72N, H72S have a slightly different Soret band with 403 and 404 nm with regard to that of WT TDO at 405 nm. Q73F presents the Soret band at 405 nm but it has slightly different maximal absorptions in the visible region compared to those in the WT TDO.

EPR properties of the His72 derivatives — Figure 7.2A-E showed the low temperature X-band EPR spectra for WT TDO and His72 derivatives. The EPR spectrum of ferric H72S shows a dominant rhombic high-spin ferric signal at g = 6.11, 5.72, a small amount of rhombic high-spin ferric signal at g = 6.99, 6.66 and a low-spin ferric signal at g = 2.98, 2.31, 1.90. H72N has a rhombic high-spin ferric signal at g = 6.11, 5.62. In addition, a small amount of high-spin ferric signal with g = 6.76 is also observed in H72N. In contrast, only one rhombic high-spin ferric signal is observed at g = 6.11, 5.70 from WT TDO. These observations indicate that the replacement of His72 does not cause significant change to the electronic structure of the ferric center. On the other hand, the replacements sometimes make the active site environment more relaxed to allow two alternative high-spin ferric coordination geometries to be present. This is especially apparent in TDO H72S (Figure 7.2B). Q73F had a predominant axial high-spin ferric signals at g = 6.00, 5.87 and a small amount of rhombic high-spin ferric signal at g = 6.18, 5.87. The interpretation is that the replacement of Gln73 instead of His72 maintains the geometry of the active site environment, although the position and orientation of the components might be perturbed due to the mutation.

The minor presence of the low-spin ferric signal at g = 2.98, 2.31, 1.90 in H72S is not observed in H72N and Q73F. By comparing these g-values with those hydroxide-bound ferric low-spin species identified in other heme-containing proteins (*135, 140, 355*), the g-values in H72S can not be assigned as such. On the other hand, g = 2.98, 2.31, 1.90 are similar to the observations in the heme proteins with imidazole in the sixth coordination position (*356, 357*). It might be explained that the replacement of His72 with a relatively small amino acid serine makes the active site more flexible for incorporation of other small molecules, such as imidazole. Since

imidazole, a histidine analogue was utilized during the purification using nickel affinity column, it can be incorporated into the active site to give rise to the low-spin signal. As for H72N, the Asn residue has a relatively large side chain, which does not allow imidazole access to the active site. Thus, the low-spin ferric species in H72S at g = 2.98, 2.31, 1.90 is assigned as an imidazole-ligated low-spin ferric heme.

Steady-state kinetics of His72 derivatives — The kinetic parameters shown in Table 7.3 were determined at 50 mM Tris pH 7.4 using L-Trp as a substrate. The mutation of H72N to Asn leads to a dramatical decrease in k_{cat} and k_{cat}/K_m with the values reduced by 630-fold and 3470-fold, respectively. The K_m value increases 5.4- fold with regard to that of the wild-type enzyme. On the other hand, the mutation of H72S causes a less pronounced 17-fold decrease of the k_{cat} with a a 1.7-fold increase of the $K_{m,}$ which lead to a 48-fold decrease of k_{cat}/K_m compared to that of WT. Meanwhile, Q73F has a limited effect on catalysis, considering both of catalysis and substrate affinity with only a 2.2-fold decrease of k_{cat} and 4.6-fold increase of K_m which collectively lead to a 10-fold decrease of $k_{cat}/K_{m.}$

pH profile of TDO and His72 derivatives — The effect of pH on WT TDO and His72 derivatives was examined by measuring the activities at various pH values in the presence of 20 mM L-Trp. Four distinct patterns are observed in Figure 7.3. WT TDO shows an unsymmetrical bell-shape with an increased activity on the acidic side and slowly decreased activity on the alkaline side. A plateau forms between pH 7.0 and pH 9.0. Q73F mutant has a similar shape to that of WT TDO, except that the entire curve shifts 1.5 pH units towards the alkaline pH. H72S and H72N display different pH-dependent shapes compared to that of the WT and Q73F enzyme, in which the enzyme activity increases with the increasing pH up to 10.0.

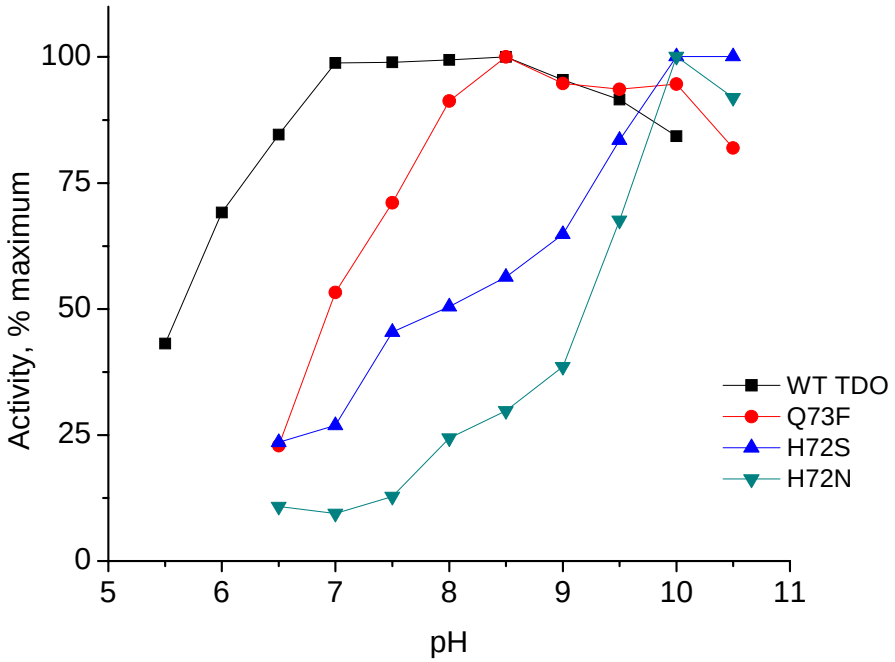

Figure 7.3. pH profile of WT TDO and His72 derivatives. The activities were normalized based on the maximal activities of each enzyme.

Previous studies have shown that WT TDO has little effect on the enzyme activity in the pH range of 6.5-8.5 (*129, 133*). The pH profile of WT TDO shown in Figure 7.2 revalidates this result. Furthermore, our results also reveal a pK_a = 6, which could be assigned for histidine residue in the active site. The replacement of Gln73 with Phe increases the hydrophobic feature of the active site environment which should result in an increased pK_a for the active site residue. The observation of an alkaline-shifted pH profile and the increased pK_a = 7 in Q73F is consistent with this anticipation. The activity of H72N is almost completely diminished at pH < 7, whereas the activity increases with the increasing of pH. H72S has a similar pH profile as that observed in H72N and both of them have a pK_a of more than 10.

All the mutations cause a decrease in the k_{cat} values and a distingulished change in their pH dependence profile suggesting that the His72 residue plays a role in the catalytic reaction.

EPR spectra of ferric His72 derivatives in the presence of L-Trp — The ferric H72S shows a spin mixture of rhombic high-spin ferric signals and a low-spin ferric signal as discussed. Upon adding L-Trp, there is a substantial decrease of the high-spin ferric signal concomitantly with the occurrence of a new low-spin ferric signal which is much more prominent than that of WT TDO under the same condition (Figure 7.4). These *g*-values at g = 2.70, 2.21, 1.79 are similar to those observed for WT TDO in the presence of L-Trp at g = 2.69, 2.19, 1.80 which is assigned as a hydroxide-bound species in Chapter 5. When the concentration of L-Trp was increased from 30 equivalents to 100 equivalents over ferric H72S as shown in Figure 7.5, the high-spin ferric signal almost vanished and a new set of low-spin ferric signal at g = 2.70, 2.21, 1.79 appeared at pH 7.4. This observation suggests that the active site structure of H72S differs from that of WT TDO in which the active site water is much close to the ferric ion center within a hydrogen bond distance upon the binding of L-Trp. This conformation facilitates the formation of low-spin hydroxide-ferric intermediate. The original imidazole-ligated ferric signal at g = 2.97, 2.32, 1.90 decreases and slightly shifts to g = 3.04, 2.31, 1.90 which indicates that the active site water competes with imidazole to bind to the active site in the presence of L-Trp.

The mutants of H72N and Q73F were also studied by EPR spectroscopy upon substrate binding (Figure 7.4). A low-spin ferric signal at g = 2.69, 2.19, 1.80 is generated at the expense of high-spin ferric signal which is similar to that observed in WT TDO and H72S. These findings are indicative of the formation of hydroxide ferric low-spin heme in H72N and Q73F. This spin transition is least efficient in Q73F relative to WT TDO and other His72 derivatives. Based on

the crystal structure of TDO, His72 provides a rigid surface for positioning the substrate bound to the active site by its ring structure. This surface would be more relaxed when His72 was mutated to Asn or Ser. It is possible that in Q73F the rigid geometry of the active site is still maintained by His72 which does not allow for the rearrangement of the hydrogen bond interaction in the active site, even if it is partially disrupted. In contrast, the original hydrogen bond interactions between His72 and L-Trp or active site water are completely lost in H72S and H72N due to the missing of His72. They might cause a significant rearrangement of the hydrogen bond interaction in the active site due to the flexibility introduced by the replacement. These results suggest that the active site hydrogen bond interaction plays a role in the spin transition in ferric TDO. The binding orientation and geometry of substrate to the active site might be perturbed by His72 which results in the increased K_m values and decreased k_{cat} of His72 mutants.

One observation of WT TDO in the presence of L-Trp is that there is a small amount of high-spin species at g = 6.71 which does not present in the absence of L-Trp (Figure 7.4A). On the contrary, the similar g = 6.66 high-spin ferric species is observed in the absence of L-Trp rather than in the presence of L-Trp in H72S. Thus, the high-spin ferric species at g = 6.7 should not be due to the substrate dependent spin transition but resulted from the different hydrogen bond interaction in the active site.

EPR spectra of ferric H72S in the presence of substrate analogues — As shown in Figure 7.6, the binding of D-Trp shifts the high-spin ferric signals of H72S to g = 6.99, 6.66 and 6.42 from the original ones at g = 6.11, 5.72 and g = 6.01, 5.45 whereas the imidazole-ligated low spin ferric species does not change. Low-spin ferric species corresponding to ferric hydroxide species

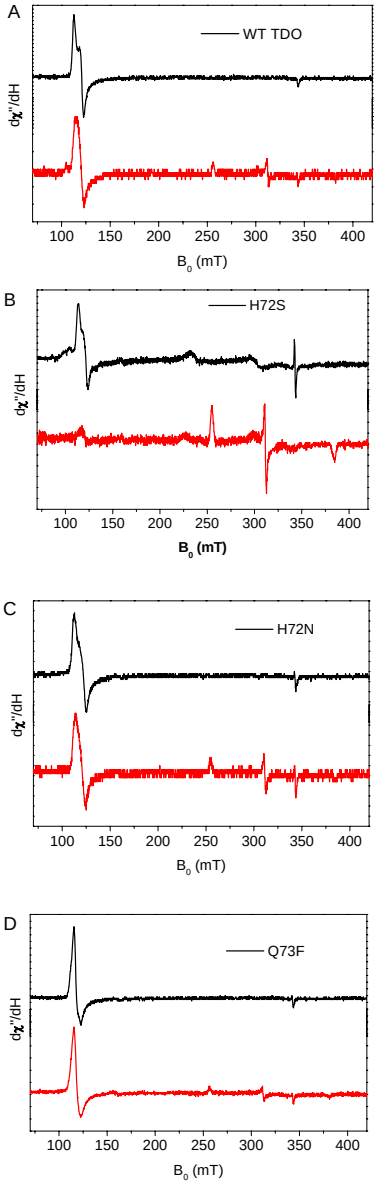

Figure 7.4. EPR spectra of WT TDO and His72 mutants treated with L-Trp. (A) WT TDO; (B) H72S; (C) H72N; (D) Q73F. Top: As-isolated purified TDO proteins; Bottom: As-isoalted TDO proteins treated with L-Trp. Experimental EPR spectra were recorded at 10 K with 3 mW microwave power at 9.4 GHz.

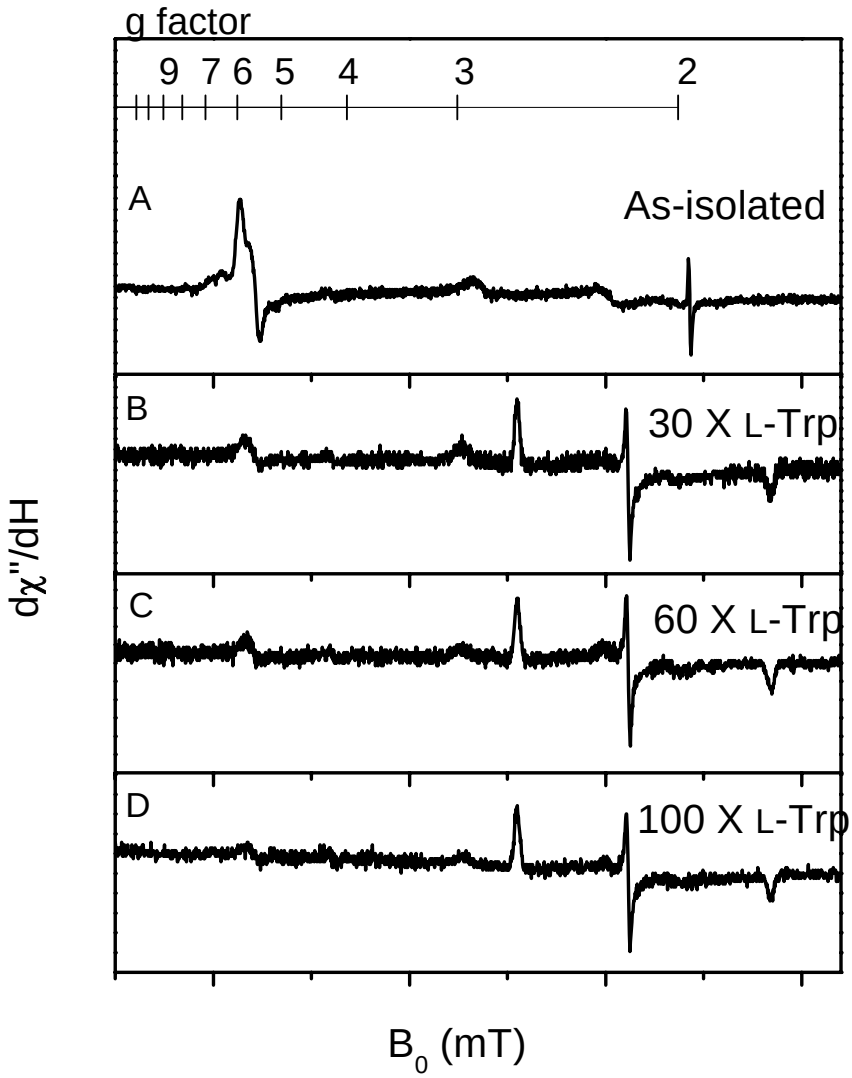

Figure 7.5. EPR spectra of ferric H72S treated with various concentration of L-Trp. (A) As-isolated purified H72S TDO. Ferric H72S was mixed with 30 equivalents of L-Trp (B), 60 equivalents of L-Trp (C) and 100 equivalents of L-Trp (D). Experimental EPR spectra were recorded at 10 K with 3 mW microwave power at 9.4 GHz.

is not observed. By comparing with that of WT TDO, these findings give clear indication that the replacement of His72 with Ser makes substrate binding more flexible, which allows D-Trp to bind to the active site of ferric H72S in a geometry differing from WT TDO. On the other hand,

low spin hydroxide ferric species is not observed upon D-Trp binding in either H72S or WT TDO which gives an indication that the formation of the low spin hydroxide ferric species in the active site is sensitive to the stereochemistry of the substrate. It is most likely due to the missing hydrogen bond interaction between D-Trp and the active site water.

Upon adding 5-OH-Trp, a set of clear low-spin ferric signals occurs at g = 2.70, 2.21, 1.78 which corresponds to the formation of a hydroxide ferric species, whereas the imidazole-ligated low-spin ferric species disappears and the high-spin species dramatically decreases and becomes more axial. This demonstrates that 5-OH-Trp binds to the active site in a similar manner relative to L-Trp and it competes with imidazole and displaces it from the active site. Adding 5-F-Trp to H72S converts half of the high-spin ferric signal to low-spin ferric signal and the remaining high-spin ferric signal becomes more axial. All of these results indicate that substrate or substrate analogues can bind to H72S regardless of the replacement of the active site histidine. However, the binding effect is sensitive to the interactions involved in the substrate analogues and the active site water.

As shown in Figure 7.6, a g = 2 signal exists in H72S. When 30 equivalents of L-Trp was added, the g = 2 signal disappeared. However, upon addition of 100 equivalents of other substrate analogues such as D-Trp, 5-F-Trp and 5-OH-Trp, the signal is still present regardless of the low-spin ferric signal transition. Since D-Trp, 5-F-Trp and 5-OH-Trp are not substrates for dioxygenation reaction catalyzed by TDO, this observation indicates that the g = 2 signal is possibly a radical signal which is relevant to the catalytic activity of H72S.

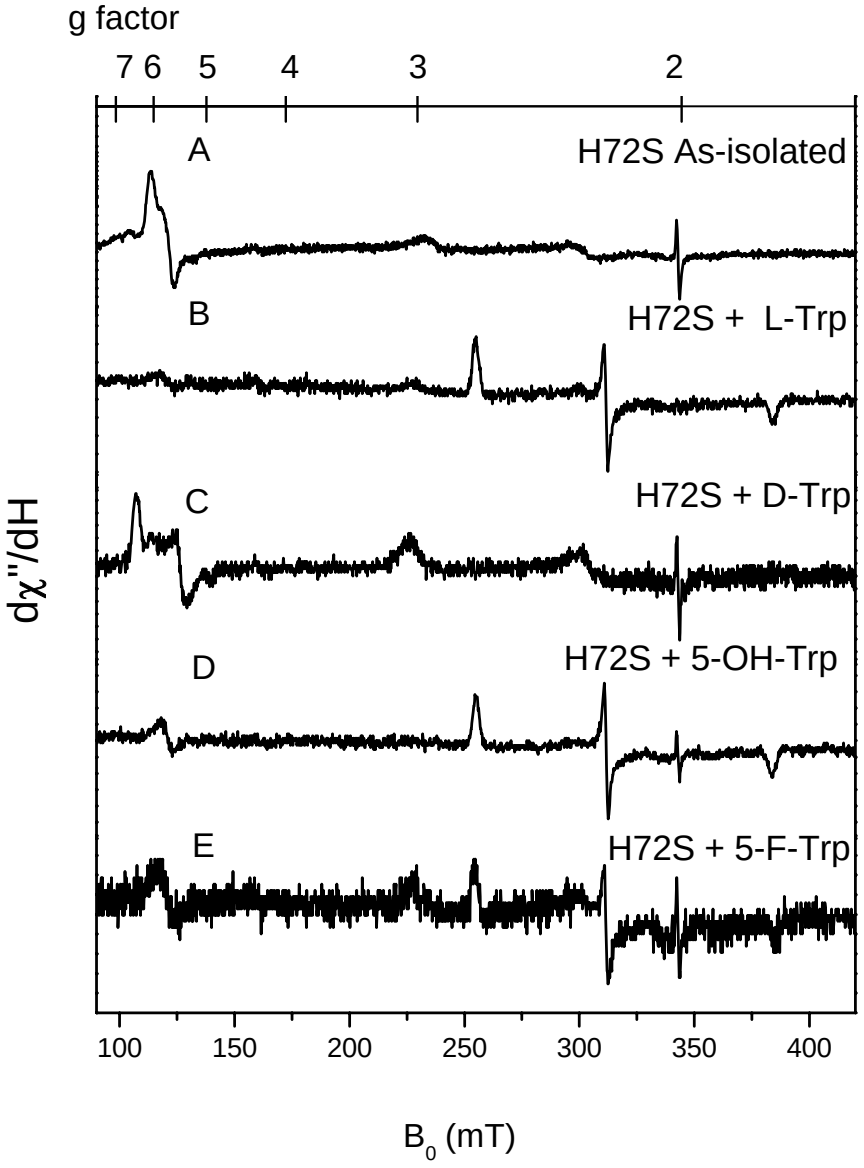

Figure 7.6. EPR spectra of 200 μM ferric H72S mixed with 20 mM substrate or substrate analogues. (A) As-isolated ferric H72S. Ferric H72S mixed with (B) L-Trp; (C) D-Trp; (D) 5-OH-Trp; (E) 5-F-Trp. Experimental EPR spectra were recorded at 10 K with 3 mW microwave power at 9.4 GHz.

EPR spectra of pH dependence of His72 and its mutants — The pH dependence profile shown in Figure 7.3 for H72N and H72S is strikingly different from that of WT TDO. The activity increases with pH with a pK_a value more than 10. This gives an indication of the participation of an alternative base such as a hydroxide ion.

The effect of pH on TDO was studied by EPR spectroscopy. TDO protein samples were exchanged to various pH using HiTrap Desalting column with buffers in 50 mM MES pH 6.0, 50 mM Tris pH 7.4 or 50 mM CHES pH 10.0 containing 10% glycerol. In WT TDO when pH was changed from 7.4 to 6.0, the EPR spectrum shows an axial high-spin ferric signal, suggesting that the more rhombic high-spin ferric species is converted to the axial species. When pH was increased to 10.0, two high-spin ferric signals are observed, the dominant rhombic one at g = 6.13, 5.7 and a small amount one at g = 6.6 (Figure 7.7).

Upon adding L-Trp to ferric TDO at pH 7.4, there are two sets of overlapping spin species as listed in Table 6.1. When pH was increased to 10.0, the g = 6.6 species was intensified and the ratio of g = 6.6 to g = 6.13 species were close to 1:2. The addition of L-Trp to ferric TDO at pH 6.0 shows an axial high-spin ferric signal and does not generate a low-spin ferric signal.

Upon changing the pH of the sample back to pH 7.4 a low-spin ferric species is again observed. These results suggest that either the increased pH from acidic to alkaline condition or the binding of substrate to the active site induces an active site conformational change in which one alternative high-spin ferric signal occurs and the original one becomes more axial. This conformational change is reversible upon changing pH.

The effect of pH on ferric H72S was investigated in the same manner as that in WT TDO. As shown in Figure 7.8, the spectrum of H72S in the absence of L-Trp at pH 6.0 exhibits a typical high-spin ferric signal at g = 6.0, 5.78, 2.0. When pH was raised to 7.4, a spin mixture occurs with a set of overlapping high-spin ferric signals and a low-spin ferric signal as discussed. Raising the pH to 10.0, the g = 6.6 high-spin ferric signal dramatically increases whereas the low-spin ferric signal corresponding to imidazole-ligated ferric heme completely disappears. It is evident that the active site conformation favors the formation of g = 6.6 high-spin ferric species and the imidazole is displaced from the active site at alkaline condition.

Upon adding L-Trp to H72S, half of the g = 6.0, 5.78, 2.0 high-spin ferric species is converted to low-spin ferric heme at pH 7.4 as discussed. In contrast, adding L-Trp to H72S at pH 10.0 induced only a small amount of low-spin ferric species and the high-spin ferric signal did not change much. H72S is unstable at pH 6.0. Based on the observation on WT TDO at pH 6.0 in the presence of L-Trp, the change of the spectrum upon adding L-Trp to H72S at pH 6.0 is not expected to be observed. Together with the pH profile of H72S, the g = 6.6 high-spin ferric species is correlated to the increased catalytic activity in which a potential acid-base catalyst with $p\mathrm{K_a}$ around 10 is involved. These suggest that the two sets of high-spin ferric species might result from two distinguished hydrogen bond networks in the active site in H72S, especially at alkaline condition.

From the crystal structure of substrate-bound H55S in xcTDO, one water molecule (W1) is in the hydrogen bond distance to the heme iron center. One additional water molecule (W2) is introduced into the position of His55 and forms a hydrogen bond with serine. At alkali pH, the g = 6.6 high spin ferric signal might result from the rearrangement of W2 in the active site to the

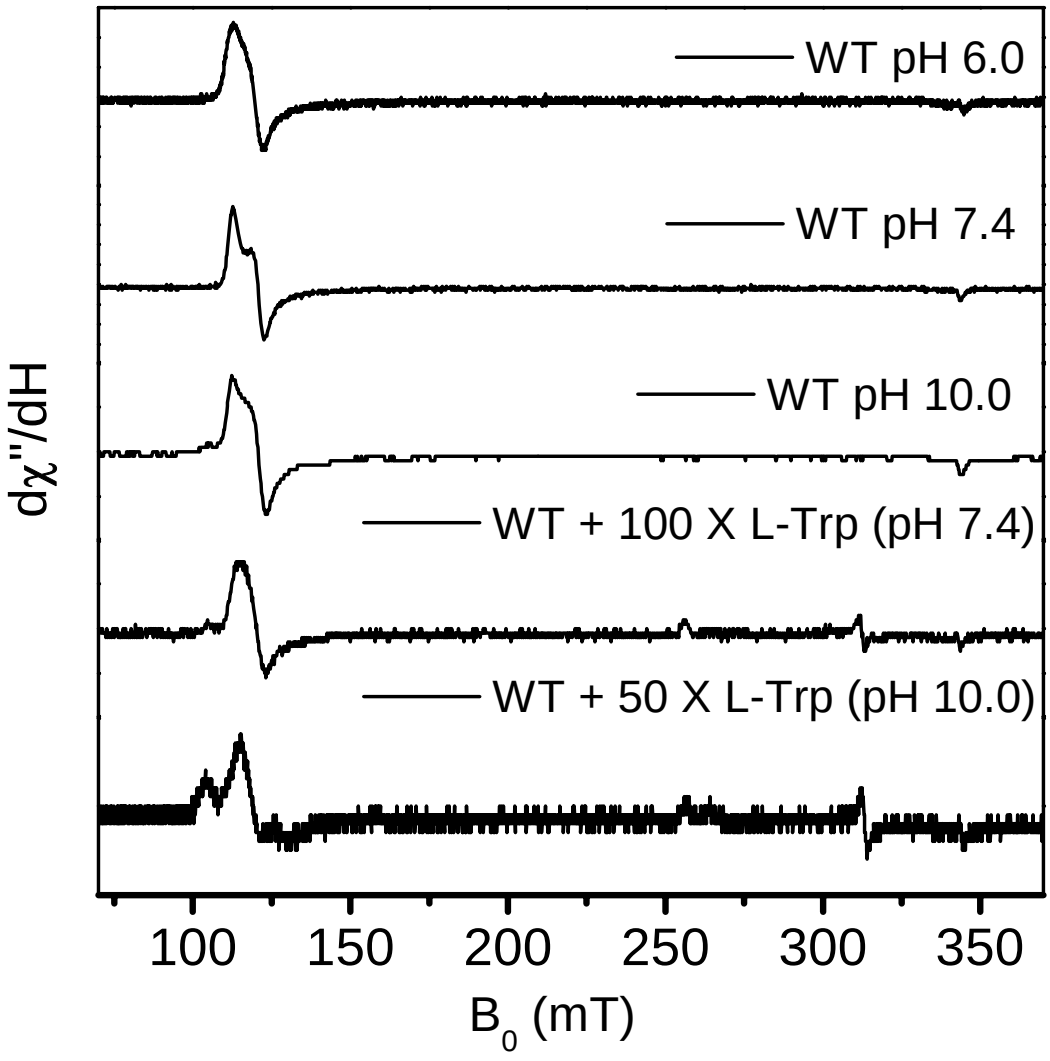

Figure 7.7. EPR spectra of the effect of pH on ferric WT TDO in the absence and presence of L-Trp. Experimental EPR spectra were recorded at 10 K with 3 mW microwave power at 9.4 GHz.

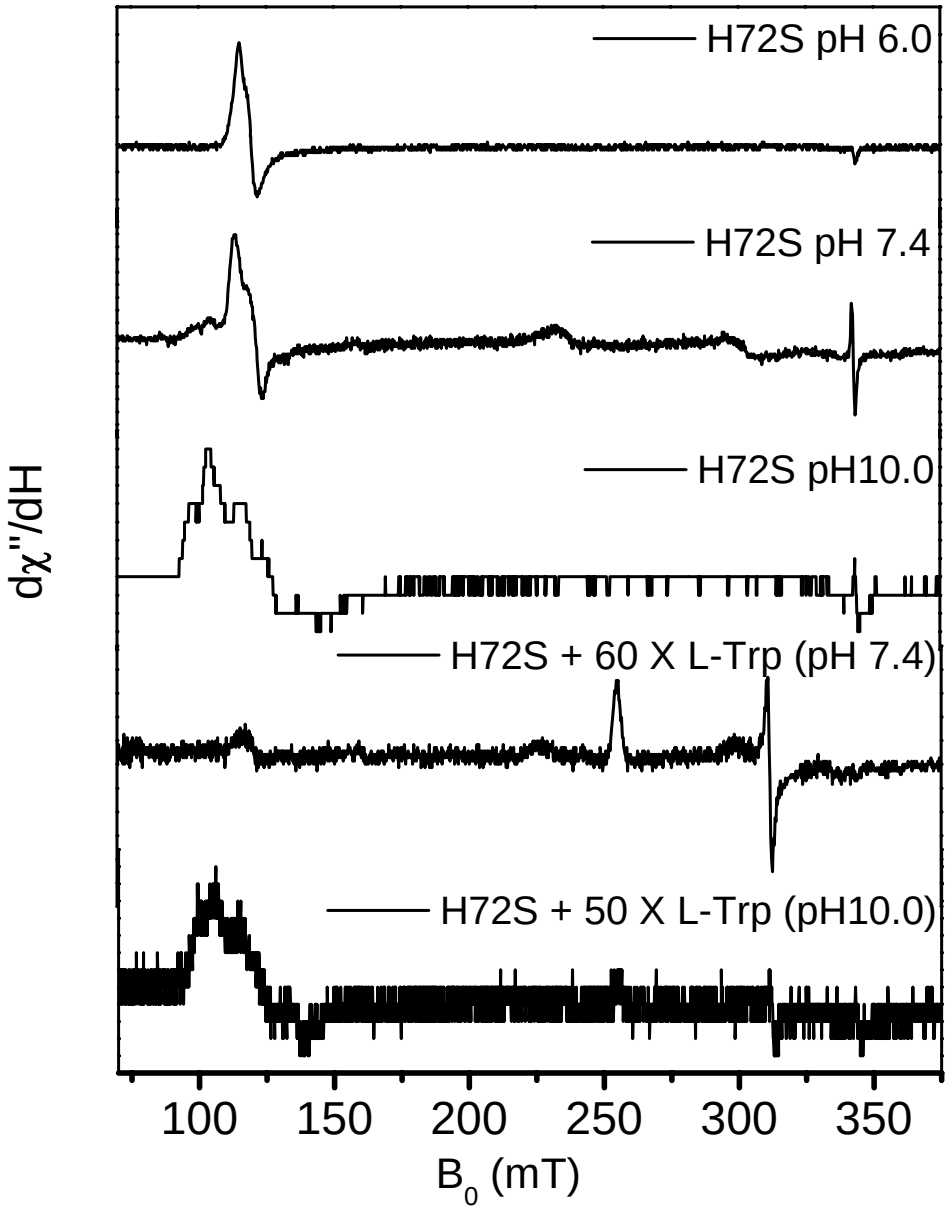

Figure 7.8. EPR spectra of the effect of pH on ferric H72S in the absence and presence of L-Trp. Experimental EPR spectra were recorded at 10 K with 3 mW microwave power at 9.4 GHz.

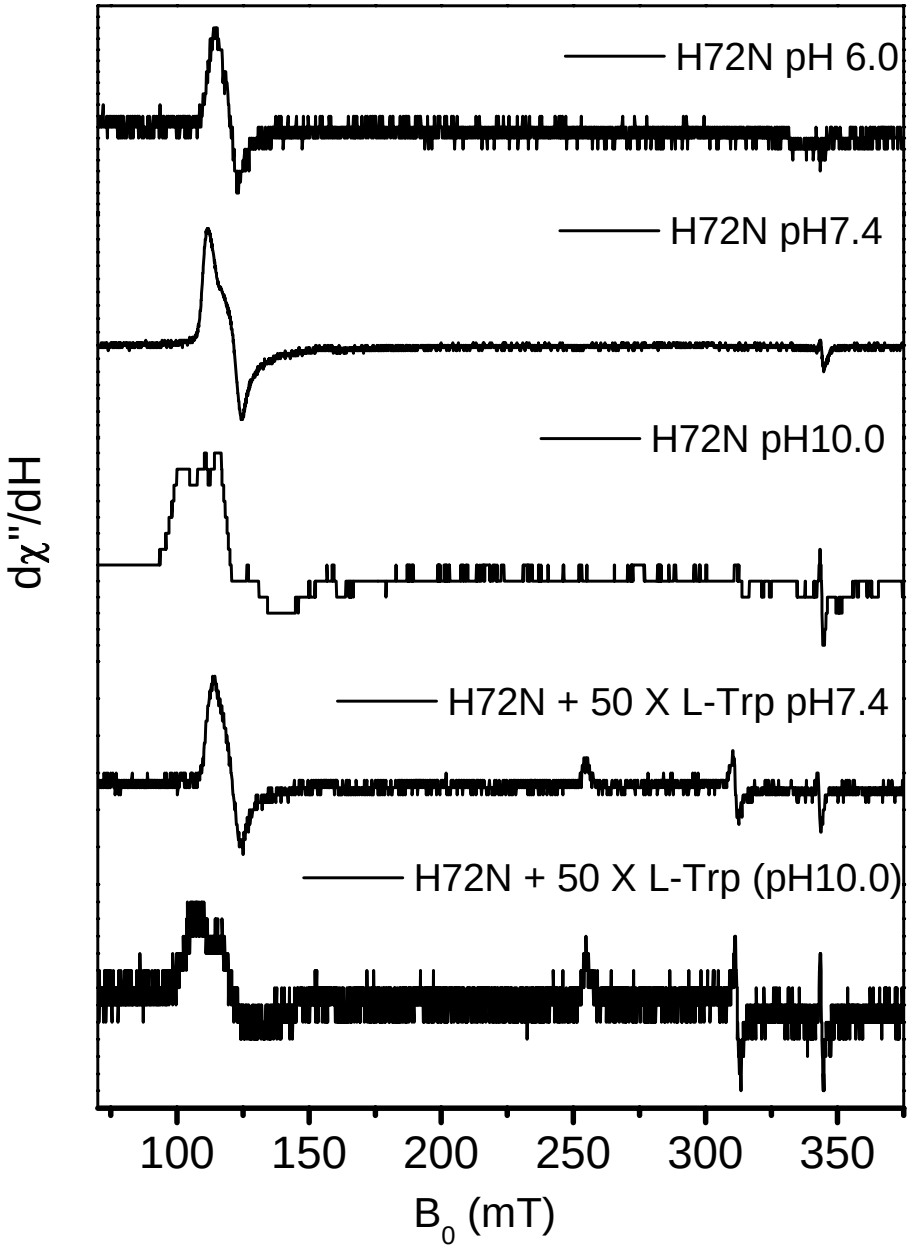

Figure 7.9. EPR spectra of the effect of pH on ferric H72N in the absence and presence of L-Trp. Experimental EPR spectra were recorded at 10 K with 3 mW microwave power at 9.4 GHz.

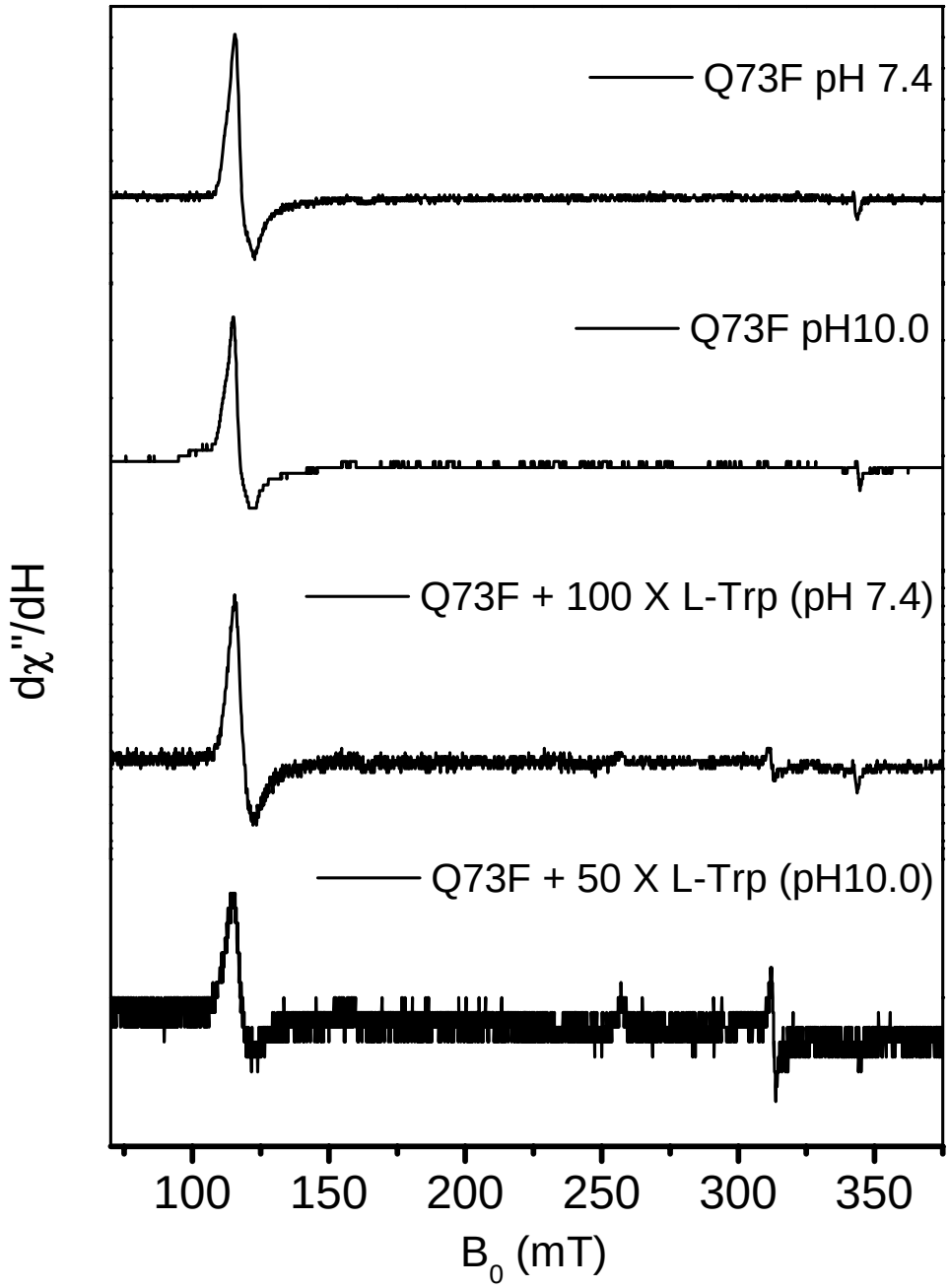

Figure 7.10. EPR spectra of the effect of pH on ferric Q73F in the absence and presence of L-Trp. Experimental EPR spectra were recorded at 10 K with 3 mW microwave power at 9.4 GHz.

position around the original His72. W2 forms a hydrogen bond with L-Trp and is presumed to function as an acid-base catalyst to partially rescue the enzyme activity. Surprisingly, a ferric hydroxide signal is not observed in H72S at pH 10.0 whereas it is present dominantly at pH 7.4. It might be explained that either in acidic or alkaline condition, the active site water molecule of H72S removes the hydrogen bonding distance from the ferric heme.

H72N mutant was also examined upon changing pH as shown in Figure 7.10. The high-spin ferric signals of H72N show a similar trend as observed in H72S. At pH 6.0, the high-spin ferric exhibits a signal at g = 6, 5.73. When pH was increased to pH 7.4, the axial ferric signal becomes much more rhombic. Two overlapping high-spin ferric signals at g = 6.78 and g = 5.94, 5.73 with 1:1 ratio is observed at pH 10.0. The g = 6.78 signal might give rise from the rearrangement of the hydrogen bond network in the active site. Upon adding L-Trp, a low-spin ferric signal is observed at g = 2.7, 2.21, 1.8 at either pH 7.4 or pH 10.0 in H72N. The high-spin ferric signals shift to g = 6.45 and g = 5.94, 5.73 at pH 10.0. The pH profile of H72N is similar to H72S in which the increased catalytic activity is in line with the increased pH. Thus, the dramatically increased g = 6.45 high-spin ferric signal might account for the catalytic activity in H72N which is similar to the observation in H72S.

In Q73F mutant, the high-spin ferric signal does not have significant changes at various pH and regardless of the presence of substrate. Only a small amount of alternative high-spin ferric signal is observed at pH 10.0 other than the original one. Upon substrate binding, the similar low-spin ferric signal corresponding to ferric hydroxide species is observed. In Q73F, the relative rigid active site environment compared to H72S and H72N maintained by His72 and the increased hydrophobic features of the Phe residue are unfavorable for the formation of the alternative high-

spin ferric signal even if at alkaline condition. On the other hand, His72 still functions as an acid-base catalyst as indicated by the pH profile of Q73F (Figure 7.3).

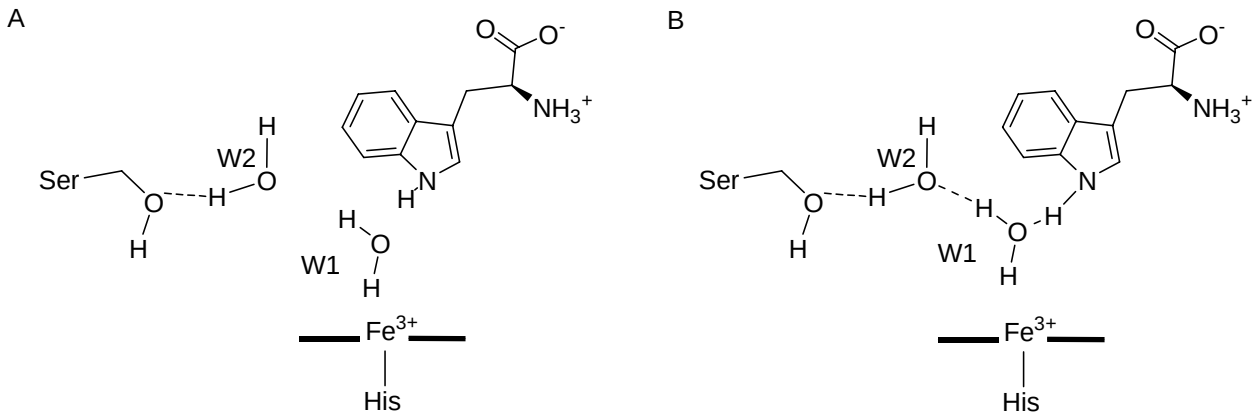

Scheme 7.1. Proposed active site hydrogen bonding interaction in H72S and H72N.

Proposed active site hydrogen bonding interaction in H72S or H72N — Although the crystal structure of H72N mutant is yet not available, a similar active site hydrogen bond network is allocated to H72N by comparing to H72S and is proposed for at neutral (A) and alkaline (B) conditions in Scheme 7.1. In H72S or H72N, an active site water molecule close to heme center is present and designated as W1 which is also observed in WT TDO from the crystal structure. Due to the replacement of His72, the hydrogen bond interaction between His72 and L-Trp is lost as well as the indole ring structure of His72 stabilizing the heme binding pocket. The binding pocket becomes more relaxed and one additional water molecule referred to W2 is introduced into the position close to Asn/Ser, forming a hydrogen bond with Asn/Ser as shown in Scheme 7.1A. When pH is increased, the conformation of the active site is rearranged which facilitates W1 to move away from the ferric ion center, and forms a hydrogen bond with Ser/Asn or W1 which is correlated to the wide extending high-spin ferric signal around g = 6.6 observed in H72S and H72N as well as in WT TDO in the presence of L-Trp, whereas the original one is

around g =6.1. Upon substrate binding, a spin mixture is observed in H72S and H72N in which W1 is within hydrogen bond distance to the ferric heme center to form a low-spin ferric hydroxide and otherwise forms a set of high-spin ferric signals. W1 is located in the active site adjacent to W2 and forms a hydrogen bond with either W2 or Ser/Asn and the NH group of L-Trp in the g = 6.6 high-spin signal (Scheme 7.1B). Based on the pH dependence EPR and pH profile, the pK_a value of W2 is around 10 which is capable of functioning as an active site acid-base catalyst to rescue dioxygenation activity in H72S and H72N (*358*).

CHAPTER 8

THE POTENTIAL LOCALIZATION OF THE PROTEIN RADICAL GENERATED IN PEROXIDE DRIVEN OXYGENATION REACTION OF OXIDIZED TDO

8.1 Introduction

Identification of the amino acid residue that harbors the radical intermediate in the presence of H_2O_2 is necessary for a complete understanding of the peroxide activation of ferric TDO. Should a protein-based radical also be generated in the Fe(II) and dioxygen process, then it will likely be located at the same site. Some protein radicals formed in other heme and non-heme enzymes are directly involved in their catalytic processes. Most stable protein-based radicals are either tyrosyl or tryptophanyl radicals (*243*), because they are easily oxidizable residues and can stabilize the radical with their π-π conjugation ring structure. There are four tyrosine and tryptophan residues that are observed around the enzyme active site and strictly conserved. These are Y130, Y43* (which is intruded from another monomer), W119 and W253 (Figure I.4). In a distal site, Tyr43 is extruded from the adjacent subunit into the active site; Y130 is close to the heme distal site and forms stacking interaction with L-Trp. In a proximal pocket, two tryptophan residues are highly conserved, W119 and W253, which surround proximal histidine and provide stacking interaction to stabilize the proximal pocket. We determined their potential involvement in the formation and localization of the protein radical by site-directed mutagenesis. The Y130F, Y43W, W119F, W253F and W119FW253F mutants were analyzed by EPR spectroscopy after the peroxide reaction.

8.2 Results and Discussion

EPR spectra of the reaction of ferric TDO with hydrogen peroxide — The reactions of ferric TDO and its derivatives with H_2O_2 were investigated using EPR spectroscopy to obtain insight into the protein radical localization in the heme active site. All the EPR samples were prepared by mixing as-isolated TDO derivatives with 6 equivalents of H_2O_2 in 50 mM Tris pH 7.4 buffer containing 10% glycerol. The samples were packed into EPR tubes and frozen in liquid nitrogen. The total time was 25 s. The EPR spectra obtained from H_2O_2-treated TDO samples of Y130F, W119F, W253F and W119F/W253F are similar to that of WT TDO in which a radical signal appeared at g = 2.003 and the high-spin ferric signal dramatically decreases (Figure 8.1A). The EPR spectrum of the Y43W mutant has a small peak at g = 2.03 which accounts for the formation of a relative small amount of a radical.

These differences in radical formation cannot yet be interpreted in detail. Based on the current observations on EPR spectra and the knowledge on the identification of protein radicals, the most probable candidate for the localization of the protein radical is tyrosine 43 (Tyr43). The UV-Vis spectrum of the ferric Y43W has a slightly different Soret band at 406 nm compared to that of WT TDO at 405 nm. Y43F was expressed in a very low yield compared to other TDO derivatives. It exhibits a dramatically shifted Soret band at 411 nm, as well as visible absorption peaks at 532 nm and 576 nm which correlate to a low-spin ferric species (Table 7.1).

EPR spectra of ferric Y43W show a typical axial high-spin ferric signal at g = 6. From crystal structure, Tyr43 is intruded into the active site from the adjacent subunit of the dimer and is 7 Å away from the heme iron center. Except for the hydrogen bond with Glu76, there is no other

hydrogen bond interaction between Tyr43 and the nearby protein matrix. The axial high-spin ferric signal in Y43W compared to other TDO derivatives with rhombic high-spin ferric signals gives an indication that Y43 is involved in the rhombicity of the active site environment via the hydrogen bond interaction with Glu76 and the stacking interaction with L-Trp. When Y43 is replaced with Trp, the hydrogen bond interactions of Tyr43 with Glu76 are disrupted which attributes to the loss of the intersubunit interaction and the potential cooperative interaction within the tetrameric protein and leads to the axial high-spin ferric signal. Although the EPR spectrum of Y43F has a very weak high-spin ferric signal at g = 6.04 and does not resolve very well, it is similar to that observed in Y43W and is consistent with the loss of the intersubunit interaction as proposed for Y43W (Figure 8.1). Y43F displays a new low-spin ferric signal at g = 2.44, 2.29, 2.09 indicating a dramatically changed active site environment in Y43F. The difficulty of expressing of Y43F might be due to the loss of the hydrogen bond interaction between Y43 and Glu76, which pushes Y43 away from the heme binding center and disrupts the proper active site pocket for heme and substrate binding. Very low activity is detected in both Y43 derivatives, with k_{cat} of 0.002 s^{-1} and 0.038 s^{-1} for Y43W and Y43F respectively. These results suggest Y43 plays an important role in catalytic reaction.

When Y43W was treated with H_2O_2, the high-spin ferric signal does not change, but a radical-like signal occurs at g = 2. This finding gives an indication that Tyr43 might not be involved in the formation of a protein radical when treated with H_2O_2.

The UV-Vis, heme occupancy and EPR spectra features of Y130F are the same as that of WT TDO. The kinetic parameters indicate that the hydroxyl group of Try130 does not provide an important contribution to K_m but contributes to the k_{cat} value of Y130F in which the k_{cat} value is

4.6-fold decreased. The radical generation of Y130F is as efficient as that of WT TDO. Thus, the protein radical is not located in Y130F.

Protein radicals are mostly seen in the proximal site of a heme binding pocket. W119F and W253F are highly conserved in the proximal pocket in TDO. When one of them was mutated to Phe, the Soret band did not change. However, the Soret band is 1 nm blue-shifted to 404 nm in W119F/W253F double mutant. The heme occupancy of the three mutants decreases to 35%, 47% and 32%, respectively. This suggests that the proximal tryptophan residues contribute to the heme binding stability and the mutations affect the heme binding in TDO. On the other hand, the three mutants do not have significant effect on the enzyme activity. The most significant effect is the 4-fold decrease of k_{cat} value in W119F/W253F.

As shown in Figure 8.1, in two tryptophan derivatives of TDO, W119F and W253F, the replacement of tryptophan with phenoalanine does not affect the radical formation, which is coupled with a decrease in the high-spin signal. In contrast, the tryptophan double mutant is affected. It concomitantly generates a relatively small portion of radical with a decreased high-spin signal. Since neither of the W119F and W253F derivatives have significant effect on radical formation, there are two possibilities for the residues: (1) Either derivative is the location for radical generation and the radical is easily harbored and transferred between them. (2) Neither derivative is the location for radical generation. Since the double mutants have significant effect on the active site environment, it disrupts the radical generation.

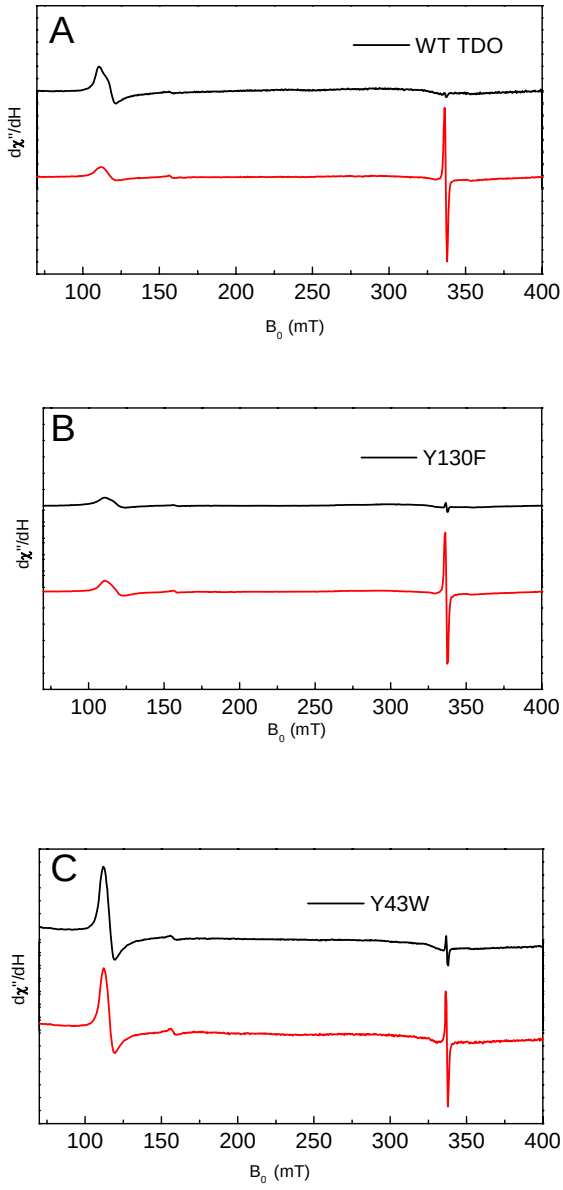
A
WT TDO
dχ''/dH
100
150
200
250
300
350
400
B0 (mT)
B
Y130F
dχ''/dH
100
150
200
250
300
350
400
B0 (mT)
C
Y43W
dχ''/dH
100
150
200
250
300
350
400
B0 (mT)

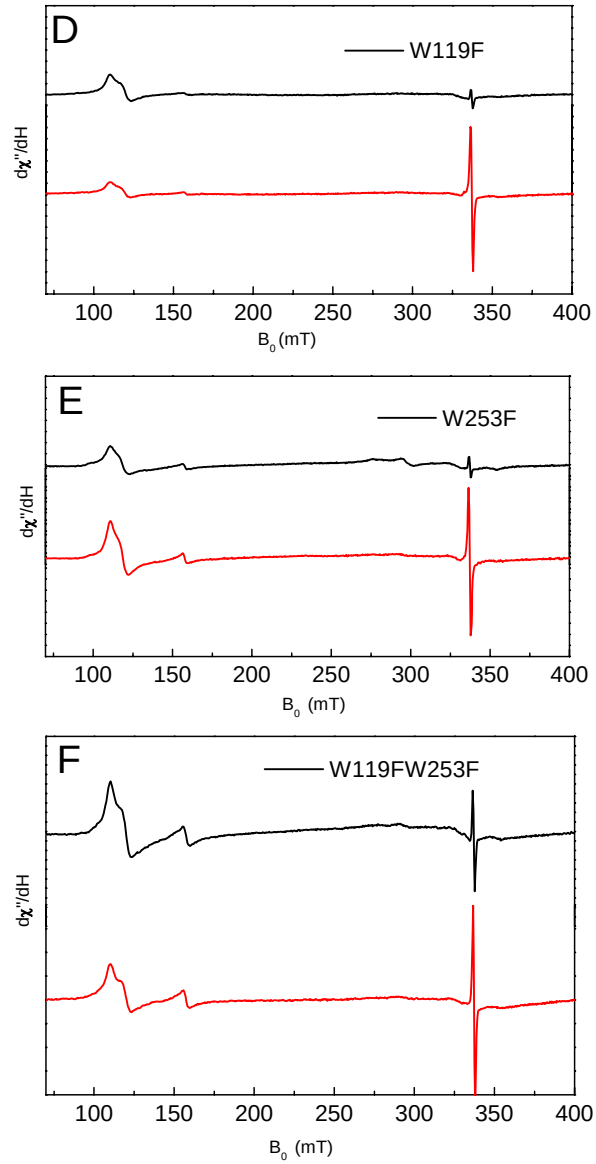

Figure 8.1. EPR spectra of ferric TDO and its derivatives treated with H_2O_2. (A) WT TDO; (B) Y130F; (C) Y43W; (D) W119F; (E) W253F; (F) W119F/W253F. Top line in each panal indicates as-isoalted purified protein; bottom line indicates as-isolated protein treated with H_2O_2. Experimental EPR spectra were recorded at 10 K with 3 mW microwave power at 9.4 GHz.

CHAPTER 9

KINETIC AND PHYSICAL EVIDENCE THAT THE DI-HEME ENZYME MAUG TIGHTLY BINDS TO A BIOSYNTHETIC PRECURSOR OF METHYLAMINE DEHYDROGENASE WITH INCOMPLETELY FORMED TRYPTOPHAN TRYPTOPHYLQUINONE

The section of chapter 9 is a direct copy of our published manuscript to Biochemistry on MauG: Kinetic and Physical Evidence that the Di-heme Enzyme MauG Tightly Binds to a Biosynthetic Precursor of Methylamine Dehydrogenase with Incompletely Formed Tryptophan Tryptophylquinone. Xianghui Li, Rong Fu, Aimin Liu and Victor L. Davidson (2008). The expression and purification of MauG protein, kinetic analysis were conducted by Dr. Xianghui Li (Department of Biochemistry, The University of Mississippi Medical Center, Jackson, Mississippi); High-resolution size-exclusion chromatography of protein mixtures was performed by Rong Fu (Department of Chemistry, Georgia State University, Atlanta). The manuscript was initially prepared by Dr. Xianghui Li. Other authors provided input for the manuscript. This work was supported by NIH grant GM-41574 (V.L.D.) and an ORAU Faculty Enhancement Award in Life Sciences (A.L.)

9.1 Abstract

Methylamine dehydrogenase (MADH) contains the protein-derived cofactor tryptophan tryptophylquinone (TTQ) which is generated by the post-translational modification of two endogenous tryptophan residues. The modifications are incorporation of two oxygens into one

tryptophan side chain, and the covalent cross-linking of that side chain to a second tryptophan residue. This process requires at least one accessory gene, *mauG*. Inactivation of *mauG* in vivo results in production of an inactive 119 kDa tetrameric $\alpha_2\beta_2$ protein precursor of MADH with incompletely synthesized TTQ. This precursor can be converted to active MADH with mature TTQ in vitro by reaction with MauG, a 42 kDa di-heme enzyme. Steady-state kinetic analysis of the MauG-dependent conversion of the precursor to mature MADH with completely synthesized TTQ yielded values of k_{cat} of 0.20 ± 0.01 s^{-1} and K_m of 6.6 ± 0.6 μM for the biosynthetic precursor protein in an in vitro assay. In the absence of an electron donor to initiate the reaction it was possible to isolate the MauG-biosynthetic precursor (enzyme-substrate) complex in solution using high-resolution size-exclusion chromatography. This stable complex is non-covalent and could be separated into its component proteins by anion exchange chromatography. In contrast to the enzyme-substrate complex, a mixture of MauG and its reaction product, mature MADH, did not elute as a complex during size-exclusion chromatography. The differential binding of MauG to its protein substrate and protein product of the reaction indicate that significant conformational changes in one or both of the proteins occur during catalysis which significantly affects the protein-protein interactions.

9.2 Introduction

Methylamine dehydrogenase (MADH) (*359*) from *Paracoccus denitrificans* catalyzes the oxidative deamination of methylamine to formaldehyde plus ammonia and then transfers substrate-derived electrons to amicyanin, a type 1 copper protein. MADH possesses a heterotetrameric $\alpha_2\beta_2$ structure. Each smaller β subunit possesses a tryptophan tryptophylquinone (TTQ) (*360*) prosthetic group, which mediates both catalysis and electron transfer. TTQ is a

protein-derived cofactor (*361*) synthesized through post-translational modification of two endogenous tryptophan residues. This modification involves the incorporation of two oxygens into *β*Trp57 and cross-linking of *β*Trp57 and *β*Trp108 (*362*). The methylamine utilization (*mau*) gene cluster that encodes the MADH subunits also contains nine other genes that relate to MADH biosynthesis and function (*363*). One of these genes, *mauG*, has been shown to be absolutely required for TTQ biosynthesis (*363-365*). The gene product, MauG, is a 42.3 kDa protein which contains two covalently-bound *c*-type hemes, one low-spin and one high-spin (*366*), which exhibit cooperative redox behavior (*367*). In contrast to typical *c*-type cytochromes, reduced MauG is oxidized by O_2, and the EPR parameters for MauG are atypical of *c*-type cytochromes and much more similar to those of hemes that bind and activate oxygen, such as ligand complexes of cytochrome P450CAM and the complex of heme oxygenase with heme (*366*).

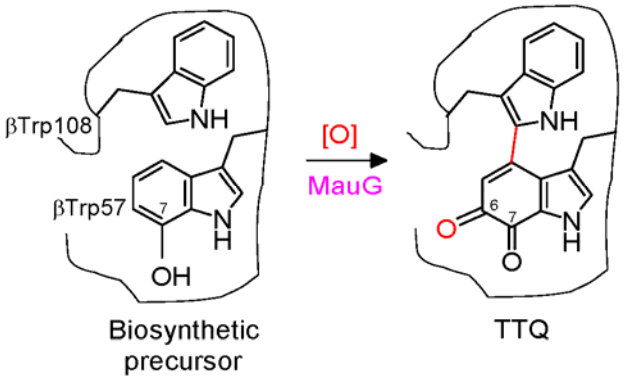

Figure 9.1. MauG-dependent TTQ biosynthesis.

A heterologous expression system for MADH was developed which included the structural genes for MADH as well as the other genes required for MADH biosynthesis (*368*). The recombinant MADH exhibits spectral and kinetic properties which are indistinguishable from native MADH. Deletion of mutation of *mauG* in this recombinant expression system results in production of a biosynthetic precursor of MADH with incompletely synthesized TTQ, in which *β*Trp57 is mono-hydroxylated at C7 and the cross-link with *β*Trp108 is absent (*364*). This tetrameric protein precursor is catalytically inactive with respect to MADH activity. It also exhibits weakened subunit-subunit interactions relative to mature MADH, as determined by non-denaturing polyacrylamide gel electrophoresis (*364*). Incubation of this precursor with MauG in vitro in the presence of either O_2 plus an electron donor or H_2O_2 results in formation of active MADH with fully synthesized TTQ with the second oxygen incorporated at C6 and the cross-link formed (Figure 9. 1), and normal strengthened subunit-subunit interactions (*365, 369, 370*).

The process of MauG-dependent TTQ biosynthesis is of interest for several reasons. It is the first description of an enzyme-mediated post-translational modification to generate a protein-derived cofactor (*361*). It is also an atypical enzyme reaction as the substrate is a 119 kDa precursor protein which is much larger than the 42.3 kD enzyme, MauG. Furthermore, the specific amino acid residue which is modified is located in the interior of the protein substrate, not on its surface. Thus, the nature of the interactions between enzyme and substrate and the structure of the enzyme-substrate complex are not obvious. Whether the conventional Michaelis-Menten theory is a tenable model for this system is unknown. In this study the interaction between MauG and its biosynthetic precursor protein substrate are characterized by steady-state kinetics and analysis by high-resolution liquid chromatography, including size-exclusion and anion-exchange separation

of protein components. The results provide kinetic properties for this unusual reaction and demonstrate that MauG is able to strongly discriminate between its substrate, the biosynthetic precursor protein, and its product, mature MADH.

9.3 Experimental Procedures

MauG was homologously expressed in *P. denitrificans* and purified as described previously (*366*). The concentration of MauG was determined using its extinction coefficient of 208,000 $M^{-1}cm^{-1}$ at 405 nm. Native MADH was purified from *P. denitrificans* as described previously (*371*) and its concentration was determined using its extinction coefficient of 26,200 $M^{-1}cm^{-1}$ at 440 nm in the oxidized form (*372*). The biosynthetic precursor of MADH which contains mono-hydroxylated βTrp57 and no crosslink to βTrp108 (*364*) was heterologously expressed in *Rhodobacter sphaeroides* and purified as described previously (*368*). The yield of this precursor protein which is very low (approximately 1 mg from 20 L cell culture) was quantitated using an extinction coefficient of 157,000 $M^{-1}cm^{-1}$ at 280 nm. Since the isolated precursor protein was not completely pure it was routinely run side by side on polyacrylamide gel electrophoresis with known concentrations of pure native MADH to verify concentration. In steady-state kinetic studies the amount of product (mature MADH) after completion of the reaction was determined from its extinction coefficient as described above, and compared with the estimated concentration of protein precursor substrate to further verify the substrate concentration in these experiments.

Steady-state kinetic studies of MauG-dependent in vitro TTQ biosynthesis from the biosynthetic precursor protein were performed using a previously described spectrophotometic method (*369*).

Reactions were performed aerobically using ambient dioxygen as the oxygen donor and NADH as an electron donor. Electron donation to MauG was mediated by an NADH-dependent oxidoreductase which is present in the preparation of the biosynthetic precursor (*369*). The reaction was monitored by the rate of appearance of the TTQ chromophore at 450 nm. This wavelength was used rather than the absorption maximum at 440 nm to minimize interference from the strong Soret peak of MauG. Data were fit to eq 1, where *S* is the concentration of the MADH biosynthetic precursor protein, *E* is the concentration of MauG, *v* is the initial reaction velocity, k_{cat} is the turnover number (V_{max}/E), and K_m is Michaelis constant.

$$v/E = k_{cat}[S]/([S] + K_m) \qquad [10.1]$$

High-resolution size-exclusion chromatography of protein mixtures was performed using a HiLoad 16/60 Superdex 200 column on an ÅKTA FPLC system (GE Healthcare Life Science). The column was equilibrated and eluted at 1 ml/min with 50 mM potassium phosphate, pH 7.5, containing 25 mM NaCl. The column was calibrated at the beginning, end, and between runs using the following molecular mass markers (Bio-rad): thyroglobin (670 kDa), γ-globulin (158 kDa), ovalbumin (44 kDa), myoglobin (17 kDa) and vitamin B_{12} (1,350 Da). Anion exchange separation of fractions obtained during size exclusion chromatography of the mixture of MauG and the MADH biosynthetic precursor was performed using a MonoQ 4.6/100 PE column with a flow rate of 1 ml/min using a linear NaCl gradient in 50 mM potassium phosphate, pH 7.5.

9.4 Results and Discussion

It was previously shown (*369*) that four diverse electron donors; ascorbate, dithiothreitol, reduced glutathione and NADH were each able to provide reducing equivalents for MauG-

dependent TTQ biosynthesis under aerobic conditions. Under anaerobic conditions in the absence of an electron donor, H_2O_2 could serve as a substrate for MauG-dependent TTQ

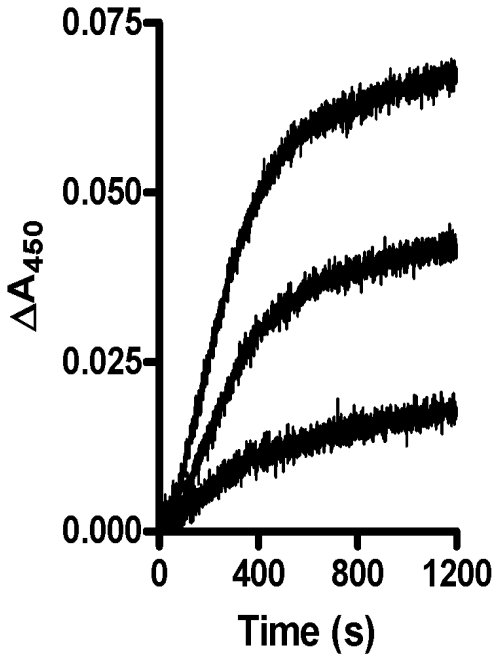

Figure 9.2. MauG-dependent TTQ biosynthesis. Time courses are shown of the absorbance change at 450 nm in the presence of varying concentrations (0.76, 1.95 and 2.63 μM) of the MADH biosynthetic precursor protein. Each reaction mixture also contained 0.23 μM MauG and 300 μM NADH in 10 mM potassium phosphate buffer, pH 7.5.

biosynthesis. NADH was used as the electron donor in the current study for the following reasons. The rates of reaction with the other three electron donors were significantly slower than with NADH. For study of the steady-state reaction parameters with respect to the biosynthetic precursor protein substrate it was necessary to chose the fastest electron donor to insure that reduction of MauG was not the rate-determining step in the reaction. While H_2O_2 was an efficient alternative substrate, when present in large excess as needed in this experiment it caused

damage to MauG. The reaction with NADH is mediated by a non-physiological NADH-dependent oxidoreductase which purifies under the same conditions used to purify the biosynthetic precursor protein (*369*). The current study exploits this opportunity to initiate the reaction with a safe and efficient source of electrons. As seen below, in this assay the rate and extent of the reaction is clearly dependent on the concentration of the biosynthetic precursor protein substrate and allows determination of the kinetic parameters of interest.

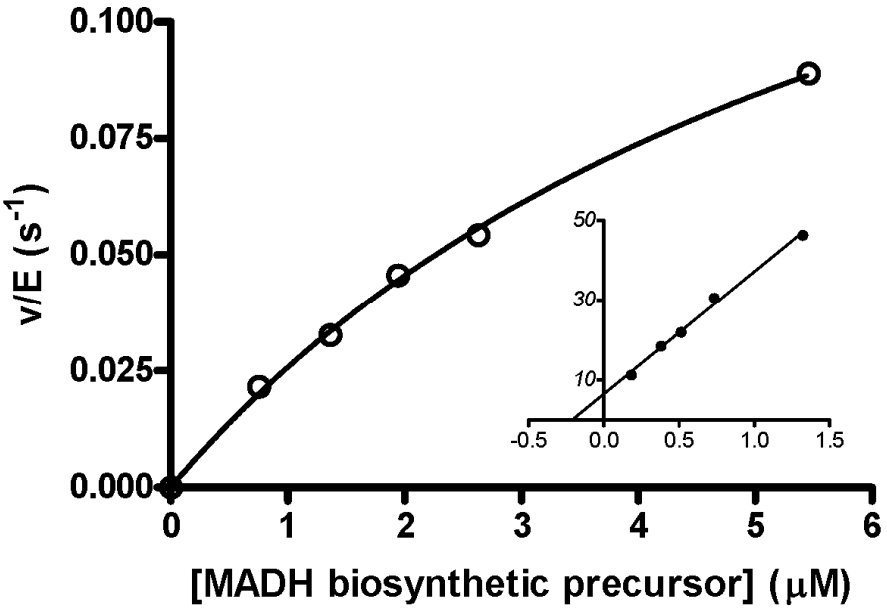

Figure 9.3. Steady-state kinetic analysis of MauG-dependent TTQ biosynthesis. Initial rates were determined from the time courses shown in Figure 9.2 as well as from additional experiments. The dependence of the initial rates of reaction on the concentration of the MADH biosynthetic precursor is plotted and the data were fit to eq 10.1. A double reciprocal plot of these data is shown in the inset.

The biosynthetic precursor protein of MADH with incompletely formed TTQ does not exhibit any visible absorbance. Mature MADH with TTQ exhibits a broad absorption peak centered at 440 nm. In these steady-state kinetic experiments the rate of product formation (i.e., appearance of MADH with completely synthesized TTQ) was monitored by following the increase in absorbance at 450 nm. The time courses of MauG-dependent TTQ biosynthesis at varying concentrations of the MADH biosynthesis precursor are shown in Figure 9.2. It should be noted that the substrate precursor protein is purified at very low levels of approximately 1 mg from 20 L cell culture, and is relatively unstable. This prohibited using much higher concentrations of substrate in these steady-state experiments. The initial rate of MauG-dependent TTQ synthesis exhibited a hyperbolic dependence on the concentration of the biosynthetic precursor protein (Figure 9.3). A fit of these data to eq 1 yielded values of K_m of 6.6 ± 0.6 μM and k_{cat} of 0.20 ± 0.01 s^{-1}. MauG-dependent TTQ biosynthesis is an unusual enzymatic reaction in that the substrate, a 119 kDa tetrameric precursor protein, is much larger than the enzyme, a 42 kDa di-heme protein. The K_m of 6.6 μM suggests that the enzyme and protein substrate exhibit a relatively strong affinity towards each other.

It is usually not possible to isolate a stable enzyme-substrate complex since once formed the conversion of substrate to product will occur. In this reaction under aerobic conditions a source of electrons is required for the reaction. Thus, by omitting a source of electrons from the reaction mixture it was possible to examine the interactions between the enzyme and substrate without the possibility of conversion of substrate to product. The interactions between MauG, the MADH biosynthetic precursor protein, and mature MADH were studied using high-resolution size-exclusion chromatography. Since no electron donor is present, even under aerobic conditions, the

biosynthetic reaction will not occur to a significant extent during the relatively rapid FPLC chromatography. The results clearly indicate that MauG forms a stable protein complex with the MADH biosynthetic precursor in solution, but not with mature MADH (Figure 9.4). MauG alone eluted primarily as a major single peak corresponding to a mass of approximately 43 kDa. The molecular weight calculated from the sequence of MauG including the hemes is 42319.7 Da. MADH alone eluted as a single peak of an apparent mass of 127 kDa. The molecular weight calculated from the sequence of MADH including posttranslational modifications is 119269.7 Da. A mixture of a 4:1 molar ratio of MauG and mature MADH resulted in two well-separated protein fractions corresponding to apparent mass of 43 and 127 kDa, respectively, with no evidence for stable complex formation between the proteins (Figure 9.4A). The MADH biosynthetic precursor protein alone eluted as a major peak at 131 kDa. The slightly larger apparent mass relative to mature MADH is consistent with previous suggestions that the MADH biosynthetic precursor has a less compact tetrameric complex structure than mature MADH (*364*). A mixture of a 2:1 molar ratio of MauG and the biosynthetic precursor protein eluted primarily as a peak corresponding to an apparent mass of 189 kDa (Figure 9.4B), indicating significant formation of a stable complex between these two proteins.

To confirm the presence of both MauG and the biosynthetic precursor of MADH in the 189 kDa peak which eluted when the mixture of the two was applied to the Superdex column, that fraction was collected and immediately subjected to strong anionic exchange chromatography over a MonoQ 4.6/100 PE column (Figure 9.5). Two fractions were obtained. Visible absorbance spectra and SDS-PAGE showed that the fraction eluting at 210 mM NaCl was MauG and the fraction eluting at 400 mM NaCl was the MADH biosynthetic precursor protein. Thus the

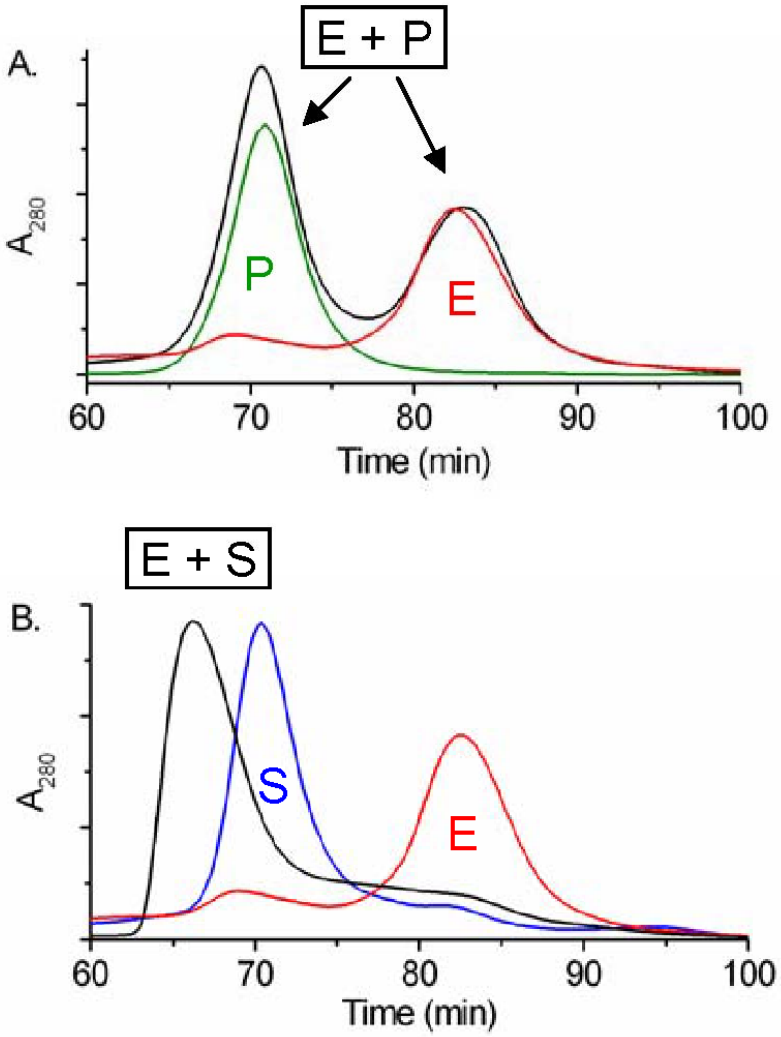

Figure 9.4. Gel filtration analysis of the enzyme MauG (E), the product of its reaction MADH (P), its substrate the MADH biosynthetic precursor (S) and mixtures of E + P and E + S. (A) MauG (E, red), MADH (P, green), and a mixture of 4:1 MauG to MADH (black). (B) MauG (E, red), the MADH biosynthetic precursor (S, blue) and a mixture of 2:1 MauG to the MADH biosynthetic precursor (black). Chromatograms of the mixtures were scaled to size with respect to absorbance to allow easier comparison of peak positions.

mixture of MauG and the biosynthetic precursor protein form a stable enzyme-substrate complex which can endure size-exclusion chromatography while the MauG-MADH enzyme-product complex cannot. These data also show that there is no covalent bond between the biosynthetic precursor protein and MauG and that the tight binding is solely due to the protein-protein interactions.

We have previously noted that the reactivity and EPR properties of MauG are similar to those of cytochrome P450s, despite the fact that MauG contains *c*-type hemes and different axial ligation (*366, 369*). The cytochrome P450 catalytic cycle is initiated by substrate binding to the oxidized enzyme with heme in the ferric state (*373*). The current study shows that MauG in the oxidized state is also capable of tightly binding its substrate. The observation that MauG binds tightly to the tetrameric MADH biosynthetic precursor, but not to mature MADH, suggests that there is a significant difference in the conformations of the precursor protein and mature MADH, or that the MADH biosynthetic precursor is a more dynamic structure than MADH, or both. It was previously reported (*374*) that a loop comprised of residues β90 – β108 on the β subunit of MADH forms about 52% of the interface between α and β subunits of MADH. This is significant as the residue at the end of loop, βTrp108, is crosslinked to form TTQ in the mature enzyme. In mature MADH, this loop is folded over TTQ and is anchored in place by the crosslink between βTrp57 and βTrp108. In the biosynthetic protein precursor substrate which lacks this crosslink, this loop would be much more flexible and disordered thereby destabilizing the subunit-subunit interactions and allowing access to the mono-hydroxylated residue βTrp57 by a processing enzyme, such as MauG. The different structural and dynamic properties of the biosynthetic precursor protein relative to mature MADH apparently allow MauG to bind its substrate

precursor protein with its active site, presumably the high-spin heme, accessible to βTrp57 for incorporation of oxygen. Once the MauG-dependent catalysis of TTQ formation is complete this loop is no longer flexible but now anchored in place. Subunit-subunit interactions are strengthened and the binding site for MauG is no longer accessible in the mature MADH.

This work describes a kinetic characterization for MauG-dependent TTQ biosynthesis in vitro. This is the first such description of an enzyme-mediated post-translational modification to generate a protein-derived cofactor. The steady-state kinetic data show that the conventional Michaelis-Menten theory is still an appropriate model for this system. The relatively small K_m for the biosynthetic precursor protein substrate suggests a strong affinity with MauG despite the fact that the substrate is nearly 3-fold larger than the enzyme itself (i.e., MauG). These kinetic results are supported by the demonstration that MauG and its natural precursor protein substrate form a complex which is sufficiently stable to sustain size-exclusion chromatography. While it is not unique that the substrate of an enzyme is a larger protein molecule, one rarely observes such a stable enzyme-substrate protein complex. In this study we were able to do so by exploiting the fact that the enzyme-substrate complex will not turn over in the absence of a reductant. In many other cases where the substrate is a big-size protein molecule, the interaction mode between the enzyme-substrate is often difficult to characterize because the reaction will proceed during chromatographic separation. However, these data do not exclude the possibility that MauG also interacts with mature MADH in solution. We have previously shown that MauG and mature MADH may undergo an interprotein redox reaction. The enzyme and the mature MADH clearly do not form such a stable protein-protein complex. This suggests that significant conformational

changes in one or both of the proteins occur during catalysis which significantly affects the protein-protein interactions.

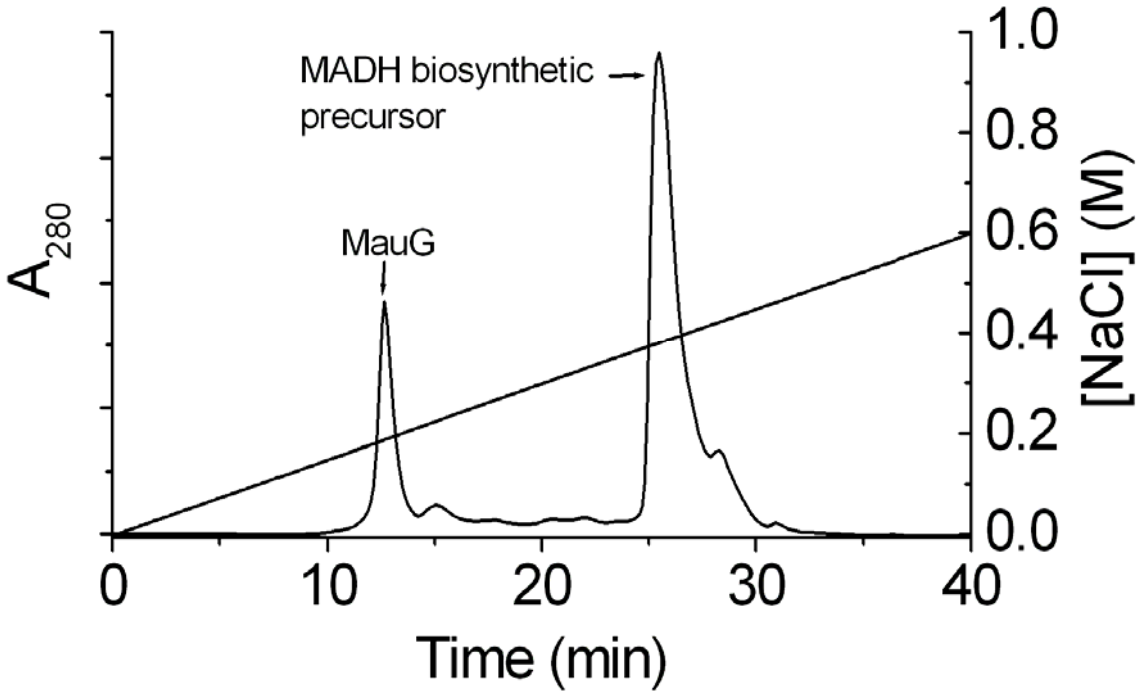

Figure 9.5. Anion exchange separation of components of the 189 kDa fraction obtained during size exclusion chromatography of the 2:1 mixture of MauG and the MADH biosynthetic precursor.

CHAPTER 10

A CATALYTIC DI-HEME *BIS*-FE(IV) INTERMEDIATE, ALTERNATIVE TO AN FE(IV)=O PORPHYRIN RADICAL

The section of chapter 10 is a direct copy of our published paper in PNAS on MauG: A Catalytic di-Heme *bis*-Fe(IV) Intermediate, Alternative to an Fe(IV)=O Porphyrin Radical. Xianghui Li, Rong Fu, Sheeyong Lee, Carsten Krebs, Victor L. Davidson, and Aimin Liu (2008). The expression and purification of ^{56}Fe-TDO and ^{57}Fe-TDO protein were conducted by Xianghui Li, Sheeyong Lee (Department of Biochemistry, The University of Mississippi Medical Center, Jackson, Mississippi); EPR experiment was conducted by Rong Fu (Department of Chemistry, Georgia State University, Atlanta); Mössbauer samples were prepared by Rong Fu and Aimin Liu. Mössbauer spectroscopy analyses were conducted by Dr. Carsten Krebs (Department of Biochemistry and Molecular Biology and Department of Chemistry, The Pennsylvania State University, University Park, Pennsylvania); The manuscript was prepared by Dr. Aimin Liu. This work was supported by National Institutes of Health grant GM41574 (V.L.D.), GM069618 and ORAU Faculty Enhancement Award in Life Sciences (A.L.), Young Investigator Award from the Arnold and Mabel Beckman Foundation and Camille Dreyfus Teacher-Scholar Award from the Camille and Henry Dreyfus Foundation (C.K.).

10.1 Abstract

High-valent iron species are powerful oxidizing agents in chemical and biological catalysis. The best characterized form of an Fe(V) equivalent described in biological systems is the

combination of a *b*-type heme with Fe(IV)=O and a porphyrin or amino acid cation radical (termed compound I). This study describes an alternative natural mechanism to store two oxidizing equivalents above the ferric state for biological oxidation reactions. MauG is an enzyme which utilizes two covalently-bound *c*-type hemes to catalyze the biosynthesis of the protein-derived cofactor tryptophan tryptophylquinone (TTQ). Its natural substrate is a monohydroxylated tryptophan residue present in a 119 kDa precursor protein. An EPR-silent di-heme reaction intermediate of MauG was trapped. Mössbauer spectroscopy revealed the presence of two distinct Fe(IV) species. One is consistent with an Fe(IV)=O (ferryl) species (δ = 0.06 mm/s, ΔE_Q = 1.70 mm/s). The other is assigned to an Fe(IV) heme species with two axial ligands from protein (δ = 0.17 mm/s, ΔE_Q = 2.54 mm/s) which has never before been described in nature. This *bis*-Fe(IV) intermediate is remarkably stable but readily reacts with its native substrate. These findings broaden our views of how proteins can stabilize a highly reactive oxidizing species and the scope of enzyme-catalyzed posttranslational modifications.

10.2 Introduction

Tryptophan tryptophylquinone (TTQ) is the protein-derived catalytic cofactor of methylamine dehydrogenase (MADH) from *Paracoccus denitrificans*, a 119 kDa heterotetrameric $\alpha_2\beta_2$ protein with a TTQ present on each β subunit (*375, 376*). TTQ biosynthesis requires incorporation of two oxygens into β Trp57 and cross-linking of the indole rings of β Trp57 and β Trp108 (Figure 10.1A). This is not a self-processing event but requires the action of at least one processing enzyme. Deletion of *mauG*, a gene in the methylamine utilization (*mau*) gene cluster (*172*), causes accumulation of a biosynthetic precursor of MADH in which βTrp57 is

monohydroxylated at C7 and the cross-link is absent (*175, 178*). Formation of mature MADH with TTQ from the biosynthetic precursor is a six-electron oxidation process; two for insertion of the second oxygen, two for formation of the cross-link, and two for the oxidation of quinol to the quinone. MauG-dependent TTQ-biosynthesis from the precursor was achieved *in vitro* using either O_2 plus electrons from an external donor, or H_2O_2 (*177, 178*).

MauG is a 42.3 kDa enzyme containing two covalently-bound *c*-type hemes, one low-spin and one high-spin (*176*). The EPR parameters of oxidized MauG are atypical of *c*-type cytochromes but similar to those of the *b*-type hemes in oxygen-binding proteins and oxygenases (*176*). The two hemes have similar intrinsic redox potentials but exhibit cooperative redox behavior indicating that facile equilibration of electrons between the two hemes occurs (*179*), even though no spin-coupling is evident from the EPR spectra (*176*). The structure of MauG has not been determined. On the basis of the CXXCH *c*-type heme binding motifs in the sequence, each heme is expected to utilize a histidine for the proximal axial ligand with the heme vinyl groups covalently attached to the two cysteine sulfurs (*377*). No additional cysteines are present in the MauG sequence so it is not possible for cysteine to provide an axial ligand for either heme as is seen in cytochrome P450s. EPR and resonance Raman studies suggested that the high-spin heme possessed a single histidine axial ligand and that the low-spin heme exhibited signals most similar to hemes with *bis*-histidine axial ligands (*176, 179*). The resonance Raman spectrum exhibited marker bands associated with the low-spin heme at frequencies similar to those of *c*-type heme proteins with *bis*-histidine coordination (*378*). However, on the basis of existing data the possibility of another amino acid residue providing the distal axial ligand cannot be excluded.

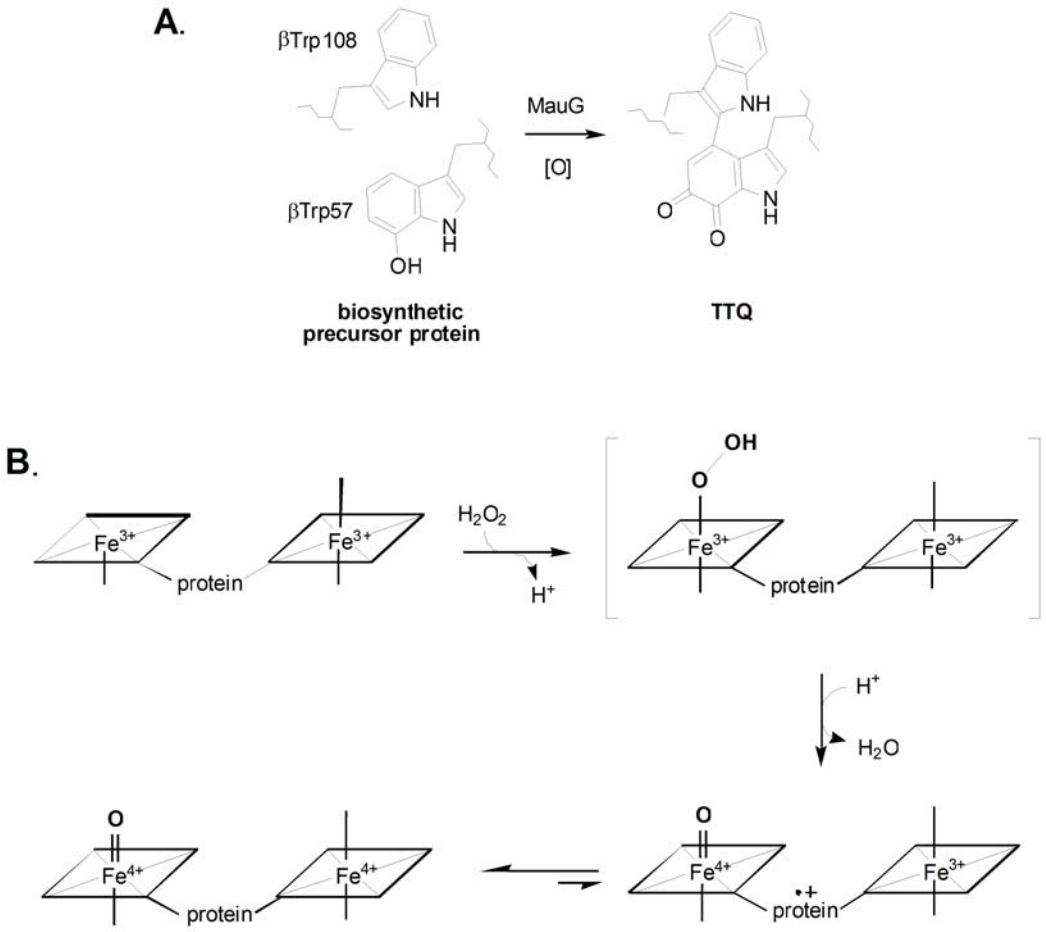

Figure 10. 1. MauG-dependent TTQ biosynthesis. (A) MauG catalyzes the formation of the protein-derive TTQ cofactor from a biosynthetic precursor protein of methylamine dehydrogenase with monohydroxylated *β*Trp57. The process requires oxidizing equivalents provided by an electron donor plus O_2 or H_2O_2. (B) Proposed mechanism for the formation of the *bis*-Fe(IV) intermediate formed by reaction of di-ferric MauG with a stoichiometric amount of H_2O_2

For heme and non-heme iron enzymes it is generally believed that the O_2-dependent and H_2O_2-dependent oxygenation mechanisms each proceed via a ferric hydroperoxy intermediate (*125, 292*) which may then lose water to yield a high-valent Fe(IV)=O (ferryl) species (*379, 380*). Ferryl heme species with a π-porphyrin or amino acid radical (known as compound I) have been observed in several enzymes (reviewed in ref. (*292, 301, 381*). Here we report EPR and

Mössbauer spectroscopic analysis of MauG oxidized by H_2O_2 in the absence and presence of itsnatural substrate (*i.e.*, the isolated biosynthetic precursor of MADH). In each case it was possible to trap and characterize an unprecedented intermediate species. Formation of mature MADH with TTQ from the biosynthetic precursor is a six-electron oxidation process; two for insertion of the second oxygen, two for formation of the cross-link, and two for oxidation of the quinol to quinone. After stoichiometric addition of H_2O_2 (*i.e.*, one-third of the total requirement) to oxidized MauG alone, a high-valent *bis*-Fe(IV) intermediate is trapped. When the biological substrate of MauG is mixed with this MauG-based di-heme *bis*-Fe(IV) intermediate, the di-ferric MauG is regenerated and a new protein-based free radical species is concomitantly observed from the substrate. These results reveal new strategies for enzyme-catalyzed and heme-dependent protein posttranslational modification reactions and for stabilization of protein-based reactive intermediates.

10.3 Results

Characterization of the product of the reaction of MauG with H_2O_2 by visible and EPR spectroscopy — To investigate the mechanism of oxygen activation by MauG, the di-heme enzyme was mixed with stoichiometric H_2O_2. Changes in the absorption spectrum of MauG occurred within 15 ms with a decrease in intensity of the Soret peak and a shift in its maximum from 405 to 407 nm (data not shown). The spectrum slowly returns to one very similar to the ferric MauG but with a slight increase and red shift in the Soret peak relative to the original ferric MauG. Parallel changes were observed in the X-band EPR spectrum (Figure 10.1B). The ferric MauG exhibits high-spin (g = 5.57, 1.99) and low-spin (g = 2.54, 2.19, 1.87) heme signals. A minor low-spin component with g values of 2.89, 2.32, and 1.52 is also apparent which was

previously assigned to a small fraction of non-reactive low-spin heme iron (*176*) which remains unchanged during the course of the experiment. After addition of H_2O_2 to ferric MauG, the reaction was quenched at various times by rapid freezing. Both hemes become EPR-silent in the first sample (2 s reaction time). No signal characteristic of compound I, the spin-coupled Fe(IV)=O ($S = 1$) and porphyrin cation radical ($S = 1/2$) (*379, 382, 383*) was observed. A weak radical-like EPR signal was observed at $g = 2.003$ which exhibits a peak-to-peak width of 1.3 millitesla. At 10 K, microwave power at half saturation ($P_{1/2}$) was estimated to be 9 μW. The combined EPR linewidth, *g*-value, and $P_{1/2}$ indicate that the $g = 2.003$ species is an organic free radical. This signal overlaps with the spectrum of the high-spin ferric heme at the $g = 2$ region, which hinders precise spin quantitation for the radical component. The best estimation derived from spin double integrations of the $g = 2$ region on the intermediate samples is that the radical-like signal represents about 1% of the protein, which is far from compensation for the loss of the two ferric heme EPR signals. This strongly suggests that the majority of both the high- and low-spin heme iron was oxidized to the EPR-silent Fe(IV) state. The high- and low-spin Fe(III) signals returned concomitant with the disappearance of the weak radical signal. Thus, the observed $g = 2$ signal is not a non-specific side-product of peroxidation but an uncoupled MauG-based cation radical which is likely in equilibrium with the two hemes (Figure 10.2).

Identification of two distinct Fe(IV) heme species in the MauG reaction intermediate by Mössbauer spectroscopy — The H_2O_2-generated MauG species was further characterized by Mössbauer spectroscopy. Since MauG possesses covalently-bound *c*-type hemes, it was not possible to reconstitute purified protein with ^{57}Fe, but necessary to isolate MauG from cells grown on ^{56}Fe-depleted minimal medium supplemented with $^{57}FeCl_2$. Figure 10.3 shows 4.2 K

Mössbauer spectra of ferric ^{57}Fe-labeled MauG before (*a*) and 45 s after addition of H_2O_2 (*b*). The dashed and solid lines in (*a*) are spin Hamiltonian simulations for the high- and low-spin hemes using typical parameters, respectively (*384*). The high- and low-spin hemes in ferric

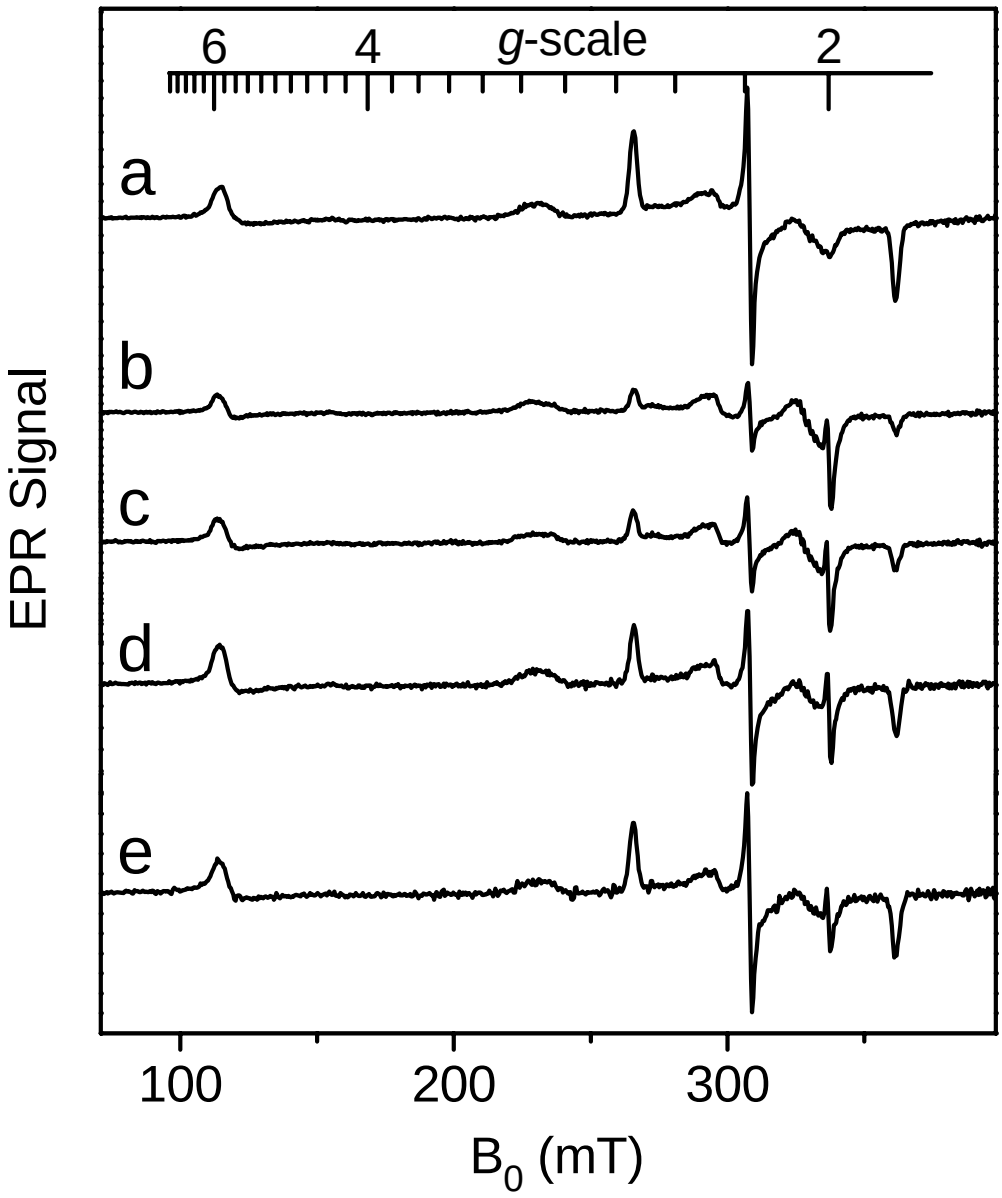

Figure 10.2. EPR analysis of the formation and decay of the intermediate formed by reaction of di-ferric MauG with a stoichiometric amount of H_2O_2. After mixing EPR spectra were recorded at time intervals of 0 (a), 0.03 (b), 2 (c), 8 (d), and 20 (e) minutes. Each sample contained 200 μM MauG. EPR parameters were temperature 10 K, microwave power 1 mW, modulation amplitude 5 G, time constant 40.96 ms, and sweep time 83.89 s. Each spectrum is the average of 5 scans.

MauG are present in an approximate 1:3 ratio rather than 1:1. This is likely due to a freezing artifact often seen in which the high-spin heme converts to low-spin on freezing (*176, 385*). It should be noted that heme quantitation, mass spectrometry and redox titrations of MauG indicated full presence of both hemes (*176, 179*). The spectrum of the H_2O_2-treated sample (hashed marks in 3*b*) contains several sharp lines that can be attributed to the intermediate, in addition to the broad, magnetically split features associated with the ferric hemes (solid line in 3*b*). There is also a small fraction of nonreactive ferric species present in both the resting and intermediate states of the enzyme, as was seen in the EPR experiment (Figure 10.1). Removal of these ferric heme signals from (*b*) yields the spectral features of the EPR-silent MauG intermediate (*c*), which can be analyzed with two quadrupole doublets using the following parameters: isomer shift (δ_1) of 0.06 mm/s and quadrupole splitting parameter (ΔE_{Q1}) of 1.70 mm/s (15 % of total Fe) and δ_2 = 0.17 mm/s and ΔE_{Q2} = 2.54 mm/s (35 % of total Fe). The isomer shift values are typical of Fe(IV) species (*384*). The quadrupole splitting parameter of Species 1 is in the range typically observed for ferryl and protonated ferryl species (*326*). The quadrupole splitting parameter of Species 2 is unusually large (ΔE_{Q2} = 2.54 mm/s) and likely describes the Fe(IV) state of the proposed six-coordinate heme with two axial amino acid ligands. Such a spin-uncoupled *bis*-Fe(IV) species has not been previously described. It is an Fe(V) equivalent. Furthermore, a six-coordinate Fe(IV) heme species with two axial amino acid ligands has also not been previously described in a protein, but analogous *bis*-ligated high-valent

inorganic porphyrin model compounds have been previously generated and in all cases a small isomer shift (δ) and large quadruple splitting (ΔE_Q) parameters are observed from those model compounds (*386, 387*). An antiferromagnetic coupled diamagnetic Fe(III)-radical has been observed in some model complexes by NMR spectroscopy (*388*). However, for MauG the 2-nm shift of the Soret band, lack of an intense EPR detectable ligand radical, and formal oxidation state of Fe(IV) revealed by Mössbauer spectroscopy eliminate the possibility of an Fe(III)-radical status for either of the Fe ions in this intermediate. Our data indicate that the two Fe(IV) species in the MauG intermediate account for approximately 50% of total iron contained in the sample, suggesting that some Fe(IV) heme has decayed to ferric MauG during the 45 s mixing/freezing period. Based on the fact that both the initial high- and low-spin hemes disappear upon peroxide oxidation (Figure 10.1), these two distinct Fe(IV) species must arise from two distinct heme sites. The ratio between the two Fe(IV) species is 3:7, suggesting that Species 1 is more reactive and thus less stable than Species 2.

Reaction of the bis-Fe(IV) MauG intermediate with its natural substrate — To determine whether the novel *bis*-Fe(IV) MauG intermediate was catalytically competent, it was mixed with its natural substrate, *i.e.*, the isolated MADH biosynthetic precursor protein (Figure 10.4). The MauG intermediate was generated by addition of one equivalent of H_2O_2 (spectrum *a*) and then immediately mixed with a stoichiometric amount of the precursor protein. Whereas in the absence of substrate the EPR-silent heme species is relatively long lived (see Figure 10.1), on addition of substrate the EPR signals of the original high- and low-spin hemes returned within the rapid mixing/freezing time (spectrum b). Furthermore, an intense new radical-like EPR signal appeared with a *g* of 2.006 determined from the baseline crossing of a 10 K spectrum. Addition

of 2 mM hydroxyurea, a known radical scavenger (*389*), caused an immediate decrease of the *g* = 2.006 EPR signal while it had little effect on the ferric heme signals (spectrum *c*). This radical intermediate is not present if hydroxyurea is pre-incubated with MauG. This demonstrates that the *g* = 2.006 EPR component (Figure 10. 4 inset) is a free radical intermediate generated during the reaction. Spin quantitation of the *g* = 2.006 signal by double integration and comparison to a *g* = 2 spin standard indicate that it corresponds to nearly stoichiometric concentration of the added precursor protein substrate. The new EPR signal exhibits a 1.9 mT peak-to-peak splitting and partially resolved hyperfine structures typical of a protein-based free radical species with an aromatic ring (*243, 390*). This new radical was also relatively long lived and remained on the MADH precursor after an anion-exchange chromatographic separation from MauG. It should be noted that this radical is observed when the reaction is initiated with stoichiometric H_2O_2 and MauG. Complete synthesis of TTQ from the precursor is a six-electron oxidation process. If excess oxidizing agents, either H_2O_2 or O_2, are added then the catalytically active mature MADH with fully synthesized TTQ is formed. This demonstrates that the novel *bis*-Fe(IV) MauG is a catalytically competent reaction intermediate in TTQ biosynthesis.

10.4 Discussion

High-valent Fe(IV)=O intermediates are frequently invoked in the catalytic cycles of Fe-dependent oxidizing enzymes (*292, 391, 392*). In heme-dependent enzymes, the two-electron oxidized intermediate (compound I) consists of an Fe(IV) species (*S* = 1) coupled to an organic

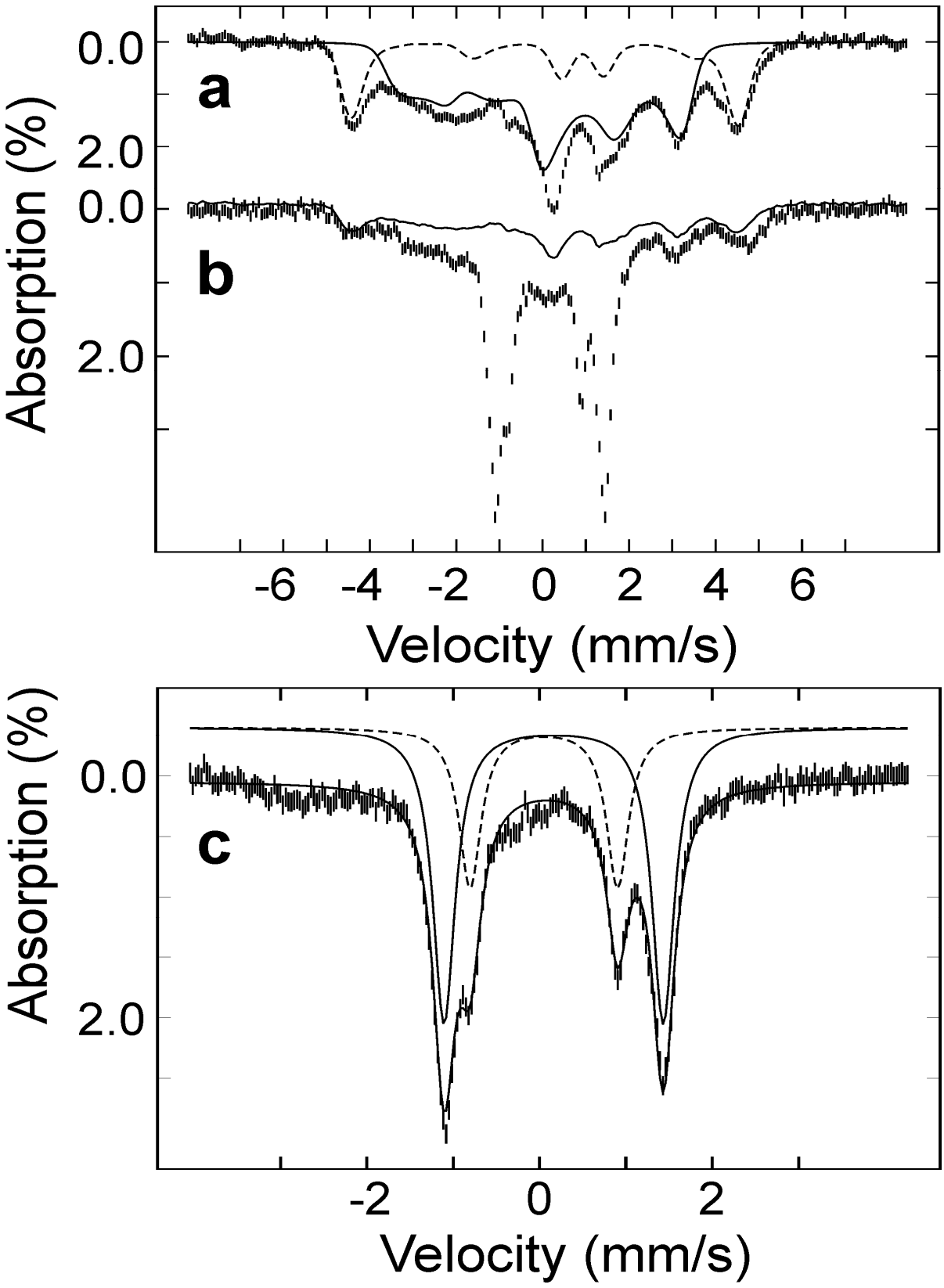
0.0
a
2.0
0.0
b
2.0
Absorption (%)
-6
-4
-2
0
2
4
6
Velocity (mm/s)
0.0
c
2.0
Absorption (%)
-2
0
2
Velocity (mm/s)

Figure 10.3. Mössbauer spectra of MauG recorded at 4.2 K in a 53-mT magnetic field. (a) The spectrum of ferric MauG (hashed marks) is overlaid with spin Hamiltonian simulations of a high-spin Fe(III) heme (25% of total Fe, dashed line) and of a low-spin Fe(III) heme (75% of total Fe, solid line) with the following parameters: $S = 5/2$, $g_{5/2} = 2$, $D_{5/2} = 10\ cm^{-1}$, $(E/D)_{5/2} = 0$, $\delta = 0.50$ mm/s, $\Delta E_Q = 2.0$ mm/s, $\eta = 0$, $\mathbf{A}/g_N\beta_N = (-18.0, -18.0, -18.0)$ T and $S = 1/2$, $\mathbf{g}_{1/2} = (1.87, 2.19, 2.54)$, $\delta = 0.25$ mm/s, $\Delta E_Q = 1.97$ mm/s, $\eta = -3$, $\mathbf{A}/g_N\beta_N = (-36.2, +9.3, +30.0)$ T. (b) The spectrum of di-ferric MauG, which was reacted with H_2O_2 for 45 s (hashed line). The solid line indicates the contribution of ferric MauG (approx. 34% of total Fe). Removal of these features yields the reference spectrum of the Fe(IV) intermediates (c), which can be simulated with two quadrupole doublets: $\delta_1 = 0.06$ mm/s and $\Delta E_{Q1} = 1.70$ mm/s (15%, dashed line) and $\delta_2 = 0.17$ mm/s and $\Delta E_{Q2} = 2.54$ mm/s (35%, solid line).

radical ($S = 1/2$) that is located on the porphyrin ring/axial ligand or a nearby amino acid residue (compound ES). The unprecedented *bis*-Fe(IV) heme MauG intermediate is in essence an electronic equivalent of compound I but with the second oxidizing equivalent stored at the second heme Fe rather than as an organic radical. A non-heme $Fe(IV)_2O_2$ species with diamond core structure and Fe-Fe distance of 2.46 Å (Intermediate Q) was trapped and characterized in methane monooxygenase (*393, 394*). However, previous studies of MauG yielded no evidence of spin-coupling between hemes (*176, 179*) and sequence homology to the structurally characterized di-heme cytochrome *c* peroxidases (*395*) suggest the heme irons of MauG are well-separated (> 20 Å) with the second oxidizing equivalent transferred via an intervening amino acid residue.

MauG is an enzyme unique in several respects. It is the first Fe-dependent oxygenase to utilize *c*-type hemes to catalyze an oxygenation reaction (*176-178*). In contrast to cytochrome P450s, the second oxidizing equivalent is not stored as a radical but on a second Fe(IV) heme. As the second heme is six-coordinate having two ligands provided by the protein our results describe the first example of a biological heme that is Fe(IV) without an exogenous ligand. This is also the first example of a *bis*-Fe(IV) system in which the two irons are not in very close proximity

and spin coupled. The *bis*-Fe(IV) MauG intermediate is also one of the most stable Fe(IV) species which has been characterized in biology. Its natural substrate is also unusual, a specific amino acid side-chain within a 119 kDa tetrameric precursor protein (*174*). Most iron-containing oxygenases and oxidases efficiently react with oxygen only in the presence of their substrates, because the generation of reactive intermediates in the absence of substrate may lead to deleterious autoxidation of the enzyme. Remarkably, the reaction of di-ferric MauG with hydrogen peroxide in the absence of its natural substrate yields a *bis*-Fe(IV) intermediate that is stable for minutes, yet this intermediate is chemically competent to oxidize its substrate.

10.5 Materials and Methods

The methods for homologous expression of MauG in *P. denitrificans* and its purification were as described previously (*176*). The concentration of MauG was determined using its extinction coefficient of 208,000 $M^{-1}cm^{-1}$ at 405 nm for the fully oxidized protein. The biosynthetic precursor of MADH with incompletely synthesized TTQ, which contains monohydroxylated *β*Trp57 and no crosslink to *β*Trp108 (*174*), was heterologously expressed in *Rhodobacter sphaeroides* (*173*) and purified as described previously (*396*). The concentration of the TTQ biosynthetic precursor of MADH was determined using its extinction coefficient of 157,000 $M^{-1}cm^{-1}$ at 280 nm.

Samples for spectroscopic analysis were prepared by rapid-freezing. For EPR analysis, samples were directly injected from a rapid freeze-quench device (times < 2 s) or transferred (times > 2 s) to EPR tubes and frozen in liquid nitrogen to avoid packing factors. X-band EPR first derivative spectra were recorded in perpendicular mode on an EMX spectrometer at 100-kHz modulation

frequency using a 4119HS high-sensitivity resonator and Oxford ITC503S temperature controller. Spin concentration of the radical species was determined by double integration of the sample spectrum obtained under non-saturating conditions and comparing the resulting intensity to that of a copper standard (1 mM $CuSO_4$, 10 mM EDTA) obtained under identical conditions. Samples for Mössbauer spectroscopy were prepared in reaction vials and transferred into sample cups before immersion in liquid nitrogen.

Separation of reaction mixtures of the H_2O_2-oxidized MauG high-valent intermediate and the MADH biosynthetic precursor was achieved using a MonoQ 4.6/100 PE column pre-equilibrated with 50 mM potassium phosphate buffer (pH 7.5) containing 25 mM NaCl and 5% glycerol (buffer A). Mixtures were applied to the column and eluted with a flow rate of 1 ml/min using a linear NaCl gradient generated over 20-column volumes from buffer A and 0-100% of buffer B (50 mM potassium phosphate buffer, pH 7.5, containing 1 M NaCl and 5% glycerol). Chromatography was performed using an ÅKTA-FPLC system (GE Healthcare Life Sciences, Piscataway, NJ).

Footnote. A.L. and V.L.D. designed research. X.L., R.F., S.L. and A.L. conducted kinetic and EPR experiments. CK performed Mössbauer analyses. AL, CK, and VLD wrote the paper.

10.6 Acknowledgements

This work was supported by National Institutes of Health grant GM41574 (V.L.D.), GM069618 and ORAU Faculty Enhancement Award in Life Sciences (A.L.), Young Investigator Award from the Arnold and Mabel Beckman Foundation and Camille Dreyfus Teacher-Scholar Award from the Camille and Henry Dreyfus Foundation (C.K.).

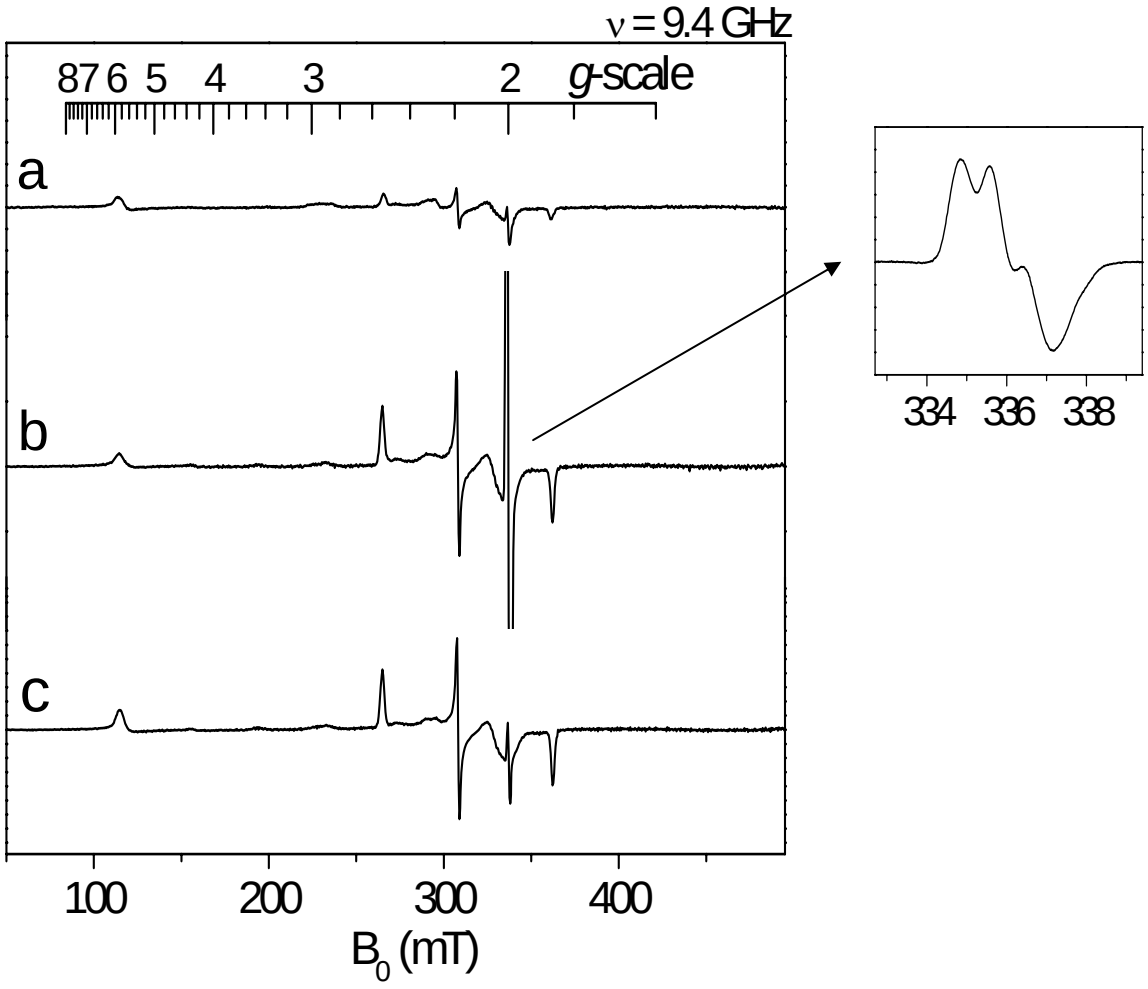

Figure 10.4. EPR analysis of the reaction of the high-valent MauG intermediate with its natural substrate. Spectrum (a) is the high-valent MauG intermediate generated from reaction of di-ferric MauG with a stoichiometric amount of H_2O_2. Spectrum (b) is (a) further reacted with a stoichiometric amount of the biosynthetic precursor of MADH for 15 s before freezing in liquid nitrogen. The inset shows a spectrum of the $g = 2$ region. Spectrum (c) is a parallel sample of (b) further reacted with 2 mM hydroxyurea for 2 min. The blow-up (indicated by an arrow) is an enlarged $g = 2$ region of spectrum (b). EPR parameters were temperature 10 K, microwave power 0.5 mW and modulation amplitude 5 G.

CHAPTER 11

A PROTEIN-BASED SUBSTRATE RADICAL IS GENERATED BY THE *BIS*-FE(IV) MAUG INTERMEDIATE

The section of chapter 11 is modified from a pre-draft of our recent studies on MauG: A Protein-Based Substrate Radical Is Generated By the *bis*-Fe(IV) MauG Intermediate and Remains Bound with MauG. Rong Fu, Xianghui Li, Victor L. Davidson and Aimin Liu.

High-resolution size-exclusion chromatography of protein mixtures and EPR experiment were performed by Rong Fu (Department of Chemistry, Georgia State University, Atlanta).

11.1 Abstract

MauG is a di-heme protein with low- and-high spin *c*-type hemes that catalyzes the biosynthesis of tryptophan tryptophylquinone (TTQ) in methylamine dehydrogenase (MADH). TTQ is formed by posttranslational modification in which two oxygens are incorporated into Trp57 which is also covalently crosslinked to Trp108. Freeze-quench experiments followed by EPR analysis were used to identify intermediates in the MauG-dependent reactions. After addition of H_2O_2 to oxidized MauG a high-valent Fe intermediate is trapped in which both hemes become EPR silent with appearance of a minor component of a MauG-based free radical (g = 2.003). The high-valent intermediate decomposes over two hours in the absence of a substrate and the EPR spectrum returns to that of the original ferric MauG (*397*). When the biological substrate of MauG, a biosynthetic precursor of MADH with Trp57 monohydroxylated and no crosslink, is mixed with the high-valent Fe intermediate the disappeared EPR signals of ferric MauG

immediately return and a protein-based free radical species with 1.9 millitesla linewidth is concomitantly observed at $g = 2.006$ at a stoichiometric amount. After separation of MauG from the MADH precursor by MonoQ chromatography the EPR spectrum of the radical remains observable only on the biosynthetic intimidate protein. Thus, the protein radical is a substrate-based intermediate that is generated at the expense of the high-valent Fe MauG intermediate. This demonstrates that the peroxide-generated MauG intermediate is catalytically competent. It reacts with its natural substrate. A radical mechanism for the TTQ biosynthesis is thus proposed.

11.2 Introduction

Tryptophan tryptophylquinone (TTQ) (*360*) is the prosthetic group of methylamine dehydrogenase (MADH) (*359*) and aromatic amine dehydrogenase (*398*). It is synthesized through the posttranslational modification of two endogenous tryptophan residues. In MADH from *Paracoccus denitrificans*, the modification involves the incorporation of two oxygen atoms into *β*Trp57 and the cross-linking between *β*Trp57 and *β*Trp108. Distinguished from many other protein-derived cofactors which are formed in a self-processing autocatalytic manner (*361*), biosynthesis of TTQ needs exogenous proteins. Included in the gene cluster which encodes the MADH subunits are four genes, *mauFEDG*, that are necessary for MADH biosynthesis (*399, 400*). Whereas deletion of *mauF*, *mauE* or *mauD* results in undetectable MADH protein subunits in cell extracts and loss of the ability of the bacterium to grow on methylamine, mutation or deletion of *mauG* *in vivo* causes accumulation of a biosynthetic precursor of MADH in which *β*Trp57 is monohydroxylated at the C7 position and the covalent cross-link is absent (*370, 401*). The second hydroxylation, cross-link formation and oxidation to the quinone could be catalyzed *in vitro* upon addition of MauG to the isolated biosynthetic precursor of MADH (*401-403*).

These observations confirm that MauG plays an essential role in the biosynthesis of TTQ.

MauG is a 42,300 Da protein containing two *c* type hemes, one low-spin and one high-spin (*404*). The two hemes have similar intrinsic redox potentials but exhibit negatively cooperative redox behavior such the the potentials for two one-electron oxidation-reductions of MauG are -159 and -254 mv (*367*). These results indicate that facile equilibration of electrons between the two hemes occurs. The substrate for MauG is a 123 kDa protein, a biosynthetic precursor of MADH with a mono-hydroxylated *β*Trp57and incompletely formed TTQ. MauG catalyzes the insertion of the second oxygen into *β*Trp57and the formation of the cross-link with *β*Trp108 (*370, 405*). In contrast to typical *c*-type cytochromes, the reduced form of MauG binds CO and is oxidizable by O_2. The sequence alignment of MauG has shown it to be 30% homologous to bacterial diheme cytochrome *c* peroxidase, but previous experiments have shown that MauG has very low peroxidase activity with artificial electron donors. Furthermore, the EPR parameters of oxidized MauG are atypical of *c*-type cytochromes or diheme cytochrome *c* peroxidases. The high-spin heme EPR signal is very similar to those of the heme oxygenase-heme complex and myoglobin. The low-spin heme EPR signal is more similar to those of ligand complexes of cytochrome P450cam (*404*). This further distinguishers MauG from the peroxidases and supports an atypical role for at least one of the *c*-type hemes of MauG.

The MauG catalyzed TTQ biosynthesis is an oxidant-dependent reaction. In the catalytic cycle, the resting ferric MauG can accept either two electrons from its electron donors and utilize molecular oxygen as its oxygen donor, or directly interact with hydrogen peroxide through a shunt pathway as do cytochrome P450 monooxygenases (*403*). It is generally believed that the O_2-dependent and H_2O_2-dependent mechanisms proceed via a ferric hydroperoxy intermediate

which loses water to yield a high-valent oxoferryl intermediate. An oxoferryl heme species with a π-porphyrin radical (compound I) and an oxoferryl heme species (compound II) have been observed in cytochrome P450s, catalase, chloroperoxidase, cytochrome *c* peroxidase and horseradish peroxidase (*187, 406*).

Here we report an optical and EPR spectroscopic analysis of MauG oxidized by H_2O_2 in the presence of its natural substrate (i.e., the isolated biosynthetic precursor of MADH). Formation of mature MADH with oxidized TTQ from the biosynthetic precursor is a six-electron oxidation process; two for the insertion of the second oxygen, two for the crosslink, and two for the oxidation of the –OH groups to the quinone. After stoichiometric addition of H_2O_2 (i.e., one-third of the total requirement) to oxidized MauG alone, a high-valent Fe intermediate is trapped in which both hemes become EPR silent with appearance of a minor component of a MauG-based free radical. When the biological substrate of MauG is mixed then with this high-valent Fe intermediate, EPR signals of ferric MauG immediately return and a new protein-based free radical species is concomitantly observed. This species was stable and could be separated from MauG by chromatography for spectroscopic analysis. These characterizations of these intermediates reveal new strategies for enzyme-catalyzed heme-dependent oxygenation reactions and for stabilization of protein-based free radicals.

11.3 Materials and Methods

Protein purification — The methods for homologous expression of MauG in *P. denitrificans* and its purification were as described previously (*404*). The concentration of MauG was determined using its extinction coefficient of 208,000 $M^{-1}cm^{-1}$ at 405 nm for the fully oxidized protein. The

biosynthetic precursor of MADH with incompletely synthesized TTQ, which contains monohydroxylated *β*Trp57 and no crosslink to *β*Trp108 (*407*), was heterologously expressed in *Rhodobacter sphaeroides* and purified as described previously (*408*). The concentration of the TTQ biosynthetic precursor of MADH was determined using its extinction coefficient of 157,000 $M^{-1}cm^{-1}$ at 280 nm.

Conventional and stopped-flow UV-Vis spectroscopy — Static absorption spectra were recorded with a Shimadzu MultiSpec-1501 spectrophotometer. For observation of rapid changes in absorption on addition of H_2O_2, spectra were recorded with an On-Line instrument RSM stopped-flow rapid scanning spectrophotometer (OLIS, Bogart, GA). In these mixing experiments one syringe contained 5 μM ferric MauG, and the other contained various concentrations of H_2O_2. The reaction temperature was controlled at 20 ºC by a water bath. All experiments were performed in 10 mM potassium phosphate buffer, pH 7.5. The concentration of H_2O_2 was calculated based on the extinction coefficient of 43.6 $M^{-1}cm^{-1}$ at 240 nm.

EPR spectroscopy — X-band EPR first derivative spectra were recorded in perpendicular mode on a Bruker (Billerica, MA) EMX spectrometer at 100-kHz modulation frequency using a 4119HS high-sensitivity resonator as described elsewhere (*409*). Measurement temperature was maintained with an ESR910 liquid helium cryostat, and LLT650/13 liquid helium transfer tube (Oxford Instruments, Concord, MA), and Oxford ITC503S and Bruker ER4131VT temperature controllers. Spin concentration was determined by double integration of the sample spectrum obtained under non-saturating conditions and comparing the resulting intensity to that of a copper standard (1 mM $CuSO_4$, 10 mM EDTA) obtained under identical conditions. EPR simulation was accomplished by using the WEPR program developed by Dr. Frank Neese (*410*).

The EPR relaxation property of the substrate/protein radical at different temperatures was analyzed from 16 EPR spectra at each given temperature obtained with increased microwave power. The values of half-saturation parameter ($P_{1/2}$) were obtained by fitting the data according to Eq 1

$$I \propto 1/(1 + P/P_{1/2})^{b/2} \quad [1]$$

where I is the EPR signal amplitude, b is an inhomogeneous broadening parameter, and P is microwave power.

All samples for EPR were prepared in 10 mM potassium phosphate buffer, pH 7.5, containing 5% glycerol. To analyze transient reaction intermediates the reaction mixtures were quenched at specific times using a Update Instrument Model 715 Rapid-freeze-quenching apparatus. Samples were transferred to EPR tubes and quickly frozen in liquid nitrogen rather than cold isopentane as the freezing agent to avoid packing factors. The entire reaction was about 15 seconds.

Separation of the reaction mixture by anion exchange chromatography — Reaction mixtures of the H_2O_2-oxidized MauG high-valent intermediate and the MADH biosynthetic precursor were loaded onto a MonoQ 4.6/100 PE column pre-equilibrated with 50mM potassium phosphate buffer (pH 7.5) containing 25 mM NaCl and 5% glycerol (buffer A). The was eluted with a flow rate of 1 ml/min using a linear NaCl gradient generated over 20 column volumes from buffer A and 0-100% of buffer B (50 mM potassium phosphate buffer, pH 7.5, containing 1 M NaCl and 5% glycerol). Chromatography was performed using an ÅKTA-FPLC system (GE Healthcare Life Sciences, Piscataway, NJ).

11.4 Results

Reaction of ferric MauG with H_2O_2 produces a long-lived intermediate in the absence of a substrate — Formation of mature MADH with oxidized TTQ from the biosynthetic precursor is a six-electron oxidation process; two for the insertion of the second oxygen, two for the formation of the crosslink, and two for the oxidation of the –OH groups to the quinone. In order to observe intermediates in this process a single equivalent of H_2O_2 was used to initiate the reaction. Upon addition of H_2O_2 rapid changes in the absorptions spectrum of MauG are observed (Figure 11.1A). The absorption intensity of the Soret peak decreases and its maximum shifts from 405 nm to 407 nm. A slight increase in absorption intensity is also seen in the region from 524 nm to 562 nm. The kinetics of the intial absorption change was further studied by rapid scan stopped-flow spectroscopy. When a five-fold excess of H_2O_2 was used in the reaction, the intermediate accumulated to the maximal amount within the dead time for mixing (*i.e.*< 2 ms). When added at approximately stoichiometric amounts the intermediate accumulated to the maximal amount in about 15 ms. The intermediate was relatively long lived with the Soret peak slowly increasing in intensity. After 20 min the absorption spectrum stabilized exhibiting features very similar to the ferric MauG but with a slight increase and red shift in the Soret peak relative to the original ferric MauG (Figure 11.1B).

In Chapter 10, a protein based radical was trapped and characterized by EPR which exhibits a 1.9 mT peak-to-peak splitting and partially resolved hyperfine structures typical of a protein-based free radical species with aromatic rings (*397*). The EPR spectrum of this new species measured under non-saturating conditions at 10 K with 0.002 mW microwave power is presented in Figure 11.2 along with spectral simulation (Figure 10.4). The $g = 2.006$ free radical signal is observable

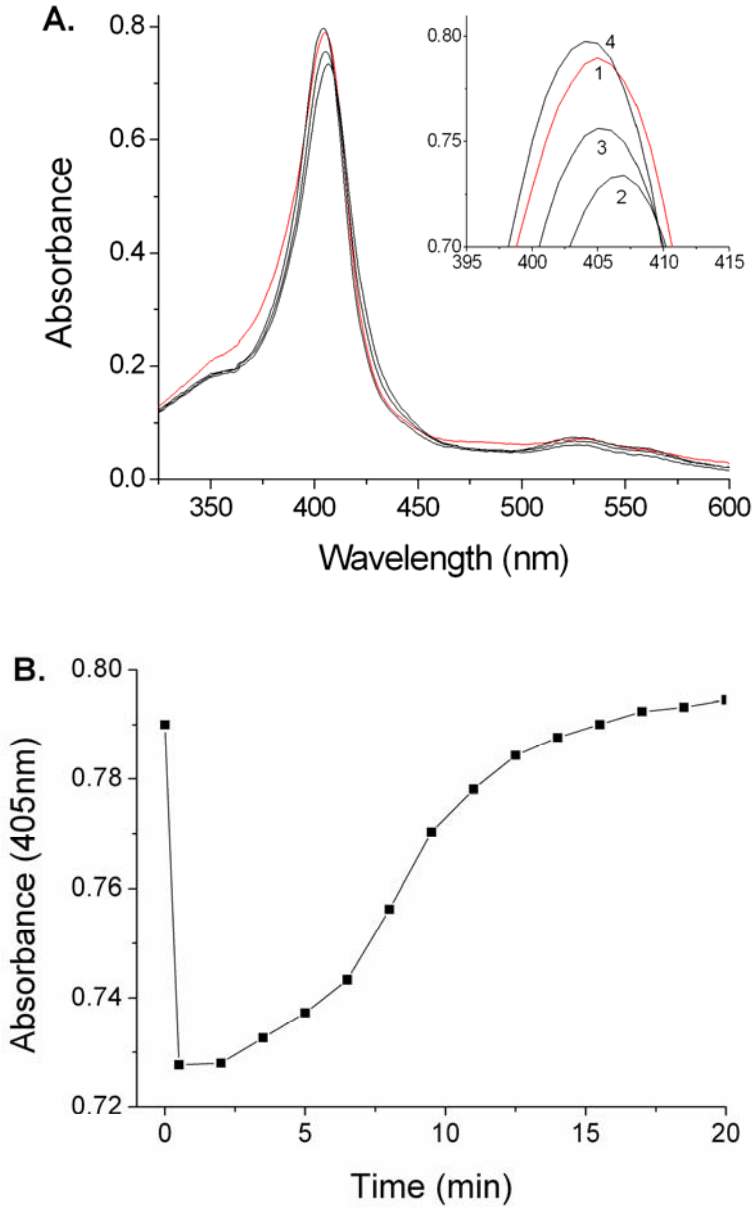

Figure 11.1. (A) Visible absorption spectral changes of the 3.8 uM ferric MauG upon addition of 7.6 uM H_2O_2 in 10 mM potassium phosphate buffer, pH 7.5, at 25ºC. The insets are a blow-up of the Soret and α and β bands. The initial ferric MauG is shown in red (trace 1), and the time-dependent change of 30 s (trace 2), 8 (trace 3) and 20 (trace 4) min after addition of H_2O_2 are shown in black. (B) Time course of absorbance changes at 405 nm after the addition of H_2O_2.

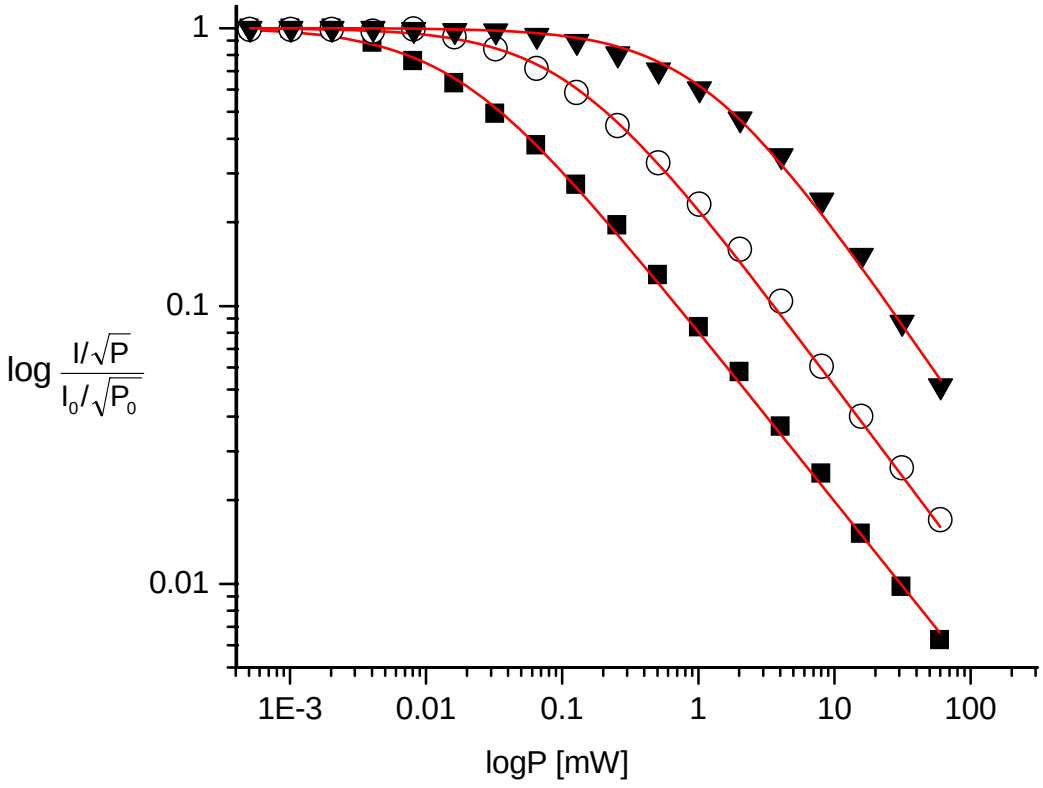

Figure 11.2. EPR spectrum of the microwave power saturation behavior the protein based radical intermediate. Protein concentration: 170 μM. Experiment conditions: temperature 10 K for the spectrum shown and various temperatures for power saturation determinations as indicated in Table 11.1, modulation amplitude 3 G, and microwave power 0.001 mW, time constant 40.96 ms, sweep time 83.89 s (single scan).

at a remarkable wide range of temperatures although the EPR signal intensity decreases at higher temperatures. Figure 3B shows the temperature dependence of the X-band EPR absorption intensity as a function of measuring temperature. Although there is an apparent linear relationship this radical component does not obey the Curie Law. The product of the double integration value and the absolute temperature should be constant when the Curie Law is followed, but this is not observed for the $g = 2.006$ spectral component. A possible reason is that

the radical sits in a rigid pocket within the protein that is less responsive to the increased free tumbling as temperature rises. This is similar to the protein-based tyrosyl radical in a class Ib ribonucleotide reductase (*320*) .

Table 11.1 EPR $P_{1/2}$ parameter of the MADH biosynthetic precursor radical intermediate.

	Temperature (K)						
	10	20	30	50	80	100	200
MADH biosynthetic precursor radical	0.013	0.0227	0.0276	0.06	0.10	0.117	1.06
Tyrosyl radical in class Ib RNR(*320*)	0.09	0.25	0.31	0.62	-	1.28	15.60

The protein radical as a MADH-based intermediat ─ The new $g = 2.006$ protein radical intermediate described above is stable for hours. The exact lifetime depends on the temperature and availability of oxidants in the environment. The signal disappears immediately on addition of excess H_2O_2. The long lifetime of the new radical intermediate provided an opportunity to isolate it from the products of the reaction mixture. The reaction mixture was subjected to ion-exchange FPLC at room temperature. Two major protein fractions eluted with a linear gradient of 0 – 1 M of NaCl and their UV-vis and EPR spectra were recorded. The first fraction was MauG which exhibited the EPR (Figure 11.3) and absorption spectra characteristic of the ferric form of the enzyme. No radical species was evident in its EPR spectrum. The second fraction was identified

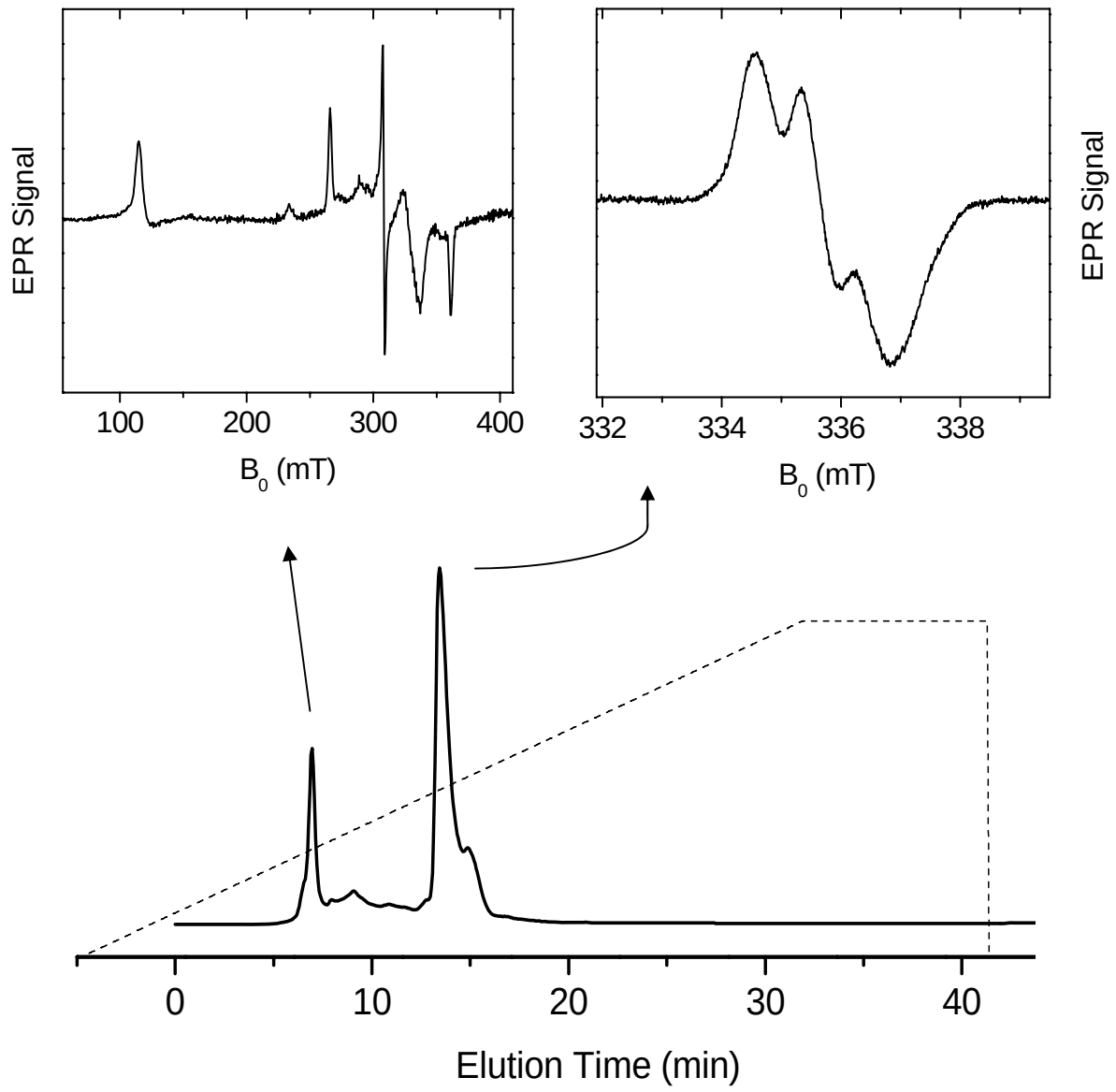

Figure 11.3. Separation of the reaction complex by MonoQ anion exchange chromatography identifies the location of the free radical intermediate. The insets are the corresponding EPR spectrum of each major elution components.

as the the MADH biosynthetic precursor which had reacted with the high-valent Fe MauG. This conclusion was based on analysis by SDS-PAGE, and the fact that it contained no heme Fe ion.

EPR analysis of this second fraction revealed a free radical signal at $g = 2.006$ with almost identical hyperfine structure as observed before the separation of the reaction mixture (Figure 11.3 inset). Thus, the free radical is protein-based and it resides in the MADH biosynthetic precursor after its reaction with the high-valent Fe heme intermediate of MauG. The EPR signal intensity decreased after separation, suggesting that the free radical less stable after the MADH precursor is released from MauG. The MonoQ separation made it possible to observe the substrate/protein based radical without the interference of the heme Fe spectral characteristics. The optical spectrum of this species is shown in Figure 11.4. The protein-based radical intermediate presents a significant 410 nm absorption peak, a 330 nm shoulder and a broad and weak feature centered at 550 nm.

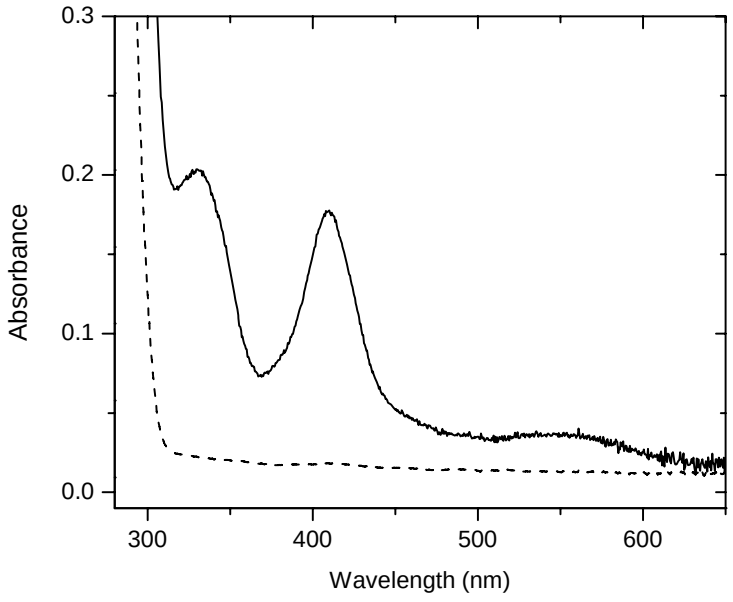

Figure 11.4. Optical spectrum of the substrate/protein radical intermediate after the MonoQ separation (solid trace). For comparison, the spectrum of substrate (biosynthetic precursor of MADH) is also shown (dashed trace).

11.5 Discussion

Conversion of the biosynthetic precursor of MADH with incompletely formed TTQ to the mature oxidized MADH is a six-electron oxidation process. Two each are required for the insertion of the second oxygen, the formation of the crosslink, and the oxidation of the –OH groups to the quinone. As a stategy to trap reactive intermediates in the biosynthetic reaction in vitro, only two oxidation equivalents were given to MauG. The product of this reaction is an unprecedented stable high-valent Fe di-heme form of MauG. Once this MauG intermediate was formed, the biosynthetic precursor protein of MADH was added. This resulted in formation of another unprecedented protein-based radical intermediate which is stable enough to be separated from MauG column chromatography.

It is well known that many hemoproteins which can activate oxygen, such as peroxidases, catalases and cytochrome P450s, generate high-valent iron-oxo complexes upon peroxide oxidation. In most of the cases, the ferric state of the hemoproteins is oxidized to an oxoferryl species (Fe^{IV}=O, S = 1) magnetically coupled with a porphyrin-π cation radical (S = 1/2) (*35*). In some other cases, such as cytochrome *c* peroxidase and cytochrome P450cam, the radical is found in a nearby amino acid, typically a tyrosine or tryptophan residue (*9, 411*). In this work, a novel high-valent iron-oxo species was captured after addition of H_2O_2 to MauG. When the high-spin heme of MauG accepts the two oxidizing equivalents from H_2O_2, one oxidizing equivalent is present as an oxoferryl species at the high-spin heme, while the other is present as ferryl species at the low-spin heme after electron transfer, presumably through intervening amino acid(s) (Figure 10.1B). This is in essence an electronic equivalent of compound I but with the

second oxidizing equivalent stored at the second heme Fe center rather than as a porphrin cation radical. This is the first example of a second heme group storing the second oxidizing equivalent in the absence of substrate. The most closely related intermediate is the elusive Fe(IV)Fe(IV) intermediate trapped for methane monooxygenase, a non-heme Fe enzyme (*412*). The characterization of this novel high-valent Fe intermediate further distinguished MauG as a novel *c*-type di-heme protein which functions as an oxygenase.

The amino acid sequence of MauG is about 30% homologous to that of diheme cytochrome *c* peroxidases. However, MauG does not present any peroxidase activity. Cytochrome *c* peroxidases contain two heme groups with redox potentials that are wildly separated (e.g., -320 and +320 mV) (*413*). In MauG, the two hemes have similar redox potentials but exhibit negative redox cooperativity suggesting that facile electron transfer between hemes occurs during oxidation and reduction (*367*), even though the two hemes do not appear to be spin-coupled to each other (*176*). The structure of the diheme peroxidases reveals a tryptophan residue positioned between the hemes in a manner that could mediate electron transfer from the high-potential heme to the low-potential heme (*55*). This tryptophan is conserved in not only the peroxidases but also in the primary sequence of MauG. The structure of MauG is not yet available, however the sequence homology suggests that the weak free radical species centered at $g = 2.005$ during peroxide oxidation of MauG could be centered on this tryptophan.

In the absence of substrate the high-valent MauG oxoferryl intermediate is relatively stable compared to the oxoferryl intermediates of other hemoproteins. This property may be attributed to storing the second oxidizing equivalent as Fe(IV) in the second heme instead of a porphyrin- or amino acid-based radical. This enhanced stability can not only protect the protein itself from

nonspecific damaging oxidation of active site amino acid residues, but also provide a longer time for binding its native substrate or conformational changes during the catalytic reaction or both. This latter feature may be critical for MauG. In contrast to most other heme-dependent oxygenases which utilize small molecules as substrates, the substrate of MauG is a 124 kDa tetramer protein, the biosynthetic precursor of MADH.

When the biosynthetic precursor of MADH is added to the MauG intermediate, the high-valent Fe species immediately returned to the ferric state and, at the same time, a protein-based free radical was quantitatively produced. This radical is relatively stable in the absence of additional peroxide and could be separated from MauG. The successful separation confirmed that the radical was based on the MADH intermediate and not MauG. It also made it possible to record the EPR and absorption spectra of the protein-based radical intermediate without interference from the intense spectral features of the heme groups in MauG. The spectral feature found in aromatic radicals with hydroxyl groups, such as 2-methylthio-4-methylphenol and tyrosyl radicals, have an absorbance around 410 nm (*414, 415*). The optical spectrum of the radical intermediate of MADH biosynthetic precursor has maxima absorbance at 330 nm and 410 nm, and a broad and weak band centered at 550 nm. It is distinguished from neutral or cationic tryptophan radicals that have absorbance at 320~340 nm and 510~580 nm (*415*). The distinctive spectral features could be due to fact that in the biosynthetic intermediate of MADH the trytophan residue which harbors the radical is hydroxylated. The relaxation properties of the g = 2.006 free radical component are also similar to the tyrosyl radical of the class Ib ribonucleotide reductase (*416*). The microwave power saturation occurred at very low values at each measured frozen temperature, and the value of $P_{1/2}$ parameter is about one magnitude low than that of the

corresponding value of the ribonucleotide reductase radical (Table 11.1). It is known that the tyrosyl radical harboring residue is about 6. 5 - 7 Å away from the nearest iron ion (*417-419*). By analogy the $g = 2.006$ radical component which we believe is on residue βTrp57 of the substrate protein intermediate may similarly be located at least 7 Å away from the nearest ferric ion in MauG in the MauG-intermediate complex. This could explain why we observe such a stable radical species prior to the oxygenation. The initial radical transfer may occur over this long distance but further reorientation of the enzyme and protein substrate within the reactive complex is required to bring residue βTrp57 close enough to the oxo-ferryl heme iron for oxygen insertion. It is noteworthy that a transient intermediate with an absorption maximum at 330 nm was also observed in the H_2O_2-dependent MauG catalyzed TTQ biosynthetic reaction in vitro in the presence of excess peroxide. That intermediate formed at a relatively rapid rate, and then decreased with a slower rate accompanied by the formation of oxidized MADH. This suggests that the radical intermediate quenched here may be the one observed transiently during the overall conversion of the biosynthetic precursor to mature oxidized MADH with completely synthesized TTQ.

The discovery of this protein-based radical intermediate is significant beyond the MauG catalytic reaction. It remains a debatable topic in the oxygenase field as to whether the oxygenation by a high-valent Fe-oxo species occurs via a radical mechanism or a concerted mechanism (*420*). Here we show that a discrete radical transfer occurs first followed by a slower oxygenation (Scheme 11.1). It is possible that this mechanism is not general but adopted by MauG because of the nature of its substrate, a specific amino acid residue within a large protein which must undergo conformational rearrangements to allow access of this residue to the reactive heme

within the enzyme-substrate complex. It is also possible that all heme-dependent oxygenases proceed via this mechanism but the unusual nature of the substrate in this reaction slowed the oxygenation reaction sufficiently to allow observation of the initial radical transfer step. MauG provides an ideal system with which to dissect the monooxygenase reaction into its two component steps, radical transfer and oxygen incorporation. The characterization of the reaction intermediates described in this paper also allows us to more completely understand of the biosynthetic route of TTQ.

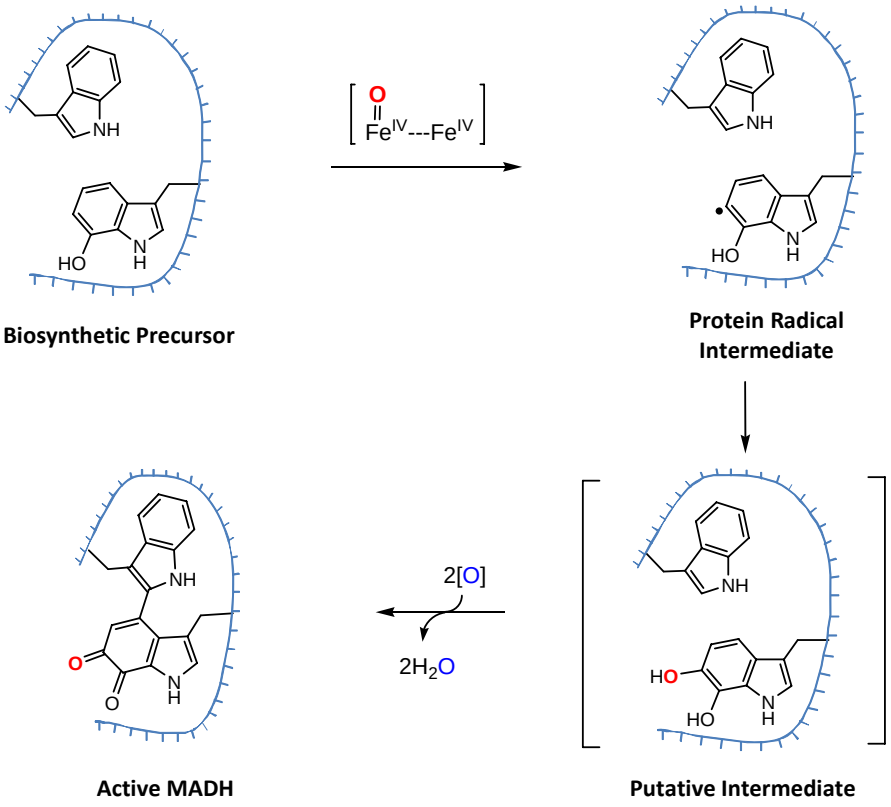

Scheme 11.1. Proposed mechanism of MauG-dependent TTQ biosynthesis.

CHAPTER 12

SUMMARY

12.1 Tryptophan 2,3-dioxygenase

Tryptophan 2,3-dioxygenase (TDO) inserts two oxygen atoms into free tryptophan to produce NFK in a four electron oxidizing process by a *b*-type heme cofactor. This enzyme is a representative of a potentially new hemoprotein dioxygenase superfamily, whose oxygenase activity remains poorly understood. Spectroscopic, biochemical, and kinetic studies of TDO were described in this dissertation in order to understand the mechanism of the activation and functionality of TDO.

TDO is catalytically active at the reduced state with a ferrous ion. In our recent study of the full-length TDO from *Ralstonia metallidurans*, we revealed two unidentified enzymatic activities of ferric TDO. We have found that the ferric form of the enzyme is catalytically active with H_2O_2 serving as the oxygen donor in the presence of L-Trp. The oxidized enzyme expresses a catalase-like activity in the absence of L-Trp, converting peroxide to O_2. Titration experiments suggest that about two moles of H_2O_2 were required for the production of one mole of NFK. Since the Fe ion cannot simultaneously coordinate two H_2O_2 molecules, the oxygen insertion from H_2O_2 must be a stepwise process. It is the first experimental evidence suggesting that oxidized TDO can utilize peroxide as a substrate for a tryptophan oxygenation. Using mass spectrometry aided with isotop labeling, we have also observed monooxygenated-L-Trp and found that one and only one

carboxylate group of NFK is solvent exchangeable. Furthermore, water did not provide oxygen atom for the peroxide-driven oxygenation.

Three enzyme-based intermediates were sequentially detected in the peroxide oxidation of ferric TDO in the absence of L-Trp. These spectroscopically distinguishable intermediates are: An Fe(IV)-oxo species coupled with a porphyrin cation radical (compound I-type), an Fe(IV)-oxo species and a distant protein radical (compound ES-type), and a ferric intermediate that is more axial than the initial ferric ion. The last two species have also been characterized by Mössbauer spectroscopy. The authentic oxyferryl species is demonstrated by an isomer shift of 0.05(2) mm/s. However, the oxyferryl species exhibits an unusually large quadrupole splitting parameter of 1.76(2) mm/s at pH 7.4. Based on DFT calculations that evaluate all the possible structural influences to the iron axial ligands, this unusual quadrupole splitting was proposed as a result of the hydrogen bonding to the oxo group due to a unique active site environment in TDO.

The TDO Fe(IV) intermediate exhibits some unexpected spectral properties, including a large quadruple splitting parameter which is greater than non-protonated Fe(IV) intermediates but smaller than the protonated Fe(IV) species reported from other hemoproteins. This is the first Fe(IV) intermediate trapped and characterized in the heme dioxygenase family.

We examined the peroxide oxidation of ferric TDO in the presence of L-Trp and observed a putative ferric hydroperoxide intermediate. Two possibilities of the O-O bond cleavage of the ferric hydroperoxide intermediate have been proposed: homolytic and heterolytic cleavage. In homolytic cleavage, one-electron reduction yields a compound II-like species and a hydroxyl radical whereas heterolytic cleavage generates a compound ES-like species with a protein radical

via two electron reductions. We have established the formation of ferrous TDO in the reaction of ferric TDO with H_2O_2 in the presence of L-Trp by Mössbauer spectroscopy. The formation of ferrous TDO is a substrate-dependent process which is involved in two electron reductions of compound II species. On the other hand, the protein radical of the compound ES-like species is catalytically competent for peroxide driven oxygenation reaction. The proposed mechanism was summarized in Scheme 12.1.

We have also found that ferric TDO could be activated via one electron reduction to form ferrous TDO when mixed with either L-Trp or substrate analogues, such as D-Trp, 5-F-Trp and 5-OH-Trp. EPR studies showed that the binding of substrate or substrate analogues to TDO induced a spin transition to form a ferric hydroxide intermediate. Mössbauer spectroscopic studies suggest that the proximal histidine of two of the dimers was in a protonated form whereas the other was in a deprotonated form. Redox potential of TDO in the absence and in the presence of L-Trp has a value of 110 mV and 190 mV, respectively. Taken together, the data support a substrate-activation scenario of ferric TDO in which the formation of ferrous TDO is accomplished by transferring one electron from substrate or substrate analogue to ferric heme through a ferric hydroxide intermediate. This process is driven by the positive features of the ferric heme center upon binding substrate or substrate analogues. The proposed mechanism is summarized in Scheme 12.1.

The role of acid-base catalysis of His72 was examined through site-directed mutagenesis analysis of H72S, H72N and Q73F. Kinetic studies and the pH profiles of WT TDO and His72 derivatives led us to propose that His72 plays a role in catalytic reaction and is probably an acid-base catalyst in the WT TDO. One hydroxide group partially rescures the catalytic activities in

H72S and H72N. The rearrangement of the active site hydrogen bond network for the hydroxide group was probed by EPR spectra of H72S, H72N, Q73F and WT TDO at various pH values of 6.0, 7.4 and 10.0.

Kinetic studies of tyrosine derivatives of Y43W and Y43F indicate that Try43 plays an important role in the catalytic reaction. In addition, Try43 is emerging as the most likely candidate for the localization of the protein radical generated during the peroxide oxidation reaction. Additional experiments would be required to further elucidate the identity of this protein radical.

12.2 A Novel Di-heme Protein MauG

MauG is a novel enzyme that utilizes two *c*-type hemes to catalyze a posttranslational modification of a 119 kDa protein. Such a modification endows endogenous tryptophan residues with a new catalytic activity. The reaction is a six-electron oxidation and the utilization of two *c*-type hemes by MauG to perform a hydroxylation reaction and the subsequent oxidation reactions is unprecedented. We have trapped novel Fe(IV) intermediate from MauG. The *bis*-Fe(IV) intermediate of MauG is an unprecedented species which stores two oxidizing equivalents as Fe(IV) on two distinct hemes. One Fe ion in the MauG intermediate is also the first example of a biological heme that is Fe(IV) but without bound exogenous oxygen ligand. The MauG *bis*-Fe(IV) intermediate is one of the most stable, yet chemically and catalytically competent Fe(IV) species that has been characterized in biology. The oxidized MauG with a *bis*-Fe(III) di-heme cofactor is also able to use H_2O_2 as a substrate for its catalytic activity. A substrate-based radical intermediate of MADH has been trapped after reaction of the substrate with the high-valent MauG species, and characterized by EPR and UV-Vis spectroscopy.

These unusual high-valent Fe intermediates expand our understanding of how nature generates, stabilizes, and utilizes powerful high-valent Fe(IV) species. These studies will elucidate fundamental relationships between the chemical structure of these intermediates and their biochemical reactivity. The studies with MauG will also be relevant to understanding the mechanisms of protein oxidation and posttranslational modification.

High-resolution size-exclusion chromatography showed that MauG can form a stable complex with the MADH biosynthetic precursor but not the mature MADH, and the maximum stoichiometry of binding of MauG to the precursor is 1:1. This study indicates that significant conformational changes in one or both of the proteins occur during catalysis. These results provide a basis for using this system as a model to study the dynamics of protein-protein interactions and the induced fit model of enzyme-substrate interactions.

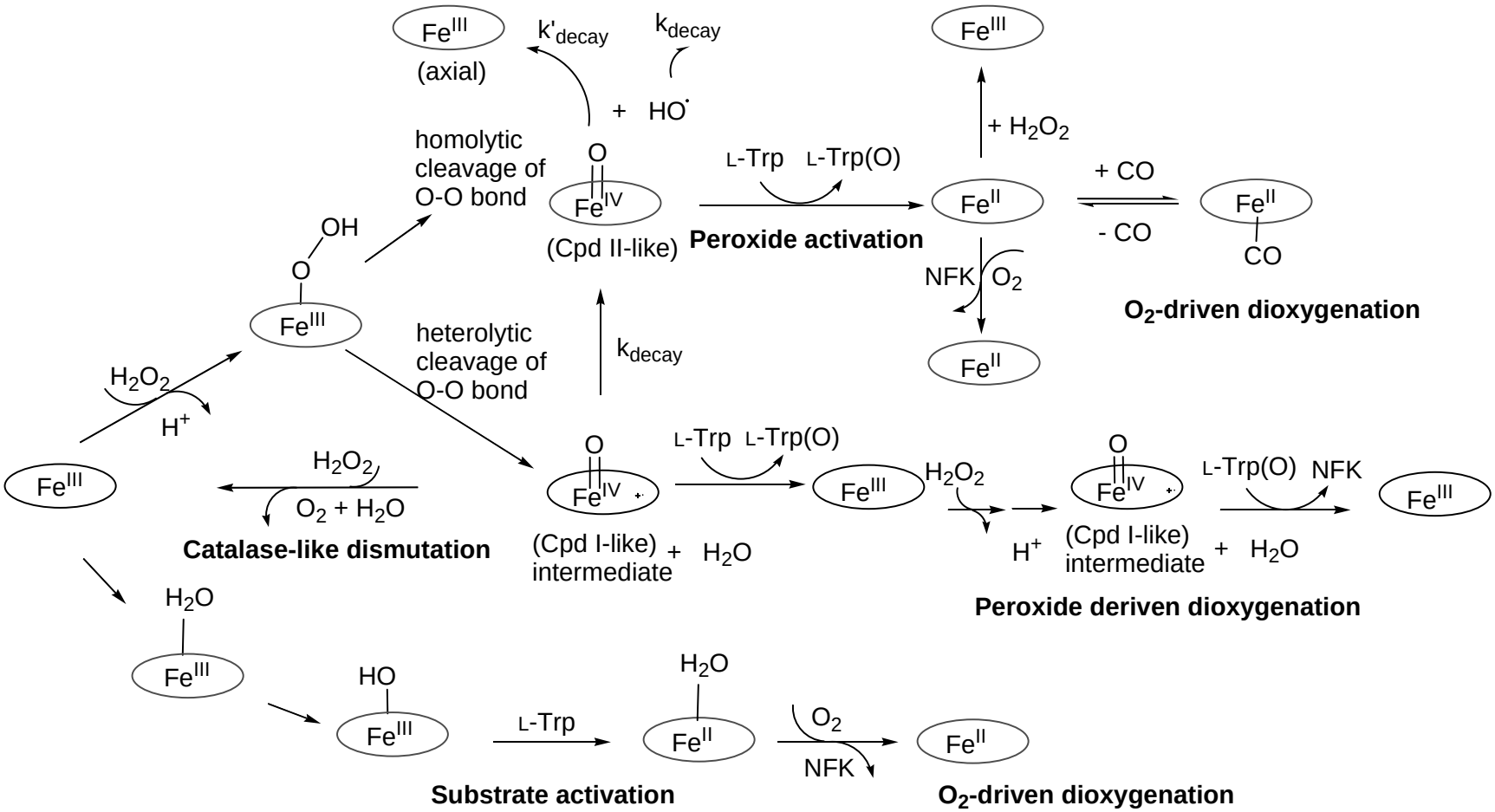

Scheme 12.1. Proposed mechanism of TDO reactions.

REFERENCES CITED

1. Schneider, S., Marles-Wright, J., Sharp, K. H., and Paoli, M. (2007) Diversity and conservation of interactions for binding heme in *b*-type heme proteins, *Nat Prod Rep 24*, 621-630.
2. Bowman, S. E., and Bren, K. L. (2008) The chemistry and biochemistry of heme *c*: Functional bases for covalent attachment, *Nat Prod Rep 25*, 1118-1130.
3. Allen, J. W., Barker, P. D., Daltrop, O., Stevens, J. M., Tomlinson, E. J., Sinha, N., Sambongi, Y., and Ferguson, S. J. (2005) Why isn't 'standard' heme good enough for *c*-type and *d1*-type cytochromes?, *Dalton Trans*, 3410-3418.
4. Sono, M., Roach, M. P., Coulter, E. D., and Dawson, J. H. (1996) Heme-containing oxygenases, *Chem Rev 96*, 2841-2888.
5. Davydov, R., Makris, T. M., Kofman, V., Werst, D. E., Sligar, S. G., and Hoffman, B. M. (2001) Hydroxylation of camphor by reduced oxy-cytochrome P450cam: Mechanistic implications of epr and endor studies of catalytic intermediates in native and mutant enzymes, *J Am Chem Soc 123*, 1403-1415.
6. Hrycay, E. G., Gustafsson, J. A., Ingelman-Sundberg, M., and Ernster, L. (1976) The involvement of cytochrome P-450 in hepatic microsomal steroid hydroxylation reactions supported by sodium periodate, sodium chlorite, and organic hydroperoxides, *Eur J Biochem 61*, 43-52.
7. Kellner, D. G., Hung, S. C., Weiss, K. E., and Sligar, S. G. (2002) Kinetic characterization of compound I formation in the thermostable cytochrome P450 CYP119, *J Biol Chem 277*, 9641-9644.

8. Schunemann, V., Jung, C., Terner, J., Trautwein, A. X., and Weiss, R. (2002) Spectroscopic studies of peroxyacetic acid reaction intermediates of cytochrome P450cam and chloroperoxidase, *J Inorg Biochem 91*, 586-596.

9. Schunemann, V., Lendzian, F., Jung, C., Contzen, J., Barra, A. L., Sligar, S. G., and Trautwein, A. X. (2004) Tyrosine radical formation in the reaction of wild type and mutant cytochrome P450cam with peroxy acids: A multifrequency EPR study of intermediates on the millisecond time scale, *J Biol Chem 279*, 10919-10930.

10. Jung, C., Schunemann, V., Lendzian, F., Trautwein, A. X., Contzen, J., Galander, M., Bottger, L. H., Richter, M., and Barra, A. L. (2005) Spectroscopic characterization of the iron-oxo intermediate in cytochrome P450, *Biol Chem 386*, 1043-1053.

11. Jung, C., Schunemann, V., and Lendzian, F. (2005) Freeze-quenched iron-oxo intermediates in cytochromes P450, *Biochem Biophys Res Commun 338*, 355-364.

12. Meunier, B., Adam, Waldemar, (Ed.) (2000) *Metal-oxo and metal-peroxo species in catalytic oxidations*, Springer, Berlin, New York.

13. Gerber, N. C., and Sligar, S. G. (1994) A role for Asp-251 in cytochrome P-450cam oxygen activation, *J Biol Chem 269*, 4260-4266.

14. Vidakovic, M., Sligar, S. G., Li, H., and Poulos, T. L. (1998) Understanding the role of the essential Asp251 in cytochrome P450cam using site-directed mutagenesis, crystallography, and kinetic solvent isotope effect, *Biochemistry 37*, 9211-9219.

15. Raag, R., Martinis, S. A., Sligar, S. G., and Poulos, T. L. (1991) Crystal structure of the cytochrome P-450cam active site mutant Thr252Ala, *Biochemistry 30*, 11420-11429.

16. Montellano, P. R. (2000) The mechanism of heme oxygenase, *Curr Opin Chem Biol 4*, 221-227.

17. Kikuchi, G., and Yoshida, T. (1976) Heme catabolism by the reconstituted heme oxygenase system, *Ann Clin Res 8 Suppl 17*, 10-17.

18. Schuller, D. J., Wilks, A., Ortiz de Montellano, P. R., and Poulos, T. L. (1999) Crystal structure of human heme oxygenase-1, *Nat Struct Biol 6*, 860-867.

19. Sugishima, M., Sakamoto, H., Higashimoto, Y., Omata, Y., Hayashi, S., Noguchi, M., and Fukuyama, K. (2002) Crystal structure of rat heme oxygenase-1 in complex with heme bound to azide. Implication for regiospecific hydroxylation of heme at the alpha-meso carbon, *J Biol Chem 277*, 45086-45090.

20. Sugishima, M., Sakamoto, H., Kakuta, Y., Omata, Y., Hayashi, S., Noguchi, M., and Fukuyama, K. (2002) Crystal structure of rat apo-heme oxygenase-1 (HO-1): Mechanism of heme binding in HO-1 inferred from structural comparison of the apo and heme complex forms, *Biochemistry 41*, 7293-7300.

21. Liu, Y., and Ortiz de Montellano, P. R. (2000) Reaction intermediates and single turnover rate constants for the oxidation of heme by human heme oxygenase-1, *J Biol Chem 275*, 5297-5307.

22. Avila, L., Huang, H. W., Damaso, C. O., Lu, S., Moenne-Loccoz, P., and Rivera, M. (2003) Coupled oxidation vs heme oxygenation: Insights from axial ligand mutants of mitochondrial cytochrome *b*5, *J Am Chem Soc 125*, 4103-4110.

23. Unno, M., Matsui, T., Chu, G. C., Couture, M., Yoshida, T., Rousseau, D. L., Olson, J. S., and Ikeda-Saito, M. (2004) Crystal structure of the dioxygen-bound heme oxygenase

from *Corynebacterium diphtheriae*: Implications for heme oxygenase function, *J Biol Chem 279*, 21055-21061.

24. Kumar, D., de Visser, S. P., and Shaik, S. (2005) Theory favors a stepwise mechanism of porphyrin degradation by a ferric hydroperoxide model of the active species of heme oxygenase, *J Am Chem Soc 127*, 8204-8213.

25. Wilks, A., Torpey, J., and Ortiz de Montellano, P. R. (1994) Heme oxygenase (HO-1). Evidence for electrophilic oxygen addition to the porphyrin ring in the formation of alpha-meso-hydroxyheme, *J Biol Chem 269*, 29553-29556.

26. Davydov, R., Matsui, T., Fujii, H., Ikeda-Saito, M., and Hoffman, B. M. (2003) Kinetic isotope effects on the rate-limiting step of heme oxygenase catalysis indicate concerted proton transfer/heme hydroxylation, *J Am Chem Soc 125*, 16208-16209.

27. Wilks, A., and Ortiz de Montellano, P. R. (1993) Rat liver heme oxygenase. High level expression of a truncated soluble form and nature of the meso-hydroxylating species, *J Biol Chem 268*, 22357-22362.

28. Davydov, R., Kofman, V., Fujii, H., Yoshida, T., Ikeda-Saito, M., and Hoffman, B. M. (2002) Catalytic mechanism of heme oxygenase through EPR and ENDOR of cryoreduced oxy-heme oxygenase and its Asp 140 mutants, *J Am Chem Soc 124*, 1798-1808.

29. Takahashi, S., Wang, J., Rousseau, D. L., Ishikawa, K., Yoshida, T., Host, J. R., and Ikeda-Saito, M. (1994) Heme-heme oxygenase complex. Structure of the catalytic site and its implication for oxygen activation, *J Biol Chem 269*, 1010-1014.

30. Schuller, D. J., Wilks, A., Ortiz de Montellano, P., and Poulos, T. L. (1998) Crystallization of recombinant human heme oxygenase-1, *Protein Sci 7*, 1836-1838.

31. Fujii, H., Dou, Y., Zhou, H., Yoshida, T., and Ikeda-Saito, M. (1998) Cobalt porphyrin heme oxygenase complex. EPR evidences for the distal heme pocket hydrogen bonding, *J Am Chem Soc 120*, 8251-8252.

32. Liu, Y., Moenne-Loccoz, P., Hildebrand, D. P., Wilks, A., Loehr, T. M., Mauk, A. G., and Ortiz de Montellano, P. R. (1999) Replacement of the proximal histidine iron ligand by a cysteine or tyrosine converts heme oxygenase to an oxidase, *Biochemistry 38*, 3733-3743.

33. Picot, D., and Garavito, R. M. (1994) Prostaglandin H synthase: Implications for membrane structure, *FEBS Lett 346*, 21-25.

34. Picot, D., Loll, P. J., and Garavito, R. M. (1994) The x-ray crystal structure of the membrane protein prostaglandin H2 synthase-1, *Nature 367*, 243-249.

35. Dolphin, D., Forman, A., Borg, D. C., Fajer, J., and Felton, R. H. (1971) Compounds I of catalase and horse radish peroxidase: *Pi*-cation radicals, *Proc Natl Acad Sci U S A 68*, 614-618.

36. Wiertz, F. G., Richter, O. M., Cherepanov, A. V., MacMillan, F., Ludwig, B., and de Vries, S. (2004) An oxo-ferryl tryptophan radical catalytic intermediate in cytochrome *c* and quinol oxidases trapped by microsecond freeze-hyperquenching (mhq), *FEBS Lett 575*, 127-130.

37. Poulos, T. L., and Kraut, J. (1980) A hypothetical model of the cytochrome *c* peroxidase . Cytochrome *c* electron transfer complex, *J Biol Chem 255*, 10322-10330.

38. Poulos, T. L., and Kraut, J. (1980) The stereochemistry of peroxidase catalysis, *J Biol Chem 255*, 8199-8205.

39. Poulos, T. L., Freer, S. T., Alden, R. A., Edwards, S. L., Skogland, U., Takio, K., Eriksson, B., Xuong, N., Yonetani, T., and Kraut, J. (1980) The crystal structure of cytochrome *c* peroxidase, *J Biol Chem 255*, 575-580.

40. Nagano, S., Tanaka, M., Watanabe, Y., and Morishima, I. (1995) Putative hydrogen bond network in the heme distal site of horseradish peroxidase, *Biochem Biophys Res Commun 207*, 417-423.

41. Sundaramoorthy, M., Terner, J., and Poulos, T. L. (1995) The crystal structure of chloroperoxidase: A heme peroxidase-cytochrome P450 functional hybrid, *Structure 3*, 1367-1377.

42. Casella, L., Gullotti, M., Ghezzi, R., Poli, S., Beringhelli, T., Colonna, S., and Carrea, G. (1992) Mechanism of enantioselective oxygenation of sulfides catalyzed by chloroperoxidase and horseradish peroxidase. Spectral studies and characterization of enzyme-substrate complexes, *Biochemistry 31*, 9451-9459.

43. Blanke, S. R., and Hager, L. P. (1988) Identification of the fifth axial heme ligand of chloroperoxidase, *J Biol Chem 263*, 18739-18743.

44. Ortiz de Montellano, P. R., Choe, Y. S., DePillis, G., and Catalano, C. E. (1987) Structure-mechanism relationships in hemoproteins. Oxygenations catalyzed by chloroperoxidase and horseradish peroxidase, *J Biol Chem 262*, 11641-11646.

45. Edwards, S. L., Nguyen, H. X., Hamlin, R. C., and Kraut, J. (1987) Crystal structure of cytochrome *c* peroxidase compound I, *Biochemistry 26*, 1503-1511.

46. Sivaraja, M., Goodin, D. B., Smith, M., and Hoffman, B. M. (1989) Identification by ENDOR of Trp191 as the free-radical site in cytochrome c peroxidase compound ES, *Science 245*, 738-740.

47. Berglund, G. I., Carlsson, G. H., Smith, A. T., Szoke, H., Henriksen, A., and Hajdu, J. (2002) The catalytic pathway of horseradish peroxidase at high resolution, *Nature 417*, 463-468.

48. Bateman, L., Leger, C., Goodin, D. B., and Armstrong, F. A. (2001) A distal histidine mutant (H52Q) of yeast cytochrome *c* peroxidase catalyzes the oxidation of H_2O_2 instead of its reduction, *J Am Chem Soc 123*, 9260-9263.

49. Hirst, J., Wilcox, S. K., Williams, P. A., Blankenship, J., McRee, D. E., and Goodin, D. B. (2001) Replacement of the axial histidine ligand with imidazole in cytochrome *c* peroxidase. 1. Effects on structure, *Biochemistry 40*, 1265-1273.

50. Hirst, J., Wilcox, S. K., Ai, J., Moenne-Loccoz, P., Loehr, T. M., and Goodin, D. B. (2001) Replacement of the axial histidine ligand with imidazole in cytochrome *c* peroxidase. 2. Effects on heme coordination and function, *Biochemistry 40*, 1274-1283.

51. Vitello, L. B., Erman, J. E., Miller, M. A., Wang, J., and Kraut, J. (1993) Effect of arginine-48 replacement on the reaction between cytochrome *c* peroxidase and hydrogen peroxide, *Biochemistry 32*, 9807-9818.

52. Satterlee, J. D., Savenkova, M. I., Foshay, M., and Erman, J. E. (2003) Temperature, pH, and solvent isotope dependent properties of the active sites of resting-state and cyanide-ligated recombinant cytochrome *c* peroxidase (H52l) revealed by proton hyperfine resonance spectra, *Biochemistry 42*, 10772-10782.

53. Bidwai, A., Witt, M., Foshay, M., Vitello, L. B., Satterlee, J. D., and Erman, J. E. (2003) Cyanide binding to cytochrome *c* peroxidase (H52l), *Biochemistry 42*, 10764-10771.

54. Choudhury, K., Sundaramoorthy, M., Hickman, A., Yonetani, T., Woehl, E., Dunn, M. F., and Poulos, T. L. (1994) Role of the proximal ligand in peroxidase catalysis. Crystallographic, kinetic, and spectral studies of cytochrome *c* peroxidase proximal ligand mutants, *J Biol Chem 269*, 20239-20249.

55. Echalier, A., Goodhew, C. F., Pettigrew, G. W., and Fulop, V. (2006) Activation and catalysis of the di-heme cytochrome *c* peroxidase from *Paracoccus pantotrophus*, *Structure 14*, 107-117.

56. Pettigrew, G. W., Echalier, A., and Pauleta, S. R. (2006) Structure and mechanism in the bacterial dihaem cytochrome *c* peroxidases, *J Inorg Biochem 100*, 551-567.

57. Foote, N., Turner, R., Brittain, T., and Greenwood, C. (1992) A quantitative model for the mechanism of action of the cytochrome *c* peroxidase of *Pseudomonas aeruginosa*, *Biochem J 283 (Pt 3)*, 839-843.

58. Foote, N., Peterson, J., Gadsby, P. M., Greenwood, C., and Thomson, A. J. (1985) Redox-linked spin-state changes in the di-haem cytochrome *c*-551 peroxidase from *Pseudomonas aeruginosa*, *Biochem J 230*, 227-237.

59. Timoteo, C. G., Tavares, P., Goodhew, C. F., Duarte, L. C., Jumel, K., Girio, F. M., Harding, S., Pettigrew, G. W., and Moura, I. (2003) Ca^{2+} and the bacterial peroxidases: The cytochrome *c* peroxidase from *Pseudomonas stutzeri*, *J Biol Inorg Chem 8*, 29-37.

60. Aasa, R., Ellfolk, N., Ronnberg, M., and Vanngard, T. (1981) Electron paramagnetic resonance studies of pseudomonas cytochrome *c* peroxidase, *Biochim Biophys Acta 670*, 170-175.

61. Villalain, J., Moura, I., Liu, M. C., Payne, W. J., LeGall, J., Xavier, A. V., and Moura, J. J. (1984) NMR and electron-paramagnetic-resonance studies of a dihaem cytochrome from *Pseudomonas stutzeri* (ATCC 11607) (cytochrome *c* peroxidase), *Eur J Biochem 141*, 305-312.

62. Chelikani, P., Fita, I., and Loewen, P. C. (2004) Diversity of structures and properties among catalases, *Cell Mol Life Sci 61*, 192-208.

63. Vainshtein, B. K., Melik-Adamyan, W. R., Barynin, V. V., Vagin, A. A., and Grebenko, A. I. (1981) Three-dimensional structure of the enzyme catalase, *Nature 293*, 411-412.

64. Murthy, M. R., Reid, T. J., 3rd, Sicignano, A., Tanaka, N., and Rossmann, M. G. (1981) Structure of beef liver catalase, *J Mol Biol 152*, 465-499.

65. Bravo, J., Verdaguer, N., Tormo, J., Betzel, C., Switala, J., Loewen, P. C., and Fita, I. (1995) Crystal structure of catalase HPII from *Escherichia coli*, *Structure 3*, 491-502.

66. Browlett, W. R., and Stillman, M. J. (1981) Evidence for heme *pi* cation radical species in compound I of horseradish peroxidase and catalase, *Biochim Biophys Acta 660*, 1-7.

67. Sevinc, M. S., Switala, J., Bravo, J., Fita, I., and Loewen, P. C. (1998) Truncation and heme pocket mutations reduce production of functional catalase HPII in *Escherichia coli*, *Protein Eng 11*, 549-555.

68. Reid, T. J., 3rd, Murthy, M. R., Sicignano, A., Tanaka, N., Musick, W. D., and Rossmann, M. G. (1981) Structure and heme environment of beef liver catalase at 2.5 Å resolution, *Proc Natl Acad Sci U S A 78*, 4767-4771.

69. Takano, T. (1977) Structure of myoglobin refined at 2.0 Å resolution. II. Structure of deoxymyoglobin from sperm whale, *J Mol Biol 110*, 569-584.

70. Takano, T. (1977) Structure of myoglobin refined at 2.0 Å resolution. I. Crystallographic refinement of metmyoglobin from sperm whale, *J Mol Biol 110*, 537-568.

71. Phillips, S. E. (1980) Structure and refinement of oxymyoglobin at 1.6 Å resolution, *J Mol Biol 142*, 531-554.

72. Quillin, M. L., Arduini, R. M., Olson, J. S., and Phillips, G. N., Jr. (1993) High-resolution crystal structures of distal histidine mutants of sperm whale myoglobin, *J Mol Biol 234*, 140-155.

73. Kitagawa, T., Ondrias, M. R., Rousseau, D. L., Ikeda-Saito, M., and Yonetani, T. (1982) Evidence for hydrogen bonding of bound dioxygen to the distal histidine of oxycobalt myoglobin and haemoglobin, *Nature 298*, 869-871.

74. Sharrock, M., Debrunner, P. G., Schulz, C., Lipscomb, J. D., Marshall, V., and Gunsalus, I. C. (1976) Cytochrome P450cam and its complexes. Mössbauer parameters of the heme iron, *Biochim Biophys Acta 420*, 8-26.

75. Ackers, G. K., Doyle, M. L., Myers, D., and Daugherty, M. A. (1992) Molecular code for cooperativity in hemoglobin, *Science 255*, 54-63.

76. Perutz, M. F. (1960) Structure of hemoglobin, *Brookhaven Symp Biol 13*, 165-183.

77. Perutz, M. F., Rossmann, M. G., Cullis, A. F., Muirhead, H., Will, G., and North, A. C. (1960) Structure of haemoglobin: A three-dimensional fourier synthesis at 5.5 Å. Resolution, obtained by x-ray analysis, *Nature 185*, 416-422.

78. Egawa, T., Shimada, H., and Ishimura, Y. (2000) Formation of compound I in the reaction of native myoglobins with hydrogen peroxide, *J Biol Chem 275*, 34858-34866.

79. Wilks, A., and Ortiz de Montellano, P. (1992) Intramolecular translocation of the protein radical formed in the reaction of recombinant sperm whale myoglobin with H_2O_2, *J Biol Chem 267*, 8827-8833.

80. Ivancich, A., Jakopitsch, C., Auer, M., Un, S., and Obinger, C. (2003) Protein-based radicals in the catalase-peroxidase of synechocystis pcc6803: A multifrequency EPR investigation of wild-type and variants on the environment of the heme active site, *J Am Chem Soc 125*, 14093-14102.

81. Matsui, T., Ozaki, S., and Watanabe, Y. (1997) On the formation and reactivity of compound I of the His-64 myoglobin mutants, *J Biol Chem 272*, 32735-32738.

82. Kato, S., Ueno, T., Fukuzumi, S., and Watanabe, Y. (2004) Catalase reaction by myoglobin mutants and native catalase: Mechanistic investigation by kinetic isotope effect, *J Biol Chem 279*, 52376-52381.

83. Watanabe, Y., Nakajima, H., and Ueno, T. (2007) Reactivities of oxo and peroxo intermediates studied by hemoprotein mutants, *Acc Chem Res 40*, 554-562.

84. Matsui, T., Ozaki, S., Liong, E., Phillips, G. N., Jr., and Watanabe, Y. (1999) Effects of the location of distal histidine in the reaction of myoglobin with hydrogen peroxide, *J Biol Chem 274*, 2838-2844.

85. Pfister, T. D., Ohki, T., Ueno, T., Hara, I., Adachi, S., Makino, Y., Ueyama, N., Lu, Y., and Watanabe, Y. (2005) Monooxygenation of an aromatic ring by F43W/H64D/V68I myoglobin mutant and hydrogen peroxide. Myoglobin mutants as a model for P450 hydroxylation chemistry, *J Biol Chem 280*, 12858-12866.

86. Finzel, B. C., Poulos, T. L., and Kraut, J. (1984) Crystal structure of yeast cytochrome c peroxidase refined at 1.7-Å resolution, *J Biol Chem 259*, 13027-13036.

87. Miller, M. A., Shaw, A., and Kraut, J. (1994) 2.2 Å structure of oxy-peroxidase as a model for the transient enzyme: Peroxide complex, *Nat Struct Biol 1*, 524-531.

88. Paoli, M., Marles-Wright, J., and Smith, A. (2002) Structure-function relationships in heme-proteins, *DNA Cell Biol 21*, 271-280.

89. Baker, R. D., Cook, C. O., and Goodwin, D. C. (2004) Properties of catalase-peroxidase lacking its C-terminal domain, *Biochem Biophys Res Commun 320*, 833-839.

90. Baker, R. D., Cook, C. O., and Goodwin, D. C. (2006) Catalase-peroxidase active site restructuring by a distant and "Inactive" Domain, *Biochemistry 45*, 7113-7121.

91. Smulevich, G., Jakopitsch, C., Droghetti, E., and Obinger, C. (2006) Probing the structure and bifunctionality of catalase-peroxidase (KatG), *J Inorg Biochem 100*, 568-585.

92. Upadhyay, A. K., Petasis, D. T., Arciero, D. M., Hooper, A. B., and Hendrich, M. P. (2003) Spectroscopic characterization and assignment of reduction potentials in the tetraheme cytochrome *c*554 from *Nitrosomonas europaea*, *J Am Chem Soc 125*, 1738-1747.

93. Igarashi, N., Moriyama, H., Fujiwara, T., Fukumori, Y., and Tanaka, N. (1997) The 2.8 Å structure of hydroxylamine oxidoreductase from a nitrifying chemoautotrophic bacterium, *Nitrosomonas europaea*, *Nat Struct Biol 4*, 276-284.

94. Bamford, V. A., Angove, H. C., Seward, H. E., Thomson, A. J., Cole, J. A., Butt, J. N., Hemmings, A. M., and Richardson, D. J. (2002) Structure and spectroscopy of the periplasmic cytochrome *c* nitrite reductase from *Escherichia coli*, *Biochemistry 41*, 2921-2931.

95. Braaz, R., Fischer, P., and Jendrossek, D. (2004) Novel type of heme-dependent oxygenase catalyzes oxidative cleavage of rubber (poly-*cis*-1,4-isoprene), *Appl Environ Microbiol 70*, 7388-7395.

96. Leys, D., Backers, K., Meyer, T. E., Hagen, W. R., Cusanovich, M. A., and Van Beeumen, J. J. (2000) Crystal structures of an oxygen-binding cytochrome *c* from *Rhodobacter sphaeroides*, *J Biol Chem 275*, 16050-16056.

97. Feigelson, P. (1976) *Pseudomonad* and hepatic L-tryptophan 2, 3-dioxygenase, *Adv Exp Med Biol 74*, 358-362.

98. Greengard, O., and Feigelson, P. (1961) The activation and induction of rat liver tryptophan pyrrolase in vivo by its substrate, *J Biol Chem 236*, 158-161.

99. Kotake, Y., Masayama, I. (1936) The intermediary metabolism of tryptophan. XVIII. The mechanism of formaiton of kynurenine from tryptophan, *Z Physiol Chem 243*, 237-244.

100. Yamamoto, S., and Hayaishi, O. (1967) Tryptophan pyrrolase of rabbit intestine. D- and L-tryptophan-cleaving enzyme or enzymes, *J Biol Chem 242*, 5260-5266.

101. Higuchi, K., and Hayaishi, O. (1967) Enzymic formation of D-kynurenine from D-tryptophan, *Arch Biochem Biophys 120*, 397-403.

102. Miller, C. L., Llenos, I. C., Dulay, J. R., Barillo, M. M., Yolken, R. H., and Weis, S. (2004) Expression of the kynurenine pathway enzyme tryptophan 2,3-dioxygenase is increased in the frontal cortex of individuals with *Schizophrenia*, *Neurobiol Dis 15*, 618-629.

103. Ishiguro, I., Naito, J., Saito, K., and Nagamura, Y. (1993) Skin L-tryptophan-2,3-dioxygenase and rat hair growth, *FEBS Lett 329*, 178-182.

104. Takikawa, O. (2005) Biochemical and medical aspects of the indoleamine 2,3-dioxygenase-initiated L-tryptophan metabolism, *Biochem Biophys Res Commun 338*, 12-19.

105. Szanto, S., Koreny, T., Mikecz, K., Glant, T. T., Szekanecz, Z., and Varga, J. (2007) Inhibition of indoleamine 2,3-dioxygenase-mediated tryptophan catabolism accelerates collagen-induced arthritis in mice, *Arthritis Res Ther 9*, R50.

106. Sun, J. X., Zhang, W. G., Chen, Y. X., Zhao, W. H., Tian, W., Yang, Y., and Liu, S. H. (2007) Indoleamine 2, 3-dioxygenase expression in cells of human acute monocyte leukemia (m(5)) and acute lymphocyte leukemia and therapeutic effect of its inhibitor 1-methyl tryptophan, *Zhongguo Shi Yan Xue Ye Xue Za Zhi 15*, 478-482.

107. MacKenzie, C. R., Heseler, K., Muller, A., and Daubener, W. (2007) Role of indoleamine 2,3-dioxygenase in antimicrobial defence and immuno-regulation: Tryptophan depletion versus production of toxic kynurenines, *Curr Drug Metab 8*, 237-244.

108. Hou, D. Y., Muller, A. J., Sharma, M. D., DuHadaway, J., Banerjee, T., Johnson, M., Mellor, A. L., Prendergast, G. C., and Munn, D. H. (2007) Inhibition of indoleamine 2,3-dioxygenase in dendritic cells by stereoisomers of 1-methyl-tryptophan correlates with antitumor responses, *Cancer Res 67*, 792-801.

109. Pellegrin, K., Neurauter, G., Wirleitner, B., Fleming, A. W., Peterson, V. M., and Fuchs, D. (2005) Enhanced enzymatic degradation of tryptophan by indoleamine 2,3-dioxygenase contributes to the tryptophan-deficient state seen after major trauma, *Shock 23*, 209-215.

110. Kurnasov, O., Goral, V., Colabroy, K., Gerdes, S., Anantha, S., Osterman, A., and Begley, T. P. (2003) NAD biosynthesis: Identification of the tryptophan to quinolinate pathway in bacteria, *Chem Biol 10*, 1195-1204.

111. Stone, T. W., and Darlington, L. G. (2002) Endogenous kynurenines as targets for drug discovery and development, *Nat Rev Drug Discov 1*, 609-620.

112. Schwarcz, R. (2004) The kynurenine pathway of tryptophan degradation as a drug target, *Curr Opin Pharmacol 4*, 12-17.

113. Stone, T. W., Mackay, G. M., Forrest, C. M., Clark, C. J., and Darlington, L. G. (2003) Tryptophan metabolites and brain disorders, *Clin Chem Lab Med 41*, 852-859.

114. Schwarcz, R., Whetsell, W. O., Jr. & Mangano, R. M. (1983) Quinolinic acid: An endogenous metabolite that produces axon-sparing lesions in rat brain, *Science 219*, 316-318.

115. Shepard, P. D., Joy, B., Clerkin, L. & Schwarcz, R. (2003) Micromolar brain levels of kynurenic acid are associated with a disruption of auditory sensory gating in the rat, *Neuropsychopharmacology 28*, 1454-1462.

116. Stone, T. W. (2001) Endogenous neurotoxins from tryptophan, *Toxicon 39*, 61-73.

117. Stone, T. W., Behan, W. M., Jones, P. A., Darlington, L. G., and Smith, R. A. (2001) The role of kynurenines in the production of neuronal death, and the neuroprotective effect of purines, *J Alzheimers Dis 3*, 355-366.

118. Stone, T. W., and Connick, J. H. (1985) Quinolinic acid and other kynurenines in the central nervous system, *Neuroscience 15*, 597-617.

119. Sanni, L. A., Thomas, S. R., Tattam, B. N., Moore, D. E., Chaudhri, G., Stocker, R., and Hunt, N. H. (1998) Dramatic changes in oxidative tryptophan metabolism along the kynurenine pathway in experimental cerebral and noncerebral malaria, *Am J Pathol 152*, 611-619.

120. Tankiewicz, A., Pawlak, D., Topczewska-Bruns, J., and Buczko, W. (2003) Kidney and liver kynurenine pathway enzymes in chronic renal failure, *Adv Exp Med Biol 527*, 409-414.

121. Hayaishi, O., Katagiri, M., Rothberg, S. (1955) Mechanism of the pyrocatechase reaction, *J Am Chem Soc 77*, 5450-5451.

122. Mason, H. S., Fowlks, W. L., Peterson E. (1955) Oxygen transfer and electron transport by the phenolase complex., *J Am Chem Soc 77*, 2914-2915.

123. Hayaishi, O., Rothberg, S., Mehler, A. H., and Saito, Y. (1957) Studies on oxygenases. Enzymatic formation of kynurenine from tryptophan, *J Biol Chem 229*, 889-896.

124. Hegg, E. L., and Que, L., Jr. (1997) The 2-His-1-carboxylate facial triad--an emerging structural motif in mononuclear non-heme iron(II) enzymes, *Eur J Biochem 250*, 625-629.

125. Kovaleva, E. G., Neibergall, M. B., Chakrabarty, S., and Lipscomb, J. D. (2007) Finding intermediates in the O_2 activation pathways of non-heme iron oxygenases, *Acc Chem Res 40*, 475-483.

126. Forouhar, F., Anderson, J. L., Mowat, C. G., Vorobiev, S. M., Hussain, A., Abashidze, M., Bruckmann, C., Thackray, S. J., Seetharaman, J., Tucker, T., Xiao, R., Ma, L. C., Zhao, L., Acton, T. B., Montelione, G. T., Chapman, S. K., and Tong, L. (2007) Molecular insights into substrate recognition and catalysis by tryptophan 2,3-dioxygenase, *Proc Natl Acad Sci USA 104*, 473-478.

127. De Laurentis, W., Khim, L., Anderson, J. L., Adam, A., Johnson, K. A., Phillips, R. S., Chapman, S. K., van Pee, K. H., and Naismith, J. H. (2007) The second enzyme in pyrrolnitrin biosynthetic pathway is related to the heme-dependent dioxygenase superfamily, *Biochemistry 46*, 12393-12404.

128. Zhang, Y., Kang, S. A., Mukherjee, T., Bale, S., Crane, B. R., Begley, T. P., and Ealick, S. E. (2007) Crystal structure and mechanism of tryptophan 2,3-dioxygenase, a heme enzyme involved in tryptophan catabolism and in quinolinate biosynthesis, *Biochemistry 46*, 145-155.

129. Forouhar, F., Anderson, J. L., Mowat, C. G., Vorobiev, S. M., Hussain, A., Abashidze, M., Bruckmann, C., Thackray, S. J., Seetharaman, J., Tucker, T., Xiao, R., Ma, L. C., Zhao, L., Acton, T. B., Montelione, G. T., Chapman, S. K., and Tong, L. (2007)

Molecular insights into substrate recognition and catalysis by tryptophan 2,3-dioxygenase, *Proc Natl Acad Sci U S A 104*, 473-478.

130. Sugimoto, H., Oda, S., Otsuki, T., Hino, T., Yoshida, T., and Shiro, Y. (2006) Crystal structure of human indoleamine 2,3-dioxygenase: Catalytic mechanism of O_2 incorporation by a heme-containing dioxygenase, *Proc Natl Acad Sci U S A 103*, 2611-2616.

131. Fukumura, E., Sugimoto, H., Misumi, Y., Ogura, T., and Shiro, Y. (2009) Cooperative binding of L-trp to human tryptophan 2,3-dioxygenase: Resonance raman spectroscopic analysis, *J Biochem*.

132. Batabyal, D., and Yeh, S. R. (2009) Substrate-protein interaction in human tryptophan dioxygenase: The critical role of H76, *J Am Chem Soc*.

133. Thackray, S. J., Bruckmann, C., Anderson, J. L., Campbell, L. P., Xiao, R., Zhao, L., Mowat, C. G., Forouhar, F., Tong, L., and Chapman, S. K. (2008) Histidine 55 of tryptophan 2,3-dioxygenase is not an active site base but regulates catalysis by controlling substrate binding, *Biochemistry 47*, 10677-10684.

134. Chauhan, N., Basran, J., Efimov, I., Svistunenko, D. A., Seward, H. E., Moody, P. C., and Raven, E. L. (2008) The role of serine 167 in human indoleamine 2,3-dioxygenase: A comparison with tryptophan 2,3-dioxygenase, *Biochemistry 47*, 4761-4769.

135. Basran, J., Rafice, S. A., Chauhan, N., Efimov, I., Cheesman, M. R., Ghamsari, L., and Raven, E. L. (2008) A kinetic, spectroscopic, and redox study of human tryptophan 2,3-dioxygenase, *Biochemistry 47*, 4752-4760.

136. Fukumura, E., Sugimoto, H., Misumi, Y., Ogura, T., and Shiro, Y. (2009) Cooperative binding of l-trp to human tryptophan 2,3-dioxygenase: Resonance Raman spectroscopic analysis, *J Biochem 145*, 505-515.

137. Sugimoto, H., Oda, S., Otsuki, T., Hino, T., Yoshida, T., and Shiro, Y. (2006) Crystal structure of human indoleamine 2,3-dioxygenase: Catalytic mechanism of O_2 incorporation by a heme-containing dioxygenase, *Proc Natl Acad Sci USA 103*, 2611-2616.

138. Henry, Y., Ishimura, Y., and Peisach, J. (1976) Binding of nitric oxide to reduced L-tryptophan-2,3-dioxygenase as studied by electron paramagnetic resonance, *J Biol Chem 251*, 1578-1581.

139. Brady, F. O., Feigelson, P., and Rajagopalan, K. V. (1973) Studies of the copper and heme cofactors of *Pseudomonad* L-tryptophan-2,3-dioxygenase by electron paramagnetic resonance spectroscopy, *Arch Biochem Biophys 157*, 63-72.

140. Papadopoulou, N. D., Mewies, M., McLean, K. J., Seward, H. E., Svistunenko, D. A., Munro, A. W., and Raven, E. L. (2005) Redox and spectroscopic properties of human indoleamine 2,3-dioxygenase and a His303Ala variant: Implications for catalysis, *Biochemistry 44*, 14318-14328.

141. Batabyal, D., and Yeh, S. R. (2007) Human tryptophan dioxygenase: A comparison to indoleamine 2,3-dioxygenase, *J Am Chem Soc 129*, 15690-15701.

142. Ishimura, Y., Nozaki, M., Hayaishi, O., Nakamura, T., Tamura, M., and Yamazaki, I. (1970) The oxygenated form of L-tryptophan 2,3-dioxygenase as reaction intermediate, *J Biol Chem 245*, 3593-3602.

143. Taniguchi, T., Sono, M., Hirata, F., Hayaishi, O., Tamura, M., Hayashi, K., Iizuka, T., and Ishimura, Y. (1979) Indoleamine 2,3-dioxygenase. Kinetic studies on the binding of superoxide anion and molecular oxygen to enzyme, *J Biol Chem 254*, 3288-3294.

144. Hirata, F., Ohnishi, T., and Hayaishi, O. (1977) Indoleamine 2,3-dioxygenase. Characterization and properties of enzyme O_2-complex, *J Biol Chem 252*, 4637-4642.

145. Ishimura, Y., Nozaki, M., and Hayaishi, O. (1967) Evidence for an oxygenated intermediate in the tryptophan pyrrolase reaction, *J Biol Chem 242*, 2574-2576.

146. Ishimura, Y., Nozaki, M., and Hayaishi, O. (1970) The oxygenated form of L-tryptophan 2,3-dioxygenase as reaction intermediate, *J Biol Chem 245*, 3593-3602.

147. Makino, R., Sakaguchi, K., Iizuka, T., and Ishimura, Y. (1980) Acid-alkaline transition and thermal spin equilibrium of the heme in ferric L-tryptophan 2,3-dioxygenases, *J Biol Chem 255*, 11883-11891.

148. Kotake, Y., and Masayama, I. (1936) The intermediary metabolism of tryptophan. XVIII. The mechanism of formation of kynurenine from tryptophan, *Z physiol Chem 243*, 237-244.

149. Sakan, T., and Hayaishi, O. (1950) Lambda-hydroxytryptophan, not an intermediate between tryptophan and kynurenine, *J Biol Chem 186*, 177-180.

150. Stanier, R. Y., Hayaishi, O., and Tsuchida, M. (1951) The bacterial oxidation of tryptophan. I. A general survey of the pathways, *J Bacteriol 62*, 355-366.

151. Stanier, R. Y., and Hayaishi, O. (1951) The bacterial oxidation of tryptophan; a study in comparative biochemistry, *Science 114*, 326-330.

152. Hayaishi, O., and Stanier, R. Y. (1952) The kynureninase of pseudomonas fluorescens, *J Biol Chem 195*, 735-740.

153. Brady, F. O. (1975) Tryptophan 2,3-dioxygenase: A review of the roles of the heme and copper cofactors in catalysis, *Bioinorganic Chemistry 5*, 167-182.

154. Makino, R., and Ishimura, Y. (1976) Negligible amount of copper in hepatic L-tryptophan 2,3-dioxygenase, *J Biol Chem 251*, 7722-7725.

155. Yamamoto, S., and Hayaishi, O. (1970) Tryptophan 2,3-dioxygenase (tryptophan pyrrolase), *Methods Enzymol 17*, 434-438.

156. Knox, W. E., Yip, A., and Reshef, L. (1970) L-tryptophan 2,3-dioxygenase (tryptophan pyrrolase) (rat liver), *Methods Enzymol 17*, 415-421.

157. Hamilton, G. A. (1969) Mechanisms of two- and four-electron oxidations catalyzed by some metalloenzymes, *Adv Enzymol Relat Areas Mol Biol 32*, 55-96.

158. Leeds, J. M., Brown, P. J., McGeehan, G. M., Brown, F. K., and Wiseman, J. S. (1993) Isotope effects and alternative substrate reactivities for tryptophan 2,3-dioxygenase, *J Biol Chem 268*, 17781-17786.

159. Thackray, S. J., Mowat, C. G., and Chapman, S. K. (2008) Exploring the mechanism of tryptophan 2,3-dioxygenase, *Biochem Soc Trans 36*, 1120-1123.

160. Macchiarulo, A., Camaioni, E., Nuti, R., and Pellicciari, R. (2008) Highlights at the gate of tryptophan catabolism: A review on the mechanisms of activation and regulation of indoleamine 2,3-dioxygenase (IDO), a novel target in cancer disease, *Amino Acids*.

161. Leeds, J., Brown, P., McGeehan, G., Brown, F., and Wiseman, J. (1993) Isotope effects and alternative substrate reactivities for tryptophan 2,3-dioxygenase, *J Biol Chem 268*, 17781-17786.

162. Lipscomb, J. D. (2008) Mechanism of extradiol aromatic ring-cleaving dioxygenases, *Current Opinion in Structural Biology 18*, 644-649.

163. Sanvoisin, J., Langley, G. J., and Bugg, T. D. H. (1995) Mechanism of extradiol catechol dioxygenases: Evidence for a lactone intermediate in the 2,3-dihydroxyphenylpropionate 1,2-dioxygenase reaction, *J Am Chem Soc 117*, 7836-7837.

164. Chauhan, N., Thackray, S. J., Rafice, S. A., Eaton, G., Lee, M., Efimov, I., Basran, J., Jenkins, P. R., Mowat, C. G., Chapman, S. K., and Raven, E. L. (2009) Reassessment of the reaction mechanism in the heme dioxygenases, *J Am Chem Soc 131*, 4186-4187.

165. Chung, L. W., Li, X., Sugimoto, H., Shiro, Y., and Morokuma, K. (2008) Density functional theory study on a missing piece in understanding of heme chemistry: The reaction mechanism for indoleamine 2,3-dioxygenase and tryptophan 2,3-dioxygenase, *J Am Chem Soc 130*, 12299-12309.

166. McIntire, W. S., Wemmer, D. E., Chistoserdov, A., and Lidstrom, M. E. (1991) A new cofactor in a prokaryotic enzyme: Tryptophan tryptophylquinone as the redox prosthetic group in methylamine dehydrogenase, *Science 252*, 817-824.

167. Davidson, V. L. (2007) Protein-derived cofactors. Expanding the scope of post-translational modifications, *Biochemistry 46*, 5283-5292.

168. Klinman, J. P. (2001) How many ways to craft a cofactor?, *Proc Natl Acad Sci USA 98*, 14766–14768.

169. Okeley, N. M., and van der Donk, W. A. (2000) Novel cofactors via post-translational modifications of enzyme active sites, *Chem Biol 7*, R159-171.

170. Chen, L., Durley, R. C., Mathews, F. S., and Davidson, V. L. (1994) Structure of an electron transfer complex: Methylamine dehydrogenase, amicyanin, and cytochrome *c*551i, *Science 264*, 86-90.

171. Chen, L., Doi, M., Durley, R. C., Chistoserdov, A. Y., Lidstrom, M. E., Davidson, V. L., and Mathews, F. S. (1998) Refined crystal structure of methylamine dehydrogenase from *paracoccus denitrificans* at 1.75 Å resolution, *J Mol Biol 276*, 131-149.

172. van der Palen, C. J., Slotboom, D. J., Jongejan, L., Reijnders, W. N., Harms, N., Duine, J. A., and van Spanning, R. J. (1995) Mutational analysis of *mau* genes involved in methylamine metabolism in *Paracoccus denitrificans*, *Eur J Biochem 230*, 860-871.

173. Graichen, M. E., Jones, L. H., Sharma, B. V., van Spanning, R. J., Hosler, J. P., and Davidson, V. L. (1999) Heterologous expression of correctly assembled methylamine dehydrogenase in *Rhodobacter sphaeroides*, *J Bacteriol 181*, 4216-4222.

174. Pearson, A. R., De La Mora-Rey, T., Graichen, M. E., Wang, Y., Jones, L. H., Marimanikkupam, S., Agger, S. A., Grimsrud, P. A., Davidson, V. L., and Wilmot, C. M. (2004) Further insights into quinone cofactor biogenesis: Probing the role of mauG in methylamine dehydrogenase tryptophan tryptophylquinone formation, *Biochemistry 43*, 5494-5502.

175. Pearson, A. R., Marimanikkuppam, S., Li, X., Davidson, V. L., and Wilmot, C. M. (2006) Isotope labeling studies reveal the order of oxygen incorporation into the tryptophan

tryptophylquinone cofactor of methylamine dehydrogenase, *J Am Chem Soc 128*, 12416-12417.

176. Wang, Y., Graichen, M. E., Liu, A., Pearson, A. R., Wilmot, C. M., and Davidson, V. L. (2003) MauG, a novel diheme protein required for tryptophan tryptophylquinone biogenesis, *Biochemistry 42*, 7318-7325.

177. Li, X., Jones, L. H., Pearson, A. R., Wilmot, C. M., and Davidson, V. L. (2006) Mechanistic possibilities in MauG-dependent tryptophan tryptophylquinone biosynthesis, *Biochemistry 45*, 13276-13283.

178. Wang, Y., Li, X., Jones, L. H., Pearson, A. R., Wilmot, C. M., and Davidson, V. L. (2005) MauG-dependent in vitro biosynthesis of tryptophan tryptophylquinone in methylamine dehydrogenase, *J Am Chem Soc 127*, 8258-8259.

179. Li, X., Feng, M., Wang, Y., Tachikawa, H., and Davidson, V. L. (2006) Evidence for redox cooperativity between *c*-type hemes of MauG which is likely coupled to oxygen activation during tryptophan tryptophylquinone biosynthesis, *Biochemistry 45*, 821-828.

180. Li, X., Fu, R., Lee, S., Krebs, C., Davidson, V. L., and Liu, A. (2008) A catalytic di-heme *bis*-Fe(IV) intermediate, alternative to an Fe(IV)=O porphyrin radical, *Proc Natl Acad Sci USA 105*, 8597-8600.

181. Braaz, R., Armbruster, W., and Jendrossek, D. (2005) Heme-dependent rubber oxygenase roxa of *Xanthomonas sp*. Cleaves the carbon backbone of poly(*cis*-1,4-isoprene) by a dioxygenase mechanism, *Appl Environ Microbiol 71*, 2473-2478.

182. Groves, J. T. (2006) High-valent iron in chemical and biological oxidations, *J Inorg Biochem 100*, 434-447.

183. Silaghi-Dumitrescu, R. (2004) The nature of the high-valent complexes in the catalytic cycles of hemoproteins, *J Biol Inorg Chem 9*, 471-476.

184. Bollinger, J. M., Jr., and Krebs, C. (2006) Stalking intermediates in oxygen activation by iron enzymes: Motivation and method, *J Inorg Biochem 100*, 586-605.

185. Rutter, R., Hager, L. P., Dhonau, H., Hendrich, M., Valentine, M., and Debrunner, P. (1984) Chloroperoxidase compound I: Electron paramagnetic resonance and Mössbauer studies, *Biochemistry 23*, 6809-6816.

186. Rutter, R., Valentine, M., Hendrich, M. P., Hager, L. P., and Debrunner, P. G. (1983) Chemical nature of the porphyrin *pi* cation radical in horseradish peroxidase compound I, *Biochemistry 22*, 4769-4774.

187. Jung, C., Lendzian, F., Schunemann, V., Richter, M., Bottger, L. H., Trautwein, A. X., Contzen, J., Galander, M., Ghosh, D. K., and Barra, A. L. (2005) Multi-frequency EPR and Mössbauer spectroscopic studies on freeze-quenched reaction intermediates of nitric oxide synthase, *Magn Reson Chem 43 Spec no.*, S84-95.

188. Lambeir, A. M., Markey, C. M., Dunford, H. B., and Marnett, L. J. (1985) Spectral properties of the higher oxidation states of prostaglandin H synthase, *J Biol Chem 260*, 14894-14896.

189. Ferguson-Miller, S., and Babcock, G. T. (1996) Heme/copper terminal oxidases, *Chem Rev 96*, 2889-2908.

190. Behan, R. K., Hoffart, L. M., Stone, K. L., Krebs, C., and Green, M. T. (2006) Evidence for basic ferryls in cytochromes P450, *J Am Chem Soc 128*, 11471-11474.

191. Terner, J., Palaniappan, V., Gold, A., Weiss, R., Fitzgerald, M. M., Sullivan, A. M., and Hosten, C. M. (2006) Resonance raman spectroscopy of oxoiron(iv) porphyrin *pi*-cation radical and oxoiron(IV) hemes in peroxidase intermediates, *J Inorg Biochem 100*, 480-501.

192. Schulz, C. E., Rutter, R., Sage, J. T., Debrunner, P. G., and Hager, L. P. (1984) Mössbauer and electron paramagnetic resonance studies of horseradish peroxidase and its catalytic intermediates, *Biochemistry 23*, 4743-4754.

193. Erman, J. E., Vitello, L. B., Mauro, J. M., and Kraut, J. (1989) Detection of an oxyferryl porphyrin *pi*-cation-radical intermediate in the reaction between hydrogen peroxide and a mutant yeast cytochrome *c* peroxidase. Evidence for tryptophan-191 involvement in the radical site of compound I, *Biochemistry 28*, 7992-7995.

194. Rutter, R., and Hager, L. P. (1982) The detection of two electron paramagnetic resonance radical signals associated with chloroperoxidase compound I, *J Biol Chem 257*, 7958-7961.

195. Benecky, M. J., Frew, J. E., Scowen, N., Jones, P., and Hoffman, B. M. (1993) EPR and ENDOR detection of compound I from *Micrococcus lysodeikticus* catalase, *Biochemistry 32*, 11929-11933.

196. Ivancich, A., Jouve, H. M., Sartor, B., and Gaillard, J. (1997) EPR investigation of compound I in proteus mirabilis and bovine liver catalases: Formation of porphyrin and tyrosyl radical intermediates, *Biochemistry 36*, 9356-9364.

197. Davydov, R. M., Smieja, J., Dikanov, S. A., Zang, Y., Que, L., Jr., and Bowman, M. K. (1999) EPR properties of mixed-valent μ-oxo and μ-hydroxo dinuclear iron complexes produced by radiolytic reduction at 77 K, *J Biol Inorg Chem 4*, 292-301.

198. Bassan, A., Blomberg, M. R., Borowski, T., and Siegbahn, P. E. (2006) Theoretical studies of enzyme mechanisms involving high-valent iron intermediates, *J Inorg Biochem 100*, 727-743.

199. Palcic, M. M., Rutter, R., Araiso, T., Hager, L. P., and Dunford, H. B. (1980) Spectrum of chloroperoxidase compound I, *Biochem Biophys Res Commun 94*, 1123-1127.

200. Harris, D., Loew, G., and Waskell, L. (2001) Calculation of the electronic structure and spectra of model cytochrome P450 compound I, *J Inorg Biochem 83*, 309-318.

201. Harris, D. L., and Loew, G. H. (1996) Investigation of the proton-assisted pathway to formation of the catalytically active, ferryl species of P450s by molecular dynamics studies of P450eryF, *J Am Chem Soc 118*, 6377-6387.

202. Hersleth, H. P., Ryde, U., Rydberg, P., Gorbitz, C. H., and Andersson, K. K. (2006) Structures of the high-valent metal-ion haem-oxygen intermediates in peroxidases, oxygenases and catalases, *J Inorg Biochem 100*, 460-476.

203. Adak, S., Mazumdar, A., and Banerjee, R. K. (1997) Low catalytic turnover of horseradish peroxidase in thiocyanate oxidation. Evidence for concurrent inactivation by cyanide generated through one-electron oxidation of thiocyanate, *J Biol Chem 272*, 11049-11056.

204. Howes, B. D., Veitch, N. C., Smith, A. T., White, C. G., and Smulevich, G. (2001) Haem-linked interactions in horseradish peroxidase revealed by spectroscopic analysis of the Phe-221-->Met mutant, *Biochem J 353*, 181-191.

205. Hewson, W. D., and Hager, L. P. (1979) Oxidation of horseradish peroxidase compound II to compound I, *J Biol Chem 254*, 3182-3186.

206. Blumberg, W. E., Peisach, J., Wittenberg, B. A., and Wittenberg, J. B. (1968) The electronic structure of protoheme proteins. I. An electron paramagnetic resonance and optical study of horseradish peroxidase and its derivatives, *J Biol Chem 243*, 1854-1862.

207. Adediran, S. A., and Lambeir, A. M. (1989) Kinetics of the reaction of compound II of horseradish peroxidase with hydrogen peroxide to form compound iii, *Eur J Biochem 186*, 571-576.

208. Liu, H. I., Sono, M., Kadkhodayan, S., Hager, L. P., Hedman, B., Hodgson, K. O., and Dawson, J. H. (1995) X-ray absorption near edge studies of cytochrome P-450-cam, chloroperoxidase, and myoglobin. Direct evidence for the electron releasing character of a cysteine thiolate proximal ligand, *J Biol Chem 270*, 10544-10550.

209. Hager, L. P., Doubek, D. L., Silverstein, R. M., Hargis, J. H., and Martin, J. C. (1972) Chloroperoxidase. IX. The structure of compound I, *J Am Chem Soc 94*, 4364-4366.

210. De Smet, L., Pettigrew, G. W., and Van Beeumen, J. J. (2001) Cloning, overproduction and characterization of cytochrome *c* peroxidase from the purple *Phototrophic bacterium Rhodobacter capsulatus*, *Eur J Biochem 268*, 6559-6568.

211. Ronnberg, M., Lambeir, A. M., Ellfolk, N., and Dunford, H. B. (1985) A rapid-scan spectrometric and stopped-flow study of compound I and compound II of *Pseudomonas* cytochrome *c* peroxidase, *Arch Biochem Biophys 236*, 714-719.

212. Tien, M., and Kirk, T. K. (1984) Lignin-degrading enzyme from phanerochaete chrysosporium: Purification, characterization, and catalytic properties of a unique H_2O_2-requiring oxygenase, *Proc Natl Acad Sci U S A 81*, 2280-2284.

213. Andrawis, A., Johnson, K. A., and Tien, M. (1988) Studies on compound I formation of the lignin peroxidase from *Phanerochaete chrysosporium*, *J Biol Chem 263*, 1195-1198.

214. Yonetani, T., and Ray, G. S. (1965) Studies on cytochrome *c* peroxidase. I. Purification and some properties, *J Biol Chem 240*, 4503-4508.

215. Rich, P. R., and Iwaki, M. (2007) A comparison of catalytic site intermediates of cytochrome *c* oxidase and peroxidases, *Biochemistry (Mosc) 72*, 1047-1055.

216. Egawa, T., Shimada, H., and Ishimura, Y. (1994) Evidence for compound I formation in the reaction of cytochrome P450cam with *m*-chloroperbenzoic acid, *Biochem Biophys Res Commun 201*, 1464-1469.

217. McLean, M. A., Maves, S. A., Weiss, K. E., Krepich, S., and Sligar, S. G. (1998) Characterization of a cytochrome P450 from the *Acidothermophilic archaea sulfolobus solfataricus*, *Biochem Biophys Res Commun 252*, 166-172.

218. Gajhede, M., Schuller, D. J., Henriksen, A., Smith, A. T., and Poulos, T. L. (1997) Crystal structure of horseradish peroxidase *c* at 2.15 Å resolution, *Nat Struct Biol 4*, 1032-1038.

219. Bonagura, C. A., Bhaskar, B., Shimizu, H., Li, H., Sundaramoorthy, M., McRee, D. E., Goodin, D. B., and Poulos, T. L. (2003) High-resolution crystal structures and spectroscopy of native and compound I cytochrome *c* peroxidase, *Biochemistry 42*, 5600-5608.

220. Engler, N., Ostermann, A., Gassmann, A., Lamb, D. C., Prusakov, V. E., Schott, J., Schweitzer-Stenner, R., and Parak, F. G. (2000) Protein dynamics in an intermediate state of myoglobin: Optical absorption, resonance Raman spectroscopy, and x-ray structure analysis, *Biophys J 78*, 2081-2092.

221. Hersleth, H. P., Dalhus, B., Gorbitz, C. H., and Andersson, K. K. (2002) An iron hydroxide moiety in the 1.35 Å resolution structure of hydrogen peroxide derived myoglobin compound II at pH 5.2, *J Biol Inorg Chem 7*, 299-304.

222. Schlichting, I., Berendzen, J., Chu, K., Stock, A. M., Maves, S. A., Benson, D. E., Sweet, R. M., Ringe, D., Petsko, G. A., and Sligar, S. G. (2000) The catalytic pathway of cytochrome P450cam at atomic resolution, *Science 287*, 1615-1622.

223. Poulos, T. L., Finzel, B. C., and Howard, A. J. (1987) High-resolution crystal structure of cytochrome P450cam, *J Mol Biol 195*, 687-700.

224. Andreoletti, P., Sainz, G., Jaquinod, M., Gagnon, J., and Jouve, H. M. (2003) High-resolution structure and biochemical properties of a recombinant *Proteus mirabilis* catalase depleted in iron, *Proteins 50*, 261-271.

225. Green, M. T. (2006) Application of Badger's rule to heme and non-heme iron-oxygen bonds: An examination of ferryl protonation states, *J Am Chem Soc 128*, 1902-1906.

226. Debrunner, P. G. (1989) Mössbauer spectroscopy of iron porphyrins., *Phys Bioinorg Chem Ser 4*, 137-234.

227. Davydov, R., Osborne, R. L., Kim, S. H., Dawson, J. H., and Hoffman, B. M. (2008) EPR and ENDOR studies of cryoreduced compounds II of peroxidases and myoglobin. Proton-coupled electron transfer and protonation status of ferryl hemes, *Biochemistry 47*, 5147-5155.

228. Murshudov, G. N., Grebenko, A. I., Brannigan, J. A., Antson, A. A., Barynin, V. V., Dodson, G. G., Dauter, Z., Wilson, K. S., and Melik-Adamyan, W. R. (2002) The structures of *Micrococcus lysodeikticus* catalase, its ferryl intermediate (compound II) and NADPH complex, *Acta Crystallogr D Biol Crystallogr 58*, 1972-1982.

229. Rovira, C. (2005) Structure, protonation state and dynamics of catalase compound II, *Chemphyschem 6*, 1820-1826.

230. Rovira, C. (2005) Study of ligand-protein interactions by means of density functional theory and first-principles molecular dynamics, *Methods Mol Biol 305*, 517-554.

231. Davydov, R., Ledbetter-Rogers, A., Martasek, P., Larukhin, M., Sono, M., Dawson, J. H., Masters, B. S., and Hoffman, B. M. (2002) EPR and ENDOR characterization of intermediates in the cryoreduced oxy-nitric oxide synthase heme domain with bound L-arginine or N(G)-hydroxyarginine, *Biochemistry 41*, 10375-10381.

232. Lang, G., Spartalian, K., and Yonetani, T. (1976) Mössbauer spectroscopic study of compound ES of cytochrome *c* peroxidase, *Biochim Biophys Acta 451*, 250-258.

233. Schulz, C. E., Devaney, P. W., Winkler, H., Debrunner, P. G., Doan, N., Chiang, R., Rutter, R., and Hager, L. P. (1979) Horseradish peroxidase compound I: Evidence for spin coupling between the heme iron and a 'free' radical, *FEBS Lett 103*, 102-105.

234. Maeda, Y., Higashimura, T., and Morita, Y. (1967) Mössbauer effect in peroxidase, *Biochem Biophys Res Commun 29*, 362-367.

235. Harami, T., Maeda, Y., Morita, Y., Trautwein, A.X., Gonser, U. (1977) Mössbauer spectroscopic determination of the electronic structure of highly oxidized iron in hemoproteins, *J ChemPhys 67*, 1164-1169.

236. Sommerfeldt, H. M., Meermann, C., Tornroos, K. W., and Anwander, R. (2008) Distinct reaction pathways of peralkylated LnIIA1III heterobimetallic complexes with substituted phenols, *Inorg Chem 47*, 4696-4705.

237. Horner, O., Oddou, J. L., Mouesca, J. M., and Jouve, H. M. (2006) Mössbauer identification of a protonated ferryl species in catalase from *Proteus mirabilis*: Density functional calculations on related models, *J Inorg Biochem 100*, 477-479.

238. Stone, K. L., Hoffart, L. M., Behan, R. K., Krebs, C., and Green, M. T. (2006) Evidence for two ferryl species in chloroperoxidase compound II, *J Am Chem Soc 128*, 6147-6153.

239. Gardner, K. A., and Mayer, J. M. (1995) Understanding C-H bond oxidations: H. And H-transfer in the oxidation of toluene by permanganate, *Science 269*, 1849-1851.

240. Silaghi-Dumitrescu, R., Reeder, B. J., Nicholls, P., Cooper, C. E., and Wilson, M. T. (2007) Ferryl haem protonation gates peroxidatic reactivity in globins, *Biochem J 403*, 391-395.

241. Ehrenberg, A., and Reichard, P. (1972) Electron spin resonance of the iron-containing protein B2 from ribonucleotide reductase, *J Biol Chem 247*, 3485-3488.

242. van der Donk, W. A., Stubbe, J., Gerfen, G. J., Bellew, B. F., and Griffin, R. G. (1995) Epr investigations of the inactivation of *E. coli* ribonucleotide reductase with 2'-azido-2'-deoxyuridine 5'-diphosphate: Evidence for the involvement of the thiyl radical of *c*225-r1, *J Am Chem Soc 117*, 8908-8916.

243. Stubbe, J., and van der Donk, W. A. (1998) Protein radicals in enzyme catalysis, *Chem Rev 98*, 705-762.

244. Ivancich, A., Jouve, H. M., and Gaillard, J. (1996) EPR evidence for a tyrosyl radical intermediate in bovine liver catalase, *J Am Cheml Soc 118*, 12852-12853.

245. Davies, M. J., and Puppo, A. (1992) Direct detection of a globin-derived radical in leghaemoglobin treated with peroxides, *Biochem J 281 (Pt 1)*, 197-201.

246. Gunther, M. R., Sturgeon, B. E., and Mason, R. P. (2000) A long-lived tyrosyl radical from the reaction between horse metmyoglobin and hydrogen peroxide, *Free Radic Biol Med 28*, 709-719.

247. Svistunenko, D. A., Dunne, J., Fryer, M., Nicholls, P., Reeder, B. J., Wilson, M. T., Bigotti, M. G., Cutruzzola, F., and Cooper, C. E. (2002) Comparative study of tyrosine radicals in hemoglobin and myoglobins treated with hydrogen peroxide, *Biophys J 83*, 2845-2855.

248. Svistunenko, D. A. (2005) Reaction of haem containing proteins and enzymes with hydroperoxides: The radical view, *Biochim Biophys Acta 1707*, 127-155.

249. Chouchane, S., Girotto, S., Yu, S., and Magliozzo, R. S. (2002) Identification and characterization of tyrosyl radical formation in *Mycobacterium tuberculosis* catalase-peroxidase (KatG), *J Biol Chem 277*, 42633-42638.

250. Ivancich, A., Mazza, G., and Desbois, A. (2001) Comparative electron paramagnetic resonance study of radical intermediates in turnip peroxidase isozymes, *Biochemistry 40*, 6860-6866.

251. Dorlet, P., Seibold, S. A., Babcock, G. T., Gerfen, G. J., Smith, W. L., Tsai, A. L., and Un, S. (2002) High-field epr study of tyrosyl radicals in prostaglandin H(2) synthase-1, *Biochemistry 41*, 6107-6114.

252. Pujols-Ayala, I., and Barry, B. A. (2004) Tyrosyl radicals in photosystem II, *Biochim Biophys Acta 1655*, 205-216.

253. Pogni, R., Baratto, M. C., Giansanti, S., Teutloff, C., Verdin, J., Valderrama, B., Lendzian, F., Lubitz, W., Vazquez-Duhalt, R., and Basosi, R. (2005) Tryptophan-based radical in the catalytic mechanism of versatile peroxidase from *Bjerkandera adusta*, *Biochemistry 44*, 4267-4274.

254. Alexander N. P. Hiner, J. I. M., Marino B. Arnao, Manuel Acosta, Daniel D. Turner, Emma Lloyd Raven, José Neptuno Rodríguez-López,. (2001) Detection of a tryptophan radical in the reaction of ascorbate peroxidase with hydrogen peroxide, *Eur J Biochem 268*, 3091-3098.

255. Whittaker, J. W. (2003) Free radical catalysis by galactose oxidase, *Chem Rev 103*, 2347-2363.

256. Whittaker, J. W. (1995) Spectroscopic studies of galactose oxidase, *Methods in Enzymology 258*, 262-277.

257. Barry, B. A., El-Deeb, M. K., Sandusky, P. O., and Babcock, G. T. (1990) Tyrosine radicals in photosystem II and related model compounds. Characterization by isotopic labeling and EPR spectroscopy, *J Biol Chem 265*, 20139-20143.

258. Hogbom, M., Galander, M., Andersson, M., Kolberg, M., Hofbauer, W., Lassmann, G., Nordlund, P., and Lendzian, F. (2003) Displacement of the tyrosyl radical cofactor in ribonucleotide reductase obtained by single-crystal high-field epr and 1.4- Å x-ray data 10.1073/pnas.0536684100, *Proc Natl Acad Sci USA 100*, 3209-3214.

259. Sjoberg, B. M., Reichard, P., Graslund, A., and Ehrenberg, A. (1978) The tyrosine free radical in ribonucleotide reductase from *Escherichia coli*, *J Biol Chem 253*, 6863-6865.

260. Sjoberg, B. M., and Graslund, A. (1977) The free radical in ribonucleotide reductase from *E. coli*, *Ciba Found Symp*, 187-196.

261. Tsai, A., Hsi, L. C., Kulmacz, R. J., Palmer, G., and Smith, W. L. (1994) Characterization of the tyrosyl radicals in ovine prostaglandin H synthase-1 by isotope replacement and site-directed mutagenesis, *J Biol Chem 269*, 5085-5091.

262. Zhang, Y., Kang, S. A., Mukherjee, T., Bale, S., Crane, B. R., Begley, T. P., and Ealick, S. E. (2007) Crystal structure and mechanism of tryptophan 2,3-dioxygenase, a heme enzyme involved in tryptophan catabolism and in quinolinate biosynthesis, *Biochemistry 46*, 145-155.

263. Kurnasov, O., Goral, V., Colabroy, K., Gerdes, S., Anantha, S., Osterman, A., and Begley, T. P. (2003) NAD biosynthesis: Identification of the tryptophan to quinolinate pathway in bacteria, *Chem Biol 10*, 1195-1204.

264. Laemmli, U. K. (1970) Cleavage of structural proteins during the assembly of the head of bacteriophage t4, *Nature 227*, 680-685.

265. Neese, F., Zumft, W. G., Antholine, W. E., and Kroneck, P. M. H. (1996) The purple mixed-valence CuA center in nitrous-oxide reductase: EPR of the copper-63-, copper-65-, and both copper-65- and [15N]histidine-enriched enzyme and a molecular orbital interpretation, *J Am Chem Soc 118*, 8692-8699.

266. Cammack, R., (Ed.) (1995) *Biogenergetics: A practical approach*, Vol. 85-109, IRL Press, New York.

267. Kurnasov, O., Goral, V., Colabroy, K., Gerdes, S., Anantha, S., Osterman, A., and Begley, T. P. (2003) NAD biosynthesis: Identification of the tryptophan to quinolinate pathway in bacteria, *Chem Biol 10*, 1195-1204.

268. Stone, T. W., and Darlington, L. G. (2002) Endogenous kynurenines as targets for drug discovery and development, *Nat Rev Drug Discov 1*, 609-620.

269. Schwarcz, R. (2004) The kynurenine pathway of tryptophan degradation as a drug target, *Curr Opin Pharmacol 4*, 12-17.

270. Robotka, H., Toldi, J., and Vcsei, L. (2008) L-kynurenine: Metabolism and mechanism of neuroprotection, *Future Neurol 3*, 169-188.

271. Guillemin, G. J., Meininger, V., and Brew, B. J. (2005) Implications for the kynurenine pathway and quinolinic acid in *Amyotrophic lateral sclerosis*, *Neurodegener Dis 2*, 166-176.

272. Guillemin, G. J., and Brew, B. J. (2002) Implications of the kynurenine pathway and quinolinic acid in alzheimer's disease, *Redox Rep 7*, 199-206.

273. Myint, A. M., Schwarz, M. J., Steinbusch, H. W. M., and Leonard, B. E. (2009) Neuropsychiatric disorders related to interferon and interleukins treatment, *Metab Brain Dis 24*, 55-68.

274. Reinhard, J. F., Jr. (2004) Pharmacological manipulation of brain kynurenine metabolism, *Ann N Y Acad Sci 1035*, 335-349.

275. Hillier, J., Hillier, J. G., and Redfern, P. H. (1975) Liver tryptophan pyrrolase activity and metabolism of brain 5-HT [5-hydroxytryptamine] in rat, *Nature 253*, 566-567.

276. Feigelson, P., and Greengard, O. (1961) Isolation of the apoprotein of the heme enzyme tryptophan pyrrolase, *Biochim Biophys Acta 50*, 200-202.

277. Thackray, S. J., Mowat, C. G., and Chapman, S. K. (2008) Exploring the mechanism of tryptophan 2,3-dioxygenase, *Biochem Soc Trans 36*, 1120-1123.

278. Batabyal, D., and Yeh, S. R. (2007) Human tryptophan dioxygenase: A comparison to indoleamine 2,3-dioxygenase, *J Am Chem Soc 129*, 15690-15701.

279. Chauhan, N., Basran, J., Efimov, I., Svistunenko, D. A., Seward, H. E., Moody, P. C. E., and Lloyd Raven, E. (2008) The role of serine 167 in human indoleamine 2,3-dioxygenase: A comparison with tryptophan 2,3-dioxygenase, *Biochemistry 47*, 4761-4769.

280. Basran, J., Rafice, S. A., Chauhan, N., Efimov, I., Cheesman, M. R., Ghamsari, L., and Lloyd Raven, E. (2008) A kinetic, spectroscopic, and redox study of human tryptophan 2,3-dioxygenase, *Biochemistry 47*, 4752-4760.

281. Batabyal, D., and Yeh, S.-R. (2009) Substrate-protein interaction in human tryptophan dioxygenase: The critical role of h76, *J Am Chem Soc 131*, 3260-3270.

282. Thackray, S. J., Bruckmann, C., Anderson, J. L. R., Campbell, L. P., Xiao, R., Zhao, L., Mowat, C. G., Forouhar, F., Tong, L., and Chapman, S. K. (2008) Histidine 55 of tryptophan 2,3-dioxygenase is not an active site base but regulates catalysis by controlling substrate binding, *Biochemistry 47*, 10677-10684.

283. Papadopoulou, N. D., Mewies, M., McLean, K. J., Seward, H. E., Svistunenko, D. A., Munro, A. W., and Raven, E. L. (2005) Redox and spectroscopic properties of human indoleamine 2,3-dioxygenase and a His303Ala variant: Implications for catalysis, *Biochemistry 44*, 14318-14328.

284. De Laurentis, W., Khim, L., Anderson, J. L. R., Adam, A., Phillips, R. S., Chapman, S. K., Van Pee, K.-H., and Naismith, J. H. (2007) The second enzyme in pyrrolnitrin biosynthetic pathway is related to the heme-dependent dioxygenase superfamily, *Biochemistry 46*, 12393-12404.

285. Li, J. S., Han, Q., Fang, J., Rizzi, M., James, A. A., and Li, J. (2007) Biochemical mechanisms leading to tryptophan 2,3-dioxygenase activation, *Arch Insect Biochem Physiol 64*, 74-87.

286. Takikawa, O. (2005) Biochemical and medical aspects of the indoleamine 2,3-dioxygenase-initiated L-tryptophan metabolism, *Biochem Biophys Res Commun 338*, 12-19.

287. Chauhan, N., Thackray, S. J., Rafice, S. A., Eaton, G., Lee, M., Efimov, I., Basran, J., Jenkins, P. R., Mowat, C. G., Chapman, S. K., and Raven, E. L. (2009) Reassessment of the reaction mechanism in the heme dioxygenases, *J Am Chem Soc 131*, 4186-4187.

288. Tanaka, T., and Knox, W. E. (1959) Nature and mechanism of the tryptophan pyrrolase (peroxidase-oxidase) reaction of *Pseudomonas* and rat liver, *J Biol Chem 234*, 1162-1170.

289. Maeno, H., and Feigelson, P. (1967) Spectral studies on the catalytic mechanism and activation of *Pseudomonas* tryptophan oxygenase (tryptophan pyrrolase), *J Biol Chem 242*, 596-601.

290. White, R. E., and Coon, M. J. (1980) Oxygen activation by cytochrome P-450, *Annu Rev Biochem 49*, 315-356.

291. Hrycay, E. G., Gustafsson, J. A., Ingelman-Sundberg, M., and Ernster, L. (1976) The involvement of cytochrome P-450 in hepatic microsomal steroid hydroxylation reactions supported by sodium periodate, sodium chlorite, and organic hydroperoxides, *Eur J Biochem 61*, 43-52.

292. Sono, M., Roach, M. P., Coulter, E. D., and Dawson, J. H. (1996) Heme-containing oxygenases, *Chem Rev 96*, 2841-2888.

293. Matsumura, H., Wakatabi, M., Omi, S., Ohtaki, A., Nakamura, N., Yohda, M., and Ohno, H. (2008) Modulation of redox potential and alteration in reactivity via the peroxide

shunt pathway by mutation of cytochrome P450 around the proximal heme ligand, *Biochemistry 47*, 4834-4842.

294. Ortiz de Montellano, P. R., and De Voss, J. J. (2002) Oxidizing species in the mechanism of cytochrome P450, *Nat Prod Rep 19*, 477-493.

295. Denisov, I. G., Hung, S. C., Weiss, K. E., McLean, M. A., Shiro, Y., Park, S. Y., Champion, P. M., and Sligar, S. G. (2001) Characterization of the oxygenated intermediate of the thermophilic cytochrome P450 CYP119, *J Inorg Biochem 87*, 215-226.

296. Mehler, A. H., and Knox, W. E. (1950) The conversion of tryptophan to kynurenine in liver. II. The enzymatic hydrolysis of formylkynurenine, *J Biol Chem 187*, 431-438.

297. Bender, M. L., and Kemp, K. C. (1957) Kinetics of the α-chymotrypsin-catalyzed oxygen exchange of carboxylic acids, *J Am Chem Soc 79*, 116-120.

298. Ronsein, G. E., Oliveira, M. C., Miyamoto, S., Medeiros, M. H., and Di Mascio, P. (2008) Tryptophan oxidation by singlet molecular oxygen [O_2(1deltag)]: Mechanistic studies using ^{18}O-labeled hydroperoxides, mass spectrometry, and light emission measurements, *Chem Res Toxicol 21*, 1271-1283.

299. Byrn, M., and Calvin, M. (1966) Oxygen-18 exchange reactions of aldehydes and ketones, *J Am Chem Soc 88*, 1916-1922.

300. Ortiz de Montellano, P. R., (Ed.) (2005) *Cytochrome P450: Structure, mechanism, and biochemistry*, 3rd Ed. ed., Plenum: New York.

301. Erman, J. E., Hager, L. P., and Sligar, S. G. (1994) Cytochrome P-450 and peroxidase chemistry, *Adv Inorg Biochem 10*, 71-118.

302. Li, X., Fu, R., Lee, S., Krebs, C., Davidson, V. L., and Liu, A. (2008) A catalytic di-heme *bis*-Fe(IV) intermediate, alternative to anFe(IV)=O porphyrin radical, *Proc Natl Acad Sci USA 105*, 8597-8600.

303. Jakopitsch, C., Vlasits, J., Wiseman, B., Loewen, P. C., and Obinger, C. (2007) Redox intermediates in the catalase cycle of catalase-peroxidases from *Synechocystis PCC 6803*, *Burkholderia pseudomallei, and Mycobacterium tuberculosis*, *Biochemistry 46*, 1183-1193.

304. Charalabous, P., Risk, J. M., Jenkins, R., Birss, A. J., Hart, C. A., and Smalley, J. W. (2007) Characterization of a bifunctional catalase-peroxidase of *Burkholderia cenocepacia*, *FEMS Immunol Med Microbiol 50*, 37-44.

305. Sagawa, T., Yomo, T., Tsugawa, S., Takeda, Y., Ihara, H., Mitamura, E. K., Urabe, I., Ohkubo, K. . (1999) A novel versatility of catalase I as a dioxygenase for indole-ring-opening dioxygenation., *Chemistry Letters 28*, 339-340.

306. Aune, T. M., and Pierce, C. W. (1982) Activation of a suppressor T-cell pathway by interferon, *Proc Natl Acad Sci USA 79*, 3808-3812.

307. Chern, C. L., Huang, R. F., Chen, Y. H., Cheng, J. T., and Liu, T. Z. (2001) Folate deficiency-induced oxidative stress and apoptosis are mediated via homocysteine-dependent overproduction of hydrogen peroxide and enhanced activation of NF-kappaB in human Hep G2 cells, *Biomed Pharmacother 55*, 434-442.

308. Droge, W. (2006) Redox regulation in anabolic and catabolic processes, *Curr Opin Clin Nutr Metab Care 9*, 190-195.

309. Rhee, S. G. (1999) Redox signaling: Hydrogen peroxide as intracellular messenger, *Exp Mol Med 31*, 53-59.

310. Schwarcz, R., Whetsell, W. O., Jr., and Mangano, R. M. (1983) Quinolinic acid: An endogenous metabolite that produces axon-sparing lesions in rat brain, *Science 219*, 316-318.

311. Brady, F. O., Forman, H. J., and Feigelson, P. (1971) The role of superoxide and hydroperoxide in the reductive activation of tryptophan-2,3-dioxygenase, *J Biol Chem 246*, 7119-7124.

312. Hirata, F., and Hayaishi, O. (1971) Possible participation of superoxide anion in the intestinal tryptophan 2,3-dioxygenase reaction, *J Biol Chem 246*, 7825-7826.

313. Li, J. S., Han, Q., Fang, J., Rizzi, M., James, A. A., and Li, J. (2007) Biochemical mechanisms leading to tryptophan 2,3-dioxygenase activation, *Arch Insect Biochem Physiol 64*, 74-87.

314. Benecky, M. J., Frew, J. E., Scowen, N., Jones, P., and Hoffman, B. M. (1993) EPR and ENDOR detection of compound I from *Micrococcus lysodeikticus* catalase, *Biochemistry 32*, 11929-11933.

315. Patterson, W. R., Poulos, T. L., and Goodin, D. B. (1995) Identification of a porphyrin pi cation radical in ascorbate peroxidase compound I, *Biochemistry 34*, 4342-4345.

316. Schunemann, V., Jung, C., Terner, J., Trautwein, A. X., and Weiss, R. (2002) Spectroscopic studies of peroxyacetic acid reaction intermediates of cytochrome P450cam and chloroperoxidase, *J Inorg Biochem 91*, 586-596.

317. Schünemanna, V., Jung, C., Trautweina, A. X., Mandon, D., and Weiss, R. (2000) Intermediates in the reaction of substrate-free cytochrome P450cam with peroxy acetic acid, *FEBS Letters 179*, 149.

318. Dawson, J. H. (1988) Probing structure-function relations in heme-containing oxygenases and peroxidases, *Science 240*, 433-439.

319. Sivaraja, M., Goodin, D. B., Smith, M., and Hoffman, B. M. (1989) Identification by endor of trp191 as the free-radical site in cytochrome *c* peroxidase compound ES, *Science 245*, 738-740.

320. Liu, A., Poetsch, S., Davydov, A., Barra, A.-L., Rubin, H., and Graeslund, A. (1998) The tyrosyl free radical of recombinant ribonucleotide reductase from *Mycobacterium tuberculosis* is located in a rigid hydrophobic pocket, *Biochemistry 37*, 16369-16377.

321. Nordlund, P., and Eklund, H. (1995) Di-iron-carboxylate proteins, *Curr Opin Struct Biol 5*, 758-766.

322. Münck, E. (2000) *Aspects of 57Fe* Mössbauer *spectroscopy*, University Science: Sausalito, CA.

323. Behan, R. K., and Green, M. T. (2006) On the status of ferryl protonation, *J Inorg Biochem 100*, 448-459.

324. Torrens, M. A., Straub, D. K., and Epstein, L. M. (1972) Mössbauer studies on oxo-bridged iron 3 prophines, *J Am Chem Soc 94*, 4160-4162.

325. Horner, O., Mouesca, J. M., Solari, P. L., Orio, M., Oddou, J. L., Bonville, P., and Jouve, H. M. (2007) Spectroscopic description of an unusual protonated ferryl species in the catalase from *Proteus mirabilis* and density functional theory calculations on related

models. Consequences for the ferryl protonation state in catalase, peroxidase and chloroperoxidase, *J Biol Inorg Chem 12*, 509-525.

326. Stone, K. L., Hoffart, L. M., Behan, R. K., Krebs, C., and Green, M. T. (2006) Evidence for two ferryl species in chloroperoxidase compound II, *J Am Chem Soc 128*, 6147-6153.

327. Behan, R. K., Hoffart, L. M., Stone, K. L., Krebs, C., and Green, M. T. (2006) Evidence for basic ferryls in cytochromes P450, *J Am Chem Soc 128*, 11471-11474.

328. Zhang, Y., and Oldfield, E. (2004) Cytochrome P450: An investigation of the Mössbauer spectra of a reaction intermediate and an Fe(IV)=O model system, *J Am Chem Soc 126*, 4470-4471.

329. Zhang, Y., Mao, J., Godbout, N., and Oldfield, E. (2002) Mössbauer quadrupole splittings and electronic structure in heme proteins and model systems: A density functional theory investigation, *J Am Chem Soc 124*, 13921-13930.

330. Zhang, Y., Mao, J., and Oldfield, E. (2002) ^{57}Fe Mössbauer isomer shifts of heme protein model systems: Electronic structure calculations, *J Am Chem Soc 124*, 7829-7839.

331. Zhang, Y., Gossman, W., and Oldfield, E. (2003) A density functional theory investigation of Fe-N-O bonding in heme proteins and model systems, *J Am Chem Soc 125*, 16387-16396.

332. Zhang, Y., and Oldfield, E. (2003) ^{57}Fe Mössbauer quadrupole splittings and isomer shifts in spin-crossover complexes: A density functional theory investigation, *The Journal of Physical Chemistry A 107*, 4147-4150.

333. Gray, H. B., (Ed.) (1989) *In iron porphyrins*, Vol. 3, VCH Publishers, New York.

334. Brady, F. O., Forman, H. J., and Feigelson, P. (1971) The role of superoxide and hydroperoxide in the reductive activation of tryptophan 2,3-dioxygenase, *J Biol Chem 246*, 7119-7124.

335. Hirata, F., and Hayaishi, O. (1971) Possible participation of superoxide anion in the intestinal tryptophan 2,3-dioxygenase reaction, *J Biol Chem 246*, 7825-7826.

336. Li, J. S., Han, Q., Fang, J., Rizzi, M., James, A. A., and Li, J. (2007) Biochemical mechanisms leading to tryptophan 2,3-dioxygenase activation, *Archives of Insect Biochemistry and Physiology 64*, 74-87.

337. Sono, M., Roach, M. P., Coulter, E. D., and Dawson, J. H. (1996) Heme-containing oxygenases, *Chemical Reviews (Washington, D C) 96*, 2841-2887.

338. White, R. E. (1991) The involvement of free radicals in the mechanisms of monooxygenases., *Pharmacol Ther 49*, 21-42.

339. Sono, M., and Dawson, J. H. (1982) Formation of low spin complexes of ferric cytochrome P-450-cam with anionic ligands. Spin state and ligand affinity comparison to myoglobin, *J Biol Chem 257*, 5496-5502.

340. Stubbe, J., and van Der Donk, W. A. (1998) Protein radicals in enzyme catalysis, *Chem Rev 98*, 705-762.

341. Isaac, I. S., and Dawson, J. H. (1999) Haem iron-containing peroxidases, *Essays Biochem 34*, 51-69.

342. Poulos, T. L. (1988) Cytochrome P450: Molecular architecture, mechanism, and prospects for rational inhibitor design, *Pharm Res 5*, 67-75.

343. Correia, M. A., Yao, K., Allentoff, A. J., Wrighton, S. A., and Thompson, J. A. (1995) Interactions of peroxyquinols with cytochromes P450 2B1, 3A1, and 3A5: Influence of the apoprotein on heterolytic versus homolytic O-O bond cleavage, *Arch Biochem Biophys 317*, 471-478.

344. McCarthy, M. B., and White, R. E. (1983) Functional differences between peroxidase compound I and the cytochrome P-450 reactive oxygen intermediate, *J Biol Chem 258*, 9153-9158.

345. Allentoff, A. J., Bolton, J. L., Wilks, A., Thompson, J. A., and Ortiz de Montellano, P. R. (1992) Heterolytic versus homolytic peroxide bond cleavage by sperm whale myoglobin and myoglobin mutants, *J Am Chem Soc 114*, 9744-9749.

346. Traylor, T. G., and Xu, F. (1990) Mechanisms of reactions of iron(III) porphyrins with hydrogen peroxide and hydroperoxides: Solvent and solvent isotope effects, *J Am Chem Soc 112*, 178-186.

347. Traylor, T. G., and Ciccone, J. P. (1989) Mechanism of reactions of hydrogen peroxide and hydroperoxides with iron(III) porphyrins. Effects of hydroperoxide structure on kinetics, *J Am Chem Soc 111*, 8413-8420.

348. Bruice, T. C. (1991) Reactions of hydroperoxides with metallotetraphenylporphyrins in aqueous solutions, *Accounts of Chemical Research 24*, 243-249.

349. Shimizu, T., Murakami, Y., and Hatano, M. (1994) Glu318 and Thr319 mutations of cytochrome P450 1A2 remarkably enhance homolytic O-O cleavage of alkyl hydroperoxides. An optical absorption spectral study, *J Biol Chem 269*, 13296-13304.

350. Rotsaert, F. A., Hallberg, B. M., de Vries, S., Moenne-Loccoz, P., Divne, C., Renganathan, V., and Gold, M. H. (2003) Biophysical and structural analysis of a novel heme *b* iron ligation in the flavocytochrome cellobiose dehydrogenase, *J Biol Chem 278*, 33224-33231.

351. Raven, E. L., Mauk, A.G. (2001) Chemical reactivity of the active site of myoglobin, *Adv InorgChem 51*, 1-49.

352. Meunier, B., Bernadou, J. (2000) *Structure & bonding*, Vol. 93, Springer, Verlag Berlin Heidelberg New York.

353. Hu, C., Noll, B. C., Schulz, C. E., and Scheidt, W. R. (2005) Proton-mediated electron configuration change in high-spin iron(II) porphyrinates, *J Am Chem Soc 127*, 15018-15019.

354. Forouhar, F., Anderson, J. L. R., Mowat, C. G., Vorobiev, S. M., Hussain, A., Abashidze, M., Bruckmann, C., Thackray, S. J., Seetharaman, J., Tucker, T., Xiao, R., Ma, L.-C., Zhao, L., Acton, T. B., Motelione, G. T., Chapman, S. K., and Tong, L. (2007) Molecular insights into substrate recognition and catalysis by tryptophan 2,3-dioxygenase, *Proc Natl Acad Sci USA 104*, 473-478.

355. Yonetani, T., and Anni, H. (1987) Yeast cytochrome *c* peroxidase. Coordination and spin states of heme prosthetic group, *J Biol Chem 262*, 9547-9554.

356. Tsai, A. L., Kulmacz, R. J., Wang, J. S., Wang, Y., Van Wart, H. E., and Palmer, G. (1993) Heme coordination of prostaglandin H synthase, *J Biol Chem 268*, 8554-8563.

357. Ikeda-Saito, M., and Iizuka, T. (1975) Studies on the heme environment of horse heart ferric cytochrome c. Azide and imidazole complexes of ferric cytochrome c, *Biochim Biophys Acta 393*, 335-342.

358. Liu, L., and Santi, D. V. (1993) Asparagine 229 in thymidylate synthase contributes to, but is not essential for, catalysis, *Proc Natl Acad Sci U S A 90*, 8604-8608.

359. Davidson, V. L. (2001) Pyrroloquinoline quinone (pqq) from methanol dehydrogenase and tryptophan tryptophylquinone (TTQ) from methylamine dehydrogenase, *Advances in Protein Chemistry 58*, 95-140.

360. McIntire, W. S., Wemmer, D. E., Chistoserdov, A., and Lidstrom, M. E. (1991) A new cofactor in a prokaryotic enzyme: Tryptophan tryptophylquinone as the redox prosthetic group in methylamine dehydrogenase, *Science 252*, 817-824.

361. Davidson, V. L. (2007) Protein-derived cofactors. Expanding the scope of post-translational modifications, *Biochemistry 46*, 5283-5292.

362. Chen, L., Doi, M., Durley, R. C., Chistoserdov, A. Y., Lidstrom, M. E., Davidson, V. L., and Mathews, F. S. (1998) Refined crystal structure of methylamine dehydrogenase from *Paracoccus denitrificans* at 1.75 Å resolution, *Journal of Molecular Biology 276*, 131-149.

363. van der Palen, C. J., Slotboom, D. J., Jongejan, L., Reijnders, W. N., Harms, N., Duine, J. A., and van Spanning, R. J. (1995) Mutational analysis of mau genes involved in methylamine metabolism in *Paracoccus denitrificans*, *Eur J Biochem 230*, 860-871.

364. Pearson, A. R., de la Mora-Rey, T., Graichen, M. E., Wang, Y., Jones, L. H., Marimanikkupam, S., Aggar, S. A., Grimsrud, P. A., Davidson, V. L., and Wilmot, C. W.

(2004) Further insights into quinone cofactor biogenesis: Probing the role of mauG in methylamine dehydrogenase TTQ formation, *Biochemistry 43*, 5494-5502.

365. Wang, Y., Li, X., Jones, L. H., Pearson, A. R., Wilmot, C. M., and Davidson, V. L. (2005) Maug-dependent in vitro biosynthesis of tryptophan tryptophylquinone in methylamine dehydrogenase, *J Am Chem Soc 127*, 8258-8259.

366. Wang, Y., Graichen, M. E., Liu, A., Pearson, A. R., Wilmot, C. W., and Davidson, V. L. (2003) MauG, a novel diheme protein required for tryptophan tryptophylquinone biogenesis, *Biochemistry 42*, 7318-7325.

367. Li, X., Feng, M., Wang, Y., Tachikawa, H., and Davidson, V. L. (2006) Evidence for redox cooperativity between *c*-type hemes of maug which is likely coupled to oxygen activation during tryptophan tryptophylquinone biosynthesis, *Biochemistry 45*, 821-828.

368. Graichen, M. E., Jones, L. H., Sharma, B. V., van Spanning, R. J., Hosler, J. P., and Davidson, V. L. (1999) Heterologous expression of correctly assembled methylamine dehydrogenase in *Rhodobacter sphaeroides*, *Journal of Bacteriology 181*, 4216-4222.

369. Zhou, W., Feng, M. Q., Li, J. Y., and Zhou, P. (2006) Studies on the preparation, crystal structure and bioactivity of ginsenoside compound k, *J Asian Nat Prod Res 8*, 519-527.

370. Pearson, A. R., Marimanikkuppam, S., Li, X., Davidson, V. L., and Wilmot, C. M. (2006) Isotope labeling studies reveal the order of oxygen incorporation into the tryptophan tryptophylquinone cofactor of methylamine dehydrogenase, *J Am Chem Soc 128*, 12416-12417.

371. Husain, M., and Davidson, V. L. (1987) Purification and properties of methylamine dehydrogenase from *Paracoccus denitrificans*, *Journal of Bacteriology 169*, 1712-1717.

372. Husain, M., Davidson, V. L., Gray, K. A., and Knaff, D. B. (1987) Redox properties of the quinoprotein methylamine dehydrogenase from *Paracoccus denitrificans*, *Biochemistry 26*, 4139-4143.

373. Sono, M., Roach, M. P., Coulter, E. D., and Dawson, J. H. (1996) Heme-containing oxygenases, *Chem Rev 96*, 28441-22887.

374. Pearson, A. R., Jones, L. H., Higgins, L., Ashcroft, A. E., Wilmot, C. W., and Davidson, V. L. (2003) Understanding quinone cofactor biogenesis in methylamine dehydrogenase through novel cofactor generation, *Biochemistry 42*, 3224-3230.

375. Davidson, V. L. (2007) Protein-derived cofactors. Expanding the scope of post-translational modifications, *Biochemistry 46*, 5283-5292.

376. Davidson, V. L. (2001) Pyrroloquinoline quinone (PQQ) from methanol dehydrogenase and tryptophan tryptophylquinone (TTQ) from methylamine dehydrogenase, *Adv Protein Chem 58*, 95-140.

377. Stevens, J. M., Daltrop, O., Allen, J. W., and Ferguson, S. J. (2004) *C*-type cytochrome formation: Chemical and biological enigmas, *Acc Chem Res 37*, 999-1007.

378. Li, X., Feng, M., Wang, Y., Tachikawa, H., and Davidson, V. L. (2006) Evidence for redox cooperativity between *c*-type hemes of maug which is likely coupled to oxygen activation during tryptophan tryptophylquinone biosynthesis, *Biochemistry 45*, 821-828.

379. Schulz, C. E., Rutter, R., Sage, J. T., Debrunner, P. G., and Hager, L. P. (1984) Mössbauer and electron paramagnetic resonance studies of horseradish peroxidase and its catalytic intermediates, *Biochemistry 23*, 4743-4754.

380. Maeda, Y., Higashimura, T., and Morita, Y. (1967) Mössbauer effect in peroxidase, *Biochem Biophys Res Commun 29*, 362-367.

381. Ortiz de Montellano, P. R. (1995) *Cytochrome P450: Structure, mechanism, and biochemistry*, 2nd ed., Plenum: New York.

382. Rutter, R., and Hager, L. P. (1982) The detection of two electron paramagnetic resonance radical signals associated with chloroperoxidase compound I, *J Biol Chem 257*, 7958-7961.

383. Benecky, M. J., Frew, J. E., Scowen, N., Jones, P., and Hoffman, B. M. (1993) Epr and endor detection of compound I from *Micrococcus lysodeikticus* catalase, *Biochemistry 32*, 11929-11933.

384. Debrunner, P. G. (1989) Mössbauer spectroscopy of iron porphyrins, *Phys Bioinorg Chem Ser 4*, 137-234.

385. Prazeres, S., Moura, J. J., Moura, I., Gilmour, R., Goodhew, C. F., Pettigrew, G. W., Ravi, N., and Huynh, B. H. (1995) Mössbauer characterization of *Paracoccus denitrificans* cytochrome *c* peroxidase. Further evidence for redox and calcium binding-induced heme-heme interaction, *J Biol Chem 270*, 24264-24269.

386. Groves, J. T., Quinn, R., McMurry, T. J., Nakamura, M., Lang, G., and Boso, B. (1985) Preparation and characterization of a dialkoxyiron(IV) porphyrin, *J Am Chem Soc 107*, 354-360.

387. Bill, E., Schunemann, V., Trautwein, A. X., Weiss, R., Fischer, J., Tabard, A., and Guilard, R. (2002) Mössbauer investigations of the hexachlorantimonate salt of the phenyliron 2,3,7,8,l2,13,17,18-octaethyl-5,10,15,20-tetraphenylporphyrinate,

[Fe(oetpp)Ph]$SbCl_6$ and x-ray structure of the phenyliron(III) precursor Fe(III)(oetpp)Ph, *Inorg Chim Acta 339*, 420-426.

388. Ikezaki, A., Tukada, H., and Nakamura, M. (2008) Control of electronic structure of a six-coordinate iron(III) porphyrin radical by means of axial ligands, *Chem Commun*, in press.

389. Karlsson, M., Sahlin, M., and Sjöberg, B. M. (1992) *Escherichia coli* ribonucleotide reductase. Radical susceptibility to hydroxyurea is dependent on the regulatory state of the enzyme, *J Biol Chem 267*, 12622-12626.

390. Gräslund, A., and Sahlin, M. (1996) Electron paramagnetic resonance and nuclear magnetic resonance studies of class I ribonucleotide reductase, *Ann Rev Biophys Biomol Struc 25*, 259-286.

391. Costas, M., Mehn, M. P., Jensen, M. P., and Que, L. (2004) Dioxygen activation at mononuclear nonheme iron active sites: Enzymes, models, and intermediates, *Chem Rev 104*, 939-986.

392. Krebs, C., Fujimori, D. G., Walsh, C. T., and Bollinger, J. M., Jr. (2007) Non-heme fe(iv)-oxo intermediates, *Acc Chem Res 40*, 484-492.

393. Lee, S. K., Fox, B. G., Froland, W. A., Lipscomb, J. D., and Münck, E. (1993) A transient intermediate of the methane monooxygenase catalytic cycle containing an $Fe^{IV}Fe^{IV}$ cluster, in *J Am Chem Soc*, pp 6450-6451.

394. Shu, L., Nesheim, J. C., Kauffmann, K., Münck, E., Lipscomb, J. D., and Que, L., Jr. (1997) An $Fe_2^{IV}O_2$ diamond core structure for the key intermediate Q of methane monooxygenase, *Science 275*, 515-518.

395. Pettigrew, G. W., Echalier, A., and Pauleta, S. R. (2006) Structure and mechanism in the bacterial dihaem cytochrome *c* peroxidases, *J Inorg Biochem 100*, 551-567.

396. Zhu, Z., Sun, D., and Davidson, V. L. (2000) Conversion of methylamine dehydrogenase to a long-chain amine dehydrogenase by mutagenesis of a single residue, *Biochemistry 39*, 11184-11186.

397. Li, X., Fu, R., Lee, S., Krebs, C., Davidson, V. L., and Liu, A. (2008) A catalytic di-heme *bis*-Fe(IV) intermediate, alternative to an Fe(IV)=O porphyrin radical, *Proc Natl Acad Sci U S A 105*, 8597-8600.

398. Govindaraj, S., Eisenstein, E., Jones, L. H., Sanders-Loehr, J., Chistoserdov, A. Y., Davidson, V. L., and Edwards, S. L. (1994) Aromatic amine dehydrogenase, a second tryptophan tryptophylquinone enzyme, *J Bacteriol 176*, 2922-2929.

399. van der Palen, C. J., Slotboom, D. J., Jongejan, L., Reijnders, W. N., Harms, N., Duine, J. A., and van Spanning, R. J. (1995) Mutational analysis of mau genes involved in methylamine metabolism in *Paracoccus denitrificans*, *Eur J Biochem 230*, 860-871.

400. van der Palen, C. J., Reijnders, W. N., de Vries, S., Duine, J. A., and van Spanning, R. J. (1997) MauE and mauD proteins are essential in methylamine metabolism of *Paracoccus denitrificans*, *Antonie van Leeuwenhoek 72*, 219-228.

401. Pearson, A. R., De La Mora-Rey, T., Graichen, M. E., Wang, Y., Jones, L. H., Marimanikkupam, S., Agger, S. A., Grimsrud, P. A., Davidson, V. L., and Wilmot, C. M. (2004) Further insights into quinone cofactor biogenesis: Probing the role of maug in methylamine dehydrogenase tryptophan tryptophylquinone formation, *Biochemistry 43*, 5494-5502.

402. Wang, Y., Li, X., Jones, L. H., Pearson, A. R., Wilmot, C. M., and Davidson, V. L. (2005) MauG-dependent in vitro biosynthesis of tryptophan tryptophylquinone in methylamine dehydrogenase, *Journal of the American Chemical Society 127*, 8258-8259.

403. Li, X., Jones, L. H., Pearson, A. R., Wilmot, C. M., and Davidson, V. L. (2006) Mechanistic possibilities in MauG-dependent tryptophan tryptophylquinone biosynthesis, *Biochemistry 45*, 13276-13283.

404. Wang, Y., Graichen, M. E., Liu, A., Pearson, A. R., Wilmot, C. M., and Davidson, V. L. (2003) MauG, a novel diheme protein required for tryptophan tryptophylquinone biogenesis, *Biochemistry 42*, 7318-7325.

405. Wang, Y., Li, X., Jones, L. H., Pearson, A. R., Wilmot, C. M., and Davidson, V. L. (2005) MauG-dependent in vitro biosynthesis of tryptophan tryptophylquinone in methylamine dehydrogenase, *J Am Chem Soc 127*, 8258-8259.

406. Makris, T. M., von Koenig, K., Schlichting, I., and Sligar, S. G. (2006) The status of high-valent metal oxo complexes in the P450 cytochromes, *J Inorg Biochem 100*, 507-518.

407. Pearson, A. R., de la Mora-Rey, T., Graichen, M. E., Wang, Y., Jones, L. H., Marimanikkupam, S., Aggar, S. A., Grimsrud, P. A., Davidson, V. L., and Wilmot, C. M. (2004) Further insights into quinone cofactor biogenesis: Probing the role of *mauG* in methylamine dehydrogenase TTQ formation, *Biochemistry 43*, 5494-5502.

408. Graichen, M. E., Jones, L. H., Sharma, B. V., van Spanning, R. J., Hosler, J. P., and Davidson, V. L. (1999) Heterologous expression of correctly assembled methylamine dehydrogenase in *Rhodobacter sphaeroides*, *J Bacteriol 181*, 4216-4222.

409. Li, T., Walker, A. L., Iwaki, H., Hasegawa, Y., and Liu, A. (2005) Kinetic and spectroscopic characterization of acmsd from *Pseudomonas fluorescens* reveals a pentacoordinate mononuclear metallocofactor, *J Am Chem Soc 127*, 12282-12290.

410. Neese, F., Zumft, W. G., Antholine, W. E., and Kroneck, P. M. H. (1996) The purple mixed-valence cua center in nitrous-oxide reductase: EPR of the copper-63-, copper-65-, and both copper-65- and [15N]histidine-enriched enzyme and a molecular orbital interpretation, *J Am Chem Soc 118*, 8692 -8699.

411. Barrows, T. P., Bhaskar, B., and Poulos, T. L. (2004) Electrostatic control of the tryptophan radical in cytochrome *c* peroxidase, *Biochemistry 43*, 8826-8834.

412. Lee, S. K., Nesheim, J. C., and Lipscomb, J. D. (1993) Transient intermediates of the methane monooxygenase catalytic cycle, *J Biol Chem 268*, 21569-21577.

413. Ellfolk, N., Ronnberg, M., Aasa, R., Andreasson, L. E., and Vanngard, T. (1983) Properties and function of the two hemes in *Pseudomonas* cytochrome *c* peroxidase, *Biochim Biophys Acta 743*, 23-30.

414. Itoh, S., Hirano, K., Furuta, A., Komatsu, M., Ohshiro, Y., Ishida, A., Takamuku, S., Kohzuma, T., Nakamura, N., and Suzuki, S. (1993) Physicochemical properties of 2-methylthio-4-methylphenol, a model compound of the novel cofactor of galactose oxidase, *Chem Lett*, 2099-2102.

415. Stubbe, J., and van der Donk, W. A. (1998) Protein radicals in enzyme catalysis, *Chem Rev 98*, 705-762.

416. Liu, A., Potsch, S., Davydov, A., Barra, A. L., Rubin, H., and Graslund, A. (1998) The tyrosyl free radical of recombinant ribonucleotide reductase from *Mycobacterium tuberculosis* is located in a rigid hydrophobic pocket, *Biochemistry 37*, 16369-16377.

417. Eriksson, M., Jordan, A., and Eklund, H. (1998) Structure of *Salmonella typhimurium NRDF* ribonucleotide reductase in its oxidized and reduced forms, *Biochemistry 37*, 13359-13369.

418. Hogbom, M., Huque, Y., Sjoberg, B. M., and Nordlund, P. (2002) Crystal structure of the di-iron/radical protein of ribonucleotide reductase from *Corynebacterium ammoniagenes*, *Biochemistry 41*, 1381-1389.

419. Uppsten, M., Davis, J., Rubin, H., and Uhlin, U. (2004) Crystal structure of the biologically active form of class IB ribonucleotide reductase small subunit from *Mycobacterium tuberculosis*, *FEBS Lett 569*, 117-122.

420. Solomon, E. I., Brunold, T. C., Davis, M. I., Kemsley, J. N., Lee, S. K., Lehnert, N., Neese, F., Skulan, A. J., Yang, Y. S., and Zhou, J. (2000) Geometric and electronic structure/function correlations in non-heme iron enzymes, *Chem Rev 100*, 235-350.